Fast Proximal Algorithms for Applications in Viscoplasticity

A thesis submitted in partial fulfilment of the requirements for the degree of Doctor of Philosophy in Computational and Applied Mathematics

Timm Treskatis

School of Mathematics and Statistics
University of Canterbury | 2016

Contents

Abstract

Numerical flow simulations for viscoplastic fluids have posed, and continue to pose major challenges. The large scale of industrially relevant flow problems coupled with the highly nonlinear and nonsmooth nature of viscoplastic materials still poses too high an obstacle even for modern computer clusters.

This research aims to provide more efficient numerical schemes for flow simulations of Bingham, Casson and Herschel-Bulkley fluids without perturbing their viscoplastic behaviour by smoothing or regularisation. Two main contributions form the focus of this thesis: firstly, a new dual formulation of such problems and secondly, their numerical solution by proximal gradient or proximal Newton-type methods.

To this end, we initially study a class of generic convex optimisation problems in Hilbert spaces. We design dual-based algorithms in the appropriate function spaces and derive properties of the primal problem that guarantee their applicability and convergence.

'Fast' or 'accelerated' proximal gradient methods can be adapted to viscoplastic flow problems, to yield strong convergence of order $O(1/k)$, as the iteration counter $k \to \infty$. This contrasts to $O(1/\sqrt{k})$ convergence of state-of-the-art solvers in viscoplasticity.

Accelerated second-order methods of Newton type are particularly advantageous for resolving the additional nonlinearity that arises in Casson and Herschel-Bulkley flow problems. We observe that these algorithms can converge several times faster than classical alternatives.

Simulations of stationary and time-dependent flows through pipe cross-sections and two-dimensional cavities demonstrate the viability and efficiency of this approach. One may anticipate that these new numerical methods bring us an important step closer towards the industrial applicability of computational viscoplasticity.

Keywords Viscoplastic Fluids, Bingham Model, Casson Model, Herschel-Bulkley Model, Fast Proximal Gradient Methods, Fast Proximal Newton-Type Methods

2010 Mathematics Subject Classification 65K15, 76A05, 90C25

Acknowledgements

Looking back over the past three years, this PhD project has provided me with new mathematical insights, many enriching encounters and countless learning experiences. They have made me grow both as a scientist and as a person. Therefore, I would like to take this opportunity to thank all those people and organisations, who have facilitated this development through their invaluable contributions.

This project has been supervised by Dr Miguel Moyers-Gonzàlez and co-supervised by Associate Professor Chris Price. I have been extremely fortunate to work with supervisors, who take the time for face-to-face meetings every single week. The vast extent of freedom they have given me for shaping this research, for trying out new directions and working independently is remarkable. In retrospect, there is no doubt that most of the results would have remained undiscovered otherwise.

Furthermore, I particularly appreciate how Miguel has opened many doors for me, by accessing his professional networks in my favour and offering his guidance to further extend the outreach of my communication as well. From Chris, I have gained a range of new computational skills and learned about the value of careful attention to detail. I am also very grateful for his insights 'behind the scenes' of academia that make me feel well-prepared for my future career. Thank you to both of you, for giving me your time and advice that amply.

Examining a PhD project is a time-consuming task as well. I appreciate that Associate Professor Regina Burachik from the University of South Australia in Adelaide and Associate Professor Sergio Gonzalez Andrade from the National Polytechnic School EPN Quito in Ecuador have offered to review this thesis.

The OptALI exchange programme (Optimisation and its Applications in Learning and Industry), funded by the European Union and the New Zealand Government, very generously provided the means for a fruitful research visit to the University of Göttingen in June and July 2014. It has been a privilege collaborating with Professor Gert Lube, Associate Professor Russell Luke and Assistant Professor Shoham Sabach during that time. Their ideas have led to a number of refinements and improvements of the work in its state at that time. Additionally, I would like to acknowledge Shoham for sharing his great experience on efficient computational techniques for solving large-scale

convex programming problems. He deserves credit for stimulating my research on FISTA and other accelerated schemes in the context of viscoplasticity.

In August 2014, the Gene Golub SIAM Summer School turned out to be an excellent opportunity for networking with fellow young researchers in closely related disciplines. During the two weeks of the summer school, Professor Roland Herzog, Dr Esther Klann, Professor Michael Stingl and Professor Winnifired Wollner walked the extra mile more than once. I left Linz with a greatly expanded skill set in optimisation, non-smooth analysis and computation. Therefore, a big 'thank you' to the organisers, to SIAM and the co-sponsors for a magnificent and memorable event.

A SIAM Student Travel Award, a Gloria Olive Student Travel Grant and the Aitken Prize of the New Zealand Mathematical Society (NZMS) allowed me to undertake another tremendously rewarding trip to the northern hemisphere in 2015. I highly esteem the scientific benefits I received from attending the British-French-German Conference on Optimisation 2015 in London, from visiting the Mathematical Institute of the University of Oxford, from participating in the SIAM Conference on Control and its Applications 2015 in Paris and the BIRS Workshop on Viscoplastic Fluids in Banff, Canada.

Several visits to the Institute for Applied Mathematics at the University of Heidelberg stand out as a further highlight of this journey. I am deeply indebted to Dr Thomas Carraro for spending his time with me so generously. Our discussions on numerical techniques for viscoplastic flow simulations have sparked a wealth of ideas for further research. Additionally, I very much appreciate his personal advice for planning my career. The proposal writing skills I learned from him will undoubtedly be of great value in the future.

For all these travels and many more conference visits in Australasia, the School of Mathematics and Statistics at the University of Canterbury has always been very generous with its support. I also acknowledge further travel grants from ANZIAM, the New Zealand branch of ANZIAM, the Australian Mathematical Society (AustMS) and CSIRO.

Furthermore, I wish to express my gratitude to the University of Canterbury for funding my research with a UC Doctoral Scholarship and for offering all its resources.

Many more people have helped me with their advice, feedback or support: Professor Amir Beck, Professor Anita Schöbel, Assistant Professor Anthony Wachs, Professor Bernhard Taureck, Professor Endre Süli, Dr Fiona Cross, Professor Ian Frigaard, Irene David, Professor Juan Carlos De los Reyes, Dr Oliver Lass, Professor Stefan Volkwein and all members of the U-CAN-SPEAK Toastmasters Club, thank you very much, indeed!

Finally, a great thank you to my family for all their support, and to my friends for making the past three years so thoroughly enjoyable.

If Dieter Rudolf had not been my grammar school teacher for mathematics and physics, I would have become an unhappy pharmacist by now. Thank you for igniting that spark of curiosity for our subject, which has given me the motivation to start and finish this project, as well as hopefully many more to come.

Chapter 1

A Phenomenological Introduction to Viscoplasticity

> Resistentiam, quæ oritur ex defectu lubricitatis partium fluidi, cæteris paribus, proportionalem esse velocitati, qua partes fluidi separantur ab invicem.
>
> *The resistance arising from the want of lubricity in the parts of a fluid is, other things being equal, proportional to the velocity with which the parts of the fluid are separated from each other.*

Isaac Newton
Philosophiæ Naturalis Principia Mathematica, 1687

Problems in fluid dynamics pose some of the greatest challenges for contemporary mathematics and computation. The inherent nonlinearity of the Navier-Stokes equations, which arises due to convection in fluid flows, gives rise to one of the most famous yet unsolved Millenium Prize Problems regarding the existence and regularity of solutions [1]. For practical flow simulations, the large scale of such problems adds further difficulty, and requires sophisticated computational techniques.

In his research on the circular motion of fluids, as cited above, Newton hypothesised that fluids are governed by a proportional relation between the flow velocity gradient, or strain rate, and the shear stress at any point in the flow domain. Today, more than three centuries later, this fundamental relation has lost some of its generality, but none of its importance. It is nowadays referred to as the constitutive equation of a Newtonian fluid, and is still considered to model the behaviour of water or air with high accuracy over a

broad range of physical parameters. As a result of modern hardware, fine-tuned numerical solvers and parallelised algorithms, simulations of Newtonian flows have widely replaced traditional experimental approaches, such as wind tunnel testing, in many industries.

Additional analytical and numerical challenges arise for more complex materials. Non-Newtonian fluids no longer obey a constitutive law with a constant proportionality parameter, but this viscosity or 'thickness' of the fluid varies depending on e.g. the local shear rate or the shear history.

Rheology

The field of rheology studies complex materials, which fall into neither of the classical categories of Newtonian liquids, perfectly plastic or ideally elastic solids. The great importance of rheological research relies on the observation that realistic materials unite several of these idealised properties at once [2, p 4]. We highlight a few examples.

1.1 Generalised Newtonian Fluids A simple deviation from Newtonian behaviour arises when the viscosity decreases, or in a few rather exotic cases, increases under shear. Such fluids are therefore termed 'shear-thinning' or 'shear-thickening'. As long as the viscosity remains finite, such behaviour is classified under generalised Newtonian flow rules.

Many emulsions and dispersions exhibit thinning under strain. The contrary effect is typically observed when flows of granular materials, such as sand, are modelled as fluids. It is a well-known effect from walking on the beach that the ground appears to harden below one's step.

1.2 Thixotropy and Rheopecty If thinning or thickening is not instantaneous, but if the material takes a finite amount of time to respond to stress, then one refers to such a rheology as thixotropic or rheopectic, respectively. [2, p 24]

Interactions between particles suspended in a fluid may give rise to complex internal structures. For colloidal suspensions with strong elastic or inelastic interactions, the breakdown or recovery of such structures may happen on an observable time scale. This kind of non-negligible dependence on the flow history constitutes a defining feature for thixotropic and rheopectic fluids.

1.3 Viscoelasticity Hooke's law of perfect elasticity, which defines a linear relation between stress and strain, can be relaxed in numerous ways to provide a more accurate description for the behaviour of real materials. Viscoelasticity is the phenomenon associated to a time-dependence of the relationship between stress and strain. Consequently, viscoelastic fluids are also described as materials 'with memory'.

Such effects are often observed when the environmental conditions, that an elastic solid is subjected to, give rise to a departure from Hookean behaviour. As such, even classical elastic solids like metals show significant viscoelastic effects at higher temperatures. Wood, too, may serve as an application of viscoelasticity. [3, p 2]

1.4 Viscoplasticity Another very important and interesting class of fluids with shear-dependent viscosity is given by viscoplastic fluids. These materials unite properties of both viscous liquids and plastic solids.

Unless the stress acting on a fluid element exceeds a critical threshold, the so-called yield stress, the fluid appears to withstand this excitation and remain solid. Shearing only becomes observable as soon as the stress reaches a magnitude greater than the yield stress. Conversely, when the stress magnitude falls below the yield limit again, fluid parcels adhere to their neighbours and macroscopically, the fluid assumes a solid state.

1.5 Rheological Controversy It has been a long debate among rheologists whether the yield stress and rigid plasticity are physically real or whether, in line with the Heraclitean 'πάντα ῥεῖ', *everything flows* so long as the time scales of observation are sufficiently large [4]–[9]. While it is not the objective of this work to participate in any rheological discussion, we may certainly draw one conclusion: there is common agreement over the fact that countless observable phenomena appear to be caused by strict viscoplasticity with a yield stress. In the sequel, we will therefore omit attributes such as 'observable' or 'apparent' and keep in mind that assuming the fluid to be solid is at the least a very useful and highly accurate approximation.

1.6 An Illustrative Experiment The characteristic viscoplastic behaviour is well known to us from every day experiences: toothpaste can be considered a prototypical example for a viscoplastic fluid. If we unscrew the lid and turn the tube upside down, taking care that we avoid applying any extra pressure with our hand, gravity causes stress within the fluid, pulling the toothpaste downwards. Still, as pictured in Figure 1.1(a) on the following page, the gravitationally induced stress is insufficient to make the toothpaste yield – it remains solid.

In a second step, we now increase the stress by squeezing the tube. As can be seen from Figure 1.1(b), we may distinguish two different flow regimes: at the tip of the tube, one can clearly identify a thin layer where sheared fluid bridges the gap between the resting wall and the moving plug. This cylindrical core, however, remains unyielded and glides downwards like a rigid body. Obscured by the toothpaste flowing out, but visible in Figure 1.1(d), are further regions of solid material, which remain attached to the wall in curved, dented or edged notches.

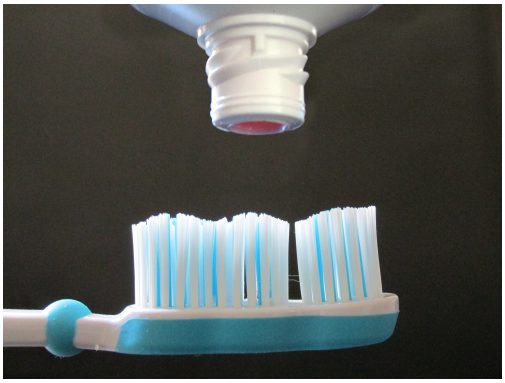

(a): Gravity alone does not cause sufficient stress to start the flow of toothpaste.

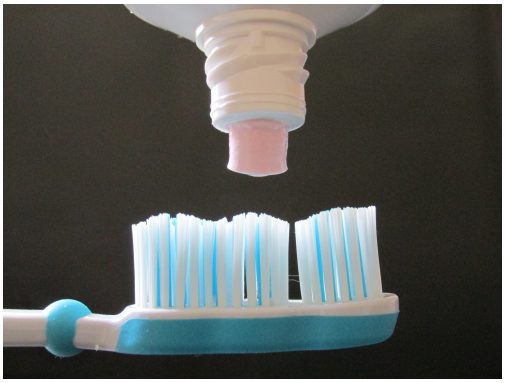

(b): With extra manual pressure, a plug is extruded. Shear only arises in a thin layer close to the wall.

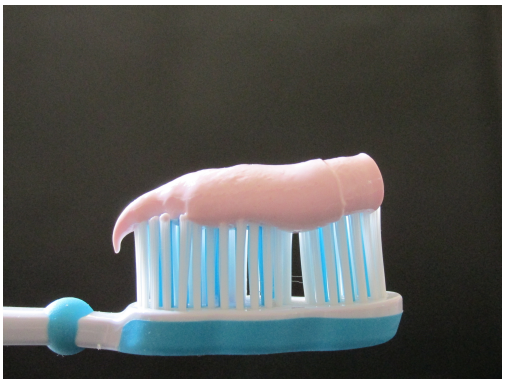

(c): Re-solidification with gravity as the only source of stress is desirable for toothpaste to avoid dripping.

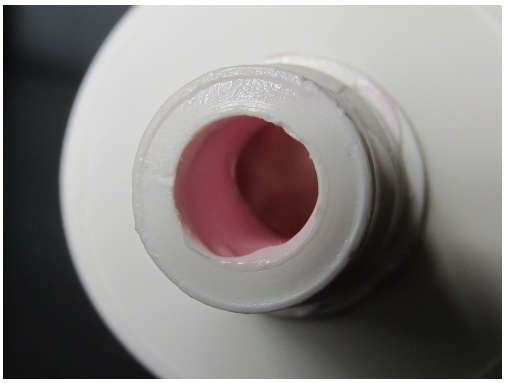

(d): Fluid in corners or indentations may never flow. For perishable viscoplastic fluids, this raises hygenic problems.

Figure 1.1: A simple experiment to illustrate the viscoplastic behaviour of toothpaste. *Photos: own work.*

As soon as the material has escaped the influence of the additional pressure, the stress magnitude no longer exceeds the yield stress and hence only a single rigid phase can be observed for the extruded part of the fluid in Figure 1.1(b) and the toothpaste continues to maintain its shape once it has come to rest on the brush in Figure 1.1(c).

1.7 Characteristic Features of Viscoplastic Fluids In summary, three main characteristics differentiate viscoplastic from Newtonian fluids:

(a) the *existence of a positive yield stress* that has to be exceeded before the fluid leaves its state of rigidity; consequently,

(b) a *separation of the flow domain* into regions with viscous shear flow and plastic

stagnation; and additionally,

(c) in the absence of sufficiently strong driving forces, *cessation of flow within finite time*.

In many industrial applications, it is a critical touchstone for any numerical scheme, whether or not it reflects this behaviour accurately. Algorithms in compliance with these requirements will therefore form the primary focus of our analytical and numerical studies in this thesis.

Viscoplastic Models

A mathematical description of fluid flow generally has to respect the physical laws of classical mechanics and thermodynamics. For the scope of this research, we restrict our attention to the very broad and most relevant class of incompressible, isotropic and isothermal flow in a domain $\Omega \subset \mathbb{R}^d$, $d \in \{2, 3\}$. In this setting, conservation of momentum and conservation of mass require that at any time t, the flow velocity $u : \Omega \to \mathbb{R}^d$, the pressure $p : \Omega \to \mathbb{R}$ and the (symmetric) deviatoric component $\tau : \Omega \to \mathbb{R}^{d\times d}_{\mathrm{sym}}$ of the total stress tensor satisfy the Navier-Stokes equations [10]

$$\varrho\,(\partial_t u + (u \cdot \nabla)u) - \operatorname{div}\tau + \nabla p = f \tag{1.1}$$

$$\operatorname{div} u = 0, \tag{1.2}$$

complemented with appropriate boundary conditions. The parameter $\varrho > 0$ represents the fluid density, and the inhomogeneity $f : \Omega \to \mathbb{R}^d$ includes the effect of all body forces, such as gravity for instance. The vector-valued divergence operator applies the scalar divergence row-wise.

While these first two equations are generic in the sense that they apply to any fluid under the aforementioned restrictions, a third, constitutive relation will specify the material-specific response to stress in terms of a strain rate $\dot\gamma : \Omega \to \mathbb{R}^{d\times d}_{\mathrm{sym}}$. This relation will also close the system: the strain rate relates back to the flow velocity, as it is given by the symmetric part $\mathcal{D}u$ of the velocity gradient, where $\mathcal{D} := (\nabla + \nabla^\top)/2$.

The Newtonian proportionality between the 'resistance arising from the want of lubricity in the parts of a fluid', i.e. the stress τ, and 'the velocity with which the parts of the fluid are separated from each other', i.e. the rate of strain $\dot\gamma$, is directly expressed by

$$\tau = 2\mu\dot\gamma \tag{1.3a}$$

with the viscosity $\mu > 0$.

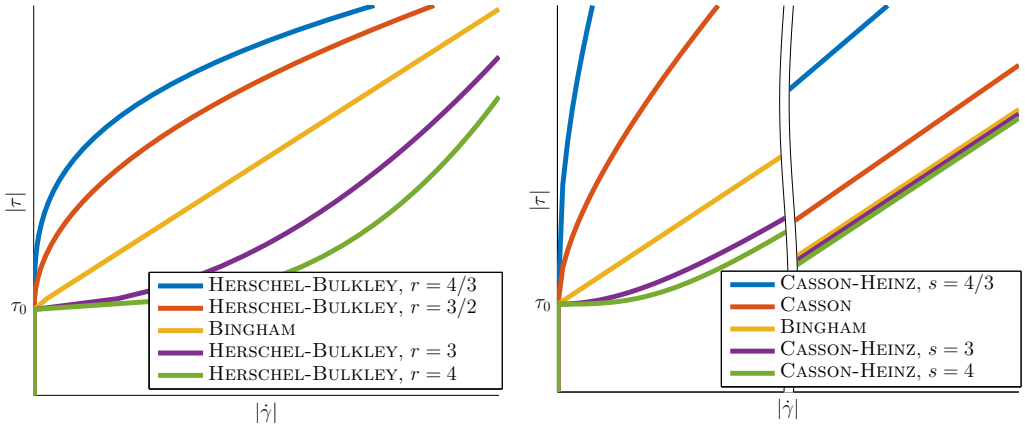

(a): A Bingham fluid is the special case of a Herschel-Bulkley fluid for $r = 2$.

(b): The effective plastic viscosity of generalised Casson fluids approaches a constant for large strain rates.

Figure 1.2: Constitutive relations for Bingham, Herschel-Bulkley and (generalised) Casson fluids. The slope of each graph can be interpreted as a measure for the effective viscosity.

1.8 Bingham Fluids First attempts to develop formal mathematical models for viscoplastic fluids date back to the first half of the 19$^{\text{th}}$ century. Bingham published his viscoplastic model in 1917 [11] and subsequently investigated its applicability to paints in experimental studies [12]. Bingham fluids are determined by two parameters: the yield stress $\tau_0 \geq 0$, and a so-called plastic viscosity $\mu > 0$, which for the yielded fluid plays a comparable role to the viscosity of a Newtonian fluid. Measuring the stress magnitude $|\tau| = \sqrt{\operatorname{tr}(\tau\tau^\top)}$ by means of the Frobenius norm, and analogously for the strain rate, Bingham prescribes

$$\begin{cases} |\tau| \leq \tau_0 & \text{if } \dot\gamma = 0 \\ \tau = 2\mu\dot\gamma + \tau_0 \dfrac{\dot\gamma}{|\dot\gamma|} & \text{if } \dot\gamma \neq 0. \end{cases} \tag{1.3b}$$

Newtonian fluids are included in this model as a special case, which is recovered by choosing the yield stress $\tau_0 = 0$. Hence, Bingham fluids can be considered as an immediate viscoplastic generalisation of a Newtonian fluid.

Despite the simplicity of the model, a large number of real fluids exhibit Bingham behaviour. Tomato sauce (ketchup) and mayonnaise belong to the most prominent representatives [13].

1.9 Herschel-Bulkley Fluids A few years later, in 1926, Herschel and Bulkley published an extension to the Bingham model [14]. Their experiments with capillary

flows of rubber-benzene solutions showed the flow characteristics of such polymer fluids are more accurately reproduced by a power-law model for the plastic viscosity. This way, they are able to incorporate phenomena such as thickening or thinning under shear into the viscoplastic constitutive relation. With a third parameter $r > 1$, the Herschel-Bulkley model reads

$$\begin{cases} |\tau| \leq \tau_0 & \text{if } \dot{\gamma} = 0 \\ \tau = 2^{r-1}\kappa|\dot{\gamma}|^{r-2}\dot{\gamma} + \tau_0 \dfrac{\dot{\gamma}}{|\dot{\gamma}|} & \text{if } \dot{\gamma} \neq 0. \end{cases} \tag{1.3c}$$

The constant κ is referred to as the fluid consistency. Clearly, by setting $r = 2$ and $\kappa = \mu$, the Herschel-Bulkley model reduces to the Bingham model. As can be seen from Figure 1.2(a) on the preceding page, $1 < r < 2$ corresponds to a shear-thinning behaviour, i.e. the effective viscosity decreases as the strain rate magnitude increases, while $r > 2$ yields shear-thickening behaviour. In the latter case, however, the power-law gives rise to an unphysical singularity at the yield limit, according to which the apparent viscosity jumps from infinity under the plastic regime, to zero straight after yielding. Therefore, the Herschel-Bulkley relations in their elementary form are rather unsuitable for modelling the yielding and unyielding of real shear-thickening fluids. This drawback could be addressed by introducing a regularisation parameter $\varepsilon > 0$, such that the effective plastic viscosity for the yielded fluid is increased in a fashion like $\mu_{\text{eff}}(|\dot{\gamma}|) = \kappa(\varepsilon^2 + (2|\dot{\gamma}|)^2)^{(r-2)/2}$ for instance [15]. However, we will not consider shear-thickening Herschel-Bulkley fluids or modified versions thereof any further.

Due to its flexibility, the Herschel-Bulkley model enjoys great popularity in a diverse range of different industries. Besides further applications in food processing [16], the scope of Herschel-Bulkley fluids comprises fresh concrete [17] in civil engineering, muds and slurries [18] arising in mining and drilling operations, waxy crude oils [19] in petrochemistry as well as lava [20], lahars [21] and soil liquefaction [22] in the geophysical sciences.

1.10 Casson Fluids An alternative generalisation of Newtonian fluids was introduced in 1959 by Casson [28]. While he initially devised a model for inks, consisting of colour pigments suspended in oil, it has found greater usage in hemodyamics as a model for blood over various intervals of shear rates [24], [29], as well as in food processing [30, p 31]. In contrast to all other models outlined here, which merely provide a fit to macroscopic phenomena, the Casson model is derived from actual physical properties, lying in the microscopic structure of a class of colloidal suspensions.

Casson fluids unite the benefits of only two parameters, as for the Bingham model, with the higher regularity at the yield limit of shear-thinning Herschel-Bulkley fluids, cf Figure 1.2. While the effective viscosity of Casson fluids approaches a positive constant

(a): Mucus [23]. *Photo: FreeImages.com / Guillaume Riesen*

(b): Blood [24]. *Photo: FreeImages.com / Marzena Osuchowicz*

(c): Glacier [25]. *Photo: FreeImages.com / Matt Hall*

(d): Lava [20]. *Photo: FreeImages.com / Jesse Adams*

(e): Tomato sauce and mayonnaise [26]. *Photo: FreeImages.com / Duygu Agar*

(f): Paint [27]. *Photo: FreeImages.com / Odan Jaeger*

Figure 1.3: Common examples for fluids with viscoplastic properties. Note the structures in the surface of many of these fluids, which do not completely fade as they would for fluids with zero yield stress.

as $|\dot\gamma| \to \infty$, shear-thinning Herschel-Bulkley fluids tend towards inviscid behaviour in this limiting case. With the same notational conventions as for the Bingham model, Casson fluids are defined through the constitutive system

$$\begin{cases} |\tau| \leq \tau_0 & \text{if } \dot\gamma = 0 \\ \tau = \left(\sqrt{2\mu|\dot\gamma|} + \sqrt{\tau_0}\right)^2 \dfrac{\dot\gamma}{|\dot\gamma|} & \text{if } \dot\gamma \neq 0. \end{cases} \tag{1.3d}$$

As will be shown later, Casson flow problems are amenable to a formulation in Hilbert spaces. Not only will this simplify the analysis of such problems compared to the treatment of Herschel-Bulkley flow in Banach spaces. It also implies that numerical solutions are about as cheaply to obtain as for Bingham fluids.

1.11 Casson-Heinz Fluids Only shortly after Casson's initial publication, Heinz found that a modified model with squared cubic roots instead of square roots provides a higher goodness of fit to experimental stress-strain curves of some fluids [31]. The obvious generalisation of Casson fluids, referred to as Casson-Heinz or generalised Casson fluids

$$\begin{cases} |\tau| \leq \tau_0 & \text{if } \dot\gamma = 0 \\ \tau = \left((2\mu|\dot\gamma|)^{s-1} + \tau_0^{s-1}\right)^{1/(s-1)} \dfrac{\dot\gamma}{|\dot\gamma|} & \text{if } \dot\gamma \neq 0, \end{cases} \tag{1.3e}$$

once more includes the Bingham model if the exponent $s > 1$ is set to $s = 2$. Shear-thickening Casson-Heinz fluids suffer from the same disadvantages as shear-thickening Herschel-Bulkley fluids. In the shear-thinning setting, however, the remarks on the analytical and numerical simplicity of the Casson model remain valid even for other choices $1 < s < 2$ than $s = 3/2$.

The model could establish itself primarily for specific foods, in particular as a standard model for milk chocolate [32, p 597] or juice concentrate [33]. Further applications exist [34], but are rare in nature.

1.12 Conclusions Naturally, it would be an endless endeavour, trying to provide an extensive list including even the most exotic model ever proposed with viscoplastic features. The subject-specific literature on food physics [35] or biomechanics [36] provides references for further reading.

It is however interesting to note, that all of the aforementioned models can be unified in a very general flow rule. In 1969, East German scientists Reher, Haroske and Kohler

[37] observed that the model

$$\begin{cases} |\tau| \leq \tau_0 & \text{if } \dot\gamma = 0 \\ \tau = \left((2\kappa|\dot\gamma|)^{r-1} + \tau_0^{s-1}\right)^{1/(s-1)} \dfrac{\dot\gamma}{|\dot\gamma|} & \text{if } \dot\gamma \neq 0. \end{cases} \tag{1.3f}$$

comprises both Herschel-Bulkley fluids (for $s = 2$) and Casson-Heinz fluids (for $r = s$). On the opposite side of the iron curtain, Ofoli, Morgan and Steffe [38] published the same discovery in 1987.

Typical viscoplastic fluids tend to exhibit a rather large plastic viscosity. In contrast, important viscous liquids, such as water and even more so air, are nearly inviscid. They therefore give rise to a singularly perturbed system of equations. This is not the case in viscoplasticity. Here, the mathematical challenges are of different nature: besides additional nonlinear terms originating from the various models for the strain-dependence of the effective viscosity, transitions between the two states of matter result in nonsmooth behaviour.

Viscoplasticity and Convex Optimisation

In our summary on the three main characteristics of viscoplastic fluids on page 4, we observed that the yield stress parameter τ_0 steers a decomposition of the flow domain into sets where the strain rate $\dot\gamma = \mathcal{D}u$ is constantly zero, and sets where it does not vanish. Readers, who are familiar with optimisation or inverse problems including an L^1-type regularisation, will recognise that this type of sparsity is a common feature in all of these settings. Hence, it comes at no more great surprise that there are indeed very tight links between such nonsmooth optimisation problems and flow problems in viscoplasticity. We delay the mathematical derivation to the second part of this thesis, but a summary of the main results shall provide a few insights at this point.

1.13 Convex Optimisation for Image Reconstruction

In the context of astronomical, medical or microscopic imaging, one is often confronted with the challenge to denoise or deblur an imperfect image. One of the most important approaches to this problem stems from convex optimisation. In order to recover a close approximation to the original, undisturbed image x, one tries to minimise a data fidelity functional F and adds a regularisation term R with weighting factor $\alpha \geq 0$:

$$\min_x F(x) + \alpha R(x). \tag{1.4}$$

A least-squares model with a suitable norm $\|\cdot\|$ offers a typical choice for measuring proximity to data,

$$F(x) = \frac{1}{2}\|\mathcal{A}x - b\|^2, \tag{1.5}$$

where b is the imperfect image and the linear operator $\mathcal{A}$ models the introduction of noise or blurring. Since such operators tend to be nearly singular, the unregularised inverse problem with $\alpha = 0$ would be highly ill-conditioned. Adding a suitable regularisation functional R becomes inevitable.

The quadratic TIKHONOV regularisation [39], which penalises large gradients of pixel values

$$R(x) = \frac{1}{2}\|\nabla x\|^2 \tag{1.6a}$$

goes hand in hand with the often undesirable side-effect of smoothing out sharp features of the image [40, p 98]. L^1-based regularisation functionals provide a remedy and preserve borders between objects or sharp contours, at the expense of rendering the problem nonsmooth. If x is a representation of the image in a FOURIER, or better, wavelet space, then

$$R(x) = \|x\| \tag{1.6b}$$

can yield competitive results [41], [42]. The corresponding equivalent of (1.6a), commonly known as TV (total variation) or ROF (RUDIN-OSHER-FATEMI) regularisation [43]

$$R(x) = \|\nabla x\| \tag{1.6c}$$

nowadays constitutes a standard approach to image denoising and deblurring. Instead of enforcing sparsity in the frequency or wavelet domain, (1.6c) gives rise to regions of constant colour. It can be shown [44] that this penalisation is exact: for the optimal solution $\bar{x}$ of (1.4), $R(\bar{x})$ monotonically decreases as the penalty parameter α increases, and there exists a finite $\alpha_0 > 0$ such that for all $\alpha \geq \alpha_0$ the optimal solution is a trivial, homogeneously coloured image, i.e. $R(\bar{x}) = 0$.

1.14 Links between Image Processing and Viscoplasticity Let us foreshadow at this stage that viscoplastic flow problems can be cast in a form very closely related to total variation image deblurring. With a convex functional F that depends on the constitutive law, we are confronted with optimisation problems of the type

$$\min_u F(u) + \tau_0\|\mathcal{D}u\|, \tag{1.7}$$

where u belongs to a closed convex set, imposing boundary conditions and possibly further constraints within an appropriate function space. The yield stress τ_0 now assumes

the role of the penalty parameter and the symmetric gradient operator $\mathcal{D}$ replaces the gradient ∇ of pixel values. This quasi-TV penalisation maintains the property of an exact penalty, which provides the mathematical explanation for the viscoplastic phenomena associated to the cessation of shear flow.

Historically, a number of numerical methods for image processing have originated in nonsmooth mechanical applications. This includes in particular methods from the framework of augmented Lagrangians [45]. In the early 2000's, Ngwa, Frigaard and Scherzer also developed Bingham [46] and Herschel-Bulkley diffusion filters for image denoising applications [47].

For the past few years and continuing to the current day, innovative algorithms for convex programming in the image processing context [48], [49] have triggered a flood of publications on more efficient approaches in this field. With this thesis, we will conversely investigate, which of these new ideas we can adapt to viscoplastic applications. Our work is motivated by the fact, that as of today, state-of-the-art methods for solving viscoplastic flow problems are still far from achieving a performance even close to computational fluid dynamics for Newtonian fluids. Three-dimensional simulations are still considered largely infeasible in viscoplasticity.

This thesis is subdivided into two parts: first, we consider convex optimisation problems of relatively generic structure, but with viscoplastic applications in mind. We address questions ranging from the well-posedness of these problems to existence and uniqueness of solutions. By taking inspiration from the latest advances in image processing, we design numerical methods, study their convergence properties and discuss further details on their computational implementation.

In the second part, we will apply these algorithms to a range of different viscoplastic flow problems. Our objective here is threefold: besides (i) verifying the theoretical results from the first part, we also (ii) assess how well each method reflects the viscoplastic characteristics of the problem. By (iii) comparing the computational performances for a variety of different options and problem sets, we shall be in the position to draw first conclusions regarding which methods should be preferred over others.

PART I

Numerical Methods for Convex Optimisation

Chapter 2

State of the Art

Due to their numerous applications in mechanics [50], signal [51] and image processing [52], mathematical finance [53], statistics [54], machine learning [55] and many other fields, convex optimisation problems have been studied intensively over the past decades. Of the vast material that is available on this topic, this chapter shall provide an overview of that research, which is most relevant to the problems considered in this thesis.

Before discussing the various algorithmic approaches to convex programming problems in Section (D), it is expedient to review important definitions, central theorems and notational conventions in Sections (A) to (C).

(A) Fundamentals of Convex Analysis

Notions of Convexity

2.1 Definition (Convex Functionals) Let $(U, \|\cdot\|_U)$ be a normed linear space and $f : U \to]-\infty, +\infty]$ an extended real-valued functional on U. f is called

(a) *convex*, if for all $u_1, u_2 \in U$ and all $t \in]0, 1[$

$$f\left((1-t)u_1 + tu_2\right) \leq (1-t)f(u_1) + tf(u_2).$$

(b) *strictly convex*, if for all $u_1, u_2 \in U$ and all $t \in]0, 1[$

$$f\left((1-t)u_1 + tu_2\right) < (1-t)f(u_1) + tf(u_2)$$

whenever $u_1 \neq u_2$ and $f(u_1), f(u_2) < +\infty$.

(c) *strongly convex*, if there exists a strong convexity parameter $\sigma > 0$, such that for

all $u_1, u_2 \in U$ and all $t \in]0,1[$

$$f\left((1-t)u_1 + tu_2\right) \leq (1-t)f(u_1) + tf(u_2) - \frac{\sigma}{2}t(1-t)\|u_1 - u_2\|_U^2.$$

In this case, we also say that f is σ-strongly convex.

The implications

$$\text{strongly convex} \implies \text{strictly convex} \implies \text{convex}$$

are clear by definition.

In geometric terms, these different types of convexity can be illustrated as follows: the graph of a convex functional, restricted to the straight line segment between any two points u_1 and u_2, lies on or below the secant connecting the points $(u_1, f(u_1))$ and $(u_2, f(u_2))$. In the strictly convex case, the secant must run strictly above the function's graph. The graph of a strongly convex function lies not only below the straight secant line, but even below a parabola with positive curvature. Here, it is crucial that $\sigma > 0$ is a global parameter, independent of the choice of the points u_1 and u_2. For the examples in Figures 2.1(b) and 2.1(c) on the next page, no such positive parameter can be found.

A simple calculation proves the following, alternative definition of strong convexity:

2.2 Lemma (Characterisation of Strong Convexity) *Let H be a real* Hilbert *space, $f : H \to]-\infty, +\infty]$ and $m : H \to \mathbb{R}, x \mapsto \frac{1}{2}\|x\|_H^2$. Then f is σ-strongly convex if and only if $f - \sigma m$ is convex.*

Properties of Convex Functions

2.3 Definition (Level Sets) Let $f : U \to]-\infty, +\infty]$.

(a) The set

$$\operatorname{dom} f := \{\, u \in U \mid f(u) < \infty \,\}$$

is called the *(effective) domain* of f. If $\operatorname{dom} f \neq \emptyset$, f is called *proper*.

(b) The *level set* of f at height $\phi \in \mathbb{R}$ is given by

$$\operatorname{level}_\phi f := \{\, u \in U \mid f(u) \leq \phi \,\}.$$

2.4 Definition (Coercivity of Convex Functionals) Let $f : U \to]-\infty, +\infty]$ be a convex functional on a normed space $(U, \|\cdot\|_U)$. f is called *coercive*, if

$$f(u) \to +\infty \qquad \text{as } \|u\|_U \to \infty.$$

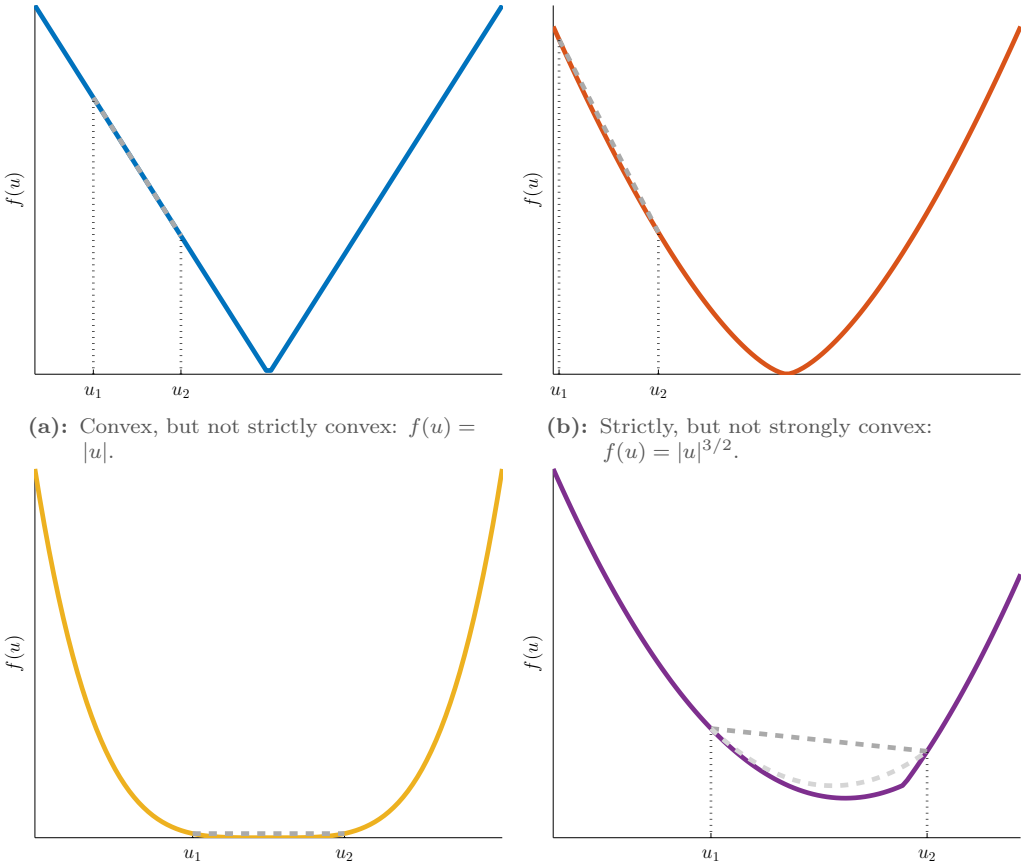

(a): Convex, but not strictly convex: $f(u) = |u|$.

(b): Strictly, but not strongly convex: $f(u) = |u|^{3/2}$.

(c): Strictly, but not strongly convex: $f(u) = |u|^4$.

(d): Strongly convex with parameter $\sigma = 2$: $f(u) = |u|^2 + |u-1|$.

Figure 2.1: Examples for convex, strictly convex and strongly convex functions. The grey dashed lines depict the graphs of an affine or parabolic majorant, as defined by the right-hand sides of the inequalities in Definition 2.1 on page 17.

Coercivity ensures that all level sets at finite heights are bounded. This property is crucial for proving the existence of minimisers of a convex functional with an unbounded domain. In particular, strong convexity or a bounded domain are sufficient conditions for coercivity.

Even if a proper and convex functional is coercive, there is still no guarantee that the functional attains its infimum. To rule out such cases as depicted in Figure 2.2(a) on the following page, an additional assumption on continuity in a relaxed sense is indispensable.

2.5 Definition (Lower Semicontinuity) A functional $f : U \to]-\infty, +\infty]$ on a Banach space U is called *(sequentially) lower semicontinuous* if for any $u \in U$ and all sequences

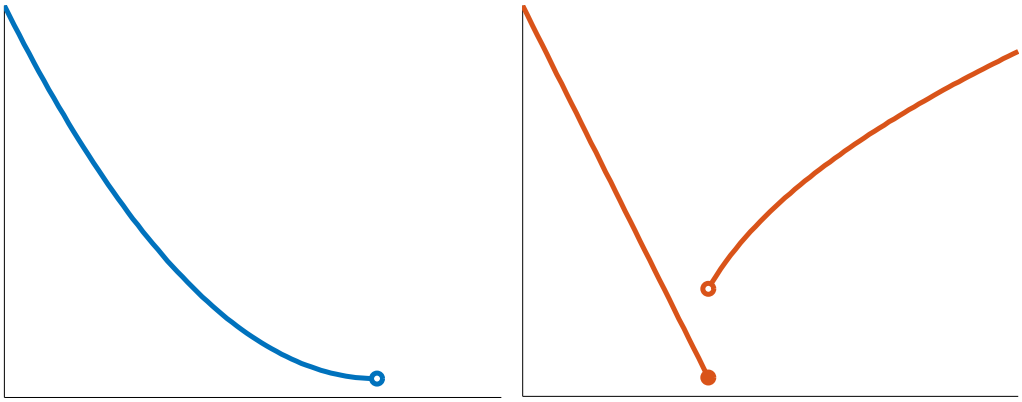

(a): Not lower semicontinuous. **(b):** Lower semicontinuous.

Figure 2.2: Lower semicontinuity for functions over the real line. The function in the left example does not assume its infimum, while the (non-convex) function on the right does.

$(u_k)_k \subset U$ with $u_k \to u$

$$\liminf_{k\to\infty} f(u_k) \geq f(u).$$

f is called *weakly (sequentially) lower semicontinuous* if this inequality even holds for all weakly convergent sequences with $u_k \rightharpoonup u$.

Clearly, all (weakly) sequentially continuous functions are also (weakly) lower semicontinuous. Also, if $C \subset U$ is a (weakly) sequentially closed convex set, then its indicator function ι_C, defined by

$$\iota_C(u) = \begin{cases} 0 & \text{if } u \in C \\ +\infty & \text{if } u \notin C, \end{cases}$$

is (weakly) lower semicontinuous. For this example, like for all convex functions, lower semicontinuity is already sufficient to guarantee weak lower semicontinuity, as stated by the following theorem.

2.6 Theorem (Lower Semicontinuity of Convex Functionals) *Let $f : U \to]-\infty, +\infty]$ be a convex functional over the* Banach *space U. The following statements are equivalent:*

(a) f is lower semicontinuous.

(b) f is weakly lower semicontinuous.

(c) For any $\phi \in \mathbb{R}$, $\operatorname{level}_\phi f$ is sequentially closed.

(d) For any $\phi \in \mathbb{R}$, $\operatorname{level}_\phi f$ is weakly sequentially closed.

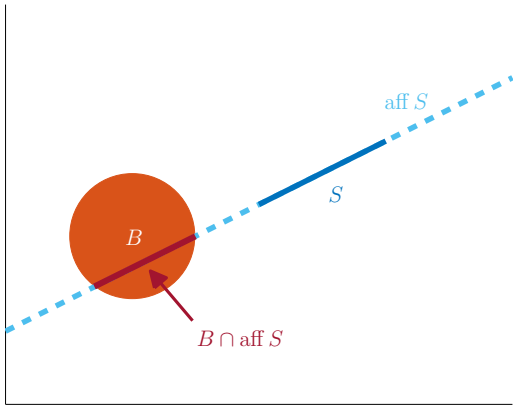

Figure 2.3: Construction of a topology for defining the relative interior of the one-dimensional set $S \subset \mathbb{R}^2$. B is an open set in the topology of $\mathbb{R}^2$. Its one-dimensional trace $B \cap \text{aff } S$ defines the corresponding open set in the relative topology on the affine hull of S.

Proof. We refer to Theorem 9.1 in [56, p 128]. □

Often, the topological notion of the interior of a set is of little use in convex analysis: when working with constraints to sets that are of lower dimension than U, their interior could become trivial in the topology of the whole space. As an example, one might take the unit disc in $\mathbb{R}^2$, which, considered as a subset of $\mathbb{R}^3$, has an empty interior. For such cases, it is more meaningful to define a natural interior by means of a suitable trace topology. This idea is formalised in the definition of the *relative* interior.

2.7 Definition (Relative Interior) (a) The *affine hull* of a set $S \subset U$, denoted by aff S, is the smallest affine subspace of U containing S.

(b) The *relative interior* of the set S is given by its interior in the relative topology of aff S.

Figure 2.3 provides an illustration of this concept. For further details, we refer to the literature on convex analysis [57].

(B) Operators on Function Spaces

Linear Operators on Normed Spaces

2.8 Definition (Bounded Linear Operators) Let $(U, \|\cdot\|_U)$ and $(V, \|\cdot\|_V)$ be two normed vector spaces. A linear operator $\mathcal{A} : U \to V$ is called

(a) *bounded*, if there exists a constant $C \in [0, +\infty[$ such that for all $u \in U$

$$\|\mathcal{A}u\|_V \leq C\|u\|_U.$$

(b) *bounded below*, if there exists a constant $c \in]0, +\infty[$ such that for all $u \in U$

$$\|\mathcal{A}u\|_V \geq c\|u\|_U.$$

It is well-known [58, p 91] that boundedness and continuity are equivalent for linear operators.

For the space of linear bounded operators between U and V we write $L(U, V)$. A norm on this space can be defined by

$$\|\mathcal{A}\|_{L(U,V)} := \sup_{\|u\|_U=1} \|\mathcal{A}u\|_V.$$

2.9 Theorem (Completeness of $L(U, V)$) *If V is complete, then $L(U, V)$ is a* Banach *space as well.*

Proof. See [58, p 104]. □

The special case $V = \mathbb{R}$ leads to a very important instance of such a complete space of operators:

2.10 Definition (Dual Space) The bounded linear functionals on a real normed vector space U constitute its *(topological) dual space* $U^* := L(U, \mathbb{R})$.

2.11 Definition (Duality Pairing) Let U be a Banach space. For elements $u \in U$ and $u^* \in U^*$, we normally use the notation $\langle u^*, u\rangle_{U^*,U} := u^*(u)$.

2.12 Definition (Adjoint Operator) Let U and V be two Banach spaces and $\mathcal{A} \in L(U, V)$. The operator $\mathcal{A}^* \in L(V^*, U^*)$, defined by

$$\langle \mathcal{A}^* v^*, u\rangle_{U^*,U} = \langle v^*, \mathcal{A}u\rangle_{V^*,V} \qquad \forall u \in U, \quad \forall v^* \in V^*$$

is called the *adjoint* of $\mathcal{A}$.

The operator $\mathcal{A}^*$ is well-defined and $\|\mathcal{A}^*\|_{L(V^*,U^*)} = \|\mathcal{A}\|_{L(U,V)}$; we refer to [58, pp 151-152] for a proof.

We recall that a BANACH space U can generally be embedded into its bi-dual space U^{**} through the linear isometry [58, p 145] $u \mapsto u^{**}$, where $u^{**} \in L(U^*, \mathbb{R})$ is defined pointwise by

$$\langle u^{**}, u^* \rangle_{U^{**},U^*} := \langle u^*, u \rangle_{U^*,U}, \qquad \forall u^* \in U^*. \tag{2.1}$$

2.13 Definition (Reflexive BANACH Space) If this embedding $U \hookrightarrow U^{**}$ is onto, we call the BANACH space U *reflexive*. That is, every element of U^{**} can be represented by a corresponding element of U such that (2.1) holds.

All HILBERT spaces are reflexive. This is one important conclusion from the following theorem and corollary, proofs for which may be found in [58, pp 123-124].

2.14 Theorem (RIESZ Representation Theorem) *Let H be a real* HILBERT *space with respect to the inner product $\langle \cdot, \cdot \rangle_H$. For any $x^* \in H^*$, there exists a unique $x \in H$ such that $\|x\|_H = \|x^*\|_{H^*}$ and $x^* = \langle x, \cdot \rangle_H$.*

2.15 Corollary (RIESZ Isomorphism) *The mapping $\mathcal{J}_H : H \cong H^*, x \mapsto x^* := \langle x, \cdot \rangle_H$ is an isometric isomorphism, referred to as the* RIESZ isomorphism. *We may therefore identify every functional $x^* \in H^*$ with its* RIESZ representative $x := \mathcal{J}_H^{-1} x^* \in H$, *where $\mathcal{J}_H^{-1} = \mathcal{J}_{H^*}$.*

For an operator $\mathcal{A} \in L(K, H)$ between two HILBERT spaces H and K, the RIESZ Theorem allows us to identify its adjoint $\mathcal{A}^* \in L(H^*, K^*)$ with the operator $\mathcal{A}' := \mathcal{J}_K^{-1} \mathcal{A}^* \mathcal{J}_H \in L(H, K)$. $\mathcal{A}'$ is often called the *dual* or *conjugate* of $\mathcal{A}$ in the literature, but sometimes [58, pp 151 & 168] naming conventions are exactly opposite as in this thesis.

In finite dimensions, typically no explicit distinction between $\mathcal{A}^*$ and $\mathcal{A}'$ is made at all. In function spaces, it is not normally desirable to identify both K^* and H^* with K and H, respectively. This also applies to the applications covered in this work, where abstract RIESZ representatives of the bounded linear functionals on K would have little meaning in practice. Therefore, no more dual operators will occur in the remainder of this thesis.

To simplify our presentation in the following, we may hide the RIESZ isomorphism $\mathcal{J}_H$ in our notation, whenever we identify the dual of H with H itself. For example, instead of $\mathcal{A}^* \mathcal{J}_H \mathcal{A}$, we simply write $\mathcal{A}^* \mathcal{A}$.

Differentiability in BANACH Spaces

We will now move on from linear functional analysis and focus on nonlinear operators $F : D \to V$ between BANACH spaces $(U, \|\cdot\|_U)$ and $(V, \|\cdot\|_V)$, where F is defined on a non-empty, open set $D \subset U$. We briefly review the different notions of differentiability, many of which collapse if U is finite-dimensional.

2.16 Definition (Directional Differentiability) Let $u \in D$ and $h \in U$. If the limit

$$\lim_{t \to 0} \frac{F(u+th) - F(u)}{t} =: F'(u)h$$

exists in V, then we call F *directionally differentiable* at u in direction h and $F'(u)h$ the corresponding *directional derivative* of F at u.

2.17 Definition (Gâteaux Differentiability) If $F : U \to V$ is directionally differentiable at $u \in D$ in all directions $h \in U$ and $F'(u) \in L(U, V)$, then we call F Gâteaux *differentiable* at u and $F'(u)$ the Gâteaux *derivative* of F at u.

2.18 Definition (Fréchet Differentiability) If, for $u \in D$, there exists $F'(u) \in L(U, V)$ such that

$$\lim_{h \to 0} \frac{\|F(u+h) - F(u) - F'(u)h\|_V}{\|h\|_U} = 0,$$

then we call F Fréchet *differentiable* at u and $F'(u)$ the Fréchet *derivative* of F at u.

It is easy to verify the implications

Fréchet differentiable $\implies$ Gâteaux differentiable $\implies$ directionally differentiable

with the same $F'(u)$ in each case.

If U is a Hilbert space and $V = \mathbb{R}$, we also use the notation $\nabla F(u) := \mathcal{J}_U^{-1} F'(u)$ for the Riesz representative of the Fréchet derivative and call ∇F the *gradient* of F.

In the context of Newton methods, a weaker notion of differentiability than the Fréchet derivative is appropriate:

2.19 Definition (Newton Differentiability) If, for $u \in D$, there exists a family $\mathcal{S} : D \rightrightarrows L(U, V)$ such that for any *slanting function* $DF \in \mathcal{S}$

$$\lim_{h \to 0} \frac{\|F(u+h) - F(u) - DF(u+h)h\|_V}{\|h\|_U} = 0,$$

then we call F *semismooth, slantly* or Newton *differentiable* at u and $DF(u)$ a *slant* or Newton *derivative* of F at u.

In contrast to the definition of the Fréchet derivative, the operator DF is evaluated at the point $u + h \in D$ rather than $u \in D$ itself. Though seemingly minor, this modification has far-reaching consequences as it gives rise to a generalisation of the Fréchet derivative:

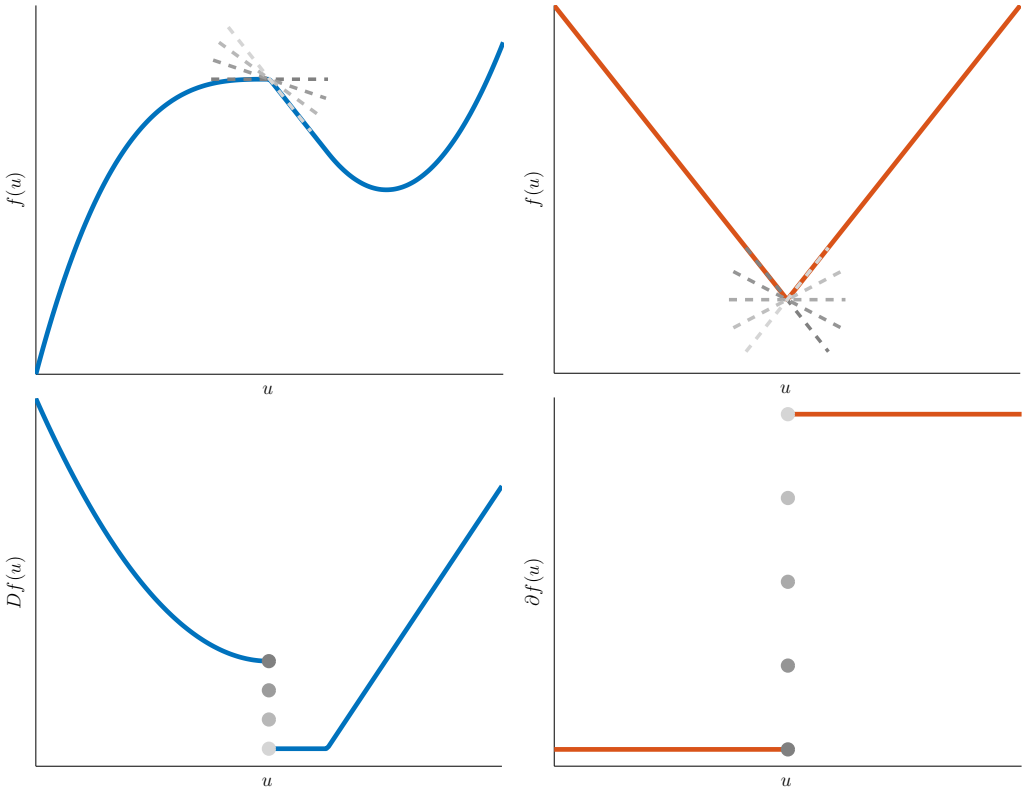

(a): A NEWTON differentiable function (top) with some NEWTON derivatives (bottom).

(b): A convex function (top) with some subderivatives (bottom).

Figure 2.4: NEWTON differentiability and subdifferentiability for functions on $\mathbb{R}$. The grey slopes and dots correspond to different NEWTON respectively subderivatives, where they are non-unique.

- Indeed, if F is FRÉCHET differentiable at u, then F' already acts as a slanting function at that point.
- If F is not FRÉCHET differentiable at u, then F might still be NEWTON differentiable at u. The point u is effectively removed from the set of arguments of DF, for which the limit in Definition 2.19 has to exist and vanish. Instead, it is already sufficient if F is FRÉCHET differentiable in an arbitrarily small environment around u, excluding u itself.

These observations can also be made from the example sketched in Figure 2.4(a).

2.20 Theorem (Characterisation of NEWTON Differentiability) *The function $F : D \to V$ is* NEWTON *differentiable, if and only if it is* LIPSCHITZ *continuous, i.e. there exists a*

Lipschitz *constant* $L \geq 0$ *such that*

$$\|F(u_1) - F(u_2)\|_V \leq L\|u_1 - u_2\|_U, \qquad \forall u_1, u_2 \in D.$$

Proof. See Theorem 2.6 in [59]. □

Convex functionals mapping U to $V = \mathbb{R}$ or $V =]-\infty, +\infty]$ facilitate a further concept of differentiability, which plays a pivotal role in optimisation:

2.21 Definition (Subdifferential) Let U be a Banach space, $f : U \to]-\infty, +\infty]$ proper, convex and $\bar{u} \in \operatorname{dom} f$. The *subdifferential* $\partial f(\bar{u})$ of f at $\bar{u}$ is defined as the set of all $u^* \in U^*$ such that

$$f(u) - f(\bar{u}) \geq \langle u^*, u - \bar{u}\rangle_{U^*,U}, \qquad \forall u \in U.$$

We refer to an element $u^* \in \partial f(\bar{u})$ as a *subderivative* (and its Riesz representative in a Hilbert space as a *subgradient*) of f at $\bar{u}$.

To illustrate this definition, Figure 2.4(b) on the previous page depicts a non-differentiable convex function with some of its subderivatives.

There are tight links between subdifferentiability and the other notions of differentiability introduced previously.

The striking similarity of the two examples depicted in Figure 2.4 on the preceding page might have already suggested that the subderivatives in Figure 2.4(b) concurrently qualify as Newton derivatives. Indeed, in the finite-dimensional setting, the definition of a subdifferential can extended beyond the class of convex functions. For a convex function, this Clarke subdifferential agrees with the subdifferential [60, p 289], and any element of the Clarke subdifferential is also a Newton derivative [61].

Furthermore, the Gâteaux derivative and subdifferential are equivalent in the following sense:

2.22 Proposition (Subdifferentiability and Gâteaux Differentiability) *Let* $f : U \to]-\infty, +\infty]$ *be proper and convex and let* $u \in \operatorname{dom} f$.

(a) If f *is* Gâteaux *differentiable at* u*, then* f *is also subdifferentiable at* u *with the singleton subdifferential* $\partial f(u) = \{f'(u)\}$.

(b) If f *is continuous and subdifferentiable at* u *with singleton subdifferential, then* f *is also* Gâteaux *differentiable at* u *with* $f'(u) \in \partial f(u)$.

Proof. See [62, pp 23-24]. □

2.23 Proposition (Properties of the Subdifferential) *Let $f : U \to]-\infty, +\infty]$ be proper, convex and lower semicontinuous. Then $\partial f(u)$ is closed and convex for all $u \in \operatorname{dom} f$ as well as non-empty for almost all $u \in \operatorname{dom} f$. Also, if f is continuous at $u \in \operatorname{dom} f$, then $\partial f(u) \neq \emptyset$.*

Proof. See [62, pp 21-22 & 32]. □

2.24 Lemma (Subdifferential Calculus) *For the subdifferentials of proper and convex functionals $f, g : U \to]-\infty, +\infty]$ we have the following rules:*

(Subadditivity)

$$\partial(f+g)(u) \supset \partial f(u) + \partial g(u), \qquad \forall u \in \operatorname{dom} f \cap \operatorname{dom} g$$

(Additivity) *If f is continuous in at least one point of $\operatorname{dom} f \cap \operatorname{dom} g$, then*

$$\partial(f+g)(u) = \partial f(u) + \partial g(u), \qquad \forall u \in \operatorname{dom} f \cap \operatorname{dom} g$$

(Positive Homogeneity) *For any $t > 0$,*

$$\partial(tf)(u) = t\partial f(u), \qquad \forall u \in \operatorname{dom} f$$

(Chain Rule for Translations) *For any $\bar{u} \in U$*

$$\partial f(\cdot - \bar{u})(u) = \partial f(u - \bar{u}), \qquad \forall u \in \bar{u} + \operatorname{dom} f$$

(Chain Rule for Bounded Linear Operators) *Let X be a* Banach *space and $\mathcal{A} \in L(X, U)$. If f is continuous in at least one point of the range of $\mathcal{A}$, then*

$$\partial(f \circ \mathcal{A})(x) = \mathcal{A}^* \partial f(\mathcal{A}x), \qquad \forall x \in \operatorname{dom} f \circ \mathcal{A}$$

Proof. Subadditivity and positive homogeneity are clear by definition. For the proofs of additivity and the chain rule for bounded linear operators, we refer to [62, pp 26-27]; the chain rule for translations is proved in [63, p 33]. □

For smooth optimisation problems, the derivative of the objective is stationary at a local minimum. The following theorem points out how the subdifferential provides a natural extension of such an optimality condition to nonsmooth, convex optimisation problems.

2.25 Theorem (Optimality Conditions) *Let U be a* Banach *space, $f : U \to]-\infty, +\infty]$ be a proper and convex functional and $\bar{u} \in \operatorname{dom} f$. Then*

$$\bar{u} \in \operatorname*{arg\,min}_{u \in U} f(u) \quad \Longleftrightarrow \quad 0 \in \partial f(\bar{u}) \quad \Longleftrightarrow \quad \forall u \in U : \quad f(u) - f(\bar{u}) \geq 0 \tag{2.2}$$

Furthermore, if there exist convex functionals f_1 and f_2, with f_2 being Gâteaux *differentiable on $\operatorname{dom} f$, such that $f = f_1 + f_2$, then*

$$\begin{aligned} \bar{u} \in \operatorname*{arg\,min}_{u \in U} f(u) \quad &\Longleftrightarrow \quad -f_2'(\bar{u}) \in \partial f_1(\bar{u}) \\ &\Longleftrightarrow \quad \forall u \in U : \quad f_1(u) - f_1(\bar{u}) + \langle f_2'(\bar{u}), u - \bar{u} \rangle_{U^*,U} \geq 0 \end{aligned} \tag{2.3}$$

Proof. The equivalences in (2.2) are clear by definition. For the more general composite case (2.3), the characterisations of optimality follow from straightforward calculations, cf [62, p 38]. □

2.26 Theorem (Existence and Uniqueness of Minimisers) *Let $f : U \to]-\infty, +\infty]$ be a proper, convex and lower semicontinuous functional over a reflexive* Banach *space U. Furthermore, let f be coercive. Then there exists $\bar{u} \in U$ such that*

$$f(\bar{u}) = \inf_{u \in U} f(u) \in]-\infty, +\infty[\,.$$

If f is strictly convex, then $\bar{u}$ is unique.

Proof. The techniques used for this proof are standard in nonlinear optimisation. One considers a minimising sequence for f and concludes from coercivity that it must be bounded. Since U is reflexive, the theorems of Banach-Alaoglu and Eberlein–Šmulian imply that the bounded sequence possesses a weakly convergent subsequence (cf [64, p 251]). The (weak) lower semicontinuity of f finally allows us to verify that the weak limit is already a point $\bar{u} \in U$ that minimises f.

For a complete presentation of this proof, we refer to [62, p 35]. □

Subderivatives for general convex functionals define a linear minorant of that functional, which can be interpreted as a generalisation of the tangent plane of a smooth function (cf the grey dashed line segments in Figure 2.4(b) on page 25). Under the assumption of strong convexity, the following lemma yields a quadratic minorant. It will play a central role in our analysis of the convergence of numerical algorithms.

2.27 Lemma (Subdifferential of Strongly Convex Functionals) *If $f : H \to]-\infty, +\infty]$ is proper σ-strongly convex on a real* Hilbert *space $(H, \langle \cdot, \cdot \rangle_H)$, then we have for any*

$\bar{x} \in \operatorname{dom} f$

$$f(x) - f(\bar{x}) \geq \langle x^*, x - \bar{x} \rangle_H + \frac{\sigma}{2}\|x - \bar{x}\|_H^2, \qquad \forall x \in H \quad \forall x^* \in \partial f(\bar{x}).$$

Proof. We can apply the characterisation of strong convexity in Hilbert spaces from Lemma 2.2 on page 18: there exists a proper convex $\tilde{f} : H \to]-\infty, +\infty]$ such that $f(x) = \tilde{f}(x) + \frac{\sigma}{2}\|x\|_H^2$, for all $x \in H$. Then, the assertion follows immediately from the definition of convexity for $\tilde{f}$ and the linearity of its subgradients. □

(C) Fenchel Duality

Fenchel's duality theory provides elegant means of deriving further conditions for the optimality of solutions. In this context, the Fenchel-Legendre transformation or conjugation of a convex functional provides a tool of enormous relevance for our work.

2.28 Definition (Convex Conjugation) Let $f : U \to]-\infty, +\infty]$ be a convex functional on a Banach space U. We define its *convex conjugate* $f^* : U^* \to]-\infty, +\infty]$ by

$$f^*(u^*) := \sup_{u \in U} \langle u^*, u \rangle_{U^*,U} - f(u).$$

We recall that the convex conjugate f^* of a convex functional f is generally convex and lower semicontinuous. It is also proper, if f is lower semicontinuous and proper. [65, pp 102-103]

Let us summarise further important features:

2.29 Lemma (Properties of Convex Conjugates) *Let $f : U \to]-\infty, +\infty]$ be proper and convex.*

(Fenchel-Moreau Theorem) $f = f^{**} \iff f$ *is lower semicontinuous.*

(Fenchel-Young Equality) *Let $u \in U$ such that $\partial f(u) \neq \emptyset$.*

$$u^* \in \partial f(u) \quad \iff \quad f^*(u^*) = \langle u^*, u \rangle_{U^*,U} - f(u)$$

(Maximising Argument) *Provided that f is proper and lower semicontinuous*

$$u \in \partial f^*(u^*) \quad \iff \quad f^*(u^*) = \langle u^*, u \rangle_{U^*,U} - f(u)$$

Proof. See [65, pp 103-105]. □

We will now review the main results of the FENCHEL theory for a specific class of convex optimisation problems. For two real BANACH spaces U and V, let $\mathcal{A} \in L(U, V)$. We define the objective $I : U \to]-\infty, +\infty]$ as the composition $I := f \circ \mathcal{A} + g$ with the two convex functionals $f : V \to]-\infty, +\infty]$ and $g : U \to]-\infty, +\infty]$. We assume $\operatorname{dom} f \cap \mathcal{A} \operatorname{dom} g \neq \emptyset$, so that f, g, $f \circ \mathcal{A}$ and I are all proper.

By means of the convex conjugates of these functionals, we can establish a lower bound on the objective I:

2.30 Theorem (Weak Duality)

$$-\infty \leq \sup_{v^* \in V^*} -f^*(v^*) - g^*(-\mathcal{A}^* v^*) \leq \inf_{u \in U} f(\mathcal{A}u) + g(u) < +\infty. \tag{2.4}$$

Proof. See [66, p 10]. □

2.31 Definition (Primal and Dual Problems, Duality Gap) With the convex primal and dual objectives $I := f \circ \mathcal{A} + g$ and $J := f^* + g^* \circ (-\mathcal{A}^*)$, respectively, we refer to

$$\inf_{u \in U} \{\, I(u) = f(\mathcal{A}u) + g(u) \,\}$$

as the *primal problem* and

$$\sup_{v^* \in V^*} \{\, -J(v^*) = -f^*(v^*) - g^*(-\mathcal{A}^* v^*) \,\}$$

as the *dual problem*. The difference

$$\left[\inf_{u \in U} I(u)\right] - \left[\sup_{v^* \in V^*} -J(v^*)\right] \in [0, +\infty]$$

between the infimum and supremum in (2.4) is called the *duality gap*.

Additional assumptions are required to turn the second inequality in (2.4) into an equality, i.e. to make the duality gap vanish. Sufficient conditions are known as *regularity conditions*, *interior point conditions* or *constraint qualifications*, two of the most important ones include [66, p 15]:

(Continuity)

$$\exists u_0 \in \operatorname{dom} g \cap \mathcal{A}^{-1} \operatorname{dom} f : \qquad f \text{ is continuous at } u_0 \tag{2.5}$$

(SLATER's condition) For finite-dimensional spaces U, V:

$$\exists u_0 \in \operatorname{relint} \operatorname{dom} f : \qquad \mathcal{A}u_0 \in \operatorname{relint} \operatorname{dom} g \tag{2.6}$$

2.32 Theorem (Strong Duality) *If a qualification condition such as (2.5) or (2.6) holds, then*

$$-\infty \leq \sup_{v^* \in V^*} -f^*(v^*) - g^*(-\mathcal{A}^* v^*) = \inf_{u \in U} f(\mathcal{A}u) + g(u) < +\infty. \tag{2.7}$$

Furthermore, there exists a solution $\bar{v}^* \in V^*$ of the dual problem.*

Proof. We refer to [66, pp 14 & 16] and the references mentioned there. □

2.33 Definition (Primal-Dual Problem) By

$$L(u, v^*) := \langle v^*, \mathcal{A}u \rangle_{V^*,V} - f^*(v^*) + g(u), \qquad \forall (u, v^*) \in U \times V^*.$$

we define the *Lagrangian* $L : U \times V^* \to [-\infty, +\infty]$. We refer to the problem of finding a saddle point $(\bar{u}, \bar{v}^*) \in U \times V^*$ of L,

$$L(\bar{u}, v^*) \leq L(\bar{u}, \bar{v}^*) \leq L(u, \bar{v}^*), \qquad \forall (u, v^*) \in U \times V^*,$$

as the *primal-dual* problem.

By definition of the Lagrangian we have

$$-J(v^*) = \inf_{u \in U} L(u, v^*), \qquad \forall v^* \in V^*$$

such that

$$\sup_{v^* \in V^*} \inf_{u \in U} L(u, v^*)$$

grants an alternative representation of the dual problem. If f is lower semicontinuous such that $f^{**} = f$ by the Fenchel-Moreau Theorem on page 29, then the Lagrangian allows us to write

$$I(u) = \sup_{v^* \in V^*} L(u, v^*) \qquad \forall u \in U$$

and

$$\inf_{u \in U} \sup_{v^* \in V^*} L(u, v^*)$$

expresses the primal problem (cf [62, p 56]).

As we will see in the following section, some numerical algorithms are designed to minimise the objective I or J of the primal respectively dual problem, while other methods

*The supremum may be $-\infty$ as the dual objective J is not necessarily proper. Clearly, this case is ruled out under the proviso that the infimum of I is finite.

compute saddle points of the Lagrangian L in the primal-dual problem. Under relatively mild assumptions, all three approaches are equivalent:

2.34 Theorem (Characterisation of Primal-Dual Solutions) *Let f, g be proper, convex and lower semicontinuous. Then $(\bar{u}, \bar{v}^*) \in (U, V^*)$ is a solution to the primal-dual problem if and only if $\bar{u} \in U$ is a solution to the primal problem, $\bar{v}^* \in V^*$ is a solution to the dual problem and the duality gap is zero.*

Proof. See [62, p 57]. □

(D) Algorithms for Convex Programming

The development and study of algorithms for (nonsmooth) convex optimisation problems has been an extremely active field of research in past years. This is reflected in the fact that many of the approaches described in this section have only been published recently.

Rather than trying to describe the no exits and winding paths through the maze of scientific progress in chronological order, we will review the literature on convex programming methods in its latest state. At the end of this section, we will still add a few remarks on the chronology of advances in this project and concurrently published related works, pointing out similarities and differences.

For our survey, we focus on highlighting the methods that are most germane to our studies. We are interested in approaches to solving the generic convex problem

$$\min_{x \in X} I(x) \tag{C}$$

on a Hilbert space $(X, \langle \cdot, \cdot \rangle_X)$ with a proper, convex, lower semicontinuous and coercive objective functional $I : X \to]-\infty, +\infty]$, such that (C) has a solution $\bar{x} \in X$. Starting with an initial guess of the solution $x^{(0)} \in X$, these methods recursively define a sequence $(x^{(k)})_{k \in \mathbb{N}_0} \subset X$, which, under suitable conditions, converges to $\bar{x}$. At a given iteration $k \in \mathbb{N}$, we also use the short-hand notations $x^- := x^{(k-1)}$, $x^\circ := x^{(k)}$ and $x^+ := x^{(k+1)}$ with superscripts for other sequences defined accordingly.

Algorithms from the Family of Subgradient Methods

A direct generalisation of the steepest descent method for smooth problems relies on successive steps in a direction based on a subgradient at the current iterate, instead of the gradient. To ensure the subdifferential is well-defined and non-empty at every iteration, we have to assume $\operatorname{dom} I = X$ and I is continuous*. Unlike negative gradients,

*Projected subgradient methods exist for the case that $\operatorname{dom} I$ is a convex set.

a negative subgradients may not point into a direction of descent, though. Therefore, the subgradient method may not decrease the objective monotonically, line searches may fail and greater care must be taken to ensure convergence of the method. Additionally, since $\partial I(\bar{x})$ may contain non-zero elements, it is generally unclear how optimality can be measured, unless the entire subdifferential is known. Although successful for a range of problems, these drawbacks imply that the algorithm in its basic form is primarily of historical relevance. [67, pp 108-111]

2.35 Algorithm (Subgradient Method)
Input: $x^{(0)} \in H$, a positive sequence $(t^{(k)})_k$ of step sizes
Initialisation: $k = 1$
Recursion: Evaluate

$$g^{(k)} \in \partial I\left(x^{(k)}\right) \tag{SGM.1}$$

and compute

$$x^{(k+1)} = x^{(k)} - t^{(k)} \frac{g^{(k)}}{\|g^{(k)}\|_H}. \tag{SGM.2}$$

If the algorithm has converged, *then return* $x^{(k+1)}$ and *stop*.

Set $k \leftarrow k + 1$ and *go to* (SGM.1) (SGM.3)

2.36 Variants of the Subgradient Method There are more modern relatives that address some of the issues. So-called 'bundle methods' accumulate iteration history to improve the convergence characteristics, including a kind of monotonicity [68], [69]. Gradient sampling methods [70]–[72] construct a local model of the objective based on a larger number of subgradient evaluations, randomly scattered around the current iterate. They are particularly suitable if the dimension of the space H is not too large, as many calls to the of the function providing subgradients—the main cost of each iteration—would be required otherwise. Some subgradient-based methods incorporate preconditioning techniques and scale the search direction by means of a variable metric. There is some evidence [73, pp 48-92], [74] that quasi-Newton updates, which successively construct an approximate Hessian of the objective, are beneficial for certain problems, even if they are nonsmooth.

Heuristics, many of them problem-specific, play a central role for algorithms of this class. Additionally, the finite-dimensional setting is often a crucial requirement. We will therefore look for alternative options and not consider the various subgradient descent

methods any further.

Primal-Dual Methods and Augmented Lagrangians

Let us return to the important class of problems, where the objective I has composite form:

$$\min_{x\in X} \{\, I(x) := f(\mathcal{A}x) + g(x) \,\}. \tag{CC}$$

In addition to the assumptions on the more general convex programming problem (C), let the operator $\mathcal{A} \in L(X, Y)$ with a second real Hilbert space $(Y, \langle\,\cdot\,,\,\cdot\,\rangle_Y)$ that we will identify with its dual. The functionals $f : Y \to]-\infty, +\infty]$ and $g : X \to]-\infty, +\infty]$ are assumed to be proper, convex and lower semicontinuous. If additionally a qualification condition holds for (CC), then Theorem 2.34 on page 32 implies that the primal problem

$$\min_{x\in X} f(\mathcal{A}x) + g(x), \tag{P}$$

the primal-dual problem

$$\min_{x\in X} \max_{\lambda\in Y} \langle \lambda, \mathcal{A}x\rangle_Y - f^*(\lambda) + g(x) \tag{PD}$$

and the dual problem

$$\max_{\lambda\in Y} -f^*(\lambda) - g^*(-\mathcal{A}^*\lambda) \tag{D}$$

are all equivalent.

2.37 Split and Augmented Formulations The primal problem (P) is clearly equivalent to the linearly constrained minimisation problem

$$\min_{(x,y)\in X\times Y} f(y) + g(x) \qquad \text{subject to } y = \mathcal{A}x, \tag{P$'$}$$

in fact, equivalent to

$$\min_{(x,y)\in X\times Y} f(y) + g(x) + \frac{\varrho}{2}\|\mathcal{A}x - y\|_Y^2 \qquad \text{subject to } y = \mathcal{A}x, \tag{P$'_\varrho$}$$

for any $\varrho \geq 0$. The corresponding saddle-point formulations

$$\max_{\lambda\in Y} \min_{(x,y)\in X\times Y} f(y) + g(x) - \langle \lambda, y - \mathcal{A}x\rangle_Y \tag{PD$'$}$$

and

$$\max_{\lambda\in Y} \min_{(x,y)\in X\times Y} f(y) + g(x) - \langle \lambda, y - \mathcal{A}x\rangle_Y + \frac{\varrho}{2}\|\mathcal{A}x - y\|_Y^2, \tag{PD$'_\varrho$}$$

reduce to (PD) if the extra variable $y \in Y$ is eliminated again by carrying out the minimisation with respect to y in (PD′) and (PD′$_\varrho$).

Analogous equivalent formulations could be derived from the dual problem in a completely symmetrical manner.

Although an additional variable has now entered the problem, hence increasing the memory footprint in a computational solution, it offers a major advantage: the two terms f and g can be formally uncoupled and therefore minimised separately. These separate minimisation problems are most of the time significantly easier than the original problem. In other words, an optimisation algorithm may relax the constraint $y = \mathcal{A}x$ in the sense that iterates do not have to satisfy this equation exactly. Surely, their sequence should still converge to a feasible solution.

We will now review classical methods, which approach one of the problems (P), (PD), (D), the split formulations (P′), (PD′) or the split and augmented formulations (P′$_\varrho$), (PD′$_\varrho$), all of which are equivalent under our assumptions.

The prototypical Uzawa *algorithm* was originally developed for concave programming problems [75]. Applied to the split problem (PD′), the Uzawa algorithm equates to simple gradient ascent in the dual problem (D), clearly under the assumption that the latter is smooth*:

$$\lambda^+ = \lambda^\circ + t^\circ \left(-\nabla f^* \left(\lambda^\circ\right) + \mathcal{A}\nabla g^* \left(-\mathcal{A}^*\lambda^\circ\right)\right).$$

We may express the gradients of convex conjugates, due to their property of the maximising argument (see Lemma 2.29 on page 29), in terms of f and g:

$$\nabla f^* \left(\lambda^\circ\right) = \operatorname*{arg\,max}_{y \in Y} \left\langle \lambda^\circ, y \right\rangle_Y - f(y) =: y^\circ$$
$$\nabla g^* \left(-\mathcal{A}^*\lambda^\circ\right) = \operatorname*{arg\,max}_{x \in X} \left\langle -\mathcal{A}^*\lambda^\circ, x \right\rangle_{X^*,X} - g(x) =: x^\circ.$$

This way, even though the Uzawa algorithm is only derived from the dual problem, we obtain effectively a primal-dual algorithm that defines a sequence $\left(x^{(k)}, y^{(k)}, \lambda^{(k)}\right)_k \subset X \times Y \times Y$, the convergence of which to a saddle point $(\bar{x}, \bar{y}, \bar{\lambda}) \in X \times Y \times Y$ follows from the convergence properties of steepest descent / ascent.

2.38 Algorithm (Uzawa Algorithm) *Input:* $\lambda^{(0)} \in Y$, a sequence $(t^{(k)})_k$ of step sizes
Initialisation: $k = 0$

*Generalisations of the Uzawa algorithm, if the dual problem is nonsmooth, rely on proximal operators, see page 41.

Recursion: Evaluate

$$x^{(k)} = \operatorname*{arg\,min}_{x \in X} g(x) + \left\langle \mathcal{A}^* \lambda^{(k)}, x \right\rangle_{X^*, X} \tag{Uz.1}$$

and

$$y^{(k)} = \operatorname*{arg\,min}_{y \in Y} f(y) - \left\langle \lambda^{(k)}, y \right\rangle_{Y} . \tag{Uz.2}$$

If the algorithm has converged, *then return* $\left(x^{(k)}, y^{(k)}, \lambda^{(k)}\right)$ and *stop*.

Update

$$\lambda^{(k+1)} = \lambda^{(k)} + t^{(k)} \left(\mathcal{A} x^{(k)} - y^{(k)} \right), \tag{Uz.3}$$

set $k \leftarrow k + 1$ and *go to* (Uz.1).

If f^* or g^* contains an indicator function, then projected gradient ascent will lead to a direct generalisation of the Uzawa Algorithm.

2.39 Motivation of Augmented Lagrangian Methods The basic Uzawa algorithm often suffers from relatively slow convergence due to a slowly decreasing residual $\mathcal{A}x^{(k)} - y^{(k)}$. This motivates *augmented Lagrangian methods*, which tackle the augmented problem formulations where this residual is penalised by means of the above quadratic terms and a (possibly varying) penalty parameter $\varrho^{(k)} > 0$. It is generally assumed that $\sup_{k \in \mathbb{N}} \varrho^{(k)} < +\infty$ to avoid the ill-conditioning issues of penalty methods. Even a bounded sequence of penalty parameters still encourages proximity of primal iterates $(x^{(k)}, y^{(k)})_k \subset X \times Y$ to the feasible manifold.

The Uzawa algorithm applied to the augmented Lagrangian in formulation (PD'_ϱ) instead of (PD') forms the first out of a set of four augmented Lagrangian methods ALG1–ALG4, which were originally proposed by Fortin, Glowinski and Le Tallec [76], [77].

2.40 Algorithm (ALG1 / Augmented-Lagrangian-Uzawa Algorithm) *Input:* $\lambda^{(0)} \in Y$, a positive sequence $(t^{(k)})_k$ of step sizes
Initialisation: $k = 0$
Recursion: Compute

$$\left(x^{(k)}, y^{(k)}\right) = \operatorname*{arg\,min}_{(x,y) \in X \times Y} f(y) + g(x) + \left\langle \lambda^{(k)}, \mathcal{A}x - y \right\rangle_{Y} + \frac{\varrho^{(k)}}{2} \left\| \mathcal{A}x - y \right\|_Y^2 \tag{ALG1.1}$$

If the algorithm has converged, *then return* $\left(x^{(k)}, y^{(k)}, \lambda^{(k)}\right)$ and *stop*.

Update

$$\lambda^{(k+1)} = \lambda^{(k)} + t^{(k)} \left(\mathcal{A}x^{(k)} - y^{(k)}\right), \tag{ALG1.2}$$

set $k \leftarrow k+1$ and *go to* (ALG1.1).

As before, the relation between gradients of the dual objective and an optimisation problem in the primal variables follows from the maximising-argument property of the subdifferential.

Unfortunately, it can be seen that the improved convergence comes at a significant cost: the penalty term re-introduces a coupling between the variables x and y. Therefore, the solution of the subproblem (ALG1.1) may be just as difficult as the original problem. An iterative method like the Uzawa algorithm is normally required for finding a solution of that subproblem, thus making every iteration computationally expensive.

Glowinski and Le Tallec [77, p 84] motivate the *alternating direction method of multipliers* (ADMM or ALG2) as the method that results from solving (ALG1.1) very inexactly, with only a single Uzawa iteration. This method can be traced back to works of Gabay and Mercier [45] and Glowinski and Marrocco [78].

2.41 Algorithm (ALG2 / Alternating Direction Method of Multipliers) *Input:* $\left(y^{(0)}, \lambda^{(0)}\right) \in Y \times Y$, a positive sequence $(t^{(k)})_k$ of step sizes
Initialisation: $k = 0$
Recursion: Compute

$$x^{(k+1)} = \operatorname*{arg\,min}_{x \in X} g(x) + \left\langle \mathcal{A}^* \lambda^{(k)}, x \right\rangle_{X^*, X} + \frac{\varrho^{(k)}}{2} \left\| \mathcal{A}x - y^{(k)} \right\|_Y^2 \tag{ALG2.1}$$

and

$$y^{(k+1)} = \operatorname*{arg\,min}_{y \in Y} f(y) - \left\langle \lambda^{(k)}, y \right\rangle_Y + \frac{\varrho^{(k)}}{2} \left\| \mathcal{A}x^{(k+1)} - y \right\|_Y^2. \tag{ALG2.2}$$

Update

$$\lambda^{(k+1)} = \lambda^{(k)} + t^{(k)} \left(\mathcal{A}x^{(k+1)} - y^{(k+1)}\right). \tag{ALG2.3}$$

If the algorithm has converged, *then return* $\left(x^{(k+1)}, y^{(k+1)}, \lambda^{(k+1)}\right)$ and *stop*.

Set $k \leftarrow k+1$ and *go to* (ALG2.1). (ALG2.4)

It is an important observation that the subproblems (ALG2.1) and (ALG2.2) may have a unique solution even if (Uz.1) and (Uz.2) do not. While we had to make strong assumptions on the regularity of the problem in order to apply the Uzawa algorithm, we can relax these for ADMM. For instance, if f is not coercive, the Uzawa algorithm may break down in step (Uz.2). In contrast, the penalty term ensures that the objective in (ALG2.2) is generally coercive and even strongly convex, making the iterate $y^{(k)}$ well-defined.

ADMM is equivalent to applying the classical Douglas-Rachford operator splitting method [79] to the inclusion problem in the first-order optimality condition (cf Theorem 2.25 on page 28) of the dual problem (D)

$$0 \in -\partial f^*(\lambda) + \mathcal{A}\partial g^*(-\mathcal{A}^*\lambda),$$

i.e. the problem of finding a root of the dual subdifferential operator. [76]

Of all augmented Lagrangian methods, ALG2 is by far the most popular one and has found widespread application in many fields of science, finance and engineering. For further details, we refer to Glowinski's recent review [80] and the references therein. Preconditoned versions and related algorithms are discussed in [81].

2.42 Reducing the Complexity of ADMM The most difficult subproblem in each iteration of ADMM is typically encountered in step (ALG2.1). The optimality condition for this problem yields a linear or possibly even nonlinear system including the operator $\mathcal{A}^*\mathcal{A}$. For finite-dimensional problems and some infinite-dimensional problems, one can effectively reduce the complexity of solving the subproblem (ALG2.1). By majorising the quadratic penalty term in a suitable way, the solution of linear (or nonlinear) systems can be replaced with only the evaluation of a matrix-vector product, at the expense of possibly shorter steps. Specifically, we split the penalty term as follows:

$$\begin{aligned}\frac{\varrho^\circ}{2}\|\mathcal{A}x - y^\circ\|_Y^2 &= \frac{\varrho^\circ}{2}\|\mathcal{A}x^\circ - y^\circ + \mathcal{A}(x - x^\circ)\|_Y^2 \\ &= \frac{\varrho^\circ}{2}\|\mathcal{A}x^\circ - y^\circ\|_Y^2 + \varrho^\circ\langle \mathcal{A}x^\circ - y^\circ, \mathcal{A}(x - x^\circ)\rangle_Y + \frac{\varrho^\circ}{2}\|\mathcal{A}(x - x^\circ)\|_Y^2.\end{aligned}$$

If $\mathcal{A}$ is bounded with operator norm $\|\mathcal{A}\|$, we can estimate the energy norm in the last term by

$$\frac{\varrho^\circ}{2}\|\mathcal{A}(x - x^\circ)\|_Y^2 \leq \frac{\varrho^\circ}{2}\|\mathcal{A}\|^2\|x - x^\circ\|_X^2 \leq \frac{1}{2\varsigma^\circ}\|x - x^\circ\|_X^2,$$

for any $\varsigma^\circ > 0$ such that $\varrho^\circ\varsigma^\circ \leq 1/\|\mathcal{A}\|^2$. Unlike the Euclidean setting, we point out that for a problem posed in function spaces, the minimisation problem including the majorising norm in X may not be any simpler than the original problem with the energy

norm: consider, for instance, the case where $\mathcal{A}$ is the gradient operator with its domain in a Sobolev space like $H^1(]0,1[)$. Since a norm on this space includes the gradient or a similar combination of derivatives, both iterations would equate to solving an elliptic problem, possibly for the same elliptic operator.

ADMM with the default penalty term majorised in this manner yields the primal-dual Chambolle-Pock algorithm [49], which is more commonly denoted in the following form:

2.43 Algorithm (Primal-Dual Chambolle-Pock Algorithm) *Input:* $\left(x^{(0)}, \lambda^{(0)}\right) \in X \times Y$, positive sequences $(\varsigma^{(k)})_k$, $(\varrho^{(k)})_k$, a sequence $(t^{(k)})_k \subset [0,1]$
Initialisation: $k = 0$, $\hat{x}^{(0)} = x^{(0)}$
Recursion: Compute the dual iterate

$$\lambda^{(k+1)} = \operatorname*{arg\,min}_{\lambda \in Y} f^*(\lambda) - \left\langle \lambda, \mathcal{A}\hat{x}^{(k)} \right\rangle_Y + \frac{1}{2\varrho^{(k)}} \left\| \lambda - \lambda^{(k)} \right\|_Y^2 \tag{CP.1}$$

and the corresponding primal iterate

$$x^{(k+1)} = \operatorname*{arg\,min}_{x \in X} g(x) + \left\langle \mathcal{A}^* \lambda^{(k+1)}, x \right\rangle_{X^*,X} + \frac{1}{2\varsigma^{(k)}} \left\| x - x^{(k)} \right\|_X^2 . \tag{CP.2}$$

Update the leading point

$$\hat{x}^{(k+1)} = x^{(k+1)} + t^{(k)} \left(x^{(k+1)} - x^{(k)} \right) . \tag{CP.3}$$

If the algorithm has converged, *then return* $\left(x^{(k+1)}, \lambda^{(k+1)}\right)$ and *stop*.

Set $k \leftarrow k+1$ and *go to* (CP.1). (CP.4)

Algorithms of this kind were initially known as *modified primal-dual hybrid gradient method*, *split inexact* Uzawa *method* or *preconditioned ADMM* [49], [81], [82]. The special case $t^{(k)} \equiv 0$ is also known as Arrow-Hurwicz Method [83]. An adaptive version thereof can be found in [84]. The article of Chambolle and Pock [49] has been cited over 1,000 times since its publication in 2011, which reflects its wide applicability and favourable features. The convergence of the method as well as of some derivatives and extensions are studied in [49], [85], [86] and several references therein.

2.44 ADMM with Symmetric Updates In favour of a more symmetric treatment of the two primal variables x and y in ADMM, Fortin and Glowinski suggest updating the dual multiplier after each subproblem (ALG2.1) and (ALG2.2) [76]. This approach is sometimes called *alternating minimisation algorithm* (AMA or ALG3). In analogy to the

link between ADMM and the Douglas-Rachford method, this alternative augmented Lagrangian method is equivalent to the Peaceman-Rachford splitting algorithm [87] applied to the optimality condition of the dual.

2.45 Algorithm (ALG3 / Alternating Minimisation Algorithm) *Input:* $\left(y^{(0)}, \lambda^{(0)}\right) \in Y \times Y$, a positive sequence $(t^{(k)})_k$ of step sizes
Initialisation: $k = 0$
Recursion: Compute

$$x^{(k+1)} = \operatorname*{arg\,min}_{x \in X} g(x) + \left\langle \mathcal{A}^* \lambda^{(k)}, x \right\rangle_{X^*, X} + \frac{\varrho^{(k)}}{2} \left\| \mathcal{A}x - y^{(k)} \right\|_Y^2 \tag{ALG3.1}$$

and update

$$\lambda^{(k+1/2)} = \lambda^{(k)} + t^{(k)} \left(\mathcal{A}x^{(k+1)} - y^{(k)} \right). \tag{ALG3.2}$$

Evaluate

$$y^{(k+1)} = \operatorname*{arg\,min}_{y \in Y} f(y) - \left\langle \lambda^{(k+1/2)}, y \right\rangle_Y + \frac{\varrho^{(k)}}{2} \left\| \mathcal{A}x^{(k+1)} - y \right\|_Y^2 \tag{ALG3.3}$$

and update again

$$\lambda^{(k+1)} = \lambda^{(k+/2)} + t^{(k)} \left(\mathcal{A}x^{(k+1)} - y^{(k+1)} \right). \tag{ALG3.4}$$

If the algorithm has converged, *then return* $\left(x^{(k+1)}, y^{(k+1)}, \lambda^{(k+1)}\right)$ and *stop*.

Set $k \leftarrow k + 1$ and *go to* (ALG3.1). (ALG3.5)

2.46 Further Modifications of ADMM A fourth augmented Lagrangian method named ALG4 seems to have first appeared in [77]. Similar to the equivalence between ALG2 and Douglas-Rachford splitting or ALG3 and Peaceman-Rachford splitting, ALG4 is designed as the primal-dual method that corresponds to the θ-method for root-finding problems of monotone operators. In each iteration, ALG4 requires the solution of two minimisation problems per primal variable and it includes a third update for the dual variable. It appears to be rarely applied in optimisation.

The penalty term in augmented Lagrangian methods offers further room for alterations. Rather than measuring proximity between $\mathcal{A}x$ and y by means of a squared norm $B(\cdot, *) := \frac{1}{2}\|\cdot - *\|^2$, other distance-like functionals have proven their viability in applications. The notion of Bregman distance provides a mathematically rigorous generalisation, which is of particular importance for problems in Banach spaces. In

such a setting, it would often be more desirable to work with powers of norms that have an exponent different from 2. The corresponding primal-dual methods are known as *nonlinear ADMM* [88], *split* Bregman *method* [89] or *nonlinear* Chambolle-Pock *algorithm* [85], [86], see also [90] for a related method.

Proximal Methods

While many of the algorithms we review under this rubric are closely related to some of the aforementioned primal-dual algorithms, they rely on completely different techniques. For all of these methods, the Moreau proximal map assumes a central role and its strong properties allow for far-reaching convergence statements. One of the greatest benefits of methods of this class can be seen in their adaptability: depending on what degree of smoothness the optimisation problem under consideration satisfies, this can easily be exploited to yield methods of provably optimal complexity. These advantages make proximal algorithms our methods of choice in this work.

2.47 Definition (Proximal Operator) For a proper, convex and lower semicontinuous functional $f : X \to]-\infty, +\infty]$ and $t > 0$ we define the *proximal map* by Moreau [91]

$$\operatorname{prox}_{tf}(x) := \operatorname*{arg\,min}_{y \in X} tf(y) + \frac{1}{2}\|x - y\|_X^2 = \operatorname*{arg\,min}_{y \in X} f(y) + \frac{1}{2t}\|x - y\|_X^2. \tag{2.8}$$

Since the functionals to be minimised in this definition are strongly convex, there is a unique solution $y \in X$ and prox_{tf} is well-defined.

2.48 Example (Proximal Operators for Common Functionals) (a) Let $f = \iota_C$ for a convex set $C \subset X$. Then, for any $x \in X$, $t > 0$

$$\operatorname{prox}_{tf}(x) = \operatorname*{arg\,min}_{y \in X} \frac{1}{2}\|x - y\|_X^2 \qquad \text{subject to } y \in C, \tag{2.9}$$

the orthogonal projection of x onto C.

(b) Let $X = \mathbb{R}^d$, $\alpha \geq 0$ and $f = \alpha|\cdot|_1$. Then, with $(\cdot)_+ := \max\{0, \cdot\}$,

$$\operatorname{prox}_{tf}(x) = \begin{pmatrix} \operatorname{sgn}(x_1)(|x_1| - \alpha t)_+ \\ \vdots \\ \operatorname{sgn}(x_d)(|x_d| - \alpha t)_+ \end{pmatrix}, \tag{2.10}$$

the so-called soft-thresholding or shrinkage-thresholding operator applied to $x \in X$.

2.49 Fixed Points of the Proximal Map By the optimality condition (2.3) on page 28, we observe that for $\bar{x} \in X$ and arbitrary $t > 0$

$$\begin{aligned} \bar{x} = \operatorname{prox}_{tf}(\bar{x}) &\iff tf(x) - tf(\bar{x}) + \langle \bar{x} - \bar{x}, x - \bar{x} \rangle_X \geq 0, \qquad \forall x \in X \\ &\iff \bar{x} \in \operatorname*{arg\,min}_{x \in X} tf(x) \\ &\iff \bar{x} \in \operatorname*{arg\,min}_{x \in X} f(x). \end{aligned}$$

Therefore, $\bar{x}$ is a minimiser for f if and only if it is a fixed point of the proximal operator.

To solve the generic convex optimisation problem (C), this fixed-point property of the proximal map motivates a Picard iteration applied to

$$\bar{x} = \operatorname{prox}_{tI}(\bar{x})$$

This procedure yields the *proximal point algorithm* [92], [93].

2.50 Algorithm (Proximal Point Method) *Input:* $x^{(0)} \in X$, a positive sequence $(t^{(k)})_k$
Initialisation: $k = 0$
Recursion: Evaluate

$$x^{(k+1)} = \operatorname{prox}_{t^{(k)} I}\left(x^{(k)}\right) \tag{PPM.1}$$

If the algorithm has converged, *then return* $x^{(k+1)}$ and *stop*.

Set $k \leftarrow k + 1$ and *go to* (PPM.1). (PPM.2)

Clearly, the algorithm is most attractive if the proximal operator is available in closed form or if it can be evaluated cheaply. Objectives with this property are normally referred to as having 'simple structure'.

The convergence of the proximal point algorithm can be derived from the firm nonexpansiveness of the proximal operator and a convergence theorem of Opial [94].

Similar to nonlinear augmented Lagrangian methods, there are nonlinear proximal point methods where the proximal map includes a Bregman distance other than the squared norm. We refer to the works of Butnariu and Iusem [95] as well as Burachik and Scheimberg [96] for further details.

It is possible to expoit an additive structure of the objective $I = \sum_j I_j$ in proximal splitting methods, which are of primary interest for large-scale optimisation problems with little known extra regularity [97], [98]. We will however focus on methods that can additionally benefit from smooth terms in the objective, allowing for first-order information to be incorporated.

2.51 Composite Convex Problems Including Smooth Terms Let us therefore return to the composite convex problem (CC), for the moment with $\mathcal{A} = \mathrm{id}_X$:

$$\min_{x \in X} \{\, I(x) = f(x) + g(x) \,\}.$$

We additionally assume that the functional f is continuously Gâteaux-differentiable with Lipschitz continuous gradient for some Lipschitz constant $L > 0$. A descent lemma [99, p 15] guarantees that that f can be majorised by a quadratic model,

$$f(y) \leq f(x) + \langle \nabla f(x), y - x \rangle_X + \frac{L}{2} \|x - y\|_X^2, \qquad \forall x, y \in X, \tag{2.11}$$

and hence $I = f + g$ can be estimated pointwise by

$$f(y) + g(y) \leq f(x) + \langle \nabla f(x), y - x \rangle_X + \frac{L}{2} \|x - y\|_X^2 + g(y) =: M_L(x, y),$$

for all $x, y \in X$. In particular,

$$\min_{y \in X} f(y) + g(y) \leq \min_{y \in X} M_L(x, y) \leq M_L(x, x) = f(x) + g(x), \qquad \forall x \in X, \tag{2.12}$$

where the minimising argument of $M_L(x, \cdot\,)$ is given by

$$\operatorname*{arg\,min}_{y \in X} M_L(x, y) = \operatorname*{arg\,min}_{y \in X} g(y) + \frac{L}{2} \left\| x - \frac{1}{L} \nabla f(x) - y \right\|_X^2 = \operatorname{prox}_{\frac{g}{L}} \left(x - \frac{1}{L} \nabla f(x) \right).$$

Furthermore, the second inequality in (2.12) is an equality, if and only if

$$\begin{aligned} x = \operatorname{prox}_{\frac{g}{L}} \left(x - \frac{1}{L} \nabla f(x) \right) &\iff \frac{1}{L} g(y) - \frac{1}{L} g(x) + \left\langle x - x + \frac{1}{L} \nabla f(x), y - x \right\rangle_X \geq 0, \\ &\qquad\qquad \forall y \in X \\ &\iff x \in \operatorname*{arg\,min}_{y \in X} \frac{1}{L} f(y) + \frac{1}{L} g(y) \\ &\iff x \in \operatorname*{arg\,min}_{y \in X} f(y) + g(y). \end{aligned}$$

Summarising, we can conclude that the recursion

$$x \mapsto \operatorname{prox}_{\frac{g}{L}} \left(x - \frac{1}{L} \nabla f(x) \right)$$

leads to a strict decrease in the value of the objective $I = f + g$, except if x is already a minimiser.

If no Lipschitz constant is known, then a value $L^{(k)} > 0$ that achieves descent can be determined in each iteration by means of a backtracking procedure [48].

2.52 Algorithm (ISTA / Proximal Gradient Method) *Input:* $x^{(0)} \in X$
Initialisation: $k = 0$
Recursion: Set $L^{(k)} = L$ or find a valid* $L^{(k)} > 0$ by backtracking and evaluate

$$x^{(k+1)} = \operatorname{prox}_{\frac{g}{L^{(k)}}}\left(x^{(k)} - \frac{1}{L^{(k)}}\nabla f\left(x^{(k)}\right)\right) \tag{ISTA.1}$$

If the algorithm has converged, *then return* $x^{(k+1)}$ and *stop*.

Set $k \leftarrow k + 1$ and *go to* (ISTA.1). (ISTA.2)

2.53 Algorithms Related to the Proximal Gradient Method This algorithm comprises a number of important special cases:

- If I is nonsmooth, i.e. $f = 0$, then (ISTA.1) is equivalent to (PPM.1) with step parameter $t^{(k)} = 1/L^{(k)}$.
- If I is smooth with Lipschitz gradient, i.e. $g = 0$, then step (ISTA.1) degenerates to steepest descent with step size $1/L^{(k)}$.
- If $g = \iota_C$ with a convex set $C \subset X$, then, according to Example 2.48(a), the proximal gradient method is equivalent to a gradient projection method.
- If $X = \mathbb{R}^d$ and $g = |\cdot|_1$, then Example 2.48(b) shows that the method corresponds to an iterative shrinkage-thresholding algorithm (ISTA) (cf [41], [100]). However, it has become common practice to refer to the proximal gradient method as ISTA, even if g has a different form [48].

Algorithms of this kind first appeared in works of Passty [101] as well as Lions and Mercier [102]. Alternative names that can be found in the literature are *majorisation-minimisation algorithm* or *proximal forward-backward splitting*, the latter primarily in the context of more general inclusion problems for monotone operators. If a splitting method of Tseng [103], which equates to ADMM with $\varrho^{(k)} = 0$ in step (ALG2.2), is applied to the dual problem, then one obtains an alternative, equivalent interpretation of ISTA [81].

The proximal gradient method unites a number of highly desirable features: it can exploit an additive decomposition of the objective into smooth and nonsmooth terms, separability of g simplifies evaluations of the proximal map, and since many functionals g

*That is: choose the approximate Lipschitz constant $L^{(k)}$ sufficiently large such that the objective does not increase, $I\left(x^{(k+1)}\right) \leq I\left(x^{(k)}\right)$.

in applications are of simple structure, each iteration typically requires little computational effort. On another hand, it often needs a very large number of iterations to reach a desired accuracy, as convergence is generally sublinear and can be very slow. The following (worst-case) convergence theorem for ISTA is proved in [48] (Remark 2.1 and Theorem 3.1).

2.54 Theorem (Convergence Rate of ISTA) *Let* $\left(x^{(k)}\right)_k \subset X$ *be generated by ISTA, where* $\left(L^{(k)}\right)_k \subset]0, +\infty[$ *is non-decreasing with* $\sup_k L^{(k)} =: \widetilde{L} < +\infty$. *For any* $\bar{x} \in \arg\min_{x \in X} I(x)$ *and* $k \in \mathbb{N}$

$$I(x^{(k)}) - I(\bar{x}) \leq \frac{\widetilde{L} \left\| x^{(0)} - \bar{x} \right\|_X^2}{2k}. \tag{2.13}$$

2.55 Improving the Convergence of Proxmal Gradient Methods The convergence result for ISTA indicates one pathway towards reducing the bound on the right-hand side of (2.13): the constant $\widetilde{L}$ or a LIPSCHITZ constant of ∇f only reflect global information on the functional f. We recall that descent methods in smooth optimisation often benefit if the negative gradient $-\nabla f(x^\circ)$ is replaced with $-\mathcal{B}^\circ \nabla f(x^\circ)$, where $\mathcal{B}^\circ$ is a positive definite operator approximating the inverse Hessian, if it exists. Analogously, one approach to preconditioning ISTA is therefore based on scaling the gradient and the proximal operator by means of a variable metric, which also reflects local curvature information of the smooth term f at the current iterate. Depending on the differentiability of f, such a variable metric could be defined from its Hessian or quasi-NEWTON approximations. Therefore, we refer to such variants of the proximal gradient algorithm as *variable metric* or NEWTON*-type methods*.

Methods of this kind for problems posed in $\mathbb{R}^d$ have been studied recently in [104]–[106], while a similar concept can already be found in an earlier work of FUKUSHIMA and MINE [107]. Proximal quasi-NEWTON methods have received a great deal of attention, see e.g. [108]–[110]. Proximal NEWTON-type methods in possibly infinite-dimensional real HILBERT spaces are considered in [111] and [112].

2.56 Scaled Topology To define another metric on X, let $\mathcal{H} \in L(X, X)$ be a self-adjoint operator satisfying $\underset{\sim}{L}\,\mathrm{id} \preccurlyeq \mathcal{H} \preccurlyeq \widetilde{L}\,\mathrm{id}$ for two constants $0 < \underset{\sim}{L} \leq L \leq \widetilde{L} < +\infty$. That is, $\mathcal{H} = \mathcal{H}^*$ and both $\mathcal{H} - \underset{\sim}{L}\,\mathrm{id}$ and $\widetilde{L}\,\mathrm{id} - \mathcal{H}$ are positive semidefinite such that $\mathcal{H}$ is bounded and bounded below. Then $\mathcal{H}$ induces a scaled inner product and a scaled norm on X by

$$\langle x, y \rangle_{\mathcal{H}} := \langle x, \mathcal{H} y \rangle_X \qquad \|x\|_{\mathcal{H}} := \sqrt{\langle x, x \rangle_{\mathcal{H}}}, \qquad \forall x, y \in X.$$

The norms $\|\cdot\|_X$ and $\|\cdot\|_{\mathcal{H}}$ are clearly equivalent, since

$$\underset{\sim}{L}\|x\|_X^2 \leq \|x\|_{\mathcal{H}}^2 \leq \widetilde{L}\|x\|_X^2, \qquad \forall x \in X \tag{2.14}$$

and $\mathcal{H}$ has an inverse $\mathcal{H}^{-1}$.

2.57 Definition (Scaled Proximal Operator) For a proper, convex and lower semicontinuous functional $f : X \to]-\infty, +\infty]$ and $t > 0$ we define the *scaled proximal map with respect to* $\mathcal{H}$

$$\operatorname{prox}_{tf}^{\mathcal{H}}(x) := \underset{y \in X}{\arg\min}\, f(y) + \frac{1}{2t}\|x - y\|_{\mathcal{H}}^2. \tag{2.15}$$

With this definition, proximal NEWTON-type methods can be derived in a similar fashion to the proximal gradient method by replacing some canonical inner products and norms on X with their scaled counterparts: firstly, with $l := L/\underset{\sim}{L}$, the left inequality in (2.14) implies that

$$M_l^{\mathcal{H}}(x, y) := f(x) + \langle \nabla f(x), y - x\rangle_X + \frac{l}{2}\|x - y\|_{\mathcal{H}}^2 + g(y)$$

majorises $I(y) = f(y) + g(y)$ for arbitrary choices of $x, y \in X$. The majorant $M_l^{\mathcal{H}}$ embodies the new quadratic model of I, which now incorporates the metric defined by $\mathcal{H}$. Secondly, for fixed $x \in X$,

$$\underset{y \in X}{\arg\min}\, M_l^{\mathcal{H}}(x, y) = \operatorname{prox}_{\frac{g}{l}}^{\mathcal{H}}\left(x - \frac{1}{l}\mathcal{H}^{-1}\nabla f(x)\right)$$

and it is easy to verify that this generalised proximal gradient recursion continues to reduce the objective, unless x is already optimal.

2.58 Algorithm (VM-ISTA / Proximal NEWTON-Type Method) *Input:* $x^{(0)} \in X$
Initialisation: $k = 0$
Recursion: Define $\mathcal{H}^{(k)}$ and solve

$$\mathcal{H}^{(k)} d^{(k)} = -\nabla f\left(x^{(k)}\right). \tag{VM-ISTA.1}$$

Set $l^{(k)} = L/\underset{\sim}{L}$ or find a valid $l^{(k)} > 0$ by backtracking and evaluate

$$x^{(k+1)} = \operatorname{prox}_{\frac{g}{l^{(k)}}}^{\mathcal{H}^{(k)}}\left(x^{(k)} + \frac{1}{l^{(k)}} d^{(k)}\right) \tag{VM-ISTA.2}$$

If the algorithm has converged, *then return* $x^{(k+1)}$ and *stop*.

Set $k \leftarrow k+1$ and *go to* (VM-ISTA.1). (VM-ISTA.3)

Alternative strategies for choosing a step size in every iteration are possible, in particular an inexact line search with sufficient descent condition [106] as known from smooth optimisation problems.

The proof for the $O(1/k)$ convergence rate of ISTA can be copied almost literally for this generalisation with variable metrics. The only extra difficulty arises from the occurrence of an entire family of different norms $(\|\cdot\|_{\mathcal{H}^{(k)}})_k$. In addition to the uniform boundedness of the operators $\left(\mathcal{H}^{(k)}\right)_k$ through the constants $\underset{\sim}{L}, \widetilde{L} > 0$, an additional relative assumption like $\mathcal{H}^{(k+1)} \preccurlyeq \left(1+\eta^{(k)}\right)\mathcal{H}^{(k)}$, for all $k \in \mathbb{N}_0$, with a summable sequence $\left(\eta^{(k)}\right)_k \subset [0,+\infty]$ is standard to derive convergence properties for proximal algorithms with variable metrics. [112]–[114]

Acceleration

Preconditioned proximal gradient methods like the variable-metric ISTA have been shown to converge within fewer, often significantly fewer iterations than the basic proximal gradient method for important applications. However, the worst-case complexity bound of $O(1/k)$ remains unchanged, unless extra regularity of the problem is assumed.

2.59 Complexity of Optimisation Algorithms for Solving (CC) It turns out that the worst-case bound of global $O(1/k)$ convergence is not optimal in the following sense [115, pp 4-7] (see also [116]): we consider the class of composite convex problems, with Lipschitz continuous f and all possible algorithms which generate a sequence of iterates $(x^{(k)})_k$ based solely on a first-order 'oracle' that can return $f\left(x^{(k)}\right)$, $g\left(x^{(k)}\right)$ and $\nabla f\left(x^{(k)}\right)$. There actually exist methods that, unlike ISTA, compute iterates which converge to a solution $\bar{x}$ such that $I\left(x^{(k)}\right) - I\left(\bar{x}\right) = O(1/k^2)$ or better. This holds true for any arbitrary optimisation problem fulfilling the regularity assumptions. Furthermore, there is no first-order method which achieves a higher order of convergence for all problems of the class [117].

Consequently, it would be desirable to adapt algorithms like ISTA or VM-ISTA in a way that their worst-case convergence improves to the optimal order of $O(1/k^2)$. Such 'fast' or 'accelerated' methods have intensely been studied over the past few years, although the fundamental concept had already appeared in the literature of the previous century in works of Nesterov [117] (see also [118]) for smooth problems and for a proximal point method in an article by Güler [119]. The topic gained momentum in recent times

following the now highly cited article of Beck and Teboulle [48] on a *fast* iterative shrinkage-thesholding algorithm (FISTA). Unlike its earlier predecessors, FISTA is an optimal $O(1/k^2)$ method that is applicable to composite convex problems with possibly both smooth and nonsmooth terms, like considered here.

2.60 Inertial Variants of Convex Programming Algorithms The key ingredient of accelerated algorithms is an extrapolation step based on the current and the immediate past iterate. From x° and x^-, a fast method computes a so-called leading point $\hat{x}^+ := x^\circ + \vartheta^\circ (x^\circ - x^-)$, where $\vartheta^\circ \in [0, 1]$. Hence, the leading point lies on the straight line segment between the current iterate x° and the point $2x^\circ - x^-$ that would result from taking a second step in the current direction $x^\circ - x^-$. Therefore, these methods are often referred to as 'inertial methods' or methods possessing 'momentum'. Function values, gradients or proximal maps are evaluated at the leading point instead of the iterate x°, to provide an estimate of higher fidelity for the next iteration.

2.61 Algorithm (FISTA / Accelerated Proximal Gradient Method) *Input:* $x^{(0)} \in X$
Initialisation: $k = 1$, $t^{(1)} = 1$, $\hat{x}^{(1)} = x^{(0)}$
Recursion: Set $L^{(k)} = L$ or find a valid $L^{(k)} > 0$ by backtracking and evaluate

$$x^{(k)} = \operatorname{prox}_{\frac{g}{L^{(k)}}} \left(\hat{x}^{(k)} - \frac{1}{L^{(k)}} \nabla f \left(\hat{x}^{(k)} \right) \right) \tag{FISTA.1}$$

If the algorithm has converged, *then return* $x^{(k)}$ and *stop*.
Compute

$$t^{(k+1)} = \frac{1 + \sqrt{1 + 4t^{(k)2}}}{2}, \tag{FISTA.2}$$

and update the leading point

$$\hat{x}^{(k+1)} = x^{(k)} + \frac{t^{(k)} - 1}{t^{(k+1)}} \left(x^{(k)} - x^{(k-1)} \right). \tag{FISTA.3}$$

Set $k \leftarrow k + 1$ and *go to* (FISTA.1). (FISTA.4)

2.62 Theorem (Convergence Rate of FISTA) *Let* $\left(x^{(k)}\right)_k \subset X$ *be generated by FISTA, where* $\left(L^{(k)}\right)_k \subset]0, +\infty[$ *is non-decreasing with* $\sup_k L^{(k)} =: \widetilde{L} < +\infty$. *For any* $\bar{x} \in \arg\min_{x \in X} I(x)$ *and* $k \in \mathbb{N}$

$$I(x^{(k)}) - I(\bar{x}) \leq \frac{2\widetilde{L} \left\| x^{(0)} - \bar{x} \right\|_X^2}{(k+1)^2}. \tag{2.16}$$

Proof. See Remark 2.1 and Theorem 4.4 in [48]. □

Properties and Variants of FISTA One of the strongest features of FISTA can be seen in the fact that from a computational perspective, the improved convergence rate has very little, if not negligible cost. In sharp contrast to bundle methods or quasi-Newton algorithms, FISTA gives rise to a very small memory footprint and there is no need for accumulating iteration history except for the last iterate. Compared to ISTA, extra computation time is needed for steps (FISTA.2) and (FISTA.3), which have no counterpart in the unaccelerated method. Evidently, the complexity of finding the weighted sum of x° and x^- is practically marginal against typical evaluations of the gradient and proximal operators in step (ISTA.1) or (FISTA.1), respectively.

The loss of monotonicity can be seen as a drawback. While the proximal gradient method decreases the objective in every iteration by design, such a property does not generally hold for its accelerated counterpart. Despite the higher convergence rate, the extrapolation step often results in iterations that overshoot the optimal region or spiralling trajectories. These characteristics are clearly visible in Figure 2.5 on the following page, where we compare the convergence of ISTA and FISTA in an archetypical composite convex problem. A monotone version of FISTA (MFISTA) can be found in [121]. Although relient on a number of heuristics, restarting schemes [120] can re-store (almost) monotone convergence as well.

The choice of extrapolation parameters $\vartheta^{(k)} := \frac{t^{(k)}-1}{t^{(k+1)}}$ with each $t^{(k)}$ defined recursively in (FISTA.2) is not unique. Alternative sequences are known that maintain the fast convergence rate of FISTA in terms of descent in the objective, but which can also simplify the convergence analysis for the iterates $\left(x^{(k)}\right)_k$ [122].

Inertial primal-dual methods with analogous extrapolational gradient steps have been investigated by several authors in recent years. Fast Douglas-Rachford and Peaceman-Rachford augmented Lagrangian methods are derived and studied in [89], [123]. Although ADMM and relatives are meanwhile well-understood, it is often difficult to derive quantitative rates of convergence. At this stage, it appears that a unified convergence theory is still missing. Nonetheless, a large number of results are available under various, sometimes rather restrictive assumptions or weakened measures of convergence [89], [124]–[130]. We refer to [49], [85], [86] for step size rules that accelerate the Chambolle-Pock algorithm for sufficiently regular problems. Chambolle and Pock also developed a fast and preconditioned primal-dual algorithm in [131]. Similarly, the variable-metric approach combined with the acceleration techniques of FISTA yields the following algorithm:

2.63 Algorithm (VM-FISTA / Accelerated Proximal Newton-Type Method) *Input:* $x^{(0)} \in X$

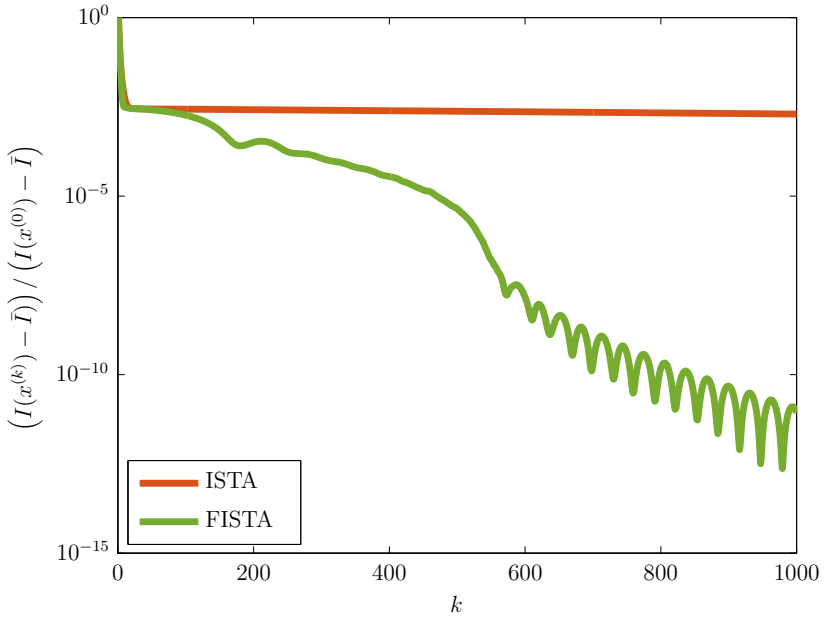

(a): Relative difference between function values at the first 1,000 iterates and the exact minimum $\bar{I} := I(\bar{x})$.

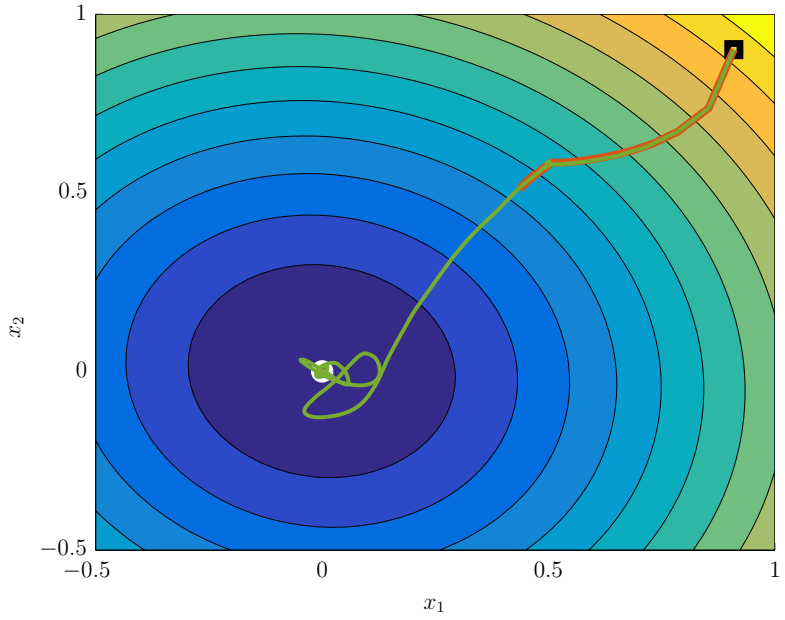

(b): Contour plot of the objective I with the trajectories of the first 500 iterates $(x^{(k)})_k$. Projection onto the two-dimensional affine subspace $\bar{x} + \operatorname{lin}\{(1,0,0,\ldots,0),(0,1,0,\ldots,0)\} \subset \mathbb{R}^d$.

Figure 2.5: Accelerating ISTA for finding $\bar{x} = \arg\min_{x\in\mathbb{R}^d} \left\{ I(x) = \frac{1}{2}|\mathcal{A}x - b|_2^2 + |x|_1 \right\}$, with $d = 2{,}000$ and data as in [120, Figure 5(a)]. In the semilogarithmic plot, function values appear to nearly stagnate for ISTA. The corresponding iterates, too, approach $\bar{x}$ very slowly compared to FISTA.

Initialisation: $k = 1$, $t^{(1)} = 1$, $\hat{x}^{(1)} = x^{(0)}$
Recursion: Define $\mathcal{H}^{(k)}$ and solve

$$\mathcal{H}^{(k)} \hat{d}^{(k)} = -\nabla f\left(\hat{x}^{(k)}\right). \tag{VM-FISTA.1}$$

Set $l^{(k)} = L/\underset{\sim}{L}$ or find a valid $l^{(k)} > 0$ by backtracking and evaluate

$$x^{(k)} = \operatorname{prox}_{\frac{g}{l^{(k)}}}^{\mathcal{H}^{(k)}}\left(\hat{x}^{(k)} + \frac{1}{l^{(k)}} \hat{d}^{(k)}\right) \tag{VM-FISTA.2}$$

If the algorithm has converged, *then return* $x^{(k)}$ and *stop*.
Compute

$$t^{(k+1)} = \frac{1 + \sqrt{1 + 4t^{(k)2}}}{2}, \tag{VM-FISTA.3}$$

and update the leading point

$$\hat{x}^{(k+1)} = x^{(k)} + \frac{t^{(k)} - 1}{t^{(k+1)}}\left(x^{(k)} - x^{(k-1)}\right). \tag{VM-FISTA.4}$$

Set $k \leftarrow k + 1$ and *go to* (VM-FISTA.1). (VM-FISTA.5)

This algorithm has also appeared in a recent preprint by Bonettini and co-authors [114], under the assumption $X = \mathbb{R}^d$. However, their analysis relies on the tools from [113] and [112] for variable-metric methods in general real Hilbert spaces. Since the operators involved are assumed to be bounded and bounded below, the restriction to the finite-dimensional case is in fact not necessary after all and the results remain valid in infinite dimensions. In particular, we have the following convergence theorem for VM-FISTA:

2.64 Theorem (Convergence Rate of VM-FISTA) *Let* $\left(\eta^{(k)}\right)_k \subset [0, +\infty[$ *be a summable sequence,* $\mathcal{H}^{(k+1)} \preccurlyeq \left(1 + \eta^{(k)}\right)\mathcal{H}^{(k)}$, *for all* $k \in \mathbb{N}$. *Then, with a constant* $C > 0$, *the sequence* $\left(x^{(k)}\right)_k \subset X$ *generated by VM-FISTA satisfies*

$$I(x^{(k)}) - I(\bar{x}) \leq \frac{C}{(k+1)^2}. \tag{2.17}$$

Proof. See Theorem 3.1 in [114]. □

Conclusions

There are, naturally, a number of further algorithmic approaches to convex programming, including interior point methods which we will not consider in our work. Even though the number of methods we have reviewed here including their various siblings is clearly extensive, most of them essentially consist of a composition of proximal or proximal-like maps. In comparison to augmented Lagrangian methods, proximal gradient and proximal NEWTON-type algorithms provide natural rules for choosing step-size parameters and can therefore do without many heuristics. We recall the optimal convergence estimates, low-cost iterations and adaptability to composite problems with smooth and nonsmooth terms as further strong bonuses. These observations make up the motivation behind this project to study these methods in particular.

2.65 Chronology Proximal NEWTON-type methods are a very recent acquisition, with the main contributions [106], [112] dating back to 2014. The early stages of this project in 2013 approached the topic from a different angle: semismooth NEWTON methods coupled with the concept of trust regions from nonlinear optimisation. Due to the cost that is required for evaluating second-order information for problems of very large scale, accelerated proximal gradient methods were expected to show comparable, if not better performance. Finally, fast proximal NEWTON-type methods promised to combine the advantages of acceleration and preconditioning with curvature information.

Let us briefly point out the interesting link between sequential quadratic programming (SQP) with trust-region constraints and proximal gradient methods with variable metrics. For simplicity*, we consider problems where g imposes a linear equality constraint with a surjective operator $\mathcal{A} \in L(X, Y)$ and $b \in Y$,

$$g = \iota_C, \qquad C := \{\, x \in X \mid \mathcal{A}x = b \,\}.$$

Since the gradient of f satisfies a LIPSCHITZ condition, Theorem 2.20 on page 25 implies that a Hessian $\nabla^2 f$ exists in the sense of NEWTON derivatives. This makes the problem of minimising $I = f + g$ amenable to semismooth NEWTON, or SQP methods. Given a feasible $x^\circ \in X$, one SQP iteration reads

$$\begin{aligned} d^\circ &\in \operatorname*{arg\,min}_{d \in X} \left\{ \langle \nabla f(x^\circ), d \rangle_X + \frac{1}{2} \langle \nabla^2 f(x^\circ) d, d \rangle_X \;\middle|\; \text{subject to } \mathcal{A}d = 0 \right\}, \\ x^+ &= x^\circ + d^\circ. \end{aligned}$$

*This approach would still be applicable for a broader class of functionals g, in particular NEWTON differentiable functionals or inequality constraints.

Unfortunately, d° may not be well-defined (consider the case $\nabla^2 f(x^\circ) = 0$ and $\nabla f(x^\circ) \neq 0$). This is where trust regions provide a remedy. With a *trust radius* $\Delta > 0$, the problem

$$\min_{d \in X} \left\{ \langle \nabla f(x^\circ), d \rangle_X + \frac{1}{2} \left\langle \nabla^2 f(x^\circ) d, d \right\rangle_X \;\middle|\; \text{subject to } \mathcal{A}d = 0 \wedge \|d\|_X \leq \Delta \right\}$$

is convex and now has a bounded domain due to the added *trust-region constraint*. It hence admits a solution. In practice, these quadratic programming (QP) problems are solved only very inexactly. It suffices that an approximate solution is feasible and meets a descent criterion (cf [132, pp 71-73 & 546-549]).

2.66 Lemma$^{(\mathrm{TT})}$ (Trust-Region SQP as VM-ISTA) *Let $x^\circ \in X$ such that $\mathcal{A}x^\circ = b$ and let $\Delta > 0$. Set $x^+ := x^\circ + d^\circ$, where d° is a solution to the trust-region constrained QP subproblem*

$$\min_{d \in X} \langle \nabla f(x^\circ), d \rangle_X + \frac{1}{2} \left\langle \nabla^2 f(x^\circ) d, d \right\rangle_X$$

subject to

$$\mathcal{A}d = 0 \quad \wedge \quad \|d\|_X \leq \Delta.$$

Then there exists $\lambda^\circ \geq 0$ such that x^+ solves the VM-ISTA subproblem

$$\min_{x \in X} \langle \nabla f(x^\circ), x - x^\circ \rangle_X + \frac{1}{2} \left\langle \left(\nabla^2 f(x^\circ) + \lambda^\circ \,\mathrm{id} \right) x - x^\circ, x - x^\circ \right\rangle_X$$

subject to

$$\mathcal{A}x = b.$$

Proof. The result can be established by an application of the Karush-Kuhn-Tucker (KKT) theory [133]: first, observe that we can re-formulate the trust-region constraint in a smooth manner:

$$\|d^\circ\|_X \leq \Delta \qquad \Longleftrightarrow \qquad 0 \leq \frac{1}{2} \left(\Delta^2 - \|d^\circ\|_X^2 \right).$$

The gradient of the right-hand side of this inequality with respect to d° is clearly $-d^\circ$.

Next, since the constraint qualification (2.5) holds by definition of the QP subproblem, there exist KKT multipliers [133] $p^\circ \in X$ and $\lambda^\circ \in \mathbb{R}$ such that

$$\begin{aligned} \nabla^2 f(x^\circ) d^\circ - \mathcal{A}^* p^\circ + \lambda^\circ d^\circ &= -\nabla f(x^\circ), \\ \mathcal{A}d^\circ &= 0, \\ 0 \leq \frac{1}{2} \left(\Delta^2 - \|d^\circ\|_X^2 \right) \perp \lambda^\circ &\geq 0, \end{aligned}$$

where the notation $\perp$ indicates that the product of the expression to the left and the expression to the right has to vanish. From the saddle-point problem in the first two KKT conditions we deduce

$$d^\circ \in \operatorname*{arg\,min}_{d \in X} \langle \nabla f(x^\circ), d \rangle_X + \frac{1}{2} \left\langle (\nabla^2 f(x^\circ) + \lambda^\circ \operatorname{id}) d, d \right\rangle_X + g(d - x^\circ).$$

With $x^+ = x^\circ + d^\circ$, this is nothing but the VM-ISTA recursion

$$x^+ \in \operatorname*{arg\,min}_{x \in X} M_1^{\mathcal{H}}(x^\circ, x),$$

if $\mathcal{H}^\circ := \nabla^2 f(x^\circ) + \lambda^\circ \operatorname{id}$. □

While generally $\nabla^2 f(x^\circ) \succcurlyeq 0$ and $\lambda^\circ \geq 0$, there may not be a lower bound $\underset{\sim}{L} > 0$ such that $\nabla^2 f(x^\circ) + \lambda^\circ \operatorname{id} \succcurlyeq \underset{\sim}{L} \operatorname{id}$. An actual iteration of VM-ISTA would have to choose $\lambda^\circ \geq \underset{\sim}{L} > 0$, if the spectrum of $\nabla^2 f(x^\circ)$ is not already bounded away from zero. In terms of the original trust-region SQP subproblem, such a modified step would still be feasible, but only optimal for a smaller trust radius $\Delta > 0$. This is a consequence of the following lemma, which contains a converse statement to the previous one.

2.67 Lemma[TT] (VM-ISTA as Trust-Region SQP) *Let $x^\circ \in X$ such that $\mathcal{A}x^\circ = b$ and choose $\lambda^\circ \geq 0$ and $l^\circ > 0$ for which $\mathcal{H}^\circ := \nabla^2 f(x^\circ)/l^\circ + \lambda^\circ \operatorname{id} \succcurlyeq \underset{\sim}{L} \operatorname{id}$. Define x^+ from x° by the VM-ISTA recursion*

$$x^+ = \operatorname{prox}_{\frac{g}{l^\circ}}^{\mathcal{H}^\circ} \left(x^\circ - \frac{1}{l^\circ} (\mathcal{H}^\circ)^{-1} \nabla f\,(x^\circ) \right).$$

Then there exists $\Delta > 0$ such that $d^\circ := x^+ - x^\circ$ is a solution of the trust-region problem

$$\min_{d \in X} \langle \nabla f(x^\circ), d \rangle_X + \frac{1}{2} \left\langle \nabla^2 f(x^\circ) d, d \right\rangle_X$$

subject to

$$\mathcal{A}d = 0 \quad \wedge \quad \|d\|_X \leq \Delta.$$

Proof. Writing out the proximal map of the VM-ISTA recursion, we obtain that x^+ is the solution of

$$\min_{x \in X} \langle \nabla f(x^\circ), x - x^\circ \rangle_X + \frac{1}{2} \left\langle \nabla^2 f(x^\circ) x - x^\circ, x - x^\circ \right\rangle_X + \frac{l^\circ \lambda^\circ}{2} \|x - x^\circ\|_X^2$$

subject to

$$\mathcal{A}x = b.$$

Hence, since as in the previous lemma sufficient regularity conditions are met, $d^\circ = x^+ - x^\circ$ solves the KKT system

$$\begin{aligned}\left(\nabla^2 f(x^\circ) + l^\circ \lambda^\circ \,\mathrm{id}\right) d^\circ - \mathcal{A}^* p^\circ &= -\nabla f(x^\circ) \\ \mathcal{A} x^\circ &= 0\end{aligned}$$

together with a multiplier $p^\circ \in X$. We now distinguish between two cases:

- If $l^\circ \lambda^\circ = 0$, then choose any $\Delta \geq \|d^\circ\|_X$.
- If $l^\circ \lambda^\circ > 0$, then set $\Delta = \|d^\circ\|_X$.

In both cases we have

$$0 \leq \frac{1}{2}\left(\Delta^2 - \|d^\circ\|_X^2\right) \perp l^\circ \lambda^\circ \geq 0$$

and we recover the KKT optimality conditions for the trust-region problem, implying that the assertion is true. □

There are efficient techniques available for solving the trust-region subproblems and for updating the trust radius from one iteration to another [134], [135]. Also the convergence of the method is unproblematic. Quantitative rate of convergence results for convex, but not necessarily strongly convex problems appear to be an open problem, though. We therefore implement proximal algorithms with their superior features in this respect, but point out that VM-ISTA can concurrently be interpreted as trust-region algorithm with a specific choice of trust radii.

Chapter 3

Proximal Algorithms in Hilbert Spaces

We develop our methodology for a broad class of composite convex minimisation problems. The central idea of our approach is to consider a formulation with split primal variables and study the corresponding dual problem. This has three main advantages: for the class of problems under consideration, the dual offers (i) attractive smoothness properties, (ii) proximal maps which are potentially far easier to evaluate than for the primal problem, and (iii) tools for deriving convergence rates in the desired topology.

We begin in Section (A) by specifying our concrete assumptions on the problem and by stating some crucial properties. In Section (B), we introduce our dual-based proximal gradient and proximal Newton-type algorithms and conclude this chapter with the analysis of their convergence in Section (C).

(A) Problem Formulations and Key Features

The optimisation problems we consider are of the form

$$\min_{x \in X} \{\, I(x) := f(\mathcal{A}x) + g(x) \,\}, \tag{P}$$

where we assume that the following prerequisites are met:

3.1 Assumption (Problem (P)) (a) X and Y are real Hilbert spaces with scalar products $\langle \cdot, \cdot \rangle_X$, $\langle \cdot, \cdot \rangle_Y$ and induced norms $\| \cdot \|_X$, $\| \cdot \|_Y$. We identify the dual of Y with the space Y itself, $Y^* \cong Y$.

(b) $f : Y \to]-\infty, +\infty]$ and $g : X \to]-\infty, +\infty]$ are proper, convex and lower semicontinuous functionals, where f is strongly convex with strong convexity parameter

$\sigma > 0$.

(c) $\mathcal{A} : X \to Y$ is a bounded linear operator with adjoint $\mathcal{A}^* : Y^* \to X^*$. We assume that $\mathcal{A}$ is bounded below on the domain of g in the following, generalised sense:

$$\exists C > 0 \quad \forall x_1, x_2 \in \operatorname{dom} g : \quad \|\mathcal{A}x_1 - \mathcal{A}x_2\|_Y \geq C\|x_1 - x_2\|_X. \tag{3.1}$$

This condition is equivalent to $\mathcal{A}$ being one-to-one and closed on $\operatorname{dom} g$ [136, pp 70-71]. As an example in finite dimensions, where $\mathcal{A}$ is a matrix, the smallest singular value of $\mathcal{A}$ defines the largest possible C.

(d) The problem satisfies a qualification condition. In Euclidean spaces, Slater's condition

$$\operatorname{relint}\left(\operatorname{dom}(f \circ \mathcal{A}) \cap \operatorname{dom} g\right) \neq \emptyset \tag{3.2}$$

serves this purpose, i.e. the functionals $f \circ \mathcal{A}$ and g have overlapping domains and the relative interior of their intersection is non-empty. Otherwise, in general Hilbert spaces, we impose the continuity condition

$$\exists x \in \operatorname{dom}(f \circ \mathcal{A} + g) : \quad f \text{ is continuous at } \mathcal{A}x. \tag{3.3}$$

3.2 Proposition (Existence and Uniqueness of Solutions) *Problem (P) admits a unique solution $\bar{x} \in X$.*

Proof. Since $f \circ \mathcal{A}$ and g have overlapping domains*, there is at least one $x \in X$ for which the objective assumes a finite value.

Boundedness below of $\mathcal{A}$ as per the inequality in (3.1) allows us to transfer the strong convexity of f to the composite function $f \circ \mathcal{A}$. Thus, the objective I is coercive:

$$f(\mathcal{A}x) + g(x) \to +\infty, \qquad \text{as } \|x\|_X \to \infty.$$

Hence, the prerequisites for Theorem 2.26 on page 28 are met, which yields the existence and uniqueness of a solution. □

3.3 Equivalent Formulations By our identification $Y^* \cong Y$, we obtain the structure

$$X \xrightarrow{\mathcal{A}} Y \cong Y^* \xrightarrow{\mathcal{A}^*} X^*$$

*the weaker condition $\operatorname{dom}(f \circ \mathcal{A}) \cap \operatorname{dom} g \neq \emptyset$ instead of the qualification condition (3.2) or (3.3), respectively, is already sufficient here

in a somewhat similar fashion to a GELFAND triple. We continue to suppress any RIESZ isomorphisms between Y and Y^* in order to simplify the notation.

Following our exposition in Section (D) of the last chapter, we may equivalently rewrite Problem (P) as the linearly constrained minimisation problem

$$\min_{(x,y)\in X\times Y} f(y) + g(x) \qquad \text{subject to } y = \mathcal{A}x \tag{P$'$}$$

to benefit from the extra flexibility of being able to minimise f and g separately. With a dual variable (or LAGRANGE multiplier) $\lambda \in Y$, we may handle the equality constraint in (P$'$) by a maximisation with respect to λ:

$$\max_{\lambda\in Y} \min_{(x,y)\in X\times Y} L(x,y,\lambda) = f(y) + g(x) - \langle \lambda, y - \mathcal{A}x\rangle_Y. \tag{PD$'$}$$

Finally, to eliminate the primal variables from the problem, we carry out the minimisation with respect to (x, y) in (PD$'$) to obtain the dual problem in terms of λ only. With the convex conjugates f^* and g^* of f and g, the dual problem reads

$$\max_{\lambda\in Y} -f^*(\lambda) - g^*(-\mathcal{A}^*\lambda). \tag{D}$$

For convenience, we re-write Problem (D) in the simpler form

$$\min_{\lambda\in Y} \{\, J(\lambda) := F(\lambda) + G(\lambda) \,\} \tag{D$'$}$$

with the convex functionals F and $G : Y \to (-\infty, +\infty]$ defined as

$$F(\lambda) := f^*(\lambda), \qquad G(\lambda) := g^*(-\mathcal{A}^*\lambda).$$

(D$'$) is the formulation that we choose for approaching the problem numerically by proximal gradient or NEWTON-type methods. Let us therefore ensure that our strategy is sensible and well-defined. Indeed, solutions to the dual problem and the necessary derivatives exist, as we point out next.

3.4 Strong Duality Since a qualification condition holds for the primal problem, and since its infimum is finite, we conclude with Theorem 2.32 on page 31 that strong duality holds. In other words, there also exists a solution $\bar{\lambda}$ of the dual problem and there is no duality gap. Hence, for an optimal solution $(\bar{x}, \bar{y}, \bar{\lambda}) \in X \times Y \times Y$,

$$f(\mathcal{A}\bar{x}) + g(\bar{x}) = -f^*(\bar{\lambda}) - g^*(-\mathcal{A}^*\bar{\lambda}), \tag{3.4}$$

and the objectives of problems (P), (P′) and (D) all assume the same value, which also agrees with $-J(\bar{\lambda})$ in (D′).

3.5 Smoothness of the Dual Problem We recall that proximal gradient methods such as FISTA (Algorithm 2.61 on page 48) and its variable metric extension VM-FISTA (Algorithm 2.63 on page 49) rely on the differentiability of at least one of the functionals F or G, with Lipschitz-continuous gradients. The functional f in the primal problem is σ-strongly convex. A classical result on convex conjugates, which we quote here for convenience, implies the desired smoothness of the functional F in the dual problem.

3.6 Lemma (First-Order Differentiability) *F is Fréchet-differentiable and the gradient satisfies a global Lipschitz condition with Lipschitz constant $1/\sigma$.*

Proof. See Theorem 18.15 (i),(vii) in [56, p 270]. □

We also recall the following property of F, which allows us to define variable metrics based on an actual second derivative:

3.7 Lemma (Second-Order Differentiability) *The gradient ∇F is globally Newton-differentiable.*

Proof. The assertion is a simple corollary of Lemma 3.6 and Theorem 2.20 on page 25. □

(B) Dual-Based Algorithms

Our objective for this section is to present numerical methods for solving (P). Since these methods are based on the dual formulation of the problem, we first express the resulting algorithms solely in terms of the data of the original problem. This also allows us to make comparisons to some related primal-dual methods, which we reviewed in Chapter 2.

3.8 New Contributions Beck and Teboulle [137] very recently developed an algorithm for composite convex problems of the form (P), where g, instead of f, is strongly convex. Our procedure is analogous as far as the application of FISTA to the dual problem is concerned. The similarity between the problem studied by the two authors and the problem under consideration here implies that we may borrow some of their ideas, which we point out in the sequel. However, there are also a number of differences between the approach of Beck and Teboulle and the methodology in this work: firstly, since we consider possibly infinite-dimensional Hilbert spaces and not just Euclidean spaces, we require different, and partially stronger regularity assumptions whenever not

necessarily equivalent properties collapse in the finite-dimensional setting. Similarly, little assumptions on the operator $\mathcal{A}$ are needed when it is coupled with the general convex functional g. The composition of the strongly convex functional f with the operator $\mathcal{A}$ in our work gives rise to some additional difficulties and requires further assumptions on $\mathcal{A}$ to achieve well-posedness and convergence. Our techniques for preconditioning by variable metrics make up a further extension to the dual FISTA algorithm in [137]. In order to obtain solutions of high accuracy as efficiently as possible, we also shed some light on various options for a computational implementation in greater detail.

Derivation of the Methods

The main step in each iteration of the accelerated proximal NEWTON-type method VM-FISTA applied to the dual problem (D′) consists in an evaluation of the scaled proximal operator at the leading point $\hat{\lambda}^\circ$

$$\lambda^\circ = \operatorname{prox}_{\frac{G}{l^\circ}}^{\mathcal{H}^\circ}\left(\hat{\lambda}^\circ - \frac{1}{l^\circ}\left(\mathcal{H}^\circ\right)^{-1}\nabla F\left(\hat{\lambda}^\circ\right)\right)$$

in steps (VM-FISTA.1) and (VM-FISTA.2) on page 51. We recall our assumptions:

- $\mathcal{H}^\circ \in L(Y,Y)$ is a self-adjoint operator, which we think of as an approximation $\mathcal{H}^\circ \approx \nabla^2 F\left(\hat{x}^\circ\right)$ to a Hessian of F at $\hat{x}^\circ$
- With the LIPSCHITZ constant $L := \frac{1}{\sigma}$ of ∇F, there exist constants $0 < \underset{\sim}{L} \leq L \leq \widetilde{L} < +\infty$, such that all operators $\mathcal{H}^\circ$ have a bounded spectrum in $\left[\underset{\sim}{L}, \widetilde{L}\right]$, or equivalently, the condition $\underset{\sim}{L}\,\mathrm{id} \preccurlyeq \mathcal{H}^\circ \preccurlyeq \widetilde{L}\,\mathrm{id}$ holds uniformly.
- $L^\circ \in \left[\underset{\sim}{L}, \widetilde{L}\right]$ is an estimate of L and $l^\circ := \frac{L^\circ}{\underset{\sim}{L}}$.

The special case without preconditioning is recovered by setting $\mathcal{H}^\circ = L^\circ\,\mathrm{id}$ and $l^\circ \equiv 1$, which yields the unscaled proximal map

$$\lambda^\circ = \operatorname{prox}_{\frac{G}{L^\circ}}\left(\hat{\lambda}^\circ - \frac{1}{L^\circ}\nabla F\left(\hat{\lambda}^\circ\right)\right)$$

of (FISTA.1) on page 48. In terms of the functionals f and g from the primal problem (P), these assignments can be formulated as follows:

3.9 Lemma$^{(\mathrm{TT})}$ (Dual Proximal Map in Terms of Primal Data) *Let $\hat{\lambda}^\circ \in Y$ be given and define*

$$\hat{y}^\circ := \operatorname*{arg\,max}_{y \in Y}\left\langle \hat{\lambda}^\circ, y\right\rangle_Y - f(y) \tag{3.5a}$$

$$\hat{x}^\circ := \operatorname*{arg\,min}_{x\in X} l^\circ g(x) + \frac{1}{2}\left\|\mathcal{A}x - \left(\hat{y}^\circ - l^\circ \mathcal{H}^\circ \hat{\lambda}^\circ\right)\right\|^2_{(\mathcal{H}^\circ)^{-1}} \tag{3.5b}$$

$$\lambda^\circ := \hat{\lambda}^\circ + \frac{1}{l^\circ}\left(\mathcal{H}^\circ\right)^{-1}\left(\mathcal{A}\hat{x}^\circ - \hat{y}^\circ\right). \tag{3.5c}$$

Then

$$\lambda^\circ = \operatorname{prox}^{\mathcal{H}^\circ}_{\frac{G}{l^\circ}}\left(\hat{\lambda}^\circ - \frac{1}{l^\circ}\left(\mathcal{H}^\circ\right)^{-1}\nabla F\left(\hat{\lambda}^\circ\right)\right). \tag{3.6}$$

In the fixed-metric case, the assignments

$$\hat{y}^\circ := \operatorname*{arg\,max}_{y\in Y}\left\langle \hat{\lambda}^\circ, y\right\rangle_Y - f(y) \tag{3.7a}$$

$$\hat{x}^\circ := \operatorname*{arg\,min}_{x\in X} L^\circ g(x) + \frac{1}{2}\left\|\mathcal{A}x - \left(\hat{y}^\circ - L^\circ\hat{\lambda}^\circ\right)\right\|^2_Y \tag{3.7b}$$

$$\lambda^\circ := \hat{\lambda}^\circ + \frac{1}{L^\circ}\left(\mathcal{A}\hat{x}^\circ - \hat{y}^\circ\right) \tag{3.7c}$$

imply

$$\lambda^\circ = \operatorname{prox}_{\frac{G}{L^\circ}}\left(\hat{\lambda}^\circ - \frac{1}{L^\circ}\nabla F\left(\hat{\lambda}^\circ\right)\right). \tag{3.8}$$

Proof. The qualification condition (3.3) guarantees that we have all the rules for subdifferential calculus in Lemma 2.24 on page 27 available. Our statements are a variation and generalisation of the analogous Lemma 3.2 in [137], but the different structure of our problem means that we have to deviate in our analysis from Beck and Teboulle to prove the assertion of this lemma.

First of all, let us verify that each assignment in (3.5) and (3.7) is well-defined. Indeed, the strict convexity of f yields the unique solvability of the maximisation problems (3.5a) and (3.7a). Also $\hat{x}^\circ$ in (3.5b) and (3.7b) are well-defined. This is a consequence of $\mathcal{A}$ being bounded below on $\operatorname{dom} g$, according to assumption (3.1).

We will verify the assertion for the general case with variable metrics only, as (3.7) is clearly recovered from (3.5) by particular choices of $\mathcal{H}^\circ$ and l° like above.

Consider the optimisation problem (3.5a) for finding $\hat{y}^\circ$. We recognise that $\hat{y}^\circ$ is the maximising argument in the definition of the conjugate $f^* = F$. With Lemma 2.29 on page 29 it follows

$$\hat{y}^\circ = \nabla F(\hat{\lambda}^\circ). \tag{3.9}$$

Let us move on to the proximal-like assignment (3.5b). The solution $\hat{x}^\circ$ is characterised by the optimality condition (cf Theorem 2.25 on page 28)

$$-\mathcal{A}^*\left(\mathcal{H}^\circ\right)^{-1}\left[\mathcal{A}\hat{x}^\circ - \left(\hat{y}^\circ - l^\circ\mathcal{H}^\circ\hat{\lambda}^\circ\right)\right] \in l^\circ \partial g\left(\hat{x}^\circ\right).$$

Meanwhile, we can re-arrange (3.5c) to $l^\circ \mathcal{H}^\circ \left(\lambda^\circ - \hat{\lambda}^\circ\right) = \mathcal{A}\hat{x}^\circ - \hat{y}^\circ$, so we may substitute

$$-\mathcal{A}^* \left(\mathcal{H}^\circ\right)^{-1} \left[l^\circ \mathcal{H}^\circ \left(\lambda^\circ - \hat{\lambda}^\circ\right) + l^\circ \mathcal{H}^\circ \hat{\lambda}^\circ\right] \in l^\circ \partial g\left(\hat{x}^\circ\right),$$

which collapses to

$$-\mathcal{A}^* \lambda^\circ \in \partial g\left(\hat{x}^\circ\right).$$

Another application of the maximising-argument property of the subdifferential yields

$$\hat{x}^\circ \in \partial g^*\left(-\mathcal{A}^* \lambda^\circ\right).$$

Recalling $G = g^* \circ (-\mathcal{A}^*)$, we infer

$$-\mathcal{A}\hat{x}^\circ \in -\mathcal{A}\partial g^*\left(-\mathcal{A}^* \lambda^\circ\right) = \partial G\left(\lambda^\circ\right). \tag{3.10}$$

By (3.5c), $\mathcal{A}\hat{x}^\circ = \hat{y}^\circ + l^\circ \mathcal{H}^\circ \left(\lambda^\circ - \hat{\lambda}^\circ\right)$, with $\hat{y}^\circ = \nabla F(\hat{\lambda}^\circ)$ according to (3.9). Hence,

$$-\nabla F(\hat{\lambda}^\circ) - l^\circ \mathcal{H}^\circ \left(\lambda^\circ - \hat{\lambda}^\circ\right) \in \partial G\left(\lambda^\circ\right).$$

Re-arranging provides us with

$$-\mathcal{H}^\circ \left[\lambda^\circ - \left(\hat{\lambda}^\circ - \frac{1}{l^\circ} \left(\mathcal{H}^\circ\right)^{-1} \nabla F\left(\hat{\lambda}^\circ\right)\right)\right] \in \frac{1}{l^\circ} \partial G\left(\lambda^\circ\right),$$

which is the optimality condition that corresponds to the problem

$$\begin{aligned} \lambda^\circ &= \operatorname*{arg\,min}_{\lambda \in Y} \frac{1}{l^\circ} G(\lambda) + \frac{1}{2} \left\| \lambda - \left(\hat{\lambda}^\circ - \frac{1}{l^\circ} \left(\mathcal{H}^\circ\right)^{-1} \nabla F\left(\hat{\lambda}^\circ\right)\right)\right\|_{\mathcal{H}^\circ}^2 \\ &= \operatorname{prox}_{\frac{G}{l^\circ}}^{\mathcal{H}^\circ} \left(\hat{\lambda}^\circ - \frac{1}{l^\circ} \left(\mathcal{H}^\circ\right)^{-1} \nabla F\left(\hat{\lambda}^\circ\right)\right). \end{aligned}$$

□

Since both (3.5) and (3.6) determine λ° uniquely, the two statements are actually equivalent. The same holds true for (3.7) and (3.8).

3.10 Primal Sequences Lemma 3.9 admits an important conclusion: even though we only tackle the dual problem with $\lambda \in Y$ as its only variable, an evaluation of the proximal map automatically supplies corresponding primal variables as intermediate results. In that respect, we essentially derive a primal-dual algorithm. From a numerical viewpoint, it is highly expedient that these approximations of the exact solution $(\bar{x}, \bar{y})$ require no extra computations. We will however see later on that a primal sequence defined from the iterate λ°, not the leading point $\bar{\lambda}^\circ$, may be preferable.

We consider three alternatives for defining a sequence $\left(x^{(k)}, y^{(k)}\right)_k \subset X \times Y$ corresponding to the dual sequence $\left(\lambda^{(k)}, \hat{\lambda}^{(k)}\right)_k \subset Y \times Y$ computed by the algorithms FISTA or VM-FISTA. The first option is given by replacing $\left(\hat{x}^\circ, \hat{y}^\circ, \hat{\lambda}^\circ\right)$ in (3.5a) and (3.5b) with $(x^\circ, y^\circ, \lambda^\circ)$. Then, for all $k \in \mathbb{N}_0$, we have

$$\begin{cases} y^{(k)} := \operatorname*{arg\,max}_{y \in Y} \left\langle \lambda^{(k)}, y \right\rangle_Y - f(y) & \text{(3.11a)} \\ x^{(k)} := \operatorname*{arg\,min}_{x \in X} l^{(k)} g(x) + \frac{1}{2} \left\| \mathcal{A}x - \left(y^{(k)} - l^{(k)} \mathcal{H}^{(k)} \lambda^{(k)} \right) \right\|^2_{\left(\mathcal{H}^{(k)}\right)^{-1}}. & \text{(3.11b)} \end{cases}$$

With the same definition for $y^{(k)}$, one could also determine a corresponding $x^{(k)}$ from a least-squares problem

$$\begin{cases} y^{(k)} := \operatorname*{arg\,max}_{y \in Y} \left\langle \lambda^{(k)}, y \right\rangle_Y - f(y) & \text{(3.12a)} \\ x^{(k)} := \operatorname*{arg\,min}_{x \in \operatorname{dom} g} \frac{1}{2} \left\| \mathcal{A}x - y^{(k)} \right\|^2_Y, & \text{(3.12b)} \end{cases}$$

which has a unique solution since g is proper and $\mathcal{A}$ bounded below on $\operatorname{dom} g$. One can expect that the latter problem is often easier to solve than (3.11b). No nonlinearities of g other than the geometry of $\operatorname{dom} g$ affect the solution of (3.12b), nor does it require assembling or even inverting the Hessian approximation $\mathcal{H}^{(k)}$. A further interesting feature is the lack of an explicit dependence on $\lambda^{(k)}$. This will shortly allow us to control the error $\left\| x^{(k)} - \bar{x} \right\|_X$ in the x-component solely by the error of the y-iterate, $\left\| y^{(k)} - \mathcal{A}\bar{x} \right\|_Y$.

For the third option, we record

$$\begin{cases} y^{(k)} := \hat{y}^{(k)} & \text{(3.13a)} \\ x^{(k)} := \hat{x}^{(k)}, & \text{(3.13b)} \end{cases}$$

the sequence of leading points, which are already available.

We are now in the position to formulate our dual-based proximal gradient and proximal Newton-type methods.

3.11 Algorithm$^{(\mathrm{TT})}$ (FISTA* / Accelerated Dual Proximal Gradient Method) *Input:* $\lambda^{(0)} \in Y$, a strong convexity parameter $\sigma > 0$ of f
Initialisation: $k = 1$, $t^{(1)} = 1$, $\hat{\lambda}^{(1)} = \lambda^{(0)}$
Recursion: Set $L^{(k)} = \frac{1}{\sigma}$ or find a valid $L^{(k)} > 0$ by backtracking and evaluate

$$\hat{y}^{(k)} := \operatorname*{arg\,max}_{y \in Y} \left\langle \hat{\lambda}^{(k)}, y \right\rangle_Y - f(y) \qquad \text{(FISTA*.1)}$$

$$\hat{x}^{(k)} := \operatorname*{arg\,min}_{x\in X} L^{(k)} g(x) + \frac{1}{2}\left\|\mathcal{A}x - \left(\hat{y}^{(k)} - L^{(k)}\hat{\lambda}^{(k)}\right)\right\|_Y^2 \tag{FISTA*.2}$$

$$\lambda^{(k)} := \hat{\lambda}^{(k)} + \frac{1}{L^{(k)}}\left(\mathcal{A}\hat{x}^{(k)} - \hat{y}^{(k)}\right) \tag{FISTA*.3}$$

If the algorithm has converged, *then* compute $\left(x^{(k)}, y^{(k)}\right)$ from (3.11), (3.12) or (3.13), *return* $\left(x^{(k)}, y^{(k)}, \lambda^{(k)}\right)$ and *stop*.
Find

$$t^{(k+1)} = \frac{1+\sqrt{1+4t^{(k)2}}}{2}, \tag{FISTA*.4}$$

and update the leading point

$$\hat{\lambda}^{(k+1)} = \lambda^{(k)} + \frac{t^{(k)}-1}{t^{(k+1)}}\left(\lambda^{(k)} - \lambda^{(k-1)}\right). \tag{FISTA*.5}$$

Set $k \leftarrow k+1$ and *go to* (FISTA*.1). (FISTA*.6)

3.12 Algorithm$^{(TT)}$ (VM-FISTA* / Accelerated Dual Proximal Newton-Type Method)
Input: $\lambda^{(0)} \in Y$, a strong convexity parameter $\sigma > 0$ of f
Initialisation: $k = 1$, $t^{(1)} = 1$, $\hat{\lambda}^{(1)} = \lambda^{(0)}$
Recursion: Define $\mathcal{H}^{(k)}$. Set $l^{(k)} = \frac{1}{L\sigma}$ or find a valid $l^{(k)} > 0$ by backtracking and evaluate

$$\hat{y}^{(k)} := \operatorname*{arg\,max}_{y\in Y}\left\langle \hat{\lambda}^{(k)}, y\right\rangle_Y - f(y) \tag{VM-FISTA*.1}$$

$$\hat{x}^{(k)} := \operatorname*{arg\,min}_{x\in X} l^{(k)} g(x) + \frac{1}{2}\left\|\mathcal{A}x - \left(\hat{y}^{(k)} - l^{(k)}\mathcal{H}^{(k)}\hat{\lambda}^{(k)}\right)\right\|^2_{\left(\mathcal{H}^{(k)}\right)^{-1}} \tag{VM-FISTA*.2}$$

$$\lambda^{(k)} := \hat{\lambda}^{(k)} + \frac{1}{l^{(k)}}\left(\mathcal{H}^{(k)}\right)^{-1}\left(\mathcal{A}\hat{x}^{(k)} - \hat{y}^{(k)}\right) \tag{VM-FISTA*.3}$$

If the algorithm has converged, *then* compute $\left(x^{(k)}, y^{(k)}\right)$ from (3.11), (3.12) or (3.13), *return* $\left(x^{(k)}, y^{(k)}, \lambda^{(k)}\right)$ and *stop*.
Find

$$t^{(k+1)} = \frac{1+\sqrt{1+4t^{(k)2}}}{2}, \tag{VM-FISTA*.4}$$

and update the leading point

$$\hat{\lambda}^{(k+1)} = \lambda^{(k)} + \frac{t^{(k)}-1}{t^{(k+1)}}\left(\lambda^{(k)} - \lambda^{(k-1)}\right). \tag{VM-FISTA*.5}$$

Set $k \leftarrow k+1$ and *go to* (VM-FISTA*.1). (VM-FISTA*.6)

Comparable Algorithms

As we outlined in our review in Chapter 2, Section (D), an array of alternative methods is available to solve composite convex minimisation problems of the form (P). Since conventional algorithms do not include the extrapolation step to determine a leading point, let us consider the non-inertial counterpart of the dual FISTA method, i.e. the dual ISTA method. With no leading point, defining an extra primal sequence becomes redundant.

3.13 Algorithm (ISTA* / Dual Proximal Gradient Method) *Input:* $\lambda^{(0)} \in Y$, a strong convexity parameter $\sigma > 0$ of f
Initialisation: $k = 1$
Recursion: Set $L^{(k)} = \frac{1}{\sigma}$ or find a valid $L^{(k)} > 0$ by backtracking and evaluate

$$y^{(k)} := \operatorname*{arg\,max}_{y \in Y} \left\langle \lambda^{(k-1)}, y \right\rangle_Y - f(y) \tag{ISTA*.1}$$

$$x^{(k)} := \operatorname*{arg\,min}_{x \in X} L^{(k)} g(x) + \frac{1}{2} \left\| \mathcal{A}x - \left(y^{(k)} - L^{(k)} \lambda^{(k-1)} \right) \right\|_Y^2 \tag{ISTA*.2}$$

$$\lambda^{(k)} := \lambda^{(k-1)} + \frac{1}{L^{(k)}} \left(\mathcal{A}x^{(k)} - y^{(k)} \right) \tag{ISTA*.3}$$

If the algorithm has converged, *then return* $\left(x^{(k)}, y^{(k)}, \lambda^{(k)}\right)$ and *stop*.

Set $k \leftarrow k + 1$ and *go to* (ISTA*.1). (ISTA*.4)

3.14 Alternating Direction Method of Multipliers We recall that the proximal gradient method applied to the dual corresponds to Tseng's splitting scheme [103].

Very closely related is the classical ADMM: the update for the dual variable in (ISTA*.3) is evidently identical to the corresponding equation (ALG2.3) on page 37, as long as the step size $t^{(k)}$ in the augmented Lagrangian method is chosen to equal $1/L^{(k)}$. Simple algebraic manipulation also shows that the minimisation problem to determine $x^{(k)}$ in (ALG2.1) is equivalent to (ISTA*.2), if the penalty parameter $\varrho^{(k)}$ of the augmented Lagrangian equals $1/L^{(k)}$ as well. Glowinski and Le Tallec [77, p 89] comment how for ALG2, experience indicates that setting $t^{(k)} = \varrho^{(k)} \equiv \varrho$ is indeed optimal. If f is twice continuously differentiable, then 'a good strategy' for fixing this constant ϱ is, according to the authors, selecting a value 'of the order of the spectral radius of the Hessian operator' of f.

For the dual proximal gradient method, the globally best choice for $1/L$ is the strong convexity parameter σ. If there exists a Hessian of f, then σ is not given by the spectral radius, i.e. the supremum of the spectrum of that Hessian operator, but by the infimum

of that spectrum.

The two methods ADMM and dual ISTA differ in their definition of the iterates $y^{(k)}$. We can re-arrange (ALG2.2) to obtain

$$y^{(k)} := \operatorname*{arg\,max}_{y \in Y} \left\langle \lambda^{(k-1)}, y \right\rangle_Y - f(y) - \frac{\varrho^{(k)}}{2} \left\| y - \mathcal{A}x^{(k)} \right\|_Y^2 ,$$

whereas in (ISTA*.1) we have $\varrho^{(k)} \equiv 0$. Here we recognise the generic character of ADMM in that it does not exploit the strong convexity of f, as it adds a quadratic term in y regardless. If, as is typically the case, a strongly convex f already contains a quadratic term, then the addition of another quadratic would not change the structure of the problem compared to (ISTA*.1), but only affect the coefficients of some polynomial terms.

We therefore conclude that the computational expenses associated with the alternating direction method of multipliers and the dual proximal gradient method are virtually identical. For problems with strongly convex f, the latter method advantageously provides a reference point for choosing the step size parameters, and no heuristics are required.

3.15 Chambolle-Pock Algorithm The subproblems that arise in the primal-dual method of Chambolle and Pock (see page 39) consist of similar evaluations of proximal mappings, apart from one notable exception: we emphasise that in contrast to the minimisation problems (FISTA*.2), (ISTA*.2) and (ALG2.1) for determining $x^{(k)}$, the corresponding problem (CP.2) does not include the operator $\mathcal{A}^*\mathcal{A}$. For finite-dimensional problems, where this normally implies a major simplification for computing $x^{(k)}$, a clear preference should be given to the Chambolle-Pock algorithm, with a step-size rule for optimal worst-case convergence behaviour. To the contrary, we refer back to our observation that in function spaces (CP.2) is not generally any easier to solve than the analogous problems of the augmented Lagrangian or dual proximal algorithms. In such applications, one would therefore not anticipate any noteworthy differences in the performance of the accelerated algorithms introduced here, and an accelerated Chambolle-Pock method.

All of these primal-dual or dual methods share in common that their iterates are not necessarily feasible. By each definition of the primal iterates, we generally have $x^{(k)} \in \operatorname{dom} g$ and $y^{(k)} \in \operatorname{dom} f$, for all $k \in \mathbb{N}$. However, $\mathcal{A}x^{(k)} \in \operatorname{dom} f$ is not necessarily true. Likewise, $y^{(k)}$ is not guaranteed to lie in the range of $\mathcal{A}$ over $\operatorname{dom} g$, as there may be no $x \in \operatorname{dom} g$ such that $y^{(k)} = \mathcal{A}x$. In fact, $y^{(k)}$ generally does not even belong to the range of $\mathcal{A}$ at all.

The solution $(\bar{x}, \bar{y})$ of (P') is feasible, of course. Strong convergence of the primal iterates $\left(x^{(k)}, y^{(k)}\right)$ towards $(\bar{x}, \bar{y})$ and the feasible manifold therefore represents a substantial touchstone for a numerical method. It turns out that the methods proposed here do in fact meet this requirement, as we will show in the following.

(C) Convergence Analysis

This section is devoted to studying the convergence of the dual-based proximal algorithms. We derive convergence rates that are

- *non-ergodic*, i.e. which refer to the approximate optimality of the k^{th} iterate itself, instead of weighted averages over iterates $i = 1, \ldots, k$,
- *global* and *non-asymptotic*, i.e. which hold true for all $k \in \mathbb{N}$.

To this end, we first derive a few auxiliary results on the various alternative choices of primal sequences. They will allow us to establish our main result: strong convergence of the primal iterates at a rate of at least $O(1/k)$, under suitable assumptions. To round off this chapter, we shall introduce some strategies for optimising the efficiency of a computational implementation.

3.16 Assumption (Parameters of the Proximal Algorithms) Let us repeat the assumptions on the step-size sequences that we have to impose for the convergence of (F)ISTA. If a backtracking strategy is used for estimating the Lipschitz constant $L = 1/\sigma$ of ∇F, then $(L^{(k)})_k \subset]0, +\infty[$ is non-decreasing and bounded above by $\widetilde{L} > 0$. Consequently, this implies analogous properties for the scaled approximate Lipschitz constants $l^{(k)} = L^{(k)}/\underset{\sim}{L}$ in the variable metric case. For VM-(F)ISTA, the Hessian approximations furthermore satisfy $\underset{\sim}{L}\,\mathrm{id} \preccurlyeq \mathcal{H}^{(k)} \preccurlyeq \widetilde{L}\,\mathrm{id}$ as well as $\mathcal{H}^{(k+1)} \preccurlyeq \left(1 + \eta^{(k)}\right)\mathcal{H}^{(k)}$, for all $k \in \mathbb{N}$ and a summable sequence $\left(\eta^{(k)}\right)_k \subset [0, +\infty]$.

The convergence theorems for the accelerated proximal gradient method (Theorem 2.62 on page 48) and the accelerated proximal Newton-type method (Theorem 2.64 on page 51) provide upper bounds for the difference between the dual objective value at the current iterate $\lambda^{(k)}$ and the minimum of J. We will therefore attempt to establish this optimality gap as a bound for the error of the primal iterates. We will discuss the situation for each of the three alternatives separately.

Properties of the Proximal-Based Primal Sequence (3.11)

If we define the primal sequence $\left(x^{(k)}\right)_k$ by evaluating the proximal map also at $\lambda^{(k)}$, in addition to $\hat{\lambda}^{(k)}$, then we encounter another minimisation problem that includes the

norm $\|\cdot\|_{(\mathcal{H}^{(k)})^{-1}}$. A uniform estimate on this norm over all $k \in \mathbb{N}$ is crucial for proving convergence of this primal sequence.

3.17 Lemma[TT] (Norms Scaled by $(\mathcal{H}^{(k)})^{-1}$) *For all $y \in Y$ and any $k \in \mathbb{N}$,*

$$\frac{1}{\widetilde{\widetilde{L}}} \|y\|_Y^2 \leq \|y\|_{(\mathcal{H}^{(k)})^{-1}}^2 \leq \frac{1}{\underset{\sim}{\underset{\sim}{L}}} \|y\|_Y^2$$

Proof. If $\mathcal{H}^{(k)}$ satisfies

$$\underset{\sim}{\underset{\sim}{L}}\, \mathrm{id} \preccurlyeq \mathcal{H}^{(k)} \preccurlyeq \widetilde{\widetilde{L}}\, \mathrm{id},$$

then also $\left(H^{(k)}\right)^{-1}$ is bounded and bounded below with

$$\frac{1}{\widetilde{\widetilde{L}}}\, \mathrm{id} \preccurlyeq \left(\mathcal{H}^{(k)}\right)^{-1} \preccurlyeq \frac{1}{\underset{\sim}{\underset{\sim}{L}}}\, \mathrm{id},$$

see [113]. Therefore, $\left(H^{(k)}\right)^{-1}$ defines an equivalent norm on Y as well and we have the bounds between $\|\cdot\|_{(\mathcal{H}^{(k)})^{-1}}$ and $\|\cdot\|_Y$ as stated in the assertion. □

In order to simplify our notation, let us introduce functionals $\tilde{f}$ and $\tilde{g}$, which arise as objectives in the subproblems (FISTA*.1) and (FISTA*.2). For $x \in X$ and $y \in Y$, we write

$$\begin{aligned} \tilde{f}\left(y; \lambda^{(k)}\right) &:= f(y) - \left\langle \lambda^{(k)}, y \right\rangle_Y \\ \tilde{g}\left(x, y; \lambda^{(k)}, \mathcal{H}^{(k)}, l^{(k)}\right) &:= g(x) + \frac{1}{2l^{(k)}} \|\mathcal{A}x - y\|_{(\mathcal{H}^{(k)})^{-1}}^2 + \left\langle \mathcal{A}x, \lambda^{(k)} \right\rangle_Y. \end{aligned}$$

When no confusion is possible, we will hide the parameters as function arguments and simply write $\tilde{f}(y)$ or $\tilde{g}(x, y)$, respectively. This way, the definition of primal sequence read

$$y^{(k)} = \operatorname*{arg\,min}_{y \in Y} \tilde{f}(y) \tag{3.14}$$

and

$$x^{(k)} = \operatorname*{arg\,min}_{x \in X} \tilde{g}\left(x, y^{(k)}\right). \tag{3.15}$$

3.18 Lemma[TT] (Bounds on the Primal Sequence) *(a) With the sequence $\left(y^{(k)}\right)_k$ in (3.11a), we have for all $k \in \mathbb{N}$*

$$\frac{\sigma}{2} \left\| y^{(k)} - \mathcal{A}\bar{x} \right\|_Y^2 \leq J(\lambda^{(k)}) - J(\bar{\lambda}).$$

(b) If there exists $K \in \mathbb{N}$ *such that* $L^{(K)} \geq L = \frac{1}{\sigma}$*, then, for all* $k \geq K$*, the sequence* $\left(x^{(k)}\right)_k$ *in (3.11b) satisfies*

$$\frac{C^2 \underline{L}}{2\widetilde{L}^2} \left\| x^{(k)} - \bar{x} \right\|_X^2 \leq J(\lambda^{(k)}) - J(\bar{\lambda}),$$

with the constant $C > 0$ *from (3.1).*

Proof. Let us remark that the convergence analysis for this choice of the primal sequence can be seen as a variation and extension to the analysis in [137] and Theorem 4.1 therein. The authors Beck and Teboulle however assume that problems of the form

$$\min_{x \in X} \langle x^*, x \rangle_{X^*,X} + g(x)$$

admit a solution, which cannot be guaranteed in our framework. We therefore have to use different arguments to establish the result here.

For $(x, y) \in X \times Y$ and $k \in \mathbb{N}$, we have

$$\begin{aligned}
-\tilde{f}(y) = \left\langle \lambda^{(k)}, y \right\rangle_Y - f(y) &\leq f^*(\lambda^{(k)}) = F(\lambda^{(k)}) \\
-\tilde{g}(x, \mathcal{A}x) = \left\langle -\mathcal{A}^*\lambda^{(k)}, x \right\rangle_{X^*,X} - g(x) &\leq g^*(-\mathcal{A}^*\lambda^{(k)}) = G(\lambda^{(k)}) \\
-\tilde{g}(x, y) \leq \left\langle -\mathcal{A}^*\lambda^{(k)}, x \right\rangle_{X^*,X} - g(x) &\leq g^*(-\mathcal{A}^*\lambda^{(k)}) = G(\lambda^{(k)}).
\end{aligned}$$

The second estimate will yield the assertion in (a), the third estimate the assertion in (b). By summing the first and second, or the first and third inequalities we obtain

$$\begin{aligned}
-\tilde{f}(y) - \gamma &\leq J(\lambda^{(k)}) \\
-\tilde{f}(y) - \tilde{g}(x, y) &\leq J(\lambda^{(k)}),
\end{aligned}$$

where $\gamma := \inf_{x \in X} \tilde{g}(x, \mathcal{A}x)$. If we evaluate the sum of $\tilde{f}$ and $\tilde{g}$ at the optimal solution $(\bar{x}, \mathcal{A}\bar{x})$, then all terms except for $f(\mathcal{A}\bar{x})$ and $g(\bar{x})$ vanish. By exploiting the strong duality principle according to (3.4), we are left with the equality

$$\tilde{f}(\mathcal{A}\bar{x}) + \tilde{g}(\bar{x}, \mathcal{A}\bar{x}) = f(\mathcal{A}\bar{x}) + g(\bar{x}) = -f^*(\bar{\lambda}) - g^*(-\mathcal{A}^*\bar{\lambda}) = -J\left(\bar{\lambda}\right).$$

As an intermediate result, we note that with $x = x^{(k)}$, $y = y^{(k)}$

$$\tilde{f}(\mathcal{A}\bar{x}) - \tilde{f}(y^{(k)}) + \tilde{g}(\bar{x}, \mathcal{A}\bar{x}) - \gamma \leq J(\lambda^{(k)}) - J(\bar{\lambda}) \tag{3.16a}$$

$$\tilde{f}(\mathcal{A}\bar{x}) - \tilde{f}(y^{(k)}) + \tilde{g}(\bar{x}, \mathcal{A}\bar{x}) - \tilde{g}(x^{(k)}, y^{(k)}) \leq J(\lambda^{(k)}) - J(\bar{\lambda}). \tag{3.16b}$$

It now remains to show that the left-hand sides of (3.16) can be bounded below by squared error norms of the primal sequence.

Since f is σ-strongly convex, so is $\tilde{f}$, and by using Lemma 2.27 on page 28, an optimality condition corresponding to (3.14) reads

$$\tilde{f}(y) - \tilde{f}(y^{(k)}) \geq \frac{\sigma}{2} \left\| y - y^{(k)} \right\|_Y^2, \qquad \forall y \in Y. \tag{3.17}$$

By definition of the infimum γ of $\tilde{g}(\,\cdot\,, \mathcal{A}\,\cdot\,)$,

$$\tilde{g}(x, \mathcal{A}x) - \gamma \geq 0, \qquad \forall x \in X. \tag{3.18a}$$

Since the scaled $(\mathcal{H}^{(k)})^{-1}$-norm is equivalent to the canonical norm on Y by Lemma 3.17, and since $\mathcal{A}$ is bounded below on $\operatorname{dom} g$ with constant $C > 0$ by (3.1), $\tilde{g}$ is strongly convex, too. Strong convexity parameters are given by $\frac{C^2}{l^{(k)}\widetilde{L}} \geq \frac{C^2 \underset{\sim}{L}}{\widetilde{L}^2}$. Thus, an optimality condition for (3.15) is found to be

$$\tilde{g}(x, y^{(k)}) - \tilde{g}(x^{(k)}, y^{(k)}) \geq \frac{C^2 \underset{\sim}{L}}{2\widetilde{L}^2} \left\| x - x^{(k)} \right\|_X^2, \qquad \forall x \in X. \tag{3.18b}$$

The result in statement (a) now follows by adding (3.17) and (3.18a) with $x = \bar{x}$ and $y = \mathcal{A}\bar{x}$:

$$\frac{\sigma}{2} \left\| y^{(k)} - \mathcal{A}\bar{x} \right\|_Y^2 \leq \tilde{f}(\mathcal{A}\bar{x}) - \tilde{f}(y^{(k)}) + \tilde{g}(\bar{x}, y^{(k)}) - \gamma \tag{3.19}$$

For part (b), we add (3.17) and (3.18b), also for $x = \bar{x}$ and $y = \mathcal{A}\bar{x}$

$$\frac{C^2 \underset{\sim}{L}}{2\widetilde{L}^2} \left\| \bar{x} - x^{(k)} \right\|_X^2 + \frac{\sigma}{2} \left\| \mathcal{A}\bar{x} - y^{(k)} \right\|_Y^2 \leq \tilde{f}(\mathcal{A}\bar{x}) - \tilde{f}(y^{(k)}) + \tilde{g}(\bar{x}, y^{(k)}) - \tilde{g}(x^{(k)}, y^{(k)}). \tag{3.20}$$

The right-hand side does not fully agree with the left-hand side in (3.16b) yet, due to the distinct terms $\tilde{g}(\bar{x}, y^{(k)})$ and $\tilde{g}(\bar{x}, \mathcal{A}\bar{x})$. Referring back to the definition of $\tilde{g}$, we deduce

$$\tilde{g}(\bar{x}, \mathcal{A}\bar{x}) = \tilde{g}(\bar{x}, y^{(k)}) - \frac{1}{2l^{(k)}} \left\| y^{(k)} - \mathcal{A}\bar{x} \right\|_{(\mathcal{H}^{(k)})^{-1}}^2.$$

To complete the proof, we therefore have to be able to absorb $-\frac{1}{2l^{(k)}} \left\| y^{(k)} - \mathcal{A}\bar{x} \right\|_{(\mathcal{H}^{(k)})^{-1}}^2$ in $\frac{\sigma}{2} \left\| y^{(k)} - \mathcal{A}\bar{x} \right\|_Y^2$. But by employing Lemma 3.17 once again, this time for the upper bound,

$$\frac{\sigma}{2} \left\| y^{(k)} - \mathcal{A}\bar{x} \right\|_Y^2 - \frac{1}{2l^{(k)}} \left\| y^{(k)} - \mathcal{A}\bar{x} \right\|_{(\mathcal{H}^{(k)})^{-1}}^2 \geq \frac{\sigma}{2} \left\| y^{(k)} - \mathcal{A}\bar{x} \right\|_Y^2 - \frac{1}{2l^{(k)} \underset{\sim}{L}} \left\| y^{(k)} - \mathcal{A}\bar{x} \right\|_Y^2$$

$$
\begin{aligned}
&= \left(\frac{1}{2L} - \frac{\underset{\sim}{L}}{2L^{(k)}\underset{\sim}{L}}\right) \left\| y^{(k)} - \mathcal{A}\bar{x} \right\|_Y^2 \\
&\geq 0, \qquad \forall k \geq K.
\end{aligned}
$$

□

Properties of the Primal Sequence (3.12) Based on Least Squares

Based on the least-squares problem (3.12b)

$$
x^{(k)} := \operatorname*{arg\,min}_{x \in \operatorname{dom} g} \frac{1}{2} \left\| \mathcal{A}x - y^{(k)} \right\|_Y^2
$$

we can define a projection operator

$$
P : Y \to Y, \quad y \mapsto \mathcal{A} \operatorname*{arg\,min}_{x \in \operatorname{dom} g} \frac{1}{2} \|\mathcal{A}x - y\|_Y^2
$$

onto $\operatorname{ran} \mathcal{A}|_{\operatorname{dom} g}$. The term 'projection' is indeed justified, as this mapping is apparently idempotent. If there already exists $\tilde{x} \in \operatorname{dom} g$ such that $y = \mathcal{A}\tilde{x}$, then the minimising argument of the least-squares problem is exactly this $\tilde{x}$, and $P(y) = \mathcal{A}\tilde{x} = y$.

3.19 Lemma$^{(\mathrm{TT})}$ (Firm Nonexpansiveness of P) *P is firmly nonexpansive, i.e. for all $y_1, y_2 \in Y$*

$$
\|P(y_1) - P(y_2)\|_Y^2 \leq \langle y_1 - y_2, P(y_1) - P(y_2) \rangle_Y .
$$

Proof. Let $y_1, y_2 \in Y$. The corresponding minimising arguments $x_1, x_2 \in \operatorname{dom} g$ of the least-squares problem satisfy the optimality conditions

$$
0 \leq \langle \mathcal{A}^* (\mathcal{A}x_1 - y_1), x - x_1 \rangle_{X^*,X} = \langle \mathcal{A}x_1 - y_1, \mathcal{A}x - \mathcal{A}x_1 \rangle_Y , \qquad \forall x \in \operatorname{dom} g \tag{3.21}
$$

$$
0 \leq \langle \mathcal{A}^* (\mathcal{A}x_2 - y_2), x - x_2 \rangle_{X^*,X} = \langle \mathcal{A}x_2 - y_2, \mathcal{A}x - \mathcal{A}x_2 \rangle_Y , \qquad \forall x \in \operatorname{dom} g. \tag{3.22}
$$

Setting $x = x_2$ in (3.21) and $x = x_1$ in (3.22) and summing both inequalities yields

$$
\begin{aligned}
0 &\leq \langle \mathcal{A}x_2 - \mathcal{A}x_1 + y_1 - y_2, \mathcal{A}x_1 - \mathcal{A}x_2 \rangle_Y \\
&= \langle y_1 - y_2, \mathcal{A}x_1 - \mathcal{A}x_2 \rangle_Y - \|\mathcal{A}x_1 - \mathcal{A}x_2\|_Y^2 \\
&= \langle y_1 - y_2, P(y_1) - P(y_2) \rangle_Y - \|P(y_1) - P(y_2)\|_Y^2 .
\end{aligned}
$$

□

In particular, it follows from Lemma 3.19 and the Cauchy-Schwarz inequality that P is nonexpansive:

3.20 Corollary (Nonexpansiveness of P)

$$
\|P(y_1) - P(y_2)\|_Y \leq \|y_1 - y_2\|_Y , \qquad \forall y_1, y_2 \in Y.
$$

Since the sequences $(y^{(k)})_k$ in both options (3.11a) and (3.12a) are identical, Lemma 3.18(a) remains valid. The corresponding error estimate for $(x^{(k)})_k$ defined by the least-squares problem (3.12b) now follows as a result of the boundedness of P by Corollary 3.20.

3.21 Lemma$^{(\mathrm{TT})}$ (Bounds on the Primal Sequence) *Let $\left(x^{(k)}\right)_k$ be the primal sequence defined in (3.12b). For all $k \in \mathbb{N}$*

$$\frac{C^2\sigma}{2}\left\|x^{(k)} - \bar{x}\right\|_X^2 \leq J(\lambda^{(k)}) - J(\bar{\lambda}),$$

with the constant $C > 0$ that quantifies the boundedness below of $\mathcal{A}$, cf inequality (3.1).

Proof. From (3.1) and Corollary 3.20 we obtain

$$C\left\|x^{(k)} - \bar{x}\right\|_X \leq \left\|\mathcal{A}x^{(k)} - \mathcal{A}\bar{x}\right\|_Y = \left\|P(y^{(k)}) - P(\mathcal{A}\bar{x})\right\|_Y \leq \left\|y^{(k)} - \mathcal{A}\bar{x}\right\|_Y.$$

Lemma 3.18(a) on page 69 provides the error estimate for $\left(y^{(k)}\right)_k$ in terms of the optimality gap in the dual objective J. □

Properties of the Leading-Point Primal Sequence (3.13)

The main drawback of using one of the previous two sequences $\left(x^{(k)}, y^{(k)}\right)_k \subset X \times Y$ is the effort associated with their computation. Each iteration becomes essentially twice as expensive as for methods without acceleration, which only require one evaluation of the proximal map.

Unfortunately, we cannot make any general statements regarding the convergence of the sequences based on the leading point, except under very strong assumptions. In particular, we cannot generally provide an estimate of $J(\hat{\lambda}^{(k)}) - J(\bar{\lambda})$.

If $(\lambda^{(k)})_k$ is norm-convergent with limit $\bar{\lambda} \in Y$, then $\left\|\lambda^{(k)} - \bar{\lambda}\right\|_Y \to 0$ as $k \to \infty$ and the leading point approaches this limit as well. Then, $J(\hat{\lambda}^{(k)}) - J(\bar{\lambda}) \to 0$. A sufficient condition for strong convergence of the iterates $\lambda^{(k)}$ is ρ-strong convexity of J, since then

$$J(\lambda^{(k)}) - J(\bar{\lambda}) \geq \frac{\rho}{2}\left\|\lambda^{(k)} - \bar{\lambda}\right\|_Y^2,$$

and the left-hand side tends to zero by the convergence theorems for FISTA and VM-FISTA. This case, however, is of little interest to us. If both the primal objective I and the dual objective J are strongly convex, then even classical methods without extrapolated gradient steps can already achieve a linear convergence rate. [49], [77].

If J is not strongly convex but still coercive, then $\left(\lambda^{(k)}\right)_k$ as a minimising sequence is bounded and so is $(\hat{\lambda}^{(k)})_k$. Hence (cf Theorem 2.26 on page 28), there are weakly

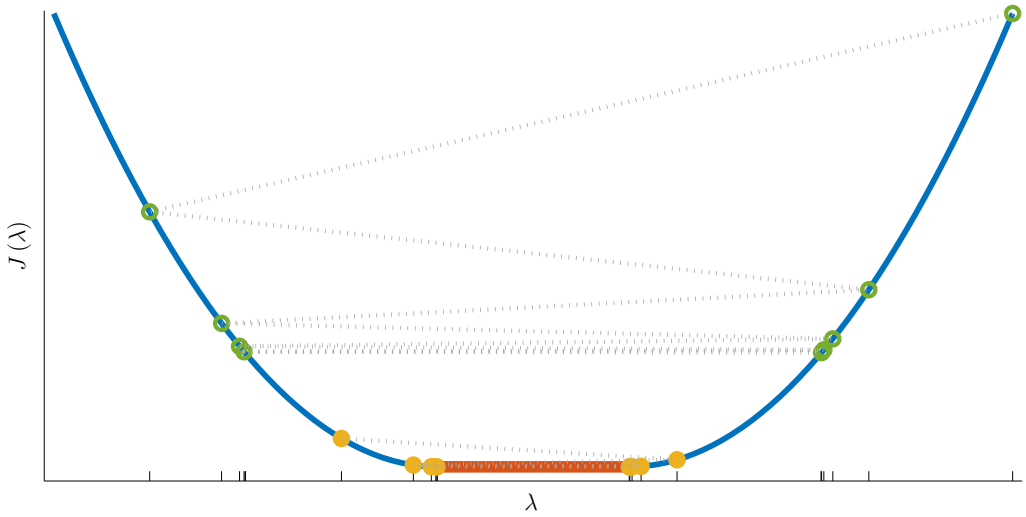

Figure 3.1: FISTA iterates $(\lambda^{(k)})_k$ (yellow) oscillating around the optimal set (red). While the function values $J(\lambda^{(k)})$ are guaranteed to converge to the global minimum, the sequence $(\hat{\lambda}^{(k)})_k$ of leading points (green) neither approaches the set of minimisers, nor do the function values $J(\hat{\lambda}^{(k)})$ approach the optimal solution, nor do the gradients become stationary.

convergent subsequences of the dual iterates and the extrapolated leading points. With a different choice of extrapolation parameters, it is possible to ensure that the entire sequence $\left(\lambda^{(k)}\right)_k$ converges weakly [122]. Another sufficient condition for convergence of the leading-point sequence (or a subsequence) to an optimal solution is therefore that Y is only of finite dimension, where the notions of strong and weak convergence collapse.

In the general case, it is well possible that $\left\|\lambda^{(k)} - \lambda^{(k-1)}\right\|_Y \not\to 0$. In Figure 3.1, we illustrate how this can cause that the leading points $(\hat{\lambda}^{(k)})_k$ may even stay bounded away from the set of optimal solutions. In consequence, we cannot rely on the corresponding primal sequence (3.13) for approximating an optimal solution.

Convergence Rates of the Primal Sequences

Quantitative rates of convergence for the primal sequences (3.11) and (3.12) now follow from the convergence properties of FISTA or VM-FISTA, respectively, combined with either Lemma 3.18 or Lemma 3.21.

3.22 Theorem$^{(\mathrm{TT})}$ (Convergene Rate for FISTA* and VM-FISTA*) *Let* $\left(x^{(k)}, y^{(k)}, \lambda^{(k)}\right)_k$ *be generated by the accelerated dual proximal gradient or* Newton*-type method.*

(a) If $\left(y^{(k)}\right)_k$ is defined by (3.11a) or (3.12a), then there exists $c > 0$ such that

$$\left\|y^{(k)} - \mathcal{A}\bar{x}\right\|_Y \leq \frac{c}{k+1}, \qquad \forall k \in \mathbb{N}. \tag{3.23}$$

(b) If $\left(x^{(k)}\right)_k$ is defined by (3.11b), and if there exists $K \in \mathbb{N}$ such that $L^{(K)} \geq L = \frac{1}{\sigma}$, then there exists $c > 0$ such that

$$\left\|x^{(k)} - \bar{x}\right\|_X \leq \frac{c}{k+1}, \qquad \forall k \geq K. \tag{3.24}$$

(c) If $\left(x^{(k)}\right)_k$ is defined by (3.12b), then there exists $c > 0$ such that

$$\left\|x^{(k)} - \bar{x}\right\|_X \leq \frac{c}{k+1}, \qquad \forall k \in \mathbb{N}. \tag{3.25}$$

By using Theorem 2.54 on page 45 for the convergence rate of ISTA, we obtain the following worst-case convergence rate of the dual proximal gradient method:

3.23 Corollary (Convergence Rate for ISTA*) *Let $\left(x^{(k)}, y^{(k)}, \lambda^{(k)}\right)_k$ be generated by the dual proximal gradient method. If there exists $K \in \mathbb{N}$ such that $L^{(K)} \geq L = \frac{1}{\sigma}$, then there exists a constant $c > 0$ such that*

$$\left\|y^{(k)} - \mathcal{A}\bar{x}\right\|_Y \leq \frac{c}{\sqrt{k}}, \qquad \forall k \in \mathbb{N} \tag{3.26}$$

$$\left\|x^{(k)} - \bar{x}\right\|_X \leq \frac{c}{\sqrt{k}}, \qquad \forall k \geq K. \tag{3.27}$$

If no majorant of the Lipschitz constant $L = \frac{1}{\sigma}$ is known and a backtracking strategy is used for finding admissible values $L^{(k)}$ or $l^{(k)}$, respectively, then clearly the least-squares projection from (3.12b) should be used to define $\left(x^{(k)}\right)_k$ in order to guarantee the convergence rate of $O(1/k)$ globally.

To put the convergence results in context, let us briefly sketch how they compare to those of similar methods: the Chambolle-Pock algorithm and the alternating direction method of multipliers.

3.24 Convergence of the Chambolle-Pock Algorithm With either (3.12) or (3.11) as primal sequence, our accelerated dual proximal algorithms compute $\left(x^{(k)}, y^{(k)}\right)_k$ solely based on the iterates $\left(\lambda^{(k)}\right)_k$, and $(\hat{x}^{(k)}, \hat{y}^{(k)})_k$ solely based on the leading points $(\hat{\lambda}^{(k)})_k$. In contrast, fast versions of the Chambolle-Pock algorithm use a weighted average between a leading point and the last iterate to compute an update for the next iterate. On the one hand, this avoids the extra computing time for determining an additional

sequence. On another hand, the known convergence results for primal-dual algorithms of this class are weaker than those in Theorem 3.22. In [49], the authors prove that there exists an index $K \in \mathbb{N}$, from which onwards convergence of order $O(1/k)$ is achieved. It appears that this result does not hold globally with $K = 1$. Accordingly, there seems to be no proof for convergence of order $O(1/k^2)$ in the dual objective values. With ergodic averages of iterates, the primal-dual gap can be shown to decrease like $O(1/k^2)$ (see [86]). In practice, non-ergodic convergence results are normally preferable, in particular if the exact solution is characterised by sparsity. Such a feature would generally be lost by averaging over all previous iterates.

3.25 Convergence of ADMM The derivation of convergence rates for augmented Lagrangian methods is a lot more intricate than for proximal methods.

Convergence itself can be guaranteed as long as the step sizes satisfy $0 < t^{(k)} < \varrho(1+\sqrt{5})/2$, with $\varrho^{(k)} \equiv \varrho > 0$. Then we have strong convergence of the primal sequence $\left(x^{(k)}, y^{(k)}\right)_k$ to the unique solution of (P′) and weak convergence of the dual sequence $\left(\lambda^{(k)}\right)_k$ to a minimiser of J [77, p 85].

Under additional regularity assumptions on f or g, the alternating direction method of multipliers converges with a linear rate [77, p 88], [138, p 322], [102, p 970]. For problems where such conditions are too restrictive, one has to expect ALG2 to converge with sublinear speed as well. In fact, Goldstein et al. can only prove sublinear convergence of order $O(1/k)$ in the dual functional, if both f and g are strongly convex [89, Theorem 1]. Referring back to Corollary 3.23, we infer that ISTA applied to the dual achieves the same convergence behaviour without such an additional assumption on g. We also refer to [89] for a recent review of further convergence results of the ADMM.

The pronounced similarity between ALG2 and ISTA* lets one conjecture that these two methods exhibit very similar convergence behaviour.

Computational Techniques

3.26 Stopping Criterion So far, we have not gone into detail how to determine 'if the algorithm has converged'. Ideally, we would find a criterion that implies near-optimality of the current iterate, while concurrently this assessment does not consume excessive computing resources.

Since $-\mathcal{A}x^{(k)} \in \partial G(\lambda^{(k)})$ and $y^{(k)} = \nabla F(\lambda^{(k)}$ by (3.10) and (3.9), a stopping criterion that tests for stationarity in the dual is given by

$$\left\| \mathcal{A}x^{(k)} - y^{(k)} \right\|_Y \leq \text{gradTol},$$

with a positive constant gradTol. For classical methods without acceleration, this expression is straightforward to evaluate as the primal iterates are already available. Also for the inertial methods FISTA* or VM-FISTA*, the primal iterate $y^{(k)}$ is typically still computable at relatively little expense: the problem (3.11a) or (3.12a), respectively, includes no operators $\mathcal{A}$ or $\mathcal{H}^{(k)}$. The iterate $x^{(k)}$, however, demands for the solution of a potentially difficult optimisation problem.

As a remedy, we suggest to proceed in the following manner:

Even though the leading-point sequence is not guaranteed to converge, one might of course hope to be in a lucky situation where it does.

1st Attempt: Test whether $\left\|\mathcal{A}\hat{x}^{(k)} - \hat{y}^{(k)}\right\|_Y \leq \text{gradTol}$

If these residuals appear to stagnate, then one can fall back to testing how much progress the algorithm is still achieving in the primal sequence $\left(y^{(k)}\right)_k$. This criterion is still relative inexpensive to evaluate. Since the primal sequences converge strongly, the difference between subsequent iterates eventually becomes arbitrarily small. We fix parameters $\text{absTol}, \text{relTol} > 0$.

2nd Attempt: Test whether $\left\|y^{(k)}\right\|_Y \leq \text{absTol}$ or else $\left\|y^{(k)} - y^{(k-1)}\right\|_Y \leq \text{relTol}\left\|y^{(k)}\right\|_Y$

Only once this criterion has been met, we evaluate the corresponding iterate $x^{(k)}$ and test for stationarity.

3rd Attempt: Test whether $\left\|\mathcal{A}x^{(k)} - y^{(k)}\right\|_Y \leq \text{gradTol}$

In summary, if the leading point sequence already converges, then the cost of (VM-)FISTA* per iteration is virtually identical to (VM-)ISTA*. Even otherwise, costly computations of iterates $x^{(k)}$ can still be avoided by an appropriate choice of absTol and relTol.

3.27 Adaptive Re-Starting In general, FISTA is not a monotone method in the sense that $J(\lambda^{(k)}) \leq J(\lambda^{(k-1)})$ needs not hold. Analogously, the primal sequence generated by the dual algorithms FISTA* or VM-FISTA* may temporarily digress from the solution $(\bar{x}, \mathcal{A}\bar{x})$. This is a well-known property of accelerated gradient schemes and can be interpreted as excessive momentum from past iterations, that causes the sequence to overshoot the minimiser and to converge in a spiralling motion.

The monotone modification termed MFISTA, which Beck and Teboulle propose in [121], requires the functional J to be evaluated at every iteration. Depending on the problem at hand, this may be computationally demanding. For some problems, J may not even be available in closed form.

O'Donoghue and Candes [120] suggest to adaptively re-start the algorithm, once an increase in the objective is detected in order to preserve monotonicity and to discard accumulated momentum of the iteration. 'Re-starting' means that the current iterate $\lambda^{(k)}$ is discarded, and the algorithm is re-initialised with $\lambda^{(k-1)}$ as initial iterate and initial leading point. Rather than observing the functional values, the authors showed a re-starting criterion based solely on the dual gradient to be similarly effective. According to this 'gradient scheme', recalling $\mathcal{A}\hat{x}^{(k)} - \hat{y}^{(k)} \in -\partial J(\mu^{(k)})$, the algorithm is re-started whenever

$$\left\langle \mathcal{A}\hat{x}^{(k)} - \hat{y}^{(k)}, \lambda^{(k)} - \lambda^{(k-1)} \right\rangle_Y < 0. \tag{3.28}$$

In that case, $\lambda^{(k)} - \lambda^{(k-1)}$ would be an ascent direction for the dual functional J at $\hat{\lambda}^{(k)}$. The authors of [120] point out that this scheme unites the benefits of increased numerical stability near the optimum on the one hand and, on the other hand, no extra computational expenditure: all quantities in (3.28) have already been computed previously.

By allowing for re-starts, the worst-case convergence rate decreases from $O(1/k)$ to $O(1/\sqrt{k})$. This is a consequence of the fact that the first step after (re-)starting is equivalent to a step in the unaccelerated dual proximal gradient method (VM-)ISTA* and we have

$$\lambda^{(k)} = \lambda^{(k-1)} + \frac{1}{l^{(k-1}} \left(\mathcal{H}^{(k-1)}\right)^{-1} \left(\mathcal{A}\hat{x}^{(k)} - \hat{y}^{(k)}\right).$$

Therefore,

$$\left\langle \mathcal{A}\hat{x}^{(k)} - \hat{y}^{(k)}, \lambda^{(k)} - \lambda^{(k-1)} \right\rangle_Y = \frac{1}{l^{(k-1)}} \left\| \mathcal{A}\hat{x}^{(k)} - \hat{y}^{(k)} \right\|^2_{(\mathcal{H}^{(k-1)})^{-1}} \not< 0$$

and this first step is generally accepted.

Surely, the rationale behind re-starting schemes is that re-initialisations only occur as isolated events, not after every single iteration. This way, the convergence rate would remain close to $O(1/k)$. A re-start would ideally result in a shortcut towards the solution and thus decrease the error more efficiently than continued iterations with full momentum. For numerical studies of this effect, we refer to [120].

PART II

Simulation of Viscoplastic Flows

Chapter 4

State of the Art

Numerical studies of viscoplastic flows have been an active topic over the past decades. Accordingly, the literature on different approaches to formulating these problems, on finding discrete approximations and suitable methods for their solution is vast.

Therefore, this chapter aims to draw a picture of the context for our approach from the perspective of viscoplasticity. First, a few more definitions and results from functional analysis are in order to provide a rigorous mathematical foundation. This is the subject of Section (A). Section (B) builds on top with a review of classical formulations and numerical methods for simulation problems of viscoplastic fluid flows.

(A) Analysis in Function Spaces

In our work, we are dealing with both finite-dimensional spaces and a number of infinite-dimensional function spaces. The following overview shall provide a summary of some of their properties.

4.1 Euclidean Topology

Unless otherwise stated, we equip $\mathbb{R}^d$ with the Euclidean scalar product and $\mathbb{R}^{d\times d}$ with the Frobenius inner product, along with the induced norms in each case:

$$\begin{aligned} &\mathbb{R}^d: && |x| := \sqrt{x^\top x} && x \cdot y := x^\top y \\ &\mathbb{R}^{d\times d}: && |A| := \sqrt{\operatorname{tr} AA^\top} && A : B := \operatorname{tr} AB^\top. \end{aligned}$$

We also make use of the equivalence of all norms on finite-dimensional spaces [139, p 122].

4.2 Multi-Index Notation We recall the compact multi-index notation for (possibly weak) partial derivatives: with $\alpha \in \mathbb{N}_0^d$, $|\alpha| := \sum_{k=1}^d \alpha_k$, we denote the corresponding differential operator by

$$D^\alpha := \frac{\partial^{|\alpha|}}{\partial x_1^{\alpha_1} \cdots \partial x_d^{\alpha_d}}.$$

4.3 Definition (Spaces of Continuous Functions) Let $\Omega \subset \mathbb{R}^d$ be a domain.

(a) For $k \in \mathbb{N}_0$, the *space of continuously differentiable functions of order* k is given by

$$C^k(\Omega) := \left\{ u : \Omega \to \mathbb{R} \;\middle|\; \forall \alpha \in \mathbb{N}_0^d, |\alpha| \leq k : D^\alpha u \text{ is continuous} \right\}.$$

These spaces are endowed with the norm defined by

$$\|u\|_{C^k(\Omega)} := \max_{0 \leq |\alpha| \leq k} \sup_{x \in \Omega} |D^\alpha u(x)|.$$

(b) For the space of continuous functions, we simply write $C(\Omega) := C^0(\Omega)$, and for the space of functions with continuous partial derivatives of any order $C^\infty(\Omega) := \bigcap_{k=0}^\infty C^k(\Omega)$.

(c) By $C_0^k(\Omega)$, $k \in \mathbb{N}_0 \cup \{\infty\}$, we denote the subspaces of functions with compact support in Ω.

4.4 Equivalence Classes of Functions In Lebesgue, Sobolev and Sobolev-Slobodeckii spaces, we consider functions that only differ from each other on sets of measure zero as equivalent. We will not introduce any special notation to distinguish between equivalence classes of functions and their representatives. Instead, we keep in mind that pointwise properties only hold *almost everywhere (a.e.)*, that is, they are violated at most on null sets.

4.5 Definition (Lebesgue, Sobolev and Sobolev-Slobodeckii Spaces) Let $\Omega \subset \mathbb{R}^d$ be measurable, $p \in [1, \infty[$, $k \in \mathbb{N}_0$, $s \in]0, \infty[\setminus \mathbb{N}$. Acting on a measurable function $u : \Omega \to \mathbb{R}$, we consider the functionals

$$\|u\|_{L^p(\Omega)} := \left(\int_\Omega |u(x)|^p \, \mathrm{d}x \right)^{1/p}$$

$$\|u\|_{L^\infty(\Omega)} := \operatorname*{ess\,sup}_{x \in \Omega} |u(x)| := \inf \{ c \geq 0 \mid |u(x)| \leq c \text{ a.e. in } \Omega \}$$

for Lebesgue spaces,

$$\|u\|_{W^{k,p}(\Omega)} := \left(\sum_{|\alpha| \leq k} \|D^\alpha u\|^p_{L^p(\Omega)} \right)^{1/p}$$
$$\|u\|_{W^{k,\infty}(\Omega)} := \max_{|\alpha| \leq k} \|D^\alpha u\|_{L^\infty(\Omega)}$$

for Sobolev spaces of integer order, and

$$\|u\|_{W^{s,p}(\Omega)} := \left(\|u\|^p_{W^{\lfloor s \rfloor,p}(\Omega)} + |u|^p_{W^{s,p}(\Omega)} \right)^{1/p}$$

with

$$|u|_{W^{s,p}(\Omega)} := \left(\sum_{|\alpha| = \lfloor s \rfloor} \int_\Omega \int_\Omega \frac{|D^\alpha u(x_1) - D^\alpha u(x_2)|^p}{|x_1 - x_2|^{d+p(s-\lfloor s \rfloor)}} \, \mathrm{d}x_1 \, \mathrm{d}x_2 \right)^{1/p}$$

for Sobolev spaces of non-integer order, also known as Sobolev-Slobodeckii spaces.

(a) We define these spaces as consisting of those (equivalence classes of) measurable functions $u : \Omega \to \mathbb{R}$, for which the respective functional assumes finite values.

(b) Additionally, we introduce $W^{k,p}_0(\Omega)$ as the closure of $C^\infty_0(\Omega)$ in $W^{k,p}(\Omega)$ and write $W^{-k,p^*}(\Omega) := W^{k,p}_0(\Omega)^*$, with $1/p + 1/p^* = 1$.

All of these spaces are Banach spaces, separable for $1 \leq p < \infty$, reflexive for $1 < p < \infty$ and, if $p = 2$, Hilbert spaces with respect to the scalar products

$$\langle u, v \rangle_{L^2(\Omega)} := \int_\Omega u(x) v(x) \, \mathrm{d}x$$
$$\langle u, v \rangle_{W^{k,2}(\Omega)} := \sum_{|\alpha| \leq k} \langle D^\alpha u, D^\alpha v \rangle_{L^2(\Omega)}$$
$$\langle u, v \rangle_{W^{s,2}(\Omega)} := \langle u, v \rangle_{W^{\lfloor s \rfloor,2}(\Omega)} + (u, v)_{W^{s,2}(\Omega)},$$

where

$$(u, v)_{W^{s,2}(\Omega)} := \sum_{|\alpha| = \lfloor s \rfloor} \int_\Omega \int_\Omega \frac{(D^\alpha u(x_1) - D^\alpha u(x_2))(D^\alpha v(x_1) - D^\alpha v(x_2))}{|x_1 - x_2|^{d+2(s-\lfloor s \rfloor)}} \, \mathrm{d}x_1 \, \mathrm{d}x_2$$

[140, pp 29 & 60], [141, p 124]. We also write $H^k(\Omega) := W^{k,2}(\Omega)$, $H^k_0(\Omega) := W^{k,2}_0(\Omega)$ and $H^s(\Omega) := W^{s,2}(\Omega)$, respectively.

4.6 Definition (Lipschitz Boundary) Let $\Omega \subset \mathbb{R}^d$ be a bounded domain with boundary $\Gamma = \partial\Omega$. We say Ω has a Lipschitz *boundary* or Ω is a Lipschitz *domain*, if the following conditions are met:

(a) there exist a finite number of points $(x_i)_{i=1,\dots,n} \subset \Gamma$ and a radius $r > 0$, such that $\Gamma \subset \bigcup_{i=1}^{n} B(x_i, r)$

(b) there exists a corresponding family of Lipschitz-continuous bijections $(h_i)_{i=1,\dots,n}$, mapping the unit ball in $\mathbb{R}^d$ onto $B(x_i, r)$, with Lipschitz-continuous inverse, such that

$$h_i(\{\, y \in B(0,1) \mid y_d = 0 \,\}) = B(x_i, r) \cap \Gamma$$
$$h_i(\{\, y \in B(0,1) \mid y_d > 0 \,\}) = B(x_i, r) \cap \Omega.$$

4.7 Theorem (Embeddings) *Let $\Omega \subset \mathbb{R}^d$ be measurable, $1 \le p, q \le \infty$, $k, l \in \mathbb{N}_0$ and $s \in]0, \infty[\setminus \mathbb{N}$.*

(a) The following non-expansive, continuous embeddings are an immediate consequence of the above definitions:

$$W_0^{k,p}(\Omega) \hookrightarrow W^{k,p}(\Omega) \qquad \text{for } k \ge 0$$
$$W^{k,p}(\Omega) \hookrightarrow W^{l,p}(\Omega) \qquad \text{for } k \ge l$$
$$W^{k,p}(\Omega) \hookrightarrow L^{p}(\Omega) \qquad \text{for } k \ge 0$$
$$W^{s,p}(\Omega) \hookrightarrow W^{k,p}(\Omega) \qquad \text{for } s > p.$$

(b) If Ω is additionally bounded, then

$$L^{q}(\Omega) \hookrightarrow L^{p}(\Omega) \qquad \text{for } q \ge p$$

[140, p 28].

(c) If Ω is also Lipschitz and $kp < d$, then

$$W^{k,p}(\Omega) \hookrightarrow L^{q}(\Omega) \qquad \text{for } p \le q \le \frac{dp}{d - kp}$$

For a proof and further Sobolev embeddings, we refer to the literature [140, pp 85-86].

4.8 Theorem (Hölder's Inequality) *Let $1 \le p, p^* \le \infty$ such that $1/p + 1/p^* = 1$. If*

$u \in L^p(\Omega)$ and $v \in L^{p^*}(\Omega)$, then $uv \in L^1(\Omega)$ and

$$\|uv\|_{L^1(\Omega)} \leq \|u\|_{L^p(\Omega)} \|v\|_{L^{p^*}(\Omega)}$$

[140, pp 24].

This statement can be extended to three functions $u \in L^p(\Omega)$, $v \in L^q(\Omega)$ and $w \in L^r(\Omega)$ with $1 \leq p, q, r \leq \infty$ such that $1/p + 1/q + 1/r = 1$ [140, pp 25]. Then their product satisfies

$$\|uvw\|_{L^1(\Omega)} \leq \|u\|_{L^p(\Omega)} \|v\|_{L^q(\Omega)} \|w\|_{L^r(\Omega)}.$$

4.9 Theorem (Duals of Lebesgue Spaces) *Let $1 < p, p^* < \infty$ such that $1/p + 1/p^* = 1$. For any $\mathcal{F} \in L^p(\Omega)^*$, there exists a unique $f \in L^{p^*}(\Omega)$ such that*

$$\mathcal{F}u = \int_\Omega f(x)u(x)\,\mathrm{d}x, \quad \forall u \in L^p(\Omega)$$

and $\|\mathcal{F}\|_{L^p(\Omega)^*} = \|f\|_{L^{p^*}(\Omega)}$. Consequently, $L^p(\Omega)^* \cong L^{p^*}(\Omega)$ [140, pp 45-47].

4.10 Theorem (Traces of Sobolev Spaces) *Let $\Omega \subset \mathbb{R}^d$ be a domain with* Lipschitz *boundary Γ, $k \in \mathbb{N}$ and $1 < p < \infty$. There exists a surjective bounded linear operator $\mathcal{T} : W^{k,p}(\Omega) \twoheadrightarrow W^{k-1/p,p}(\Gamma)$ such that*

$$u \in C^\infty(\bar{\Omega}) \Rightarrow \mathcal{T}u = u|_\Gamma$$

[142, p 47], [143, pp 86-96].

An informal interpretation of this statement reads: by projecting a function to the boundary of the domain, one loses one p^{th} of a derivative.

Even if $u \notin C^\infty(\bar{\Omega})$, we will apply the notation $u|_\Gamma$ for $\mathcal{T}u$.

4.11 Product Spaces We also work with vector-valued and tensor-valued functions, which assume values in $\mathbb{R}^d$ or $\mathbb{R}^{d\times d}$. For products of Lebesgue, Sobolev or Sobolev-Slobodeckii spaces, we define a product norm by replacing absolute values of function values in Definition 4.5 with the Euclidean or Frobenius norm, respectively. The inner products generalise to the multi-valued case in a similarly natural manner, by replacing products of function values in $\mathbb{R}$ with the canonical scalar products of $\mathbb{R}^d$ or $\mathbb{R}^{d\times d}$.

The following two inequalities are crucial for the well-posedness of our problems and numerical algorithms:

4.12 Theorem (Poincaré's Inequality) *Let $\Omega \subset \mathbb{R}^d$ be a bounded domain and $1 < p < \infty$. There exists $C > 0$ such that for all $u \in W_0^{1,p}(\Omega)$*

$$\|u\|_{L^p(\Omega)} \leq C\|\nabla u\|_{L^p(\Omega)^d}.$$

Analogously, for vector-valued functions $u \in W_0^{1,p}(\Omega)^d$

$$\|u\|_{L^p(\Omega)^d} \leq C\|\nabla u\|_{L^p(\Omega)^{d\times d}}.$$

[140, p 183].

4.13 Theorem (Korn's Inequality) *Let $\Omega \subset \mathbb{R}^d$ be a bounded domain with* Lipschitz *boundary and $1 < p < \infty$. There exists $C > 0$ such that for all $u \in W_0^{1,p}(\Omega)^d$*

$$\|\nabla u\|_{L^p(\Omega)^{d\times d}} \leq C\|\mathcal{D}u\|_{L^p(\Omega)^{d\times d}},$$

with the symmetric gradient operator $\mathcal{D} := (\nabla + \nabla^\top)/2$ [144, p 371].

Poincaré's and Korn's inequalities imply that the seminorms defined by $\|\nabla u\|_{(L^p(\Omega))^{d\times d}}$ and $\|\mathcal{D}u\|_{(L^p(\Omega))^{d\times d}}$ are actually norms on $W_0^{1,p}(\Omega)^d$ and equivalent to the canonical norm on this space.

(B) Numerical Methods for Viscoplastic Fluid Flows

After these theoretical preliminaries, let us now turn towards applications of our work. First, we present the precise connection between flow problems in viscoplasticity and convex programming. We then review classical strategies for simulating the flow of viscoplastic materials. It turns out that the community of numerical analysts is divided into two groups: those that employ classical methods for nonsmooth optimisation, as discussed in Section (D) of Chapter 2, and others that smooth or otherwise regularise the problem at the outset. A discussion of the benefits and drawbacks of each approach shall conclude this section.

Formulations of Stationary and Instationary Flow Problems

From our introductory remarks in Chapter 1 we recall that a mathematical model for a broad class of fluid flows is made up of three building blocks: physics imposes two conservation laws—conservation of momentum and mass—with their mathematical formulation in the Navier-Stokes equations. Rheology contributes a model for the material-dependent relation between stress and strain. We consider the models named

after Bingham, Casson and Herschel-Bulkley. For convenience, we recapitulate our notation for the different variables:

$$\begin{aligned} u(t,x) &\in \mathbb{R}^d && \text{flow velocity} \\ \dot\gamma(t,x) = \mathcal{D}u(t,x) &\in \mathbb{R}^{d\times d}_{\mathrm{sym}} && \text{strain rate} \\ p(t,x) &\in \mathbb{R} && \text{pressure} \\ \tau(t,x) &\in \mathbb{R}^{d\times d}_{\mathrm{sym}} && \text{(deviatoric part of the) stress} \end{aligned}$$

The corresponding functions are defined on the time interval $t \in [0,T]$ with $T > 0$, and for $x \in \Omega \subset \mathbb{R}^d$. The flow domain shall be two- or three-dimensional. We denote its boundary by $\Gamma = \partial\Omega$. Furthermore, the problem is defined by the following data:

$$\begin{aligned} f(t,x) &\in \mathbb{R}^d && \text{density of body forces} \\ u_0(x) &\in \mathbb{R}^d && \text{initial flow velocity} \\ u_{\mathrm{D}}(t,x) &\in \mathbb{R}^d && \text{velocity on the boundary} \\ \varrho &> 0 && \text{density} \end{aligned}$$

4.14 Strong Formulations Assuming sufficient regularity of all functions so that the following statements are well-defined, we seek solutions to the Navier-Stokes equations

$$\varrho\left(\partial_t u + (u\cdot\nabla)\,u\right) - \operatorname{div}\tau + \nabla p = f \qquad \text{in }]0,T[\times\Omega \tag{4.1}$$

$$\operatorname{div} u = 0 \qquad \text{in }]0,T[\times\Omega \tag{4.2}$$

complemented with the initial and boundary conditions

$$u = u_0 \qquad \text{in } \Omega \tag{4.3}$$

$$u = u_{\mathrm{D}} \qquad \text{on }]0,T[\times\Gamma \tag{4.4}$$

and either the Bingham model

$$\begin{cases} |\tau| \le \tau_0 & \text{if } \dot\gamma = 0 \\ \tau = 2\mu\dot\gamma + \tau_0 \dfrac{\dot\gamma}{|\dot\gamma|} & \text{if } \dot\gamma \neq 0, \end{cases} \tag{4.5a}$$

the Casson model

$$\begin{cases} |\tau| \le \tau_0 & \text{if } \dot\gamma = 0 \\ \tau = \left(\sqrt{2\mu|\dot\gamma|} + \sqrt{\tau_0}\right)^2 \dfrac{\dot\gamma}{|\dot\gamma|} & \text{if } \dot\gamma \neq 0, \end{cases} \tag{4.5b}$$

or the Herschel-Bulkley model

$$\begin{cases} |\tau| \leq \tau_0 & \text{if } \dot{\gamma} = 0 \\ \tau = 2^{r-1}\kappa|\dot{\gamma}|^{r-2}\dot{\gamma} + \tau_0 \dfrac{\dot{\gamma}}{|\dot{\gamma}|} & \text{if } \dot{\gamma} \neq 0. \end{cases} \tag{4.5c}$$

We recall that $\mu, \kappa > 0$, $\tau_0 \geq 0$ and $1 < r \leq 2$.

If the flow has reached a steady state, then $\partial_t u + (u \cdot \nabla)\, u = 0$ and all functions and parameters lose their time-dependence. This way, the momentum equation simplifies to

$$-\operatorname{div} \tau + \nabla p = f \qquad \text{in } \Omega. \tag{4.6}$$

4.15 Weak Formulations: A Synopsis There are two classical weak formulations of the Bingham flow problem in Sobolev spaces, which can be traced back to the work of Duvaut and Lions [145], [146]: (i) a parabolic variational inequality of the second kind for the flow velocity u, or equivalently (ii) a semismooth system of equations that additionally contains a (non-unique) multiplier. A closely related multiplier formulation was also studied by Basov and Shelukhin in [147], [148]. Mutatis mutandis, the same principles yield variational formulations for fluid flows governed by the Casson and Herschel-Bulkley models with their extra nonlinearities. Such an extension of the Basov-Shelukhin approach to Herschel-Bulkley fluids is studied in [15], [149].

After applying an appropriate time-discretisation scheme, or for stationary problems, these weak formulations correspond to a first-order optimality condition of a nonsmooth composite convex minimisation problem, calling for an application of the methods from the first part of this work.

We first introduce a number of definitions and then present these different formulations explicitly.

4.16 Function Spaces for Variational Formulations Let $\Omega \subset \mathbb{R}^d$ be bounded and Lipschitz. Since the Navier-Stokes equations in three spatial dimensions give rise to numerous yet unanswered questions, we assume $d = 2$ whenever we consider instationary problems. For the flow velocity, we consider the spaces

$$\begin{aligned} U_{0*} &:= \left\{ u \in W^{1,r}(\Omega)^d \;\middle|\; \operatorname{div} u = 0 \right\} \\ U_{*0} &:= \left\{ u \in W^{1,r}(\Omega)^d \;\middle|\; u|_\Gamma = 0 \right\} \\ U_{00} &:= \left\{ u \in W^{1,r}(\Omega)^d \;\middle|\; \operatorname{div} u = 0 \wedge u|_\Gamma = 0 \right\} \end{aligned}$$

with $r = 2$ for Bingham and Casson fluids. In this notation, the first subscript of U summarises any constraints on the divergence of the flow velocity, the second subscript

reflects boundary conditions that are incorporated into U.

Due to the regularity imposed on the domain, outward-pointing normal vectors $\vec{n}$ with unit length exist almost everywhere on Γ. This allows us to define the space of admissible boundary values by

$$U_{\mathrm{D}} := \left\{ u_{\mathrm{D}} \in W^{1-1/r,r}(\Gamma)^d \;\middle|\; \int_\Gamma u_{\mathrm{D}} \cdot \vec{n} \,\mathrm{d}s = 0 \right\},$$

where the condition on compatibility with $\operatorname{div} u = 0$ arises from Gauss's divergence theorem. For a given $u_{\mathrm{D}} \in U_{\mathrm{D}}$ we introduce

$$\begin{aligned} U_{0\mathrm{D}} &:= \left\{ u \in W^{1,r}(\Omega)^d \;\middle|\; \operatorname{div} u = 0 \wedge u|_\Gamma = u_{\mathrm{D}} \right\} \\ U_{*\mathrm{D}} &:= \left\{ u \in W^{1,r}(\Omega)^d \;\middle|\; \operatorname{div} u = 0 \wedge u|_\Gamma = 0 \right\} \end{aligned}$$

as convex sets that contain admissible velocity fields.

Moving on to an appropriate function space for the strain-rate tensors, we set

$$Q := L^r(\Omega)^{d\times d}_{\mathrm{sym}} = \left\{ \dot\gamma \in L^r(\Omega)^{d\times d} \;\middle|\; \dot\gamma = \dot\gamma^\top \right\}$$

and $S := Q^*$ for the space containing stress tensors.

It is easy to derive a less abstract representation of S. As a consequence of Theorem 4.9, we may identify $(L^r(\Omega)^{d\times d})^*$ with $L^{r^*}(\Omega)^{d\times d}$. Let now $\dot\gamma \in Q$ and $\tau \in L^{r^*}(\Omega)^{d\times d}$. Then the symmetry of $\dot\gamma$ implies

$$\begin{aligned} \langle \tau, \dot\gamma \rangle_{L^{r^*}(\Omega)^{d\times d}, L^r(\Omega)^{d\times d}} &= \int_\Omega \sum_{i,j=1}^d \tau_{ij}\dot\gamma_{ij} \,\mathrm{d}x \\ &= \int_\Omega \sum_{i=1}^d \tau_{ii}\dot\gamma_{ii} \,\mathrm{d}x + \int_\Omega \sum_{i<j=1}^d (\tau_{ij} + \tau_{ji})\dot\gamma_{ij} \,\mathrm{d}x. \end{aligned}$$

Hence, we conclude that two elements $\tau, \tilde\tau \in L^{r^*}(\Omega)^{d\times d}$ paired in duality with $\dot\gamma \in Q$ yield the same real number, as long as $\tau_{ij} + \tau_{ji} = \tilde\tau_{ij} + \tilde\tau_{ji}$, for all $i, j \in \{1, \ldots, d\}$. From each class of all $\tau \in L^{r^*}(\Omega)^{d\times d}$, which are equivalent in this sense, we select the unique symmetric representative and may thus identify

$$S = L^{r^*}(\Omega)^{d\times d}_{\mathrm{sym}} = \left\{ \tau \in L^{r^*}(\Omega)^{d\times d} \;\middle|\; \tau = \tau^\top \right\}.$$

Finally, we introduce for the pressure

$$P := L^{r^*}(\Omega)$$
$$P_0 := L_0^{r^*}(\Omega) = \left\{ p \in L^{r^*}(\Omega) \,\middle|\, \int_\Omega p \,\mathrm{d}x = 0 \right\}.$$

4.17 Functionals for Variational Formulations To shorten our notation, we define the trilinear form $c : W^{1,r}(\Omega)^d \times W^{1,r}(\Omega)^d \times W^{1,r}(\Omega)^d \to \mathbb{R}$

$$c(u, v, w) := \int_\Omega ((u \cdot \nabla)\, v) \cdot w \,\mathrm{d}x$$

the functional $j : L^r(\Omega)^{d\times d} \to \mathbb{R}$

$$j(\dot\gamma) := \tau_0 \int_\Omega |\dot\gamma| \,\mathrm{d}x$$

and, depending on the constitutive law, $a : L^r(\Omega)^{d\times d} \times L^r(\Omega)^{d\times d} \to \mathbb{R}$

$$a(\dot\gamma, \dot\delta) := 2\mu \int_\Omega \dot\gamma : \dot\delta \,\mathrm{d}x \qquad \text{(Bingham)}$$
$$a(\dot\gamma, \dot\delta) := 2\mu \int_\Omega \dot\gamma : \dot\delta \,\mathrm{d}x + 2\sqrt{2\mu\tau_0} \int_\Omega \frac{\dot\gamma}{\sqrt{|\dot\gamma|}} : \dot\delta \,\mathrm{d}x \qquad \text{(Casson)}$$
$$a(\dot\gamma, \dot\delta) := 2^{r-1}\kappa \int_\Omega |\dot\gamma|^{r-2}\dot\gamma : \dot\delta \,\mathrm{d}x \qquad \text{(Herschel-Bulkley)}$$

Obviously, the potentially problematic terms in the nonlinear form a of the Casson and Herschel-Bulkley models vanish in the limiting case $\dot\gamma \to 0$. Therefore, by setting $a(0, \dot\delta) :\equiv 0$, a is always well-defined (and continuous). The same holds true for the nonsmooth functional j, we refer back to the embedding in Part (b) of Theorem 4.7 on page 84. The situation is less clear for the convective functional c. Proofs for its continuity in two spatial dimensions and in the Hilbert space setting can be found in classical textbooks on the analysis of the Navier-Stokes equations, e.g. [10, p 108], [150, p 106] or [151, p 284]. This covers the cases of Bingham or Casson fluids. For unsteady, inertial flows of Herschel-Bulkley fluids, we have to restrict the permissible range of exponents r in order to guarantee that c remains finite:

4.18 Lemma$^{(TT)}$ (Boundedness of the Trilinear Form c) *Let $d = 2$ and $\frac{3}{2} \le r \le 2$. Then*

there exists a constant $C > 0$ such that

$$|c(u,v,w)| \le C\|u\|_{W^{1,r}(\Omega)^2}\|v\|_{W^{1,r}(\Omega)^2}\|w\|_{W^{1,r}(\Omega)^2},$$

for all $u, v, w \in W^{1,r}(\Omega)^2$.

Proof. Observe that c is given by a sum of terms of the form $\int_\Omega u_i \frac{\partial v_j}{\partial x_i} w_j \,\mathrm{d}x$, with $i, j \in \{1, 2\}$.

It is easily verified that $\frac{3}{2} \le r \le 2$ implies

$$r < 4 \le \frac{2r}{r-1} \le 6 \le \frac{2r}{2-r}.$$

Therefore, the SOBOLEV embedding in Part (c) of Theorem 4.7, which for $d = 2$ reads

$$W^{1,r}(\Omega) \hookrightarrow L^q(\Omega) \qquad \text{for } r \le q \le \frac{2r}{2-r},$$

is true in particular for $q := \frac{2r}{r-1}$. Hence, $u_i, w_j \in L^q(\Omega)$. Since $\frac{1}{q} + \frac{1}{r} + \frac{1}{q} = 1$, HÖLDER's inequality applied to $\int_\Omega u_i \frac{\partial v_j}{\partial x_i} w_j \,\mathrm{d}x$ yields the assertion. □

4.19 Scalar Potentials Corresponding to the Forms a For all of the three models under consideration, the bilinear or nonlinear form a possesses special structure: it is integrable. In each case, one can find a functional $b : L^r(\Omega)^{d\times d} \to \mathbb{R}$, such that $a(\dot\gamma, \dot\delta) = \langle b'(\dot\gamma), \dot\delta\rangle_{L^{r^*}(\Omega)^{d\times d}, L^r(\Omega)^{d\times d}}$, for all $\dot\gamma, \dot\delta \in L^r(\Omega)^{d\times d}$. Explicitly, we have

$$b(\dot\gamma) := \mu \int_\Omega |\dot\gamma|^2 \,\mathrm{d}x \qquad \text{(BINGHAM)}$$

$$b(\dot\gamma) := \mu \int_\Omega |\dot\gamma|^2 \,\mathrm{d}x + \frac{4\sqrt{2\mu\tau_0}}{3} \int_\Omega |\dot\gamma|^{3/2} \,\mathrm{d}x \qquad \text{(CASSON)}$$

$$b(\dot\gamma) := \frac{2^{r-1}\kappa}{r} \int_\Omega |\dot\gamma|^r \,\mathrm{d}x. \qquad \text{(HERSCHEL-BULKLEY)}$$

This representation is classical for BINGHAM fluids [145], [146], [152] and HERSCHEL-BULKLEY fluids [76]. For these consitutive models, $(b \circ \mathcal{D})'$ equates to the r-Laplacian operator, possibly modulo a constant factor. A different elliptic operator is associated to the CASSON model. For the special case of steady and unidirectional pipe flow, such a formulation has appeared in [153].

Following Duvaut and Lions [145], [146] we can now formulate the problem of viscoplastic flow in this manner:

4.20 Definition (Unsteady Viscoplastic Flow as Variational Inequality Problem) For $t \in]0,T[$, let boundary conditions $u_{\mathrm{D}}(t) \in U_{\mathrm{D}}$, an initial condition $u_0 \in U_{0\mathrm{D}}$ and $f(t) \in U_{00}^*$ be given*. We refer to $(u(t))_{t\in]0,T[} \subset U_{0\mathrm{D}}$ as a *weak solution of the unsteady viscoplastic flow problem*, if

$$\begin{aligned} &\varrho\left(\langle \partial_t u(t), v-u(t)\rangle_{U_{00}^*,U_{00}} + c(u(t),u(t),v-u(t))\right) + a(\mathcal{D}u(t),\mathcal{D}v-\mathcal{D}u(t)) \\ &\quad + j(\mathcal{D}v) - j(\mathcal{D}u(t)) \geq \langle f(t), v-u(t)\rangle_{U_{00}^*,U_{00}} \qquad \forall v \in U_{0\mathrm{D}},\ \text{a.e. } t \in]0,T[\end{aligned} \tag{4.7}$$

and

$$u(0) = u_0. \tag{4.8}$$

4.21 Theorem (Multiplier Formulation of Unsteady Viscoplastic Flow) *A function $u(t) \in U_{0D}$ satisfies the system (4.7)-(4.8) if and only if there exists a multiplier $q(t) \in S$ such that*

$$\begin{aligned} &\varrho\left(\langle \partial_t u(t), v\rangle_{U_{00}^*,U_{00}} + c(u(t),u(t),v)\right) + a(\mathcal{D}u(t),\mathcal{D}v) \\ &\qquad + \langle q(t),\mathcal{D}v\rangle_{Q^*,Q} = \langle f(t),v\rangle_{U_{00}^*,U_{00}} \qquad \forall v \in U_{00},\ a.e.\ t \in]0,T[\end{aligned} \tag{4.9}$$

and

$$|q(t,x)| \leq \tau_0 \qquad a.e.\ on\ ]0,T[\times\Omega \tag{4.10}$$

$$q(t,x) : \mathcal{D}u(t,x) = \tau_0\,|\mathcal{D}u(t,x)| \qquad a.e.\ on\ ]0,T[\times\Omega \tag{4.11}$$

with the initial condition

$$u(0) = u_0. \tag{4.12}$$

4.22 Alternative Weak Formulations of Unsteady Viscoplastic Flow The multiplier q corresponds to the plastic contribution to the extra stress tensor, i.e.

$$q = \tau_0 \frac{\dot\gamma}{|\dot\gamma|}$$

whenever $\dot\gamma \neq 0$. Other authors, like Basov and Shelukhin [147], [148], employ the extra stress τ as multiplier and replace the system (4.10)-(4.11) with the requirement,

*We use the notation $u(t) := u(t,\cdot)$, so that $t \mapsto u(t)$ can be interpreted as a curve in $W^{1,r}(\Omega)^d$, parameterised by the time t. Analogous definitions hold for the remaining time-dependent variables and data.

that the constitutive relations (4.5) be fulfilled almost everywhere. It is easy to see (cf [15]) that the velocity part of a solution $(u(t), \tau(t))$ to the Basov-Shelukhin formulation is also a weak solution in the sense of Duvaut and Lions.

4.23 Well-Posedness of the Initial Condition It is a priori unclear whether there exists a weak solution for which the mapping $t \mapsto u(t)$ possesses sufficient regularity to define a trace at time $t = 0$, so that the initial condition makes sense. Classical existence results for solutions of the Navier-Stokes equations can ensure that $t \mapsto u(t)$ is continuous at almost all times t, which is clearly sufficient for the trace at $t = 0$ to be well-defined. The extension of such an existence result to the Bingham flow problem appears in [146, p 303], and continuity almost everywhere follows with Theorem 1 of [154, p 473].

In L^r-based Sobolev spaces, existence results for the Navier-Stokes equations with well-posed initial conditions are available under 'smallness of data' conditions [155, pp 52-56]. Generalisations to an existence theory for Herschel-Bulkley fluids appear to be very scarce. The main result in this respect is due to Eberlein and Růžička [149], who established the existence of a weak solution* under homogeneous boundary conditions and a mild assumption on the initial data. In their setting, $t \mapsto u(t)$ is continuous almost everywhere and thus the initial condition is sensible. For related results on the existence and regularity of solutions to viscoplastic flow problems, we also refer to [15], [156]–[164].

4.24 Definition (Stationary Viscoplastic Flow as Variational Inequality Problem) Let $u_{\mathrm{D}} \in U_{\mathrm{D}}$ and $f \in U_{00}^*$. We refer to $u \in U_{0\mathrm{D}}$ as a *weak solution of the stationary viscoplastic flow problem*, if

$$a(\mathcal{D}u, \mathcal{D}v - \mathcal{D}u) + j(\mathcal{D}v) - j(\mathcal{D}u) \geq \langle f, v - u \rangle_{U_{00}^*, U_{00}} \qquad \forall v \in U_{0\mathrm{D}}. \tag{4.13}$$

We are now in the position to establish the connection between the abstract convex programming problems in the first part of this thesis and the viscoplastic flow problems, that form its second part. Due to the integrability of a, we recognise that the variational inequality (4.13) states an optimality condition for a convex optimisation problem. Therefore, Theorem 2.25 on page 28 provides the following characterisation of weak solutions in the stationary case:

4.25 Theorem (Characterisation of Weak Solutions) *A velocity field $\bar{u} \in U_{0D}$ is a weak solution of the stationary viscoplastic flow problem, if an only if*

$$\bar{u} = \operatorname*{arg\,min}_{u \in U_{0D}} b(\mathcal{D}u) + j(\mathcal{D}u) - \langle f, u \rangle_{U_{00}^*, U_{00}}, \tag{4.14}$$

*A weak solution in the sense of Basov and Shelukhin

A characterisation by means of a multiplier can be derived in complete analogy to Theorem 4.21.

Let us remark that even in the instationary setting, we can still apply our methodology for convex optimisation problems. Two examples for suitable time-discretisation schemes, which lead to very similar convex programs, are the subject of Chapter 7. Consequently, whenever we refer to approaches to solving the steady flow problems, there are normally analogous approaches for unsteady flow problems, once these have been appropriately semi-discretised in time.

We also point out that despite contrary claims in the literature [153, p 141], for any of the three constitutive models a weak solution of the stationary flow problem exists and is unique:

4.26 Theorem (Existence and Uniqueness of Weak Solutions) *There exists a unique weak solution $\bar{u} \in U_{0D}$ of the stationary viscoplastic flow problem (4.13) or (4.14).*

Proof. The objective in (4.14) is clearly proper, strictly convex, continuous, coercive and the underlying function space is reflexive, since $1 < r < \infty$. Therefore, Theorem 2.26 is applicable and yields the desired result. □

4.27 Genuinely Nonsmooth Methods for Numerical Solutions Since the Bingham and Casson flow problems are posed in Hilbert Spaces, the traditional methods that we reviewed in Chapter 2, Section (D) are immediately applicable. In contrast, the Herschel-Bulkley model demands for nonlinear methods in Banach spaces. Owing to the fact that the physical memory and the processing capabilities of a computer are only finite, algorithms in infinite-dimensional function spaces are not actually implementable. Instead, one has to apply a discretisation scheme to be able to compute approximate solutions to the subproblems that arise in every iteration. This approach, where one computes approximations to iterates in function spaces, is commonly termed 'first optimise, then discretise'.

To avoid the difficulties of a nonlinear algorithm for the Herschel-Bulkley problem, it is common [78], [76, pp 129-131] to fully discretise the entire optimisation problem. The resulting problem is then posed in $\mathbb{R}^n$, with $n \in \mathbb{N}$ typically very large. The main advantage of this 'first-discretise-then-optimise' approach consists in the Hilbert space structure of $\mathbb{R}^n$. The solution of problems, which are not originally posed in Hilbert spaces, simplifies tremendously.

On another hand, a discretisation right at the outset concurrently defines the discretisation schemes for the dual problem and any additional variables as well. It is, however, often desirable to tailor finite-dimensional approximations to characteristic features of each variable. This is generally only possible within the 'first-optimise-then-discretise'

framework. Furthermore, the latter approach allows for very desirable strong statements on mesh-independent convergence, see e.g. [165], [166].

An Uzawa Algorithm for the Bingham flow problem already appeared in 1972 [167]. The alternating direction method of multipliers (ADMM / ALG2) for the same problem was introduced a decade later in [76], [168]. It has since been applied extensively, also for Casson and discretised Herschel-Bulkley flow problems. We exemplarily refer to [153], [169]–[173] for some representative works. ADMM can be considered state-of-the-art in numerical viscoplasticity.

Some authors have investigated alternative numerical schemes that are less generic in nature but more specifically adapted to the structure of the viscoplastic optimality conditions in particular. He and Glowinski [174] study a fictitious time-dependent problem whose steady state corresponds to the stationary Bingham problem. They then recover this stationary limit by stepping through time according to the backward Euler method. Their methodology is closely related to the proximal point algorithm. In a similar fashion, Aposporidis and co-authors [175]–[177] propose another Picard iteration for solving a multiplier formulation of the optimality condition (4.13) for stationary Bingham flow. Even more specific tools with limited applicability to general flow probles were used in [178], [179].

Regularised Approximations

It appears that smoothed and regularised formulations of the viscoplastic flow problem clearly dominate in the literature. Rather than solving any of the aforementioned nonsmooth problems, many authors first segue to a modified formulation with higher regularity, which is hence amenable to solutions by fast Newton-type methods. We provide a brief overview of such approaches, focussing on the Bingham model, since the procedure is completely analogous for Casson or Herschel-Bulkley fluids. We then argue why we choose to tackle the original nonsmooth problem in this work.

4.28 Bercovier-Engelman Modification In [180], Bercovier and Engelman suggest to surmount the nondifferentiability of viscoplastic flow problems by replacing

$$|\dot{\gamma}| \approx \sqrt{\varepsilon^2 + |\dot{\gamma}|^2}$$

in the constitutive relations (4.5). This way, the denominator may no longer vanish and the differentiation between the two different cases $\dot{\gamma} \neq 0$ and $\dot{\gamma} = 0$ can be dropped. For

three different values of $\varepsilon > 0$, we plot the modified Bingham model

$$\tau = 2\mu\dot{\gamma} + \tau_0 \frac{\dot{\gamma}}{\sqrt{\varepsilon^2 + |\dot{\gamma}|^2}} \tag{4.15}$$

along with the original constitutive relation in Figure 4.1(a) on the facing page.

4.29 Papanastasiou Regularisation A closely related modification is due to Papanastasiou. In his article [181], he advocates to replace the $O(1/\varepsilon)$ approximation of Bercovier and Engelman with an exponential model. The Bingham model with Papanastasiou modification reads

$$\tau = 2\mu\dot{\gamma} + \tau_0 \frac{\left(1 - e^{-|\dot{\gamma}|/\varepsilon}\right)\dot{\gamma}}{|\dot{\gamma}|}, \tag{4.16}$$

with $\tau := 0$ where $\dot{\gamma} = 0$. Figure 4.1(b) shows the qualitatively similar behaviour to the Bercovier-Engelman model.

4.30 Bi-Viscosity Model Clearly, the previous two regularisations affect the original viscoplastic models globally. Moreover, they also result in fully smooth approximations. Another model that attempts to reflect the inherent nonsmoothness of viscoplastic problems more accurately, while introducing only a local modification, is given by the bi-viscosity approximation. The quasi-infinite viscosity of a Bingham fluid under the plastic regime $\dot{\gamma} = 0$ is approximated by a very large, but still finite value.

Tanner and Milthorpe [182] published this idea in 1983. More recently, Gonzalez Andrade and De los Reyes [183]–[187] contributed in-depth studies of this approach, where they derive the model from a Tikhonov regularisation in the dual problem, or equivalently, a Huber regularisation of the primal problem.

For three different values of the regularisation parameter $\varepsilon > 0$, we provide a sketch of the semismooth bi-viscosity model

$$\tau = 2\mu\dot{\gamma} + \tau_0 \frac{\dot{\gamma}}{\max\left(\varepsilon\tau_0, |\dot{\gamma}|\right)} \tag{4.17}$$

in Figure 4.1(c).

4.31 C^2-Regularisation of the Dual Glowinski and collaborators [188]–[192] put forward a different approach: the inequality (4.10) in the multiplier formulation reflects the

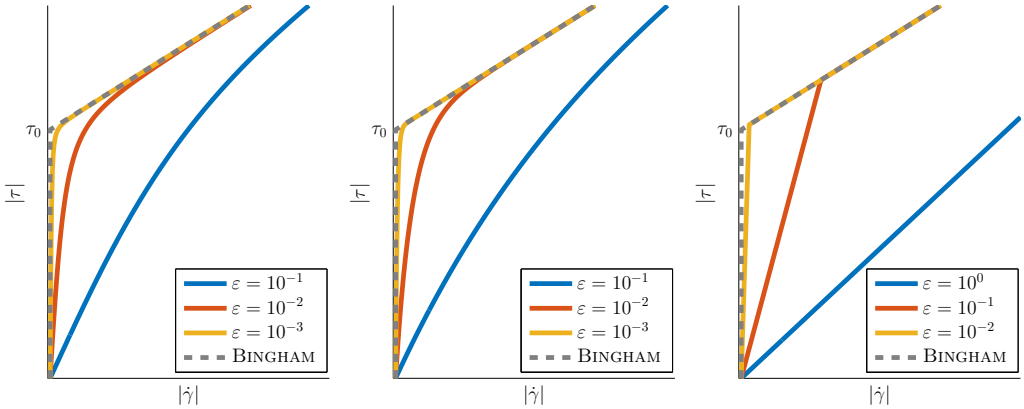

(a): Smooth approximation of Bercovier and Engelman [180].

(b): Smooth regularisation according to Papanastasiou [181] with exponential decay.

(c): Semismooth bi-viscosity model of Tanner/Milthrope [182] and Gonzalez Andrade/De los Reyes [183]–[187].

Figure 4.1: Common regularised approximations of the Bingham model. While the first two models lead to a global modification, the third regularisation acts only locally near the yield surface.

fact that

$$\begin{cases} |q| \leq \tau_0 & \text{if } \dot\gamma = 0 \\ |q| = \tau_0 \dfrac{|\dot\gamma|}{|\dot\gamma|} = \tau_0 & \text{if } \dot\gamma \neq 0. \end{cases}$$

Rather than enforcing equality in the second case strictly, the authors penalise violations of the constraint $|q| \leq \tau_0$ by replacing it with the term

$$\frac{1}{6\varepsilon} \int_\Omega \left(|q|^2 - \tau_0^2 \right)_+^3 \, \mathrm{d}x \tag{4.18}$$

in the dual objective, for $\varepsilon > 0$. We recall the notation $(\,\cdot\,)_+ := \max\{0, \cdot\}$.

In terms of citation numbers, it appears that methods of viscosity regularisation have proved far more popular than this penalty approach. One possible explanation could be that numerical solutions under the bi-viscosity approximation require fewer subproblems to be solved, as Gonzalez Andrade and De los Reyes observed in [183], [184]. This is true in particular for the Bercovier-Engelman and Papanastasiou modifications.

4.32 Genuinely Nonsmooth Vs Regularised Formulations It can be seen as the main advantage of regularised formulations that they allow for very efficient numerical methods of Newton-type, with fast, locally superlinear or quadratic convergence rate. This

contrasts sharply to methods from convex optimisation for the original nonsmooth formulation, where only a sublinear rate can generally be established. Furthermore, for each of the aforementioned regularisation methods (4.15)-(4.18) with corresponding solutions u_ε, it is straightforward to prove strong convergence to the exact solution u [175], [185], [188], [193],

$$\|u_\varepsilon - u\|_{W^{1,r}(\Omega)^d} \to 0, \qquad \text{as } \varepsilon \to 0.$$

In practice, conditioning deteriorates as $\varepsilon \to 0$. This implies that one has to find a compromise between goodness of fit to the original formulation (small ε) and stability of the method (not too small ε). By means of a path-following strategy, Gonzalez Andrade and De los Reyes are able to compute reliable approximations for far smaller regularisation parameters than previously attainable [183], [184].

In summary, if the objective of a viscoplastic flow simulation consists solely in finding an accurate approximation to the exact velocity fields, then a regularised formulation is most appropriate.

Even though such an approximate solution u_ε can be arbitrarily close to the exact solution, it does not generally reflect the characteristic features of viscoplastic flow fields. We recall from Chapter 1 that our aim is to compute solutions, which exhibit

(a) the *existence of a positive yield stress* that has to be exceeded before the fluid leaves its state of rigidity; consequently,

(b) a *separation of the flow domain* into regions with viscous shear flow and plastic stagnation; and additionally,

(c) in the absence of sufficiently strong driving forces, *cessation of flow within finite time*.

Formulations based on viscosity regularisation violate all three of these criteria by design.

Regarding the first feature (a), Moyers-González and Frigaard [169] demonstrate that even under arbitratily small excitations, solutions to regularised models predict slow flow although the actual flow rate is exactly zero, cf also [193], [194].

Due to its nonsmoothness, bi-viscosity formulations still suggest a natural way of defining distinct regions in the flow domain as demanded for by criterion (b); an approach followed in [183]–[187]. When the fully smooth Bercovier-Engelman or Papanastasiou models are employed, then a threshold has to be set with some degree of arbitrariness. Still, recovering the actual yielded and unyielded regions under a regularised problem formulation is very difficult. In fact, it appears that convergence of these approximate plug and shear regions has not been proved yet, and such a statement may not even hold

[194]. Hence, we have to assume that approximate regions stemming from regularised formulations may exhibit different geometrical features, or, in the worst case, even have a different topology. We will re-visit this topic in detail when we present our numerical results in subsequent chapters.

Incidentally, some authors have shown that numerical solutions may still reflect the third phenomenon (c), even if a regularised formulation is employed. Chatzimina and co-authors report finite stopping times for Bingham-Papanastasiou fluids [195], [196]. De los Reyes and Gonzalez Andrade observe the same behaviour for solutions to a bi-viscosity approximation of Bingham flow [186]. Although the analytical solution u_ε to a problem with finite viscosity tends to zero only asymptotically [197, pp 187-189], it is the finite arithmetic precision in conjunction with round-off and discretisation errors of any numerical scheme, which cause the contrary—and in this case rather desirable—artefact of certain numerical approximations.

Let us outline the contributions that we wish to accomplish with our methodology: we target applications where a mere quantitative approximation to the velocity field is insufficient. An accurate determination of yielded and unyielded regions lies in the focal point of our attention. Consequently, it is imperative that we employ numerical methods, which preserve the characteristic features of the genuinely nonsmooth formulation. We address the drawback of slow convergence of state-of-the-art methods, such as ADMM, by accelerated schemes and preconditioning techniques, as derived in the first part of this work. The following three chapters are therefore devoted to assessing the performance of this new approach, in comparison to the alternative methods that we reviewed in this section.

Chapter 5

Stationary Pipe Flow

This chapter is devoted to studying the problem of viscoplastic fluid flow at steady state through infinitely long pipes. As sketched in Figure 5.1, this restriction implies that we effectively search a one-dimensional velocity profile over a two-dimensional flow domain. In the literature, this set up is occasionally referred to as '1.5-dimensional flow problem' [198]. Despite its relative simplicity, it serves as a very common touchstone for numerical methods. The imposed restrictions allow for a more far-reaching analysis than flow problems in more general geometries, thus offering a number of analytical results for comparisons with numerical approximations.

We proceed as follows: in Section (A), we derive an implementable form of our methods from the first part. Our first numerical experiments in Section (B) focus on the convergence properties of the new algorithms, compared to state-of-the-art alternatives. Further simulations in Section (C) shall explore the capability of the different methods

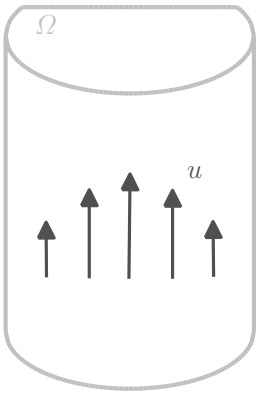

Figure 5.1: Sketch of the pipe-flow geometry: the duct extends infinitely in the vertical direction with a homogeneous cross-section $\Omega \subset \mathbb{R}^2$. The flow velocity u is a scalar field that can only vary in the two horizontal directions.

with respect to the challenge of identifying regions of stagnant or shear flow, as well as detecting the plastic limit of no flow at all.

(A) Explicit Form of the Proximal Algorithms

Governing Equations

To begin with, let us derive a simplified form of the governing equations, taking into account the assumptions on the flow geometry. Initially, the flow domain $\Omega \subset \mathbb{R}^3$ is unbounded in x_3-direction, and only the third component of the flow velocity does not necessarily vanish. Hence,

$$u(x_1, x_2, x_3) = (0, 0, u_3(x_1, x_2))^\top .$$

Therefore, the incompressibility condition $\operatorname{div} u = 0$ is generally satisfied. Additionally,

$$\dot\gamma = \mathcal{D}u = \frac{1}{2} \begin{pmatrix} 0 & 0 & \frac{\partial u_3}{\partial x_1} \\ 0 & 0 & \frac{\partial u_3}{\partial x_2} \\ \frac{\partial u_3}{\partial x_1} & \frac{\partial u_3}{\partial x_2} & 0 \end{pmatrix}$$

and without loss of generality, the stress τ possesses the same sparsity pattern. For the Frobenius norm of the strain rate we have

$$|\dot\gamma| = \frac{1}{\sqrt{2}} \sqrt{\left(\frac{\partial u_3}{\partial x_1}\right)^2 + \left(\frac{\partial u_3}{\partial x_2}\right)^2} = \frac{1}{\sqrt{2}} \left| \begin{pmatrix} \frac{\partial u_3}{\partial x_1} \\ \frac{\partial u_3}{\partial x_2} \end{pmatrix} \right| = \frac{1}{\sqrt{2}} \left| \nabla u_3 \right| ,$$

where ∇ refers to the gradient operator in two dimensions. Motivated by these observations, we introduce new variables and parameters

$$\tilde u := u_3 \qquad \tilde{\dot\gamma} := \begin{pmatrix} \dot\gamma_{13} \\ \dot\gamma_{23} \end{pmatrix} \qquad \tilde\tau := \begin{pmatrix} \tau_{13} \\ \tau_{23} \end{pmatrix} \qquad \tilde\tau_0 := \frac{\tau_0}{\sqrt{2}} \qquad \tilde\kappa := 2^{1-\frac{r}{2}} \kappa$$

as well as the cross-section

$$\tilde\Omega := \Omega \cap \left\{ x \in \mathbb{R}^3 \;\middle|\; x_3 = 0 \right\}$$

and we drop the tilde in our notation for the remainder of this chapter. Accordingly, we work with the Sobolev spaces

$$U := U_{00} := W_0^{1,r}(\Omega), \qquad Q := L^r(\Omega)^2 \qquad \text{and} \qquad S := L^{r^*}(\Omega)^2.$$

After these preliminaries, we can now state the minimisation problem, which, according to Theorem 4.25 on page 93, characterises weak solutions to the problem under consideration.

5.1 Formulation of Steady Viscoplastic Duct Flow as Minimisation Problem Let $f \in L^{r^*}(\Omega)$ be given. Then find the solution $\bar{u} \in U$ of the convex programming problem

$$\min_{u \in U} \left\{ I(u) := b(\nabla u) + j(\nabla u) - \langle f, u \rangle_{L^{r^*}(\Omega), L^r(\Omega)} \right\} \tag{VP-P}$$

where

$$b(\nabla u) = \frac{\mu}{2} \int_\Omega |\nabla u|^2 \, \mathrm{d}x \qquad \text{(Bingham)}$$

$$b(\nabla u) = \frac{\mu}{2} \int_\Omega |\nabla u|^2 \, \mathrm{d}x + \frac{4\sqrt{\mu \tau_0}}{3} \int_\Omega |\nabla u|^{3/2} \, \mathrm{d}x \qquad \text{(Casson)}$$

$$b(\nabla u) = \frac{\kappa}{r} \int_\Omega |\nabla u|^r \, \mathrm{d}x \qquad \text{(Herschel-Bulkley)}$$

and

$$j(\nabla u) = \tau_0 \int_\Omega |\nabla u| \, \mathrm{d}x.$$

Moreover, the duality pairing reads in explicit form

$$\langle f, u \rangle_{L^{r^*}(\Omega), L^r(\Omega)} = \int_\Omega f u \, \mathrm{d}x.$$

5.2 Discretisation of the Herschel-Bulkley Flow Problem To be able to apply our methodology for the Hilbert space setting, we now have to discretise the optimisation problem that models the flow of Herschel-Bulkley fluids. In a manner to be specified later on, we have to approximate the flow velocity $u \approx u_h$, where u_h belongs to a finite-dimensional subspace $U_h \subset U$. The problem is then constrained to U_h.

Strictly speaking, we would now have to differentiate between such finite-dimensional subspaces, whenever we refer to the Herschel-Bulkley problem, while we concurrently work with the original function spaces for the Bingham and Casson problems. In an attempt to provide a clearer picture, we will not make such a distinction between U and U_h for now. Instead, we opt for a purely formal presentation of the approach in the given function spaces. It shall therefore be emphasised at this point that in order to

re-establish a mathematically rigorous formulation for Herschel-Bulkley fluids, one has to replace all variables with their finite-dimensional counterparts.

5.3 Problem (VP-P) as Composite Convex Problem There are several possible ways to split (VP-P) into a composite objective with convex and strongly convex terms. In the literature on viscoplasticity, one frequently encounters the formulation

$$\min_{(u,\dot\gamma)\in U\times Q} [b(\dot\gamma)] + \left[j(\nabla u) - \langle f, u\rangle_{L^{r^*}(\Omega),L^r(\Omega)}\right] \qquad \text{subject to} \qquad \dot\gamma = \nabla u$$

or the corresponding first-order optimality conditions. A Lagrange multiplier associated to the linear constraint is exactly the plastic component q of the extra stress tensor. A step-by-step derivation of the dual problem, which assumes the form of an elliptic optimal control problem with pointwise inequality constraint on the control, can be found in [184].

Authors, who apply ADMM to viscoplastic flow problems, typically consider the alternative splitting

$$\min_{(u,\dot\gamma)\in U\times Q} [b(\dot\gamma) + j(\dot\gamma)] + \left[-\langle f, u\rangle_{L^{r^*}(\Omega),L^r(\Omega)}\right] \qquad \text{subject to} \qquad \dot\gamma = \nabla u \qquad \text{(VP-P')}$$

instead [76], [153], [169], [171]. This way, a dual multiplier corresponds to an admissible stress field τ.

Subproblems Arising in the Proximal Algorithms

It is justified to raise the question why we do not consider proximal algorithms applied to the primal problem (VP-P) directly. At least for Bingham fluids, the functional b is differentiable with Lipschitz continuous gradients. Furthermore, the functional j possesses simple structure, and recalling Example 2.48 on page 41, proximal maps are in fact available in closed form.

This is, however, no longer true for the composition $j\circ\nabla$. Each evaluation of a proximal operator would necessitate the solution of a subproblem, which again requires an iterative solution. This situation is comparable to image de-blurring problems with total-variation regularisation, which can be approached by iterative solutions of de-noising problems, cf [121]. Furthermore, the functionals b associated with Casson and shear-thinning Herschel-Bulkley fluids do not meet the smoothness criterion of Lipschitz continuous gradients. Instead of applying accelerated proximal gradient methods, one would have to revert to a proximal point algorithm with its inferior performance.

In conclusion, a dual-based approach appears far more promising for facilitating efficient numerical methods. We will now derive the explicit form of the proximal-type mappings

that arise in the methods (F)ISTA* and VM-(F)ISTA*. It turns out that, indeed, these assume a simple form for all three viscoplastic fluids.

5.4 Assumptions on the Primal Problem In Assumption 3.1 on page 57, we summarised the prerequisites that have to be met so that these algorithms become applicable. We briefly validate these assumptions for the problem (VP-P):

(a) U and Q (or their discretised counterparts) are, indeed, HILBERT spaces.

(b) All of the functionals b, j and the duality pairing with f are proper, convex and continuous, in particular lower semicontinuous. For BINGHAM and CASSON fluids, b is apparently μ-strongly convex. For HERSCHEL-BULKLEY fluids, b is not globally strongly convex, but since $r \in]1,2]$, b is strongly convex on the bounded sets of Q. This weaker assumption is effectively equivalent to global strong convexity, as long as the sequences generated by a numerical method remain bounded.

(c) The gradient operator $\nabla : U \to Q$ is bounded by definition of the canonical norm on $U = W_0^{1,r}(\Omega)$. It is also bounded below in the sense of (3.1) due to POINCARÉ's inequality.

(d) The qualification condition (3.3) holds, since $b + j$ is in particular continuous at 0, for instance.

Next, we state an auxiliary result.

5.5 Lemma$^{(\mathrm{TT})}$ (Unique Solution of a Variational Inequality) *Let $\tau \in S$. The variational inequality*

$$\langle b'(\bar{\dot\gamma}) - \tau, \dot\gamma - \bar{\dot\gamma}\rangle_{Q^*,Q} + j(\dot\gamma) - j(\bar{\dot\gamma}) \geq 0, \qquad \forall \dot\gamma \in Q$$

admits a unique solution $\bar{\dot\gamma} \in Q$, which is given by

$$\bar{\dot\gamma} = \frac{1}{\mu}\left(|\tau| - \tau_0\right)_+ \frac{\tau}{|\tau|} \qquad \text{(BINGHAM)}$$

$$\bar{\dot\gamma} = \frac{1}{\mu}\left(\sqrt{|\tau|} - \sqrt{\tau_0}\right)_+^2 \frac{\tau}{|\tau|} \qquad \text{(CASSON)}$$

$$\bar{\dot\gamma} = \frac{1}{\kappa^{r^*-1}}\left(|\tau| - \tau_0\right)_+^{r^*-1} \frac{\tau}{|\tau|}. \qquad \text{(HERSCHEL-BULKLEY)}$$

Here, and from now on, we define $0 \cdot \frac{\tau}{|\tau|} := 0$ for $\tau = 0$.

Proof. The variational inequality represents an optimality condition of the strictly convex minimisation problem

$$\min_{\dot\gamma \in Q} b(\dot\gamma) + j(\dot\gamma) - \langle \tau, \dot\gamma\rangle_{Q^*,Q},$$

hence the solution is unique.

Let us exemplarily verify that $\bar{\dot{\gamma}}$ in the asserted form is indeed one, and thus the only solution of the variational inequality for the case of Herschel-Bulkley fluids*. Since $r^* - 1 = \frac{1}{r-1}$, we have

$$b'(\bar{\dot{\gamma}}) = \kappa|\bar{\dot{\gamma}}|^{r-2}\bar{\dot{\gamma}} = (|\tau| - \tau_0)_+ \frac{\tau}{|\tau|}.$$

Therefore, with $q := \dot{\gamma} - \bar{\dot{\gamma}}$,

$$\begin{aligned}
\langle b'(\bar{\dot{\gamma}}) - \tau, q\rangle_{Q^*,Q} &= \left\langle (|\tau| - \tau_0)_+ \frac{\tau}{|\tau|} - \tau, q \right\rangle_{Q^*,Q} \\
&= \int\limits_{\{\,|\tau|>\tau_0\,\}} (|\tau| - \tau_0)\frac{\tau}{|\tau|} \cdot q \,\mathrm{d}x - \int\limits_{\Omega} \tau \cdot q \,\mathrm{d}x \\
&= -\int\limits_{\{\,|\tau|\le\tau_0\,\}} \tau \cdot q \,\mathrm{d}x - \tau_0 \int\limits_{\{\,|\tau|>\tau_0\,\}} \frac{\tau}{|\tau|} \cdot q \,\mathrm{d}x.
\end{aligned}$$

From the Cauchy-Schwarz inequality we derive for the first integral

$$-\int\limits_{\{\,|\tau|\le\tau_0\,\}} \tau \cdot q \,\mathrm{d}x \ge -\int\limits_{\{\,|\tau|\le\tau_0\,\}} |\tau||q| \,\mathrm{d}x \ge -\tau_0 \int\limits_{\{\,|\tau|\le\tau_0\,\}} |q| \,\mathrm{d}x = -\tau_0 \int\limits_{\{\,|\tau|\le\tau_0\,\}} |q + \bar{\dot{\gamma}}| \,\mathrm{d}x,$$

where the last equality holds since $\bar{\dot{\gamma}} = 0$ almost everywhere in $\{\,|\tau| \le \tau_0\,\}$. Similarly, we conclude

$$\begin{aligned}
-\tau_0 \int\limits_{\{\,|\tau|>\tau_0\,\}} \frac{\tau}{|\tau|} \cdot q \,\mathrm{d}x &= -\tau_0 \int\limits_{\{\,|\tau|>\tau_0\,\}} \frac{\tau}{|\tau|} \cdot q \,\mathrm{d}x - \tau_0 \int\limits_{\{\,|\tau|>\tau_0\,\}} |\bar{\dot{\gamma}}| \,\mathrm{d}x + \tau_0 \int\limits_{\Omega} |\bar{\dot{\gamma}}| \,\mathrm{d}x \\
&= -\tau_0 \int\limits_{\{\,|\tau|>\tau_0\,\}} \frac{\tau}{|\tau|} \cdot \left(q + |\bar{\dot{\gamma}}| \frac{\tau}{|\tau|} \right) \mathrm{d}x + \tau_0 \int\limits_{\Omega} |\bar{\dot{\gamma}}| \,\mathrm{d}x \\
&\ge -\tau_0 \int\limits_{\{\,|\tau|>\tau_0\,\}} \left| q + |\bar{\dot{\gamma}}| \frac{\tau}{|\tau|} \right| \mathrm{d}x + \tau_0 \int\limits_{\Omega} |\bar{\dot{\gamma}}| \,\mathrm{d}x \\
&= -\tau_0 \int\limits_{\{\,|\tau|>\tau_0\,\}} |q + \bar{\dot{\gamma}}| \,\mathrm{d}x + \tau_0 \int\limits_{\Omega} |\bar{\dot{\gamma}}| \,\mathrm{d}x,
\end{aligned}$$

where we used $\frac{\tau}{|\tau|} = \frac{\bar{\dot{\gamma}}}{|\bar{\dot{\gamma}}|}$ almost everywhere on $\{\,|\tau| > \tau_0\,\}$ in the last step.

*This includes Bingham fluids by setting $r := 2$ and $\mu := \kappa$. The calculation for Casson fluids is completely analogous.

Overall, we have now established

$$\begin{aligned}\langle b'(\bar{\dot\gamma}) - \tau, q\rangle_{Q^*,Q} &\geq -\tau_0 \int\limits_{\{\,|\tau|\leq\tau_0\,\}} |q+\bar{\dot\gamma}|\,\mathrm{d}x - \tau_0 \int\limits_{\{\,|\tau|>\tau_0\,\}} |q+\bar{\dot\gamma}|\,\mathrm{d}x + \tau_0 \int\limits_\Omega |\bar{\dot\gamma}|\,\mathrm{d}x \\ &= -\tau_0 \int\limits_\Omega |q+\bar{\dot\gamma}|\,\mathrm{d}x + \tau_0 \int\limits_\Omega |\bar{\dot\gamma}|\,\mathrm{d}x \\ &= -j(q+\bar{\dot\gamma}) + j(\bar{\dot\gamma}),\end{aligned}$$

which proves the assertion. □

We now present the dual problem for viscoplastic duct flow, which our methods are based on. To the best of our knowledge, this dual formulation has not appeared in the literature so far.

5.6 Proposition[TT] (Dual Duct Flow Problem) *The dual problem associated with the split primal formulation (VP-P′) reads*

$$\min_{\tau\in S} F(\tau) \qquad \textit{subject to} \qquad -\operatorname{div}\tau = f, \tag{VP-D′}$$

where the constraint is to be understood in the weak sense, i.e. for all $u \in U$ it holds

$$\langle \tau, \nabla u\rangle_{Q^*,Q} = \langle f, u\rangle_{L^{r^*}(\Omega),L^r(\Omega)}.$$

The objective F is given by

$$F(\tau) = \frac{1}{2\mu}\int\limits_\Omega (|\tau|-\tau_0)_+^2\,\mathrm{d}x \qquad \text{(Bingham)} \tag{5.1a}$$

$$F(\tau) = \frac{1}{2\mu}\int\limits_\Omega \left(\sqrt{|\tau|}-\sqrt{\tau_0}\right)_+^3 \left(\sqrt{|\tau|}+\frac{1}{3}\sqrt{\tau_0}\right)\mathrm{d}x \qquad \text{(Casson)} \tag{5.1b}$$

$$F(\tau) = \frac{1}{r^*\kappa^{r^*-1}}\int\limits_\Omega (|\tau|-\tau_0)_+^{r^*}\,\mathrm{d}x \qquad \text{(Herschel-Bulkley)} \tag{5.1c}$$

Proof. Let $\tilde f := b + j$ and $\tilde g := -\langle f, \cdot\,\rangle_{L^{r^*}(\Omega),L^r(\Omega)}$. Then, the primal objective is given by $I = \tilde f \circ \nabla + \tilde g$. With Definition 2.31 on page 30, we conclude that the corresponding dual problem reads

$$\min_{\tau\in S}\left\{\, J(\tau) := \tilde f^*(\tau) + \tilde g^*(-\nabla^*\tau)\,\right\}.$$

It is obvious that $\nabla^* = -\operatorname{div}$ in the weak sense on U. Moreover, by definition of the

convex conjugate, it follows that for any $u^* \in U^*$

$$\tilde{g}^*(u^*) = \sup_{u \in U} \langle u^*, u \rangle_{U^*,U} + \langle f, u \rangle_{L^{r^*}(\Omega),L^r(\Omega)} = \iota_{\{\,\cdot = -f\,\}}(u^*).$$

This leads to the constraint in (VP-D′).

For the conjugate of $\tilde{f}$, we obtain for any $\tau \in S$

$$\tilde{f}^*(\tau) = \sup_{\dot{\gamma} \in Q} \langle \tau, \dot{\gamma} \rangle_{Q^*,Q} - b(\dot{\gamma}) - j(\dot{\gamma}).$$

An equivalent optimality condition reads

$$\langle b'(\bar{\dot{\gamma}}) - \tau, \dot{\gamma} - \bar{\dot{\gamma}} \rangle_{Q^*,Q} + j(\dot{\gamma}) - j(\bar{\dot{\gamma}}) \geq 0, \qquad \forall \dot{\gamma} \in Q$$

and Lemma 5.5 provides the maximising argument $\bar{\dot{\gamma}}$ in terms of τ. Simple arithmetic manipulations now yield the asserted form of $F(\tau) = \langle \tau, \bar{\dot{\gamma}} \rangle_{Q^*,Q} - b(\bar{\dot{\gamma}}) - j(\bar{\dot{\gamma}})$. □

By the property of the maximising argument of the subdifferential (cf Lemma 2.29 on page 29), the expressions for $\bar{\dot{\gamma}}$ in Lemma 5.5 are equal to $\nabla F(\tau)$. The Hessian $\nabla^2 F(\tau)$ is crucial for defining variable metrics.

5.7 Lemma$^{(\mathrm{TT})}$ (Hessian of the Dual Objective) *With the functional F defined in Proposition 5.6, a Hessian in the sense of* Newton *derivatives is given by*

$$\nabla^2 F(\tau) = \frac{1}{\mu} \begin{pmatrix} 1 - \frac{\tau_0 \tau_2^2}{|\tau|^3} & \frac{\tau_0 \tau_1 \tau_2}{|\tau|^3} \\ \frac{\tau_0 \tau_1 \tau_2}{|\tau|^3} & 1 - \frac{\tau_0 \tau_1^2}{|\tau|^3} \end{pmatrix} \quad \text{a.e. in } \{\, |\tau| > \tau_0 \,\} \tag{5.2a}$$

$$\nabla^2 F(\tau) \equiv 0 \quad \text{a.e. in } \{\, |\tau| \leq \tau_0 \,\} \qquad \text{(Bingham)} \tag{5.2b}$$

and, in the sense of Fréchet *derivatives, by*

$$\nabla^2 F(\tau) = \frac{1}{\mu} \begin{pmatrix} \frac{\tau_1^2 \sqrt{|\tau| c + \tau_2^2 c^2}}{|\tau|^3} & \frac{\sqrt{\tau_0} \tau_1 \tau_2 c}{|\tau|^3} \\ \frac{\sqrt{\tau_0} \tau_1 \tau_2 c}{|\tau|^3} & \frac{\tau_2^2 \sqrt{|\tau| c + \tau_1^2 c^2}}{|\tau|^3} \end{pmatrix} \qquad \text{(Casson)} \tag{5.2c}$$

$$\nabla^2 F(\tau) = \frac{1}{\kappa^{r^*-1}} \begin{pmatrix} \frac{\tau_1^2 h_1}{|\tau|^2} + \frac{\tau_2^2 h_2}{|\tau|^3} & \frac{\tau_1 \tau_2 h_1}{|\tau|^2} - \frac{\tau_1 \tau_2 h_2}{|\tau|^3} \\ \frac{\tau_1 \tau_2 h_1}{|\tau|^2} - \frac{\tau_1 \tau_2 h_2}{|\tau|^3} & \frac{\tau_2^2 h_1}{|\tau|^2} + \frac{\tau_1^2 h_2}{|\tau|^3} \end{pmatrix}. \qquad \text{(Herschel-Bulkley)} \tag{5.2d}$$

We use the abbreviations $c := (\sqrt{|\tau|} - \sqrt{\tau_0})_+$, $h_1 := (r^* - 1)(|\tau| - \tau_0)_+^{r^*-2}$ *and* $h_2 := (|\tau| - \tau_0)_+^{r^*-1}$.

Proof. These calculations were verified with Maple 2015. □

5.8 Lemma$^{(TT)}$ (FISTA* and VM-FISTA* for Steady Viscoplastic Duct Flow) *(a) The steps (FISTA*.1) and (VM-FISTA*.1) are equivalent to*

$$\hat{\dot\gamma}^{(k)} := \frac{1}{\mu}\Big(|\hat\tau^{(k)}| - \tau_0\Big)_+ \frac{\hat\tau^{(k)}}{|\hat\tau^{(k)}|} \qquad \text{(Bingham)} \tag{5.3a}$$

$$\hat{\dot\gamma}^{(k)} := \frac{1}{\mu}\left(\sqrt{|\hat\tau^{(k)}|} - \sqrt{\tau_0}\right)_+^2 \frac{\hat\tau^{(k)}}{|\hat\tau^{(k)}|} \qquad \text{(Casson)} \tag{5.3b}$$

$$\hat{\dot\gamma}^{(k)} := \frac{1}{\kappa^{r^*-1}}\Big(|\hat\tau^{(k)}| - \tau_0\Big)_+^{r^*-1} \frac{\hat\tau^{(k)}}{|\hat\tau^{(k)}|}. \qquad \text{(Herschel-Bulkley)} \tag{5.3c}$$

(b) Step (FISTA.2) is equivalent to the* Poisson-Dirichlet *problem: find $\hat u^{(k)} \in U$, such that*

$$-\Delta\hat u^{(k)} = L^{(k)} f - \operatorname{div}(\hat{\dot\gamma}^{(k)} - L^{(k)}\hat\tau^{(k)}) \qquad \text{in } \Omega \tag{5.4a}$$

$$\hat u^{(k)} = 0 \qquad \text{on } \Gamma \tag{5.4b}$$

in the weak sense, i.e.

$$\int_\Omega \nabla\hat u^{(k)} \cdot \nabla v \,\mathrm{d}x = L^{(k)} \int_\Omega f v \,\mathrm{d}x + \int_\Omega (\hat{\dot\gamma}^{(k)} - L^{(k)}\hat\tau^{(k)}) \cdot \nabla v \,\mathrm{d}x, \qquad \forall v \in U.$$

(c) Step (VM-FISTA.2) is equivalent to the scaled* Poisson-Dirichlet *problem: find $\hat u^{(k)} \in U$, such that*

$$-\operatorname{div}(\mathcal{H}^{(k)})^{-1}\nabla\hat u^{(k)} = l^{(k)} f - \operatorname{div}((\mathcal{H}^{(k)})^{-1}\hat{\dot\gamma}^{(k)} - l^{(k)}\hat\tau^{(k)}) \qquad \text{in } \Omega \tag{5.5a}$$

$$\hat u^{(k)} = 0 \qquad \text{on } \Gamma \tag{5.5b}$$

in the weak sense, i.e. $\forall v \in U$

$$\int_\Omega (\mathcal{H}^{(k)})^{-1}\nabla\hat u^{(k)} \cdot \nabla v \,\mathrm{d}x = l^{(k)} \int_\Omega f v \,\mathrm{d}x + \int_\Omega ((\mathcal{H}^{(k)})^{-1}\hat{\dot\gamma}^{(k)} - l^{(k)}\hat\tau^{(k)}) \cdot \nabla v \,\mathrm{d}x.$$

Proof. (a) follows from Lemma 5.5; (b) and (c) are the first-order optimality conditions of (FISTA*.2) and (VM-FISTA*.2), respectively, written out in explicit form. □

(a): Velocity nodes

(b): Strain-rate and stress nodes

Figure 5.2: Finite elements for simulations of pipe flows.

Discretisation

For our numerical studies in this chapter, we employ a discretisation with continuous piecewise linear finite elements for the flow velocity u and a piecewise constant approximation for the extra stress τ.

5.9 Finite-Element Spaces To avoid technicalities, we assume that $\Omega_h := \Omega$ is already polygonal with boundary $\Gamma_h := \partial\Omega_h$, and we let $\mathcal{T}_h$ be a regular triangulation (cf [199, Sec 2.2]) on the closure $\bar{\Omega}_h$. The parameter $h > 0$ denotes the maximum edge length of any triangle $T \in \mathcal{T}_h$. With $\mathbb{P}_k$ denoting the space of polynomials in two variables of degree at most k, we set

$$
\begin{aligned}
U_h &:= \left\{ u_h \in C(\bar{\Omega}_h) \;\middle|\; u_h|_{\Gamma_h} = 0 \quad \wedge \quad u_h|_T \in \mathbb{P}_1, \quad \forall T \in \mathcal{T}_h \right\} \\
Q_h &:= \left\{ \dot{\gamma}_h \in L^r(\Omega_h)^2 \;\middle|\; \dot{\gamma}_h|_T \in \mathbb{P}_0^2, \quad \forall T \in \mathcal{T}_h \right\} \\
S_h &:= \left\{ \tau_h \in L^{r^*}(\Omega_h)^2 \;\middle|\; \tau_h|_T \in \mathbb{P}_0^2, \quad \forall T \in \mathcal{T}_h \right\}.
\end{aligned}
$$

In Figure 5.2, we provide a sketch of these finite elements.

5.10 Discrete Subproblems We can interpret (5.3) pointwise for the discretised problem. The discrete counterparts of problems (5.4) and (5.5) read: given $\hat{\dot{\gamma}}_h^{(k)} \in Q_h$ and $\hat{\tau}_h^{(k)} \in S_h$, find $\hat{u}_h^{(k)} \in U_h$ such that, for all $v_h \in U_h$

$$
\int_{\Omega_h} \nabla \hat{u}^{(k)} \cdot \nabla v_h \,\mathrm{d}x = L^{(k)} \int_{\Omega_h} f v_h \,\mathrm{d}x + \int_{\Omega_h} (\hat{\dot{\gamma}}_h^{(k)} - L^{(k)} \hat{\tau}_h^{(k)}) \cdot \nabla v_h \,\mathrm{d}x
$$

or

$$\int_{\Omega_h} (\mathcal{H}_h^{(k)})^{-1} \nabla \hat{u}^{(k)} \cdot \nabla v_h \, \mathrm{d}x = l^{(k)} \int_{\Omega_h} f v_h \, \mathrm{d}x + \int_{\Omega_h} ((\mathcal{H}_h^{(k)})^{-1} \hat{\gamma}_h^{(k)} - l^{(k)} \hat{\tau}_h^{(k)}) \cdot \nabla v_h \, \mathrm{d}x,$$

respectively. It is an elementary result that the symmetry and ellipticity of the (scaled) Laplacian are preserved under this discretisation. Hence, both discrete problems have a unique solution $\hat{u}_h^{(k)}$ as well. [199, p 41]

We implement our methods in MATLAB and execute our programs with the Student Version of MATLAB R2013a 64-bit on a laptop running Fedora Linux 23 KDE with IntelCORE i7 CPU 4x2.50 GHz.

For algorithms with a fixed metric, we pre-compute a CHOLESKY factorisation of the discrete Laplacian and solve for $\hat{u}_h^{(k)}$ by backward substitution. If the metric may vary from one iteration to another, we resort to the \-operator in MATLAB.

(B) Convergence Properties

When we refer to the convergence of our method, we have to distinguish between two distinct contributions:

(a) convergence of the finite-element discretisation as $h \to 0$

(b) convergence of the optimisation algorithms as $k \to \infty$

Let $\bar{u} \in U$ be the solution to (VP-P) and, for $h > 0$, $\bar{u}_h := \lim_{k\to\infty} u_h^{(k)}$; the limit referring to strong convergence in U_h. This way, we can write

$$\left\| u_h^{(k)} - \bar{u} \right\|_U \leq \left\| u_h^{(k)} - \bar{u}_h \right\|_U + \left\| \bar{u}_h - \bar{u} \right\|_U .$$

We recall that POINCARÉ's inequality implies the equivalence of $\|\cdot\|_U$ and the energy norm $\|\nabla \cdot\|_Q$, which, from now on, we simply denote by $\|\cdot\|$.

Let us first study the convergence of our discretisation scheme.

Convergence of the Finite-Element Discretisation

5.11 Analytical Solutions The symmetry of a circular cross-section effectively renders the problem of viscoplastic flow through a cylindrical duct one-dimensional. Analytical solutions for the velocity profiles under each of the three constitutive models are available in closed form and have been published in the literature.

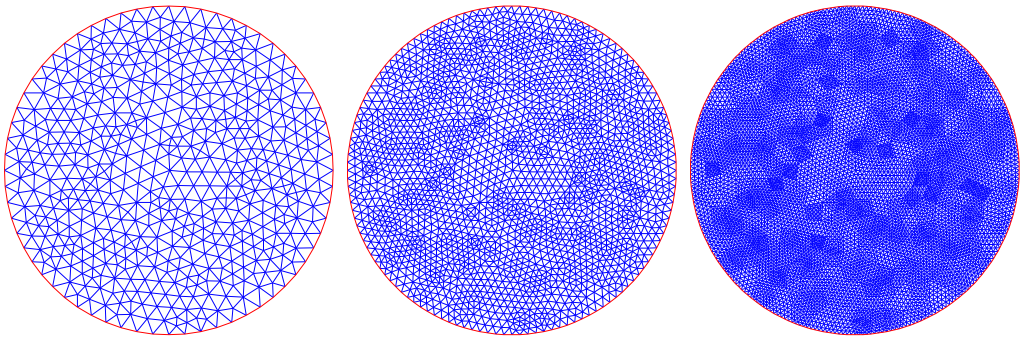

Figure 5.3: Meshes for analysing the convergence of the finite-element discretisation.

We consider the unit circle* $\Omega = B(0,1)$. We set $\mu := \kappa := 1$, $f := 1$, $r := |x|$ and $r_0 := 2\tau_0$. Analytical solutions under this setting have appeared in [200]–[202] (cf [153]):

$$\bar{u}(r) := \frac{1}{4}\left((1-r_0)^2 - (r-r_0)_+^2\right) \qquad \text{(Bingham)}$$

$$\bar{u}(r) := \begin{cases} \frac{1}{4}\left((1-\sqrt{r_0})^3\left(1+\frac{1}{3}\sqrt{r_0}\right)\right. \\ \left. -\left(\sqrt{r}-\sqrt{r_0}\right)_+^3\left(\sqrt{r}+\frac{1}{3}\sqrt{r_0}\right)\right) \end{cases} \qquad \text{(Casson)}$$

$$\bar{u}(r) := \frac{1}{2^{r^*-1}r^*}\left((1-r_0)^{r^*} - (r-r_0)_+^{r^*}\right). \qquad \text{(Herschel-Bulkley)}$$

5.12 Mesh Generation Initially, we obtain a mesh $\mathcal{T}_h$ by using the `initmesh` function from the PDE Toolbox of MATLAB with a maximum edge length of $h = 0.1$. We then successively refine this mesh $\mathcal{T}_h \to \mathcal{T}_{h/2}$ by connecting the edge midpoints in each triangle†. This is accomplished with the function `refinemesh`. Figure 5.3 shows the initial mesh with the first two refinements. For investigating the convergence rate of the discretisation, we refine the grid four times. Accordingly, we have data available for five different meshes in total.

5.13 Numerical Results We approximate $\bar{u}_h$ by solving (VP-P) on U_h, until the optimality condition

$$\left\|\nabla u_h^{(k)} - \dot{\gamma}_h^{(k)}\right\| \leq \text{gradTol}$$

is satisfied to a very high accuracy. We set $\text{gradTol} = 10^{-8}$. Surely, in view of the small tolerance, the numerical method for finding this approximation only plays a subordinate

*This domain clearly violates our assumption of a polygonal shape. Therefore, approximations $\Omega_h \approx \Omega$ introduce an additional error. For our numerical convergence studies, we assume this contribution to be negligible.

†For edges that fall on the boundary $\partial\Omega_h$, new vertices lie on the curved boundary $\partial\Omega$ instead.

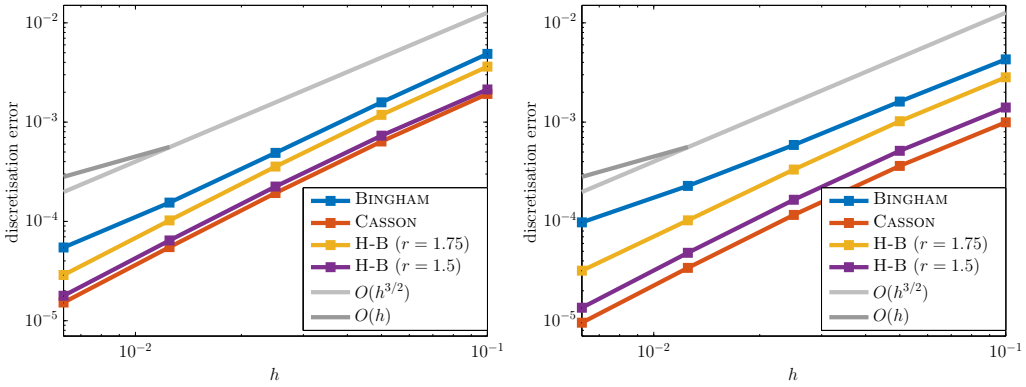

(a): $\tau_0 = 0.1$ **(b):** $\tau_0 = 0.2$

Figure 5.4: Discretisation errors $\|\bar{u}_h - \bar{u}\|$ for different values of h. The results demonstrate strong convergence of order $O(h)$ for Bingham fluids, of order $O(h^{3/2})$ for the other models, as $h \to 0$.

role. For our computations, we apply the accelerated dual proximal gradient method FISTA*.

The results are shown in Figure 5.4. It is evident that the approximation errors decay like $O(h^{3/2})$ in the global energy norm for Casson and Herschel-Bulkley fluids. The graphs corresponding to Bingham fluids clearly exhibit a deteriorating convergence rate for the finer grids under consideration. This observation is little surprising, due to the lower regularity of the solution $\bar{u}$ for Bingham fluids: in the latter case, we have $\bar{u} \in C^1(\Omega)$ but $\bar{u} \notin C^2(\Omega)$. In contrast, the solutions to the Casson and Herschel-Bulkley flow problems satisfy at least $\bar{u} \in C^2(\Omega)$, with the maximum regularity depending on the value of r.

We also point out that our convergence results are consistent with results published in the literature on related problems [203, p 57].

Convergence of the Optimisation Algorithms

Let us now assess the convergence rate of the various optimisation algorithms, i.e. the convergence $u_h^{(k)} \to \bar{u}_h$ as $k \to \infty$, for fixed $h > 0$. We recall the worst-case convergence rates from the first part of this thesis: $O(1/\sqrt{k})$ for conventional algorithms and $O(1/k)$ for accelerated methods.

We wish to answer a number of questions:

(a) How does the *actual convergence rate* of the accelerated dual proximal gradient method FISTA* compare with ADMM as the state of the art in viscoplasticity?

(b) Which definition should be chosen for the *primal sequence* in an accelerated method?

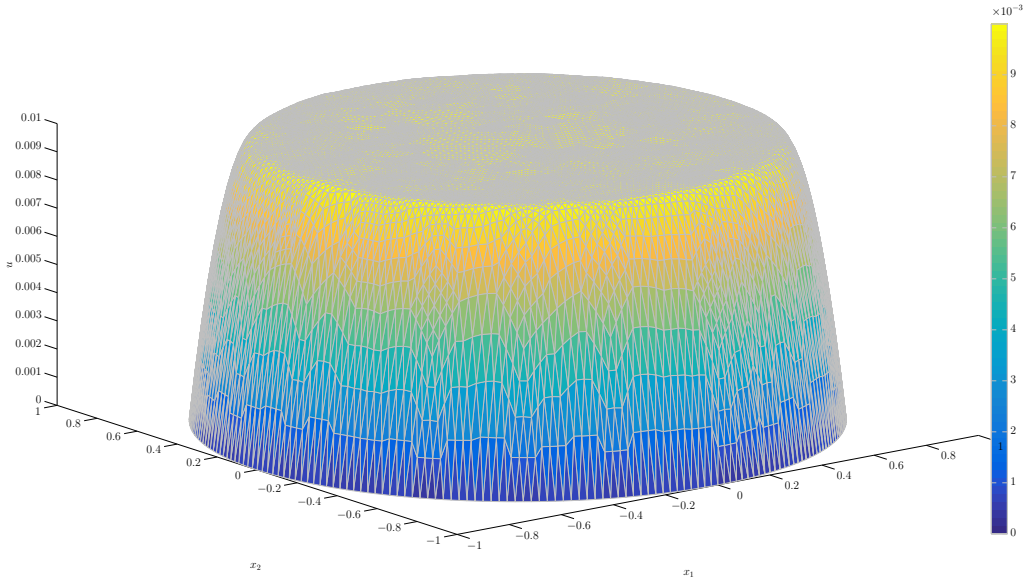

Figure 5.5: Velocity profile u for the flow of a BINGHAM fluid through the circular pipe ($\tau_0 = 0.4$). The plug flow zone in the centre is a remarkable feature.

(c) How does *preconditioning with second-order information* affect the speed of convergence and computation times?

For now, we investigate these issues for flow problems through the circular pipe. These specific results can then provide some first guidance for further studies in more complex settings, which form part of the following chapter.

The following simulations are carried out on the mesh $\mathcal{T}_h$ with $h = 0.025$ that results after two refinements of the initial grid. Furthermore, we fix $\tau_0 := 0.4$.

5.14 FISTA* Vs ADMM for BINGHAM Flow We begin by computing an approximation to $\bar{u}_h$. To this end, we carry out 50,000 iterations with FISTA* and set $\bar{u}_h \approx u_h^{(50,000)}$. At the last iteration, the residual $\|\nabla u_h^{(50,000)} - \dot{\gamma}_h^{(50,000)}\| \approx 7.5 \cdot 10^{-11}$. We therefore consider this reference solution to be virtually exact on the given grid.

In the next step, we record the convergence history for ADMM, ISTA* and FISTA*, with its three different primal sequences, over the first 10,000 iterations. To maintain comparability between the different algorithms, we keep the step size fixed. For the proximal methods, we use the globally optimal value of $L^{(k)} \equiv \frac{1}{\mu} = 1$. Accordingly, we also set $\varrho^{(k)} = t^{(k)} \equiv 1$ for ADMM. All variables, which require an initial guess, are set to zero for each method.

The convergence data is shown in Figure 5.6(a) on page 116, along with graphs

corresponding to $O(1/\sqrt{k})$, $O(1/k)$ and $O(1/k^2)$.

We observe immediately that all three primal sequences for FISTA* lie almost equally close to the reference solution. Also the errors of the sequences defined by ADMM and ISTA* are visually indistinguishable. Considering the very similar recursions of both methods, this result is little surprising.

The effect of the acceleration in this example is in fact more significant than predicted by the worst-case convergence estimates. From about the 20^{th} iteration onwards, FISTA* generates sequences, which, despite increasing fluctuations, overall approach the exact solution at a rate of $O(1/k^2)$. This rate is not only higher than the guaranteed order of $O(1/k)$, but it also compares very favourably against the two methods without acceleration. For ADMM and ISTA* we notice a worst-case decay of the error, i.e. convergence like $O(1/\sqrt{k})$, for the first few hundred iterations. Only from about $k = 500$ onwards, the rate increases to $O(1/k)$.

As a first hypothesis for explaining this behaviour, we conjecture that this switch is related to the identification of active and inactive sets, i.e. regions of shear or plug flow. Once these have been pinpointed, the Bingham problem essentially simplifies to a perturbed quadratic optimisation problem. With further examples in the next chapter, we shall investigate this phenomenon in more detail.

Let us emphasise the logarithmic scaling of the axes in Figure 5.6(a). Visible differences are therefore a lot more dramatic than they may appear at first sight. For instance, we infer from the graph that ADMM and ISTA* require 10,000 iteration to reduce the error to about $7 \cdot 10^{-5}$. In contrast, the fast proximal algorithms achieve the same accuracy after little more than 100 steps. At least for the sequence of leading points, this reduction in iteration numbers translates into an equivalent reduction in computation time. Even if one of the other two primal sequences is used, which require up to twice the computational cost per iteration, the speedup through acceleration remains enormous.

5.15 ADMM for Casson and Herschel-Bulkley Flow Applied to the constitutive models of Casson or Herschel-Bulkley fluids, the subproblem (ALG2.2) results in a nonlinear equation, solutions of which are not generally available in closed form [153]. Consequently, each iteration necessitates an iterative solution, e.g. by Newton's method, making ADMM prohibitively expensive for such applications.

Even though this problem can be overcome by setting the penalty parameter $\varrho^{(k)}$ in this subproblem to zero, i.e. by applying ISTA* instead, this workaround does not seem to be well-known among numerical practitioners in viscoplasticity.

Given the similarity of the two methods ADMM and ISTA*—apart from the complexity of this one subproblem—we only consider ISTA* as a representative of state-of-the-art

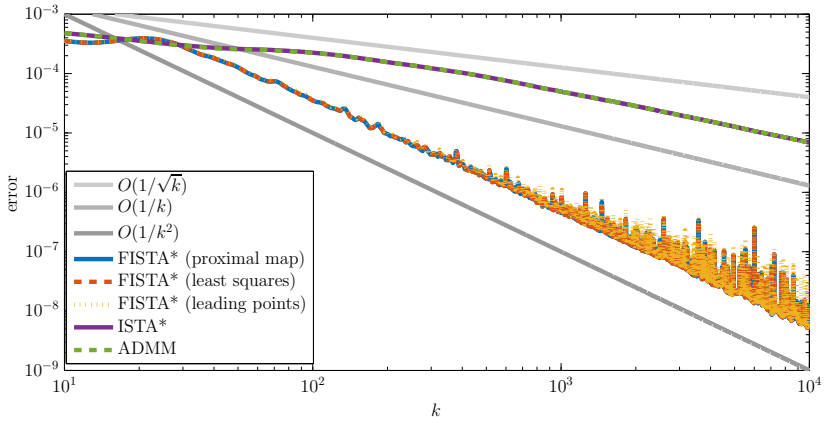

(a): Bingham flow with $\tau_0 = 0.4$.

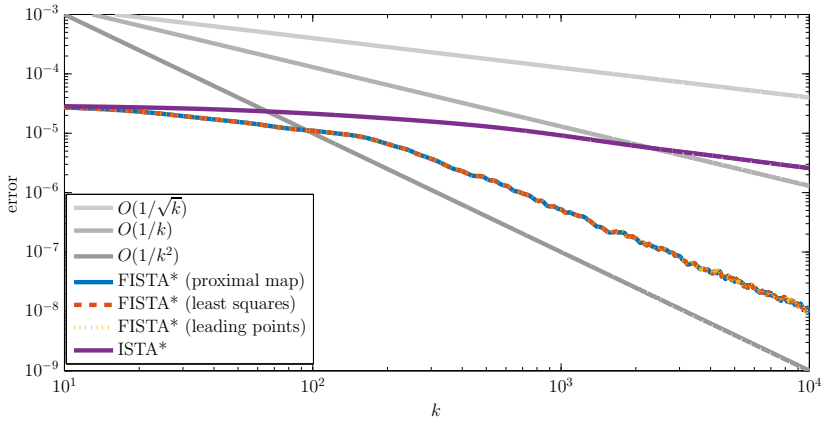

(b): Casson flow with $\tau_0 = 0.4$.

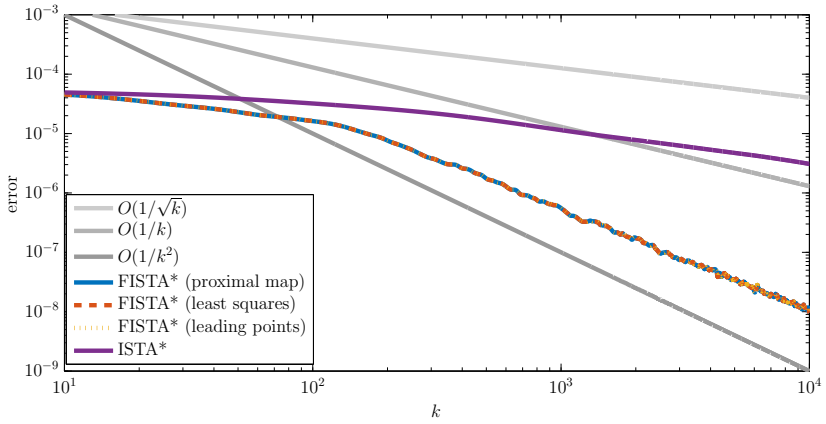

(c): Herschel-Bulkley flow with $\tau_0 = 0.4$ and $r = 1.5$.

Figure 5.6: Convergence of FISTA*, ISTA* and ADMM for the viscoplastic duct flow problems. Error $\|u_h^{(k)} - \bar{u}_h\|$ for the first 10,000 iterations.

methods for Casson and Herschel-Bulkley flow problems.

5.16 FISTA* Vs ISTA* for Casson Flow We follow the same strategy as for the assessment of convergence rates for Bingham flow. After 50,000 iterations of FISTA*, we obtain a reference solution for the duct flow problem of a Casson fluid with a dual gradient residual of approximately $6.5 \cdot 10^{-10}$.

The results shown in Figure 5.6(b) on the facing page are overall comparable to those of the Bingham flow problem. The convergence behaviour of all three primal sequences of FISTA* is essentially equivalent. Compared to the Bingham setting, deviations from monotonicity are only very minor. The convergence rate, however, does not appear to quite reach $O(1/k^2)$, but is definitely higher than $O(1/k)$.

In contrast, the convergence of ISTA* is extremely slow for this problem. After about 1,000 iterations, the predicted worst-case rate of $O(1/\sqrt{k})$ is attained.

Once more we observe two different regimes in the convergence history, which are also more apparent for the accelerated algorithms in this case. After a very slow decay of the errors up to $k = 100$, a remarkable descent can be observed once the iterates fall within a radius of about 10^{-5} around the reference solution.

5.17 FISTA* Vs ISTA* for Herschel-Bulkley Flow For studying the convergence of the conventional and fast algorithms applied to the descretised Herschel-Bulkley problem, we focus on the strongly shear-thinning and hence particularly challenging setting with $r = \frac{3}{2}$.

Since an admissible strong convexity parameter on the set of all iterates is a priori unknown, it is necessary to verify whether each iteration achieves descent in the dual objective. We initialise the dual proximal gradient methods FISTA* and ISTA* with $L^{(0)} := 1$. As it turns out, this step size is already feasible for all 50,000 or 10,000 iterations, respectively. For their computations with ADMM, Huilgol and You [153] report convergence with $\varrho^{(k)} = t^{(k)} \equiv 1$ as well.

At the 50,000$^{\text{th}}$ iteration, the norm of the dual gradient has decreased to about $6.1 \cdot 10^{-10}$ in this case.

The convergence history shares the same features as for the simulations of Casson flow, and the above remarks are equally valid to describe Figure 5.6(c). The higher smoothness of the dual objectives for Casson and shear-thinning Herschel-Bulkley fluids provides a plausible explanation for their similar convergence behaviour.

This concludes our initial investigation of the different first-order algorithms. We now turn towards those methods, which additionally exploit curvature information of F.

5.18 Proximal Newton-Type Methods To ensure the convergence of variable-metric extensions of the dual-based proximal gradient method, we recall that the operators $\mathcal{H}^{(k)}$ have to meet two criteria, which do not generally hold for an actual Hessian $\nabla^2 F$, evaluated at the iterates or leading points:

(Uniform Boundedness) There exist constants $\underset{\sim}{L}, \widetilde{L} > 0$ such that for all iterations $k \in \mathbb{N}$ we have

$$\underset{\sim}{L}\,\mathrm{id} \preccurlyeq \mathcal{H}^{(k)} \preccurlyeq \widetilde{L}\,\mathrm{id} \tag{5.6}$$

(Relative Boundedness) There exists a summable sequence $\left(\eta^{(k)}\right)_k \subset [0, +\infty[$ such that for all $k \in \mathbb{N}$

$$\mathcal{H}^{(k+1)} \preccurlyeq \left(1 + \eta^{(k)}\right) \mathcal{H}^{(k)} \tag{5.7}$$

We propose two Hessian-based preconditioners.

For the first choice of the variable metric, we choose a convex combination of the Hessian $\nabla^2 F(\hat{\tau}^{(k)})$ and $L\,\mathrm{id}$, where L is a Lipschitz constant of the dual gradient or an estimate thereof. With a weighting factor $\alpha \in]0, 1]$, we set

$$\mathcal{H}^{(k)} := \alpha L\,\mathrm{id} + (1 - \alpha)\nabla^2 F(\hat{\tau}^{(k)}). \tag{5.8a}$$

This sequence of preconditioners apparently verifies the condition (5.6) with $\underset{\sim}{L} = \alpha L$ and $\widetilde{L} = L$, if L is a Lipschitz constant of ∇F. Otherwise $\widetilde{L} = \alpha L + (1 - \alpha) L_{(\nabla F)}$, where the latter parameter denotes an actual Lipschitz constant.

The condition (5.7) imposes a constraint only asymptotically, as $k \to \infty$. As we stop our algorithms after a finite number of steps, (5.7) is automatically verified. Due to the finite precision of actual computations, it might still be desirable to implement such a criterion for large k. One possible choice is given by the following adaptation: for $k > k_0 \in \mathbb{N}$, replace $\mathcal{H}^{(k)}$ with $\tilde{\mathcal{H}}^{(k)}$, defined by the convex combination

$$\tilde{\mathcal{H}}^{(k)} := \frac{1}{(k - k_0)^2} \mathcal{H}^{(k)} + \left(1 - \frac{1}{(k - k_0)^2}\right) L\,\mathrm{id}$$

which puts increasing emphasis on the second term. Since the sequence defined by $1/(k - k_0)^2$ is summable, there exists $c > 0$ such that (5.7) holds with $\eta^{(k)} := c/k^2$, for all $k \in \mathbb{N}$. We will not study such modifications any further, but instead refer to [114].

In the duct-flow setting, the Hessian and the preconditioners pointwise assume values of symmetric (2×2)-matrices, which are invertible at relatively low cost. For two-dimensional flow problems, like those considered in the next chapter, the dimension of these matrices already increases to 3×3, and for fully three-dimensional flow problems to 6×6. This motivates a search for a diagonal preconditioner, which would ideally capture

a similar amount of second-order information as the full Hessian, while its inverses are straightforward to compute. As an alternative to (5.8a), we therefore suggest

$$\mathcal{H}^{(k)} := \alpha L \,\mathrm{id} + (1-\alpha)\,\mathrm{diag}\left(\nabla^2 F(\hat{\tau}^{(k)})\right). \tag{5.8b}$$

Here, the operator diag maps all off-diagonal elements to zero, i.e. for $A \in \mathbb{R}^{d\times d}$

$$\mathrm{diag}\, A := \begin{pmatrix} a_{11} & 0 & 0 \\ 0 & \ddots & 0 \\ 0 & 0 & a_{dd} \end{pmatrix}.$$

5.19 Alternative Preconditioning Strategies in Viscoplasticity Our suggested approach exhibits certain analogies to recently published ideas of Aposporidis and co-workers [177]: the authors explore preconditioning strategies for a Picard iteration on the primal Bingham problem, where the preconditioners are defined from the viscosity regularisation of Bercovier-Engelman.

In a similar fashion, the constant αL added to the Hessian gives rise to a Tikhonov regularisation of the dual problem. Transferred back to primal problem, this approach to preconditioning can likewise be interpreted as a viscosity regularisation.

5.20 Backtracking Procedure For Newton-type methods, a global worst-case estimate of the step-size would defeat the purpose of incorporating second-order information in the first place. Hence, we initialise VM-FISTA* with $l^{(0)} = 1$ and, if necessary, increase $l^{(k)}$ only slightly. We recall that the sequence $\left(l^{(k)}\right)_k$ is not permitted to decrease. Hence, increasing $l^{(k)}$ too aggressively would result in unnecessarily small steps from the current iteration onwards.

While it is common for line searches in smooth nonlinear optimisation to decrease the step size by a factor of 2 in a backtracking procedure, we increase the scaled Lipschitz parameter only by 10%. This yields the following strategy (cf [48]):

5.21 Algorithm (Backtracking) *Input:* $l^{(k)} > 0$, the current leading point $\hat{\tau}_h^{(k)}$

Compute $\hat{\hat{\gamma}}_h^{(k)}$ from (5.3) (BT.1)

Solve (5.5) for $\hat{u}_h^{(k)}$ (BT.2)

Evaluate $\tau_h^{(k)} := \hat{\tau}_h^{(k)} + \frac{1}{l^{(k)}}\left(\mathcal{H}_h^{(k)}\right)^{-1}\left(\nabla \hat{u}_h^{(k)} - \hat{\hat{\gamma}}_h^{(k)}\right)$ (BT.3)

If $F(\tau_h^{(k)}) \le F(\hat{\tau}_h^{(k)}) + \left\langle \nabla F(\hat{\tau}_h^{(k)}), \tau_h^{(k)} - \hat{\tau}_h^{(k)} \right\rangle_{S^*,S} + \frac{l^{(k)}}{2}\left\| \tau_h^{(k)} - \hat{\tau}_h^{(k)} \right\|^2_{\mathcal{H}^{(k)}}$ (BT.4)

then return $(\hat{u}_h^{(k)}, \hat{\hat{\gamma}}_h^{(k)})$ and $\tau_h^{(k)}$, *else* set $l^{(k)} \leftarrow 1.1 \cdot l^{(k)}$ and *go to* (BT.1) (BT.5)

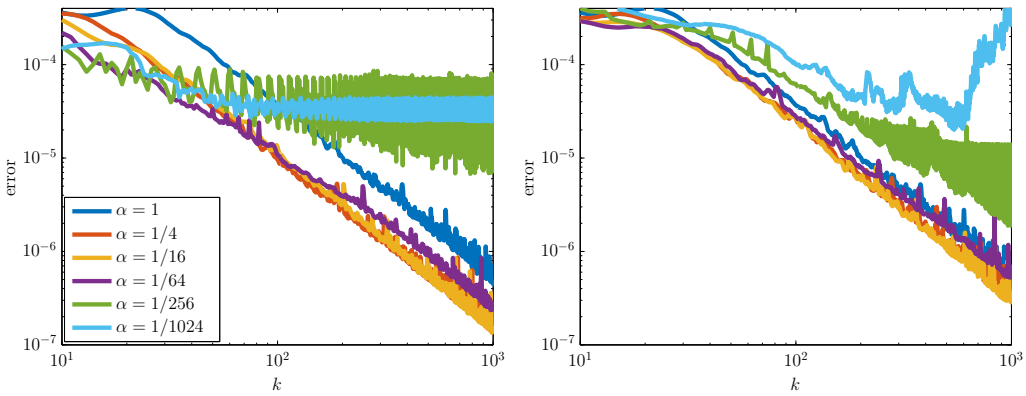

(a): Full Hessian-based preconditioning.

(b): Diagonal preconditioning.

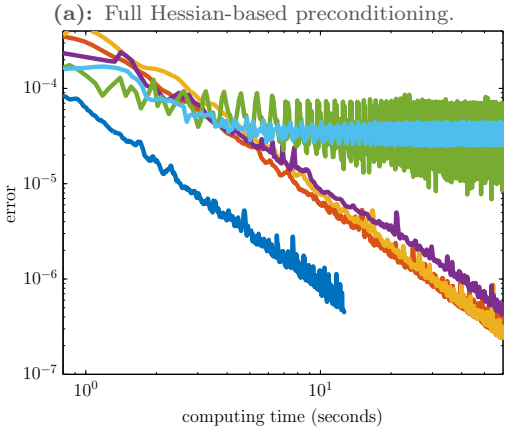

(c): Full Hessian-based preconditioning.

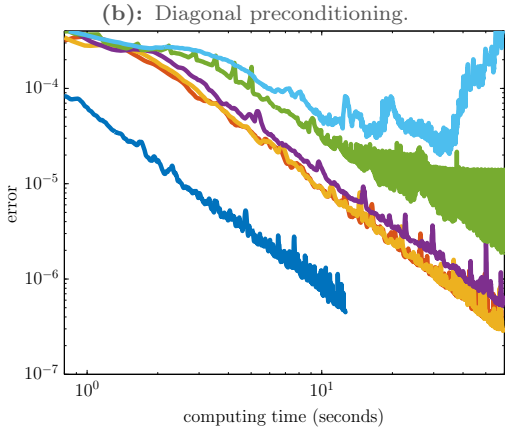

(d): Diagonal preconditioning.

Figure 5.7: Convergence history of accelerated proximal Newton-type methods (VM-FISTA*) for Bingham flow, plotted against the iteration counter or the computing time. The value $\alpha = 1$ corresponds to no preconditing, i.e. the accerated dual proximal gradient method FISTA*.

5.22 VM-FISTA* for Viscoplastic Duct Flow We now assess the effect of using either the full Hessian as in (5.8a) or its diagonal entries, according to (5.8b), for preconditioning.

In the first case, we invert the Hessian by means of the explicit formula

$$A^{-1} = \frac{1}{a_{11}a_{22} - 2a_{12}} \begin{pmatrix} a_{22} & -a_{12} \\ -a_{12} & a_{11} \end{pmatrix}$$

for a symmetric (2×2)-matrix A. In the second case, we only compute the diagonal entries a_{11} and a_{22} to assemble

$$(\operatorname{diag} A)^{-1} = \begin{pmatrix} \frac{1}{a_{11}} & 0 \\ 0 & \frac{1}{a_{22}} \end{pmatrix}.$$

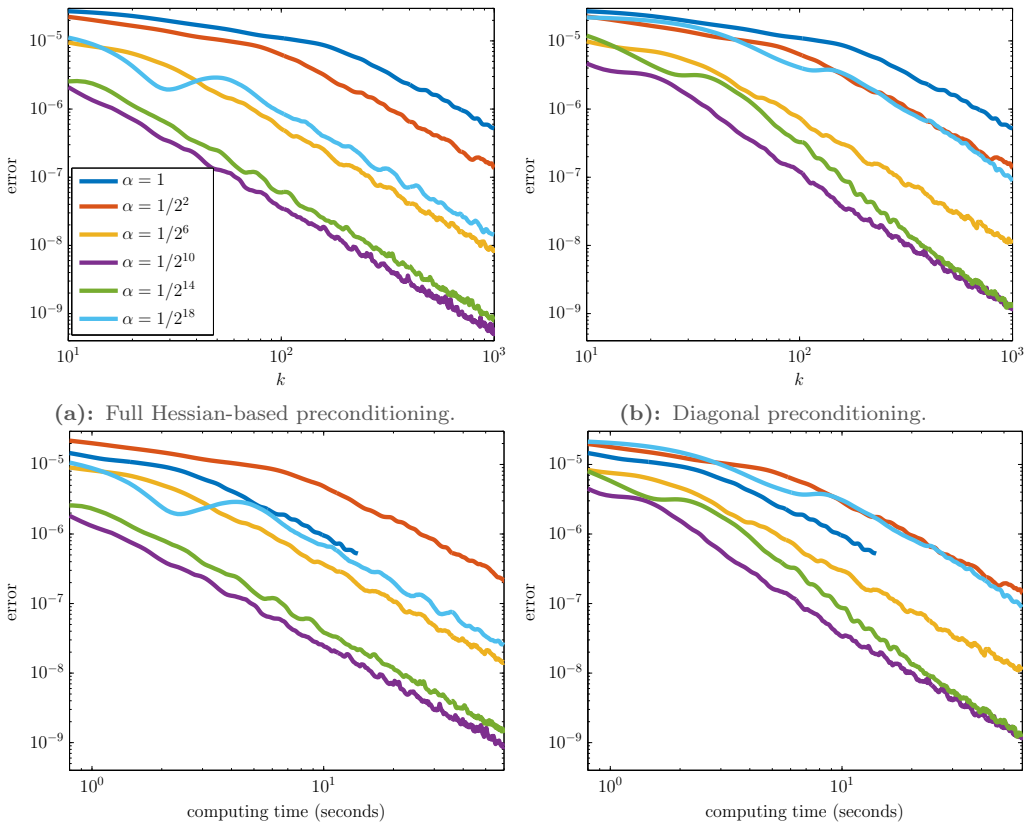

(a): Full Hessian-based preconditioning.

(b): Diagonal preconditioning.

(c): Full Hessian-based preconditioning.

(d): Diagonal preconditioning.

Figure 5.8: Convergence history of accelerated proximal NEWTON-type methods (VM-FISTA*) for CASSON flow.

Let us first analyse the results for BINGHAM flow, which are shown in Figure 5.7 on the preceding page. From the first plot, we observe that the larger values of the weighting factor α in (5.8a) result in faster convergence of the method, compared to the accelerated dual proximal gradient method without preconditioning ($\alpha = 1$). For the parameters shown here, preconditioning yields at best half the error for the same number of iterations. However, Figure 5.7(c) shows that the computational expense associated with assembling and inverting the Hessian outweighs the benfits of improved convergence: at any given time (not iteration), approximations obtained from FISTA* are more accurate by about one order of magnitude than those of VM-FISTA*.

As expected, the diagonal preconditioner (5.8b) can not quite achieve the same reduction of the error per iteration. This can be seen from Figure 5.7(b). The performance over time, however, is very similar to variable metrics that include the full Hessian.

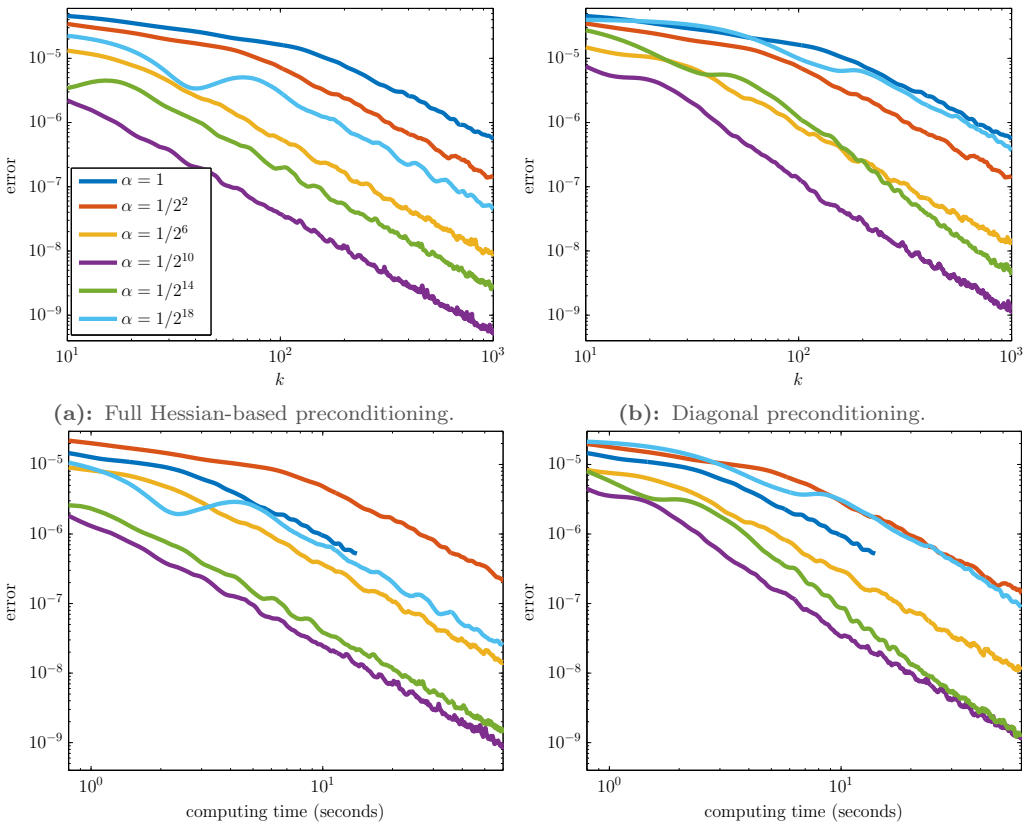

(a): Full Hessian-based preconditioning.

(b): Diagonal preconditioning.

(c): Full Hessian-based preconditioning.

(d): Diagonal preconditioning.

Figure 5.9: Convergence history of accelerated proximal Newton-type methods (VM-FISTA*) for Herschel-Bulkley flow ($r = 1.5$).

Too small choices of α lead to instabilities or even divergence, as the condition of the preconditioners deteriorates. This issue could be addressed by modifying the preconditioner as for the above $\tilde{\mathcal{H}}^{(k)}$. However, we can conclude that the proximal gradient method FISTA* with fixed metric provides the most efficient approach to solving the Bingham flow problem.

The results for the Casson and Herschel-Bulkley flow problems paint a completely different picture. As can be seen from the graphs in Figures 5.8 and 5.9, variable metrics achieve errors that are smaller by several orders of magnitude than for FISTA* with its fixed metric. This remains true even if one takes the extra computational cost into consideration.

For both Casson and Herschel-Bulkley flow, the optimal value of α out of those selected here is $\alpha = 1/1024$. Smaller and larger choices reduce the error less efficiently.

However, it is important to note that for a wide range of weighting factors, the algorithm VM-FISTA* achieves superior performance over FISTA*. This implies major advantages for flow simulations in applications, where it would be impractical to first experiment with different values of α until the convergence behaviour has become satisfactory.

5.23 Conclusions Based on these results, we may draw first conclusions and provide some answers to the above questions:

(a) How does the actual convergence rate of the accelerated dual proximal gradient method FISTA* compare with ADMM as the state of the art in viscoplasticity?

—*Convergence rates of up to* $O(1/k^2)$ *compared to* $O(1/k)$ *or even* $O(1/\sqrt{k})$ *imply reductions in iteration numbers and computing times by several orders of magnitude.*

(b) Which definition should be chosen for the primal sequence in an accelerated method?

—*The simulations so far indicate no noteworthy differences. Therefore, primal approximations based on the leading point are most sensible if they converge, as this procedure implies no extra computational cost.*

(c) How does preconditioning with second-order information affect the speed of convergence and computation times?

— *Preconditioning does not provide any benefits for the* Bingham *flow problem considered. In contrast, for* Casson *and* Herschel-Bulkley *problems, we observe further, very significant acceleration of the convergence.*

(C) Numerical Experiments

To conclude our investigations of duct-flow problems, we assess how well numerical solutions reflect characteristic properties of a viscoplastic fluid. We first concentrate on identifying the plastic limit, where the flow stops completely. Finally, we study geometric features of the two different flow regions.

Detection of the Plastic Limit

Leaving all other parameters unchanged, we now consider the flow of a Bingham fluid through a duct, where the cross-section is given by a square with edge length equal to one. If the yield stress is sufficiently large, then the pressure gradient $f = 1$ is insufficient to make the fluid flow. Methods that rely on a regularised formulation are unable to compute solutions which exhibit the same feature.

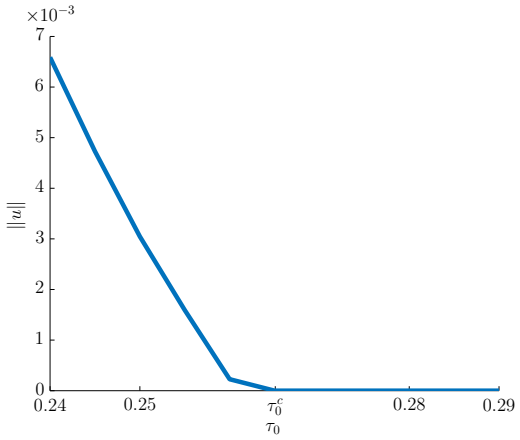

Figure 5.10: The flow rate decreases to exactly zero if the yield stress exceeds the critical value τ_0^c.

5.24 Critical Yield Stress By analytical means, Mosolov and Miasnokov [204] determine the critical yield stress $\tau_0^c = \frac{1}{2+\sqrt{\pi}} \approx 0.2651$ in this geometry. If and only if $\tau_0 \geq \tau_0^c$, then the exact solution is given by $\bar{u} = 0$.

On a mesh with $h = \frac{1}{128}$, we solve the Bingham flow problem for 11 homogeneously spaced values $\tau_0 \in [0.24, 0.29]$ and compute the energy norm of the solution after 100 iterations of FISTA*. In Figure 5.10, we also mark the theoretical value for the plastic limit. Although the finite resolution of the mesh limits the accuracy of the numerical solution, theoretical and numerical results show very good agreement.

In [169], Moyers-González and Frigaard show that sophisticated workarounds are required to achieve a similarly good fit if the augmented Lagrangian method ADMM is used instead of FISTA*.

5.25 Visualisation of Yielded and Unyielded Areas The idea behind one of the most common methods to determine stagnant regions in the flow is to visualise areas where $|\tau| \leq \tau_0$ and $|\tau| > \tau_0$ in two different colours. However, in its basic form, this approach does not normally provide satisfactory results, as numerical errors near the interface become visible in the form of colourful noise. A traditional remedy [170], [185], [205] exploits the fact that the solution tends to be more regular and converges a lot faster in yielded flow regions and therefore the shape of sets with $|\tau| \leq (1+\varepsilon)\tau_0$ for a positive 'correction factor' ε is typically far smoother. Nevertheless, the main drawback of this postprocessing step is that it introduces a systematic error by overestimating the actual unyielded regions.

We propose another means of visualising the yield surfaces: in Figure 5.11, we plot the

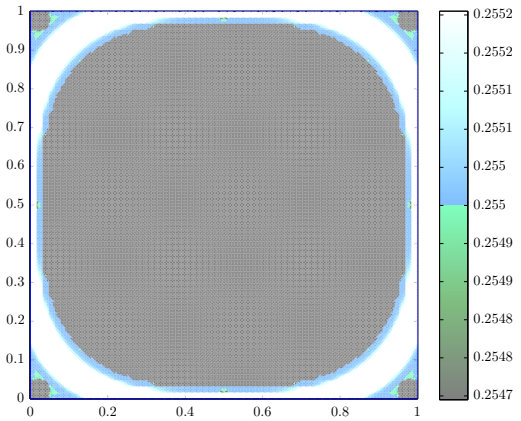

(a): $\tau_0 = 0.255$.

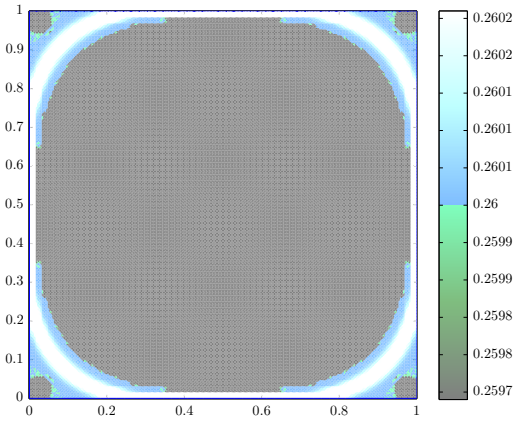

(b): $\tau_0 = 0.26$.

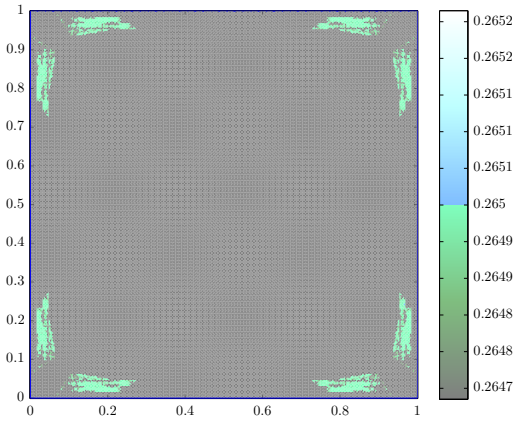

(c): $\tau_0 = 0.265$.

Figure 5.11: Magnitude of the extra stress tensor. Unyielded areas are shaded in gray and green, yielded areas in blue and white.

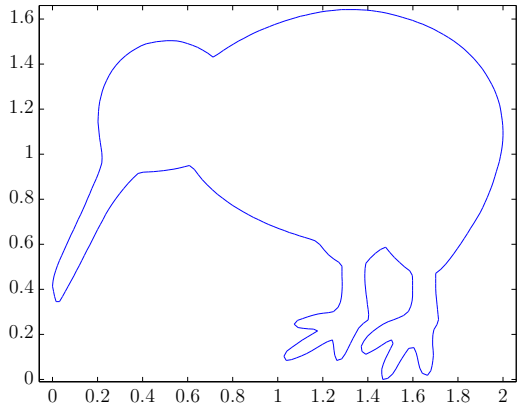

Figure 5.12: Geometry of the kiwi-shaped duct.

magnitude of the extra stress tensor $|\tau|$ in a window of $\pm 0.1\%$ around the yield stress τ_0. Stress magnitudes below the critical value appear in gray-green, yielded regions are displayed as blue-white. Therefore, the interface between yielded and unyielded regions, as predicted by the numerical solution, lies at the sharp transition from blue to green. Meanwhile, since the classification into 'yielded' and 'unyielded' is least reliable near $|\tau| = \tau_0$ due to numerical errors, the width of blue and green shaded areas serves as an indicator of uncertainty in the identification of flow regions. As for the 'correction factor' ε, there is of course some arbitrariness in choosing the width of the interval around the yield stress, which defines the span of the colour gradients. However, this width never introduces any systematic errors into the visualisation, as the discontinuity in our colourbar always occurs exactly at the value τ_0.

As can be seen from the three graphs in Figure 5.11, the fluid is at rest in the corners of the domain and moves like a rigid column in the centre of the pipe. As $\tau_0 \nearrow \tau_0^c$, the outer and inner regions of rigidity approach each other until the entire cross-section is occupied with solid material.

Flow Through a Kiwi

The flow domains that we used for our simulations so far were characterised by geometric simplicity, high symmetry and a convex shape. Our final experiments shall confirm whether the superior performance of our methods was merely related to any of these properties, or whether they turn out similarly efficient in a more complex setting.

A duct shaped like a kiwi, which is shown in Figure 5.12, is neither geometrically simple, nor symmetric, nor convex. Before progressing to a comparison of how the different algorithms perform in this setting, we compute approximations to the plug flow regions

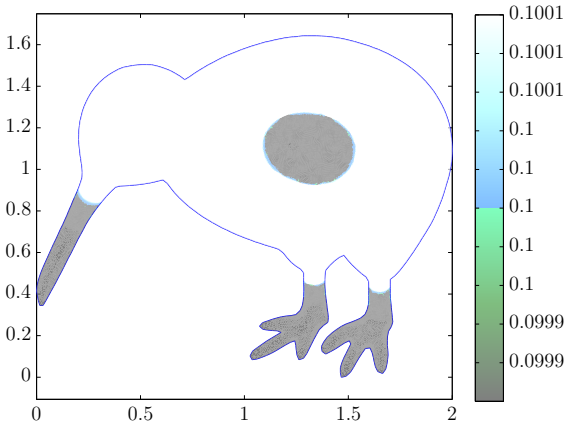

(a): $\tau_0 = 0.1$.

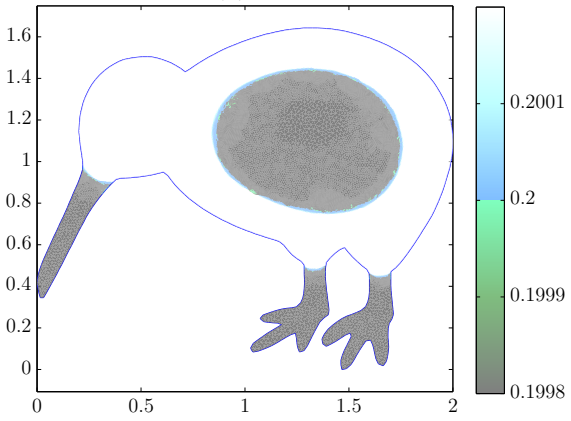

(b): $\tau_0 = 0.2$.

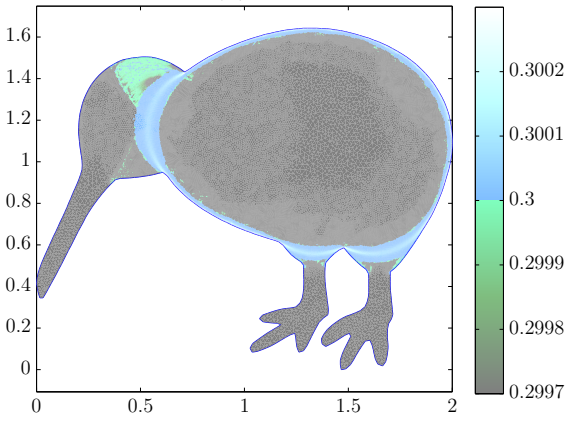

(c): $\tau_0 = 0.3$.

Figure 5.13: Yielded and unyielded regions for BINGHAM flow through the kiwi.

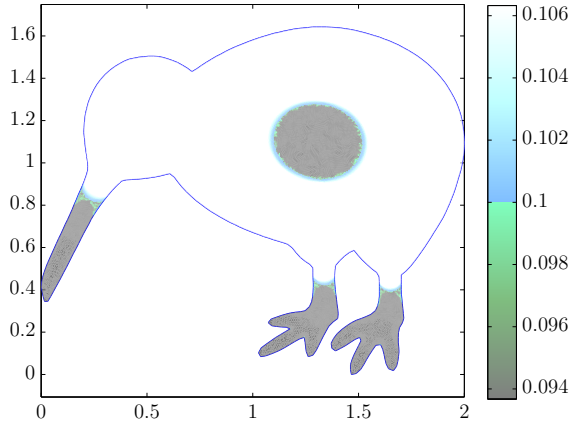

(a): $\tau_0 = 0.1$.

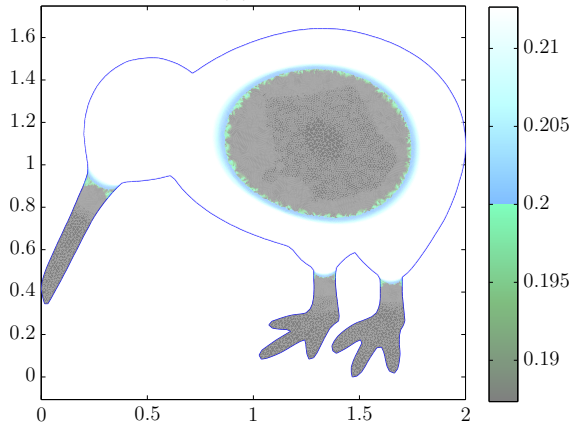

(b): $\tau_0 = 0.2$.

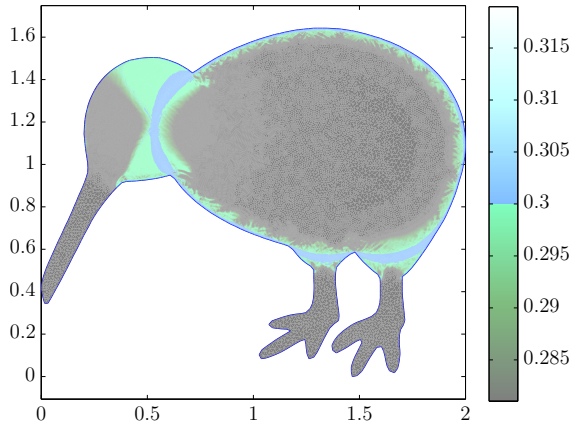

(c): $\tau_0 = 0.3$.

Figure 5.14: Yielded and unyielded regions for Casson flow through the kiwi.

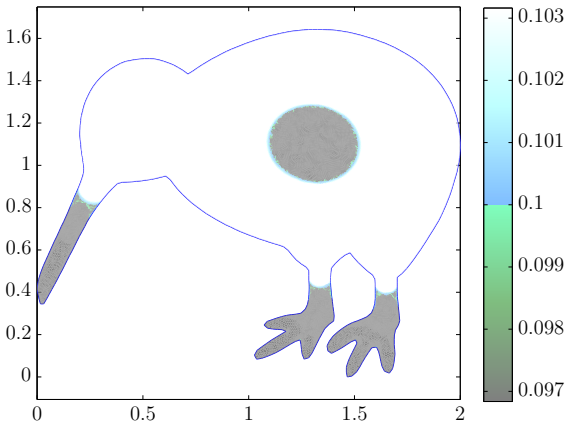

(a): $\tau_0 = 0.1$.

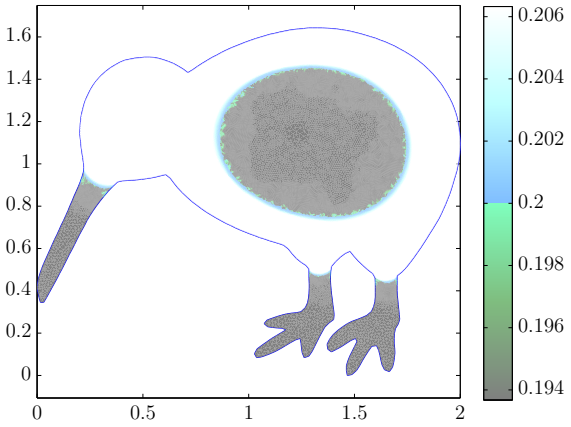

(b): $\tau_0 = 0.2$.

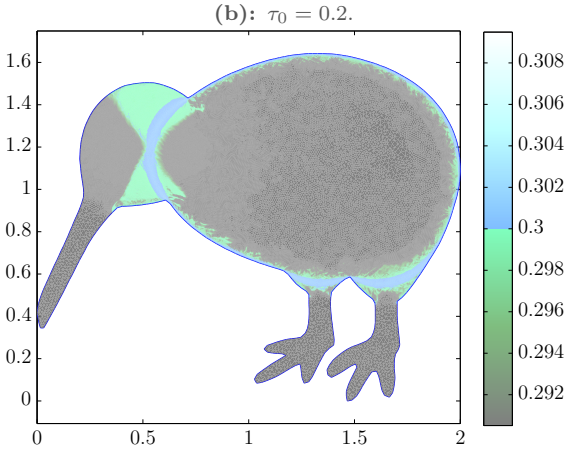

(c): $\tau_0 = 0.3$.

Figure 5.15: Yielded and unyielded regions for Herschel-Bulkley flow through the kiwi ($r = 1.5$).

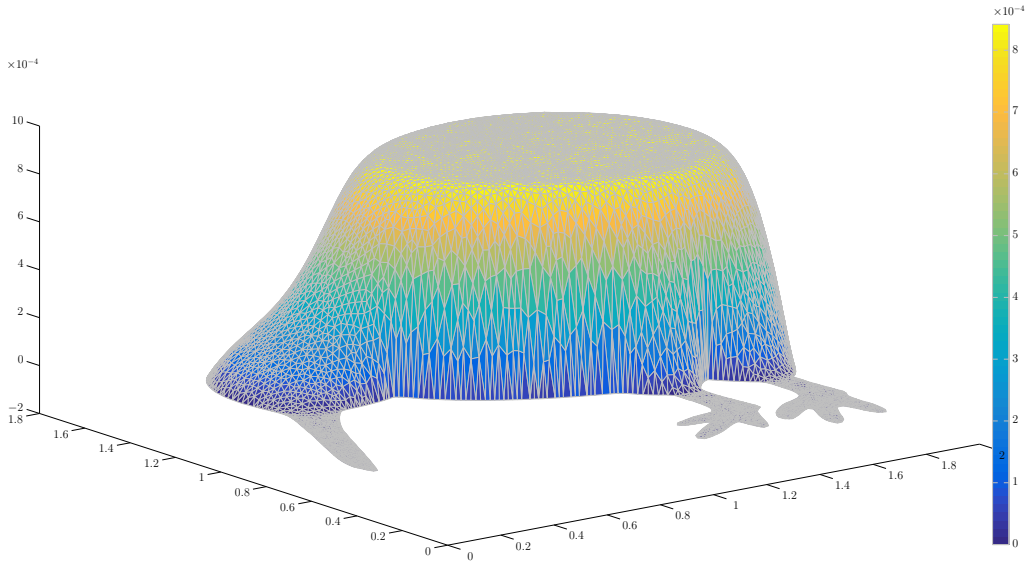

Figure 5.16: Velocity profile u for the flow of a Herschel-Bulkley fluid through the kiwi pipe ($\tau_0 = 0.2$, $r = 1.5$). The flow profiles for Bingham and Casson fluids with the same yield stress are very similar.

for different parameters.

5.26 Visualisation of Yielded and Unyielded Areas We carry out simulations for the three different constitutive models and three different values of the yield stress, $\tau_0 \in \{\, 0.1, 0.2, 0.3 \,\}$. The largest value of the yield stress lies close to the plastic limit, which poses a challenge for the optimisation algorithms.

For simulations of Bingham fluids, we use the accelerated dual proximal gradient method FISTA*. For the other two models, we apply its variable-metric extension, with the full Hessian included in the preconditioner. By trying different powers of 2 for the weighting factor α, we find that $\alpha = 1/16$ yields the fastest convergence if $\tau_0 = 0.1$, $\alpha = 1/128$ is optimal in this respect for $\tau_0 = 0.2$ and $\alpha = 1/1024$ for $\tau_0 = 0.3$. In all cases, the primal sequence is computed from the leading point and we stop the algorithms as soon as the residual falls below gradTol $= 10^{-8}$.

The corresponding results are visualised in Figures 5.13 to 5.15. A typical velocity profile is depicted in Figure 5.16.

In tight areas and corners of the duct, viscoplastic fluids easily get stuck. This is confirmed by the results, which show no flow in parts of the beak and the feet, depending on the value of the yield stress. Very close to yield limit, only a thin liquid layer lubricates between the large solid plug and the pipe wall or rigid material attached to it. The

contours of the different yielded and unyielded regions appear plausible and agree with theoretical results as far as these are available [204].

Algorithm	Iterations	Time (s)	Speedup
ADMM	2839	17.3	1.0
ISTA*	2834	16.7	1.0
FISTA*	161	1.05	15
VM-FISTA* (5.8a)	273	13.6	1.2
VM-FISTA* (5.8b)	416	14.8	1.1

Table 5.1: Bingham flow through the kiwi. Iterations and computing time until convergence. The speedup factors refer to ISTA*.

Algorithm	Iterations	Time (s)	Speedup
ISTA*	3950	24.3	1.0
FISTA*	288	1.83	13
VM-FISTA* (5.8a)	23	1.20	20
VM-FISTA* (5.8b)	39	1.50	16

Table 5.2: Casson flow through the kiwi. ADMM would require Newton's method in every iteration, resulting in computing times many times larger. This can be avoided by using ISTA* instead.

Algorithm	Iterations	Time (s)	Speedup
ISTA*	3957	22.3	1.0
FISTA*	290	1.71	14
VM-FISTA* (5.8a)	23	1.25	19
VM-FISTA* (5.8b)	38	1.49	16

Table 5.3: Herschel-Bulkley flow through the kiwi ($r = 1.5$). In comparison to a state-of-the-art method, tteration numbers and computing times of the new algorithms are smaller by several orders of magnitude.

5.27 Performance of State-of-the-Art and New Algorithms Finally, we compare the iteration numbers and computation times that different methods require to meet a given tolerance.

We consider the problem with intermediate yield stress, $\tau_0 = 0.2$ and stop each algorithm as soon as the residual reaches gradTol $= 10^{-6}$. For the Newton-type methods, we set $\alpha = 1/128$.

Tables 5.1 to 5.3 summarise the outcome of this experiment. The results are in agreement with our previous observations. For all three flow problems, at least one of

our new methods converges at least 15 times faster than classical algorithms. Compared to ISTA*, all of the accelerated methods reduce the computing time, which is required to find an approximate solution to the Casson and Herschel-Bulkley flow problems, to only a small fraction. Also for the simulation of a Bingham fluid, FISTA* and VM-FISTA* with either preconditioner lead to convergence within a shorter time frame. However, as observed for the circular pipe, this improvement is only significant for the dual-based method with a fixed metric.

We remark that these data only reflect a snapshot of the convergence properties in so far, as they only refer to one specific tolerance on the residual. As a result of the higher convergence rate of accelerated methods, the speedup factors cannot be extrapolated proportionally to smaller tolerances. In this respect, the data presented in the above tables provides rather conservative estimates of the performance increase due to acceleration and/or preconditioning in favour of state-of-the-art methods. As decreasing tolerances on the residual go hand in hand with increasing speedup factors, computing times quickly become practically infeasible for ADMM and ISTA*. Accordingly, accelerated schemes unveil their full potential for simulations of high fidelity.

Chapter 6

Stationary Flow through Cavities

Fully two-dimensional flow problems overall possess a very similar structure to '1.5-dimensional' pipe flow. Consequently, our derivation of the explicit form of the dual-based proximal algorithms remains unaltered in large parts. Mainly three different features require extra attention:

(a) the incompressibility condition $\operatorname{div} u = 0$ is no longer satisfied by default and therefore the pressure enters as a new variable,

(b) inhomogeneous DIRICHLET boundary conditions for the flow velocity imply that the primal problem is constrained to a convex set, which generally constitutes only an affine subspace,

(c) the flow velocity is now vector-valued, while the rate-of-strain and deviatoric stress tensors possess three independent components.

The sketch in Figure 6.1 outlines the geometric setting of a typical problem.

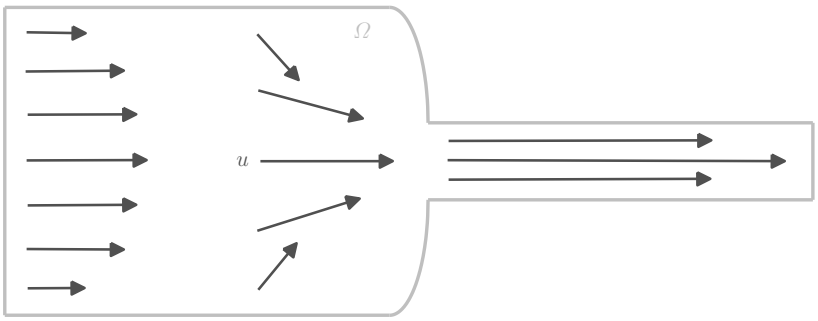

Figure 6.1: Sketch of the geometry for flows through cavities: the flow velocity u is a two-dimensional vector field on the domain $\Omega \subset \mathbb{R}^2$.

This chapter is structured in analogy to the previous one. In Section (A), we implement the necessary changes to the problem formulation and subproblems of each algorithm. Due to the great deal of similarity to pipe flow problems, we skip proofs and detailed calculations, as far as they are analogous to those in Chapter 5. Numerical studies of convergence properties are the subject of Section (B), before we conclude with further simulations in Section (C).

(A) Explicit Form of the Proximal Algorithms

Governing Equations

The two-dimensional geometry of the flow domain $\Omega \subset \mathbb{R}^2$ allows us to set the third component of the flow velocity to zero. With $u(x_1, x_2, x_3) = (u_1(x_1, x_2), u_2(x_1, x_2), 0)^\top$, the strain rate becomes

$$\dot{\gamma} = \mathcal{D}u = \begin{pmatrix} \frac{\partial u_1}{\partial x_1} & \frac{1}{2}\frac{\partial u_1}{\partial x_2} + \frac{1}{2}\frac{\partial u_2}{\partial x_1} & 0 \\ \frac{1}{2}\frac{\partial u_1}{\partial x_2} + \frac{1}{2}\frac{\partial u_2}{\partial x_1} & \frac{\partial u_2}{\partial x_2} & 0 \\ 0 & 0 & 0 \end{pmatrix}.$$

Its Frobenius norm obviously agrees with the Frobenius norm of the top left (2×2)-block only. We therefore define the restricted variables

$$\tilde{u} := \begin{pmatrix} u_1 \\ u_2 \end{pmatrix} \qquad \tilde{\dot{\gamma}} := \begin{pmatrix} \dot{\gamma}_{11} & \dot{\gamma}_{12} \\ \dot{\gamma}_{21} & \dot{\gamma}_{22} \end{pmatrix} \qquad \tilde{\tau} := \begin{pmatrix} \tau_{11} & \tau_{12} \\ \tau_{21} & \tau_{22} \end{pmatrix}$$

where $\dot{\gamma}_{12} = \dot{\gamma}_{21}$ and $\tau_{12} = \tau_{21}$. We now adapt our notation and remove the tilde when we refer to these variables.

To reduce memory requirements, it is advantageous to exploit $\mathbb{R}^{2\times 2}_{\mathrm{sym}} \cong \mathbb{R}^3$ for a computational implementation. For this isomorphism to be isometric, the latter space must be equipped with a scaled inner product $\star$ instead of the Euclidean dot product $\cdot$, so that for $A, B \in \mathbb{R}^{2\times 2}_{\mathrm{sym}}$

$$A : B = a_{11}b_{11} + a_{22}b_{22} + 2a_{12}b_{12} = \begin{pmatrix} a_{11} \\ a_{22} \\ a_{12} \end{pmatrix} \star \begin{pmatrix} b_{11} \\ b_{22} \\ b_{12} \end{pmatrix}.$$

The appropriate function spaces for problems of flows through cavities are those of Chapter 4, Section (B) with $d = 2$. For convenience, we repeat the explicit form of the primal problem in this setting.

6.1 Formulation of 2D Steady Viscoplastic Flow as Minimisation Problem Let $f \in L^{r^*}(\Omega)^2$ and $u_{\mathrm{D}} \in U_{\mathrm{D}}$ be given. Then find the solution $\bar{u} \in U_{0\mathrm{D}}$ of the convex programming problem

$$\min_{u \in U_{0\mathrm{D}}} \left\{ I(u) := b(\mathcal{D}u) + j(\mathcal{D}u) - \langle f, u \rangle_{L^{r^*}(\Omega)^2, L^r(\Omega)^2} \right\} \tag{VP-P}$$

where

$$b(\mathcal{D}u) = \mu \int_\Omega |\mathcal{D}u|^2 \,\mathrm{d}x \qquad \text{(Bingham)}$$

$$b(\mathcal{D}u) = \mu \int_\Omega |\mathcal{D}u|^2 \,\mathrm{d}x + \frac{4\sqrt{2\mu\tau_0}}{3} \int_\Omega |\mathcal{D}u|^{3/2} \,\mathrm{d}x \qquad \text{(Casson)}$$

$$b(\mathcal{D}u) = \frac{2^{r-1}\kappa}{r} \int_\Omega |\mathcal{D}u|^r \,\mathrm{d}x \qquad \text{(Herschel-Bulkley)}$$

and

$$j(\mathcal{D}u) = \tau_0 \int_\Omega |\mathcal{D}u| \,\mathrm{d}x.$$

Moreover, the duality pairing reads in explicit form

$$\langle f, u \rangle_{L^{r^*}(\Omega)^2, L^r(\Omega)^2} = \int_\Omega f \cdot u \,\mathrm{d}x.$$

6.2 Problem (VP-P) as Composite Convex Problem The boundary conditions now give rise to an extra term in the split problem formulation. In order to re-write (VP-P) in the form of (P′), we employ the indicator function of the set $U_{0\mathrm{D}}$, which incorporates both the incompressibility constraint and the set trace of the velocity on Γ.

$$\begin{gathered} \min_{(u,\dot{\gamma}) \in U_{0*} \times Q} \left[b(\dot{\gamma}) + j(\dot{\gamma}) \right] + \left[-\langle f, u \rangle_{L^{r^*}(\Omega)^2, L^r(\Omega)^2} + \iota_{U_{0\mathrm{D}}}(u) \right] \\ \text{subject to} \qquad \dot{\gamma} = \mathcal{D}u. \end{gathered} \tag{VP-P′}$$

As for pipe flows of Herschel-Bulkley fluids, some of the following problems may not be well-posed in the corresponding function spaces. They should be understood in a purely formal sense.

Subproblems Arising in the Proximal Algorithms

6.3 Assumptions on the Primal Problem To verify Assumption 3.1 on page 57 for (VP-P), the same arguments as for duct flow problems apply to justify that conditions (a) and (b) hold in the two-dimensional setting as well. Only the statements (c) and (d) do not follow in the same way.

(c) The symmetric part of the gradient operator is apparently bounded. To establish boundedness below on $U_{0\mathrm{D}}$, consider two functions $u_1, u_2 \in U_{0\mathrm{D}}$. Their difference $u_1 - u_2 \in U_{00} \subset W_0^{1,r}(\Omega)^2$. On this space, Korn's inequality (Theorem 4.13) holds and together with the multivariate form of Poincaré's inequality (Theorem 4.12) it follows the existence of $C > 0$ such that

$$\|u_1 - u_2\|_{W_0^{1,r}(\Omega)^2} \leq C \, \|\mathcal{D}u_1 - \mathcal{D}u_2\|_{L^r(\Omega)^{2\times 2}} \, .$$

(d) According to the trace theorem (Theorem 4.10) and since $u_{\mathrm{D}} \in U_{\mathrm{D}}$ satisfies a condition for compatibility with the incompressibility constraint, $U_{0\mathrm{D}} \neq \emptyset$. Furthermore, $b + j$ is continuous. Hence, the qualification condition (3.3) is met.

The following dual formulation of two-dimensional viscoplastic flow appears to be new. The derivation follows the exact same steps as in Chapter 5.

6.4 Proposition$^{(\mathrm{TT})}$ (Dual 2D Flow Problem) *The dual problem associated with the split primal formulation (VP-P′) reads*

$$\begin{aligned} &\min_{\tau \in S} F(\tau) \\ &\textit{subject to} \qquad \langle \tau, \mathcal{D}\,\cdot \rangle_{Q^*,Q} = \langle f, \cdot \rangle_{L^{r^*}(\Omega)^2, L^r(\Omega)^2} \quad \textit{on } U_{00}^* \end{aligned} \tag{VP-D′}$$

The objective F is given by

$$F(\tau) = \frac{1}{4\mu} \int_\Omega (|\tau| - \tau_0)_+^2 \, \mathrm{d}x \qquad \text{(Bingham)} \tag{6.1a}$$

$$F(\tau) = \frac{1}{4\mu} \int_\Omega \left(\sqrt{|\tau|} - \sqrt{\tau_0}\right)_+^3 \left(\sqrt{|\tau|} + \frac{1}{3}\sqrt{\tau_0}\right) \mathrm{d}x \qquad \text{(Casson)} \tag{6.1b}$$

$$F(\tau) = \frac{1}{2r^*\kappa^{r^*-1}} \int_\Omega (|\tau| - \tau_0)_+^{r^*} \, \mathrm{d}x \qquad \text{(Herschel-Bulkley)} \tag{6.1c}$$

6.5 Lemma$^{(\mathrm{TT})}$ (Derivatives of the Dual Objective) *The functional F is* Fréchet

differentiable with

$$\nabla F(\tau) = \frac{1}{2\mu}\left(|\tau| - \tau_0\right)_+ \frac{\tau}{|\tau|} \qquad \text{(Bingham)} \tag{6.2a}$$

$$\nabla F(\tau) = \frac{1}{2\mu}\left(\sqrt{|\tau|} - \sqrt{\tau_0}\right)_+^2 \frac{\tau}{|\tau|} \qquad \text{(Casson)} \tag{6.2b}$$

$$\nabla F(\tau) = \frac{1}{2\kappa^{r^*-1}}\left(|\tau| - \tau_0\right)_+^{r^*-1} \frac{\tau}{|\tau|}. \qquad \text{(Herschel-Bulkley)} \tag{6.2c}$$

For second derivatives, we use the identification $\tau(x) \in \left(\mathbb{R}^3, \star\right)$ *almost everywhere. For* Bingham *fluids, a Hessian in the sense of* Newton *derivatives is given by*

$$\begin{aligned}
\left(\nabla^2 F(\tau)\right)_{11} &= \frac{1}{2\mu}\left(1 - \frac{\tau_0(\tau_2^2 + 2\tau_3^2)}{|\tau|^3}\right) \\
\left(\nabla^2 F(\tau)\right)_{22} &= \frac{1}{2\mu}\left(1 - \frac{\tau_0(\tau_1^2 + 2\tau_3^2)}{|\tau|^3}\right) \\
\left(\nabla^2 F(\tau)\right)_{33} &= \frac{1}{2\mu}\left(1 - \frac{\tau_0(\tau_1^2 + \tau_2^2)}{|\tau|^3}\right) \\
\left(\nabla^2 F(\tau)\right)_{12} &= \frac{1}{2\mu}\left(\frac{\tau_0\tau_1\tau_2}{|\tau|^3}\right) \\
\left(\nabla^2 F(\tau)\right)_{13} &= \frac{1}{2\mu}\left(\frac{2\tau_0\tau_1\tau_3}{|\tau|^3}\right) \\
\left(\nabla^2 F(\tau)\right)_{23} &= \frac{1}{2\mu}\left(\frac{2\tau_0\tau_2\tau_3}{|\tau|^3}\right)
\end{aligned} \tag{6.3a}$$

almost everywhere in $\{\, |\tau| > \tau_0 \,\}$ *and* $\nabla^2 F(\tau) = 0$ *almost everywhere in* $\{\, |\tau| \leq \tau_0 \,\}$. *With the other two constitutive models, the Hessian exists in the sense of* Fréchet. *For* Casson *fluids, its entries read*

$$\begin{aligned}
\left(\nabla^2 F(\tau)\right)_{11} &= \frac{1}{2\mu}\left(\frac{c^2}{|\tau|} + \frac{c\sqrt{\tau_0}\tau_1^2}{|\tau|^3}\right) \\
\left(\nabla^2 F(\tau)\right)_{22} &= \frac{1}{2\mu}\left(\frac{c^2}{|\tau|} + \frac{c\sqrt{\tau_0}\tau_2^2}{|\tau|^3}\right) \\
\left(\nabla^2 F(\tau)\right)_{33} &= \frac{1}{2\mu}\left(\frac{c^2}{|\tau|} + \frac{2c\sqrt{\tau_0}\tau_3^2}{|\tau|^3}\right) \\
\left(\nabla^2 F(\tau)\right)_{12} &= \frac{1}{2\mu}\frac{c\sqrt{\tau_0}\tau_1\tau_2}{|\tau|^3} \\
\left(\nabla^2 F(\tau)\right)_{13} &= \frac{1}{2\mu}\frac{2c\sqrt{\tau_0}\tau_1\tau_3}{|\tau|^3} \\
\left(\nabla^2 F(\tau)\right)_{23} &= \frac{1}{2\mu}\frac{2c\sqrt{\tau_0}\tau_2\tau_3}{|\tau|^3}
\end{aligned} \tag{6.3b}$$

and for Herschel-Bulkley *fluids*

$$
\begin{aligned}
\big(\nabla^2 F(\tau)\big)_{11} &= \frac{1}{2\kappa^{r^*-1}}\left(\frac{h_1\tau_1^2}{|\tau|^2} + \frac{h_2(|\tau| - \tau_1^2)}{|\tau|^3}\right)\\
\big(\nabla^2 F(\tau)\big)_{22} &= \frac{1}{2\kappa^{r^*-1}}\left(\frac{h_1\tau_2^2}{|\tau|^2} + \frac{h_2(|\tau| - \tau_2^2)}{|\tau|^3}\right)\\
\big(\nabla^2 F(\tau)\big)_{33} &= \frac{1}{2\kappa^{r^*-1}}\left(\frac{2h_1\tau_3^2}{|\tau|^2} + \frac{h_2(|\tau| - 2\tau_3^2)}{|\tau|^3}\right)\\
\big(\nabla^2 F(\tau)\big)_{12} &= \frac{1}{2\kappa^{r^*-1}}\left(\frac{h_1\tau_1\tau_2}{|\tau|^2} - \frac{h_2\tau_1\tau_2}{|\tau|^3}\right)\\
\big(\nabla^2 F(\tau)\big)_{13} &= \frac{1}{2\kappa^{r^*-1}}\left(\frac{2h_1\tau_1\tau_3}{|\tau|^2} - \frac{2h_2\tau_1\tau_3}{|\tau|^3}\right)\\
\big(\nabla^2 F(\tau)\big)_{23} &= \frac{1}{2\kappa^{r^*-1}}\left(\frac{2h_1\tau_2\tau_3}{|\tau|^2} - \frac{2h_2\tau_2\tau_3}{|\tau|^3}\right)
\end{aligned}
\tag{6.3c}
$$

with the auxiliary expressions $c := (\sqrt{|\tau|} - \sqrt{\tau_0})_+$, $h_1 := (r^*-1)(|\tau| - \tau_0)_+^{r^*-2}$ *and* $h_2 := (|\tau| - \tau_0)_+^{r^*-1}$.

We now proceed to the problems that form part of the evaluation of each proximal map. Instead of simple Poisson problems, we are now confronted with the solution of a Stokes problem in every iteration.

6.6 Lemma[(TT)] (FISTA* and VM-FISTA* for Steady Viscoplastic Duct Flow) *(a) The steps (FISTA*.1) and (VM-FISTA*.1) are equivalent to*

$$\hat{\dot\gamma}^{(k)} := \frac{1}{2\mu}\Big(|\hat\tau^{(k)}| - \tau_0\Big)_+ \frac{\hat\tau^{(k)}}{|\hat\tau^{(k)}|} \qquad \text{(Bingham)} \tag{6.4a}$$

$$\hat{\dot\gamma}^{(k)} := \frac{1}{2\mu}\left(\sqrt{|\hat\tau^{(k)}|} - \sqrt{\tau_0}\right)_+^2 \frac{\hat\tau^{(k)}}{|\hat\tau^{(k)}|} \qquad \text{(Casson)} \tag{6.4b}$$

$$\hat{\dot\gamma}^{(k)} := \frac{1}{2\kappa^{r^*-1}}\Big(|\hat\tau^{(k)}| - \tau_0\Big)_+^{r^*-1} \frac{\hat\tau^{(k)}}{|\hat\tau^{(k)}|}. \qquad \text{(Herschel-Bulkley)} \tag{6.4c}$$

(b) Step (FISTA.2) is equivalent to the* Stokes *problem: find the unique solution* $(\hat u^{(k)}, \hat p^{(k)}) \in U_{*D} \times P_0$, *such that*

$$-\Delta\hat u^{(k)} + \nabla\hat p^{(k)} = L^{(k)} f - \operatorname{div}(\hat{\dot\gamma}^{(k)} - L^{(k)}\hat\tau^{(k)}) \qquad \text{in } \Omega \tag{6.5a}$$

$$\hat u^{(k)} = u_D \qquad \text{on } \Gamma \tag{6.5b}$$

in the weak sense, i.e. $\forall u \in U_{*0}, \forall p \in P$

$$\int_\Omega \mathcal{D}\hat{u}^{(k)} : \mathcal{D}u \,\mathrm{d}x - \int_\Omega \hat{p}^{(k)} \operatorname{div} u \,\mathrm{d}x = L^{(k)} \int_\Omega f \cdot u \,\mathrm{d}x + \int_\Omega (\hat{\hat{\gamma}}^{(k)} - L^{(k)}\hat{\tau}^{(k)}) : \mathcal{D}u \,\mathrm{d}x$$
$$\int_\Omega p \operatorname{div} \hat{u}^{(k)} \,\mathrm{d}x = 0.$$

(c) *Step (VM-FISTA*.2) is equivalent to the scaled* Stokes *problem: find the unique solution* $(\hat{u}^{(k)}, \hat{p}^{(k)}) \in U_{*D} \times P_0$*, such that*

$$-\operatorname{div}(\mathcal{H}^{(k)})^{-1}\mathcal{D}\hat{u}^{(k)} + \nabla \hat{p}^{(k)} = l^{(k)} f - \operatorname{div}((\mathcal{H}^{(k)})^{-1}\hat{\hat{\gamma}}^{(k)} - l^{(k)}\hat{\tau}^{(k)}) \quad \text{in } \Omega \tag{6.6a}$$
$$\hat{u}^{(k)} = u_D \quad \text{on } \Gamma \tag{6.6b}$$

in the weak sense, i.e. $\forall u \in U_{*0}, \forall p \in P$

$$\int_\Omega (\mathcal{H}^{(k)})^{-1}\mathcal{D}\hat{u}^{(k)} \cdot \mathcal{D}u \,\mathrm{d}x - \int_\Omega \hat{p}^{(k)} \operatorname{div} u \,\mathrm{d}x = l^{(k)} \int_\Omega f \cdot u \,\mathrm{d}x + \int_\Omega ((\mathcal{H}^{(k)})^{-1}\hat{\hat{\gamma}}^{(k)} - l^{(k)}\hat{\tau}^{(k)}) \cdot \nabla u \,\mathrm{d}x$$
$$\int_\Omega p \operatorname{div} \hat{u}^{(k)} \,\mathrm{d}x = 0.$$

Proof.

(a) follows from the previous Lemma.

(b) The problem (FISTA*.2) explicitly reads

$$\hat{u}^{(k)} = \operatorname*{arg\,min}_{u \in W^{1,r}(\Omega)^2} \left\{ L^{(k)} \left(-\langle f, u \rangle_{U_{00}^*, U_{00}} + \iota_{U_{0D}}(u) \right) + \frac{1}{2} \left\| \mathcal{D}u - (\hat{\hat{\gamma}}^{(k)} - L^{(k)}\hat{\tau}^{(k)}) \right\|_Q^2 \right\}.$$

We fix $u_0 \in U_{0D}$. Since $U_{*D} = u_0 + U_{*0}$, we can characterise $\hat{u}^{(k)}$ equivalently by $\hat{u}^{(k)} = u_0 + \tilde{u}^{(k)}$, where $\tilde{u}^{(k)}$ is the solution of

$$\min_{u \in U_{*0}} \frac{1}{2} \left\| \mathcal{D}(u + u_0) - (\hat{\hat{\gamma}}^{(k)} - L^{(k)}\hat{\tau}^{(k)}) \right\|_Q^2 - L^{(k)} \langle f, u \rangle_{U_{00}^*, U_{00}}$$
$$\text{subject to } \operatorname{div} u = 0.$$

Since a constraint qualification holds, there exists a Lagrange multiplier $\hat{p}^{(k)} \in P$

which satisfies the optimality conditions

$$\begin{aligned}\left\langle \mathcal{D}(\tilde{u}^{(k)} + u_0) - (\hat{\dot{\gamma}}^{(k)} - L^{(k)}\hat{\tau}^{(k)}), \mathcal{D}u \right\rangle_{Q^*,Q} - \left\langle \operatorname{div} u, \hat{p}^{(k)} \right\rangle_{P^*,P} &= L^{(k)}\langle f, u\rangle_{U_{00}^*,U_{00}} \\ \left\langle \operatorname{div} \tilde{u}^{(k)}, p \right\rangle_{P^*,P} &= 0,\end{aligned}$$

for all $u \in U_{*0}$ and all $p \in P$. By rearranging and backsubstitution of $u^{(k)}$ we obtain

$$\begin{aligned}\left\langle \mathcal{D}u^{(k)}, \mathcal{D}u \right\rangle_{Q^*,Q} - \left\langle \operatorname{div} u, \hat{p}^{(k)} \right\rangle_{P^*,P} &= L^{(k)}\langle f, u\rangle_{U_{00}^*,U_{00}} + \left\langle \hat{\dot{\gamma}}^{(k)} - L^{(k)}\hat{\tau}^{(k)}, \mathcal{D}u \right\rangle_{Q^*,Q} \\ \left\langle \operatorname{div} \tilde{u}^{(k)}, p \right\rangle_{P^*,P} &= 0,\end{aligned}$$

for all $u \in U_{*0}$ and all $p \in P$.

Finally, the uniqueness of $u^{(k)} \in U_{*\mathrm{D}}$ is a consequence of the strict convexity of the problem. The uniqueness of the pressure $p \in P_0$ is proved by simple calculations that can be found in Section 19 of [206], see also Sections 26.5.1-3.

(c) follows from an analogous proof to (b).

□

Discretisation

While the finite-element discretisation of duct-flow problems is straightforward, greater care has to be taken in the fully two-dimensional case. For a stable approximation, is is crucial to ensure that like its continuous counterpart, discrete divergence operator maps the discrete velocity space onto the discrete pressure space. Consequently, the velocity needs sufficiently many degrees of freedom, which is formulated rigorously in the so-called inf-sup condition or Ladyzhenskaya-Babuška-Brezzi (LBB) condition (cf [207, pp 284-287]).

6.7 Finite-Element Spaces We assume again that Ω is a polygonal domain and we let $\mathcal{T}_h$ be a regular triangulation on $\bar{\Omega}$.

Following Glowinski [206, p 303], we apply the $\mathbb{P}_1$-iso-$\mathbb{P}_2/\mathbb{P}_1$ element of Bercovier and Pironneau [208] for discretising the velocity and pressure, respectively. We recall that $\mathbb{P}_k$ denotes the space of polynomials in two variables of degree at most k, so that the corresponding finite element spaces are given by

$$U_{*0,h} := \left\{ u_h \in C(\bar{\Omega})^2 \;\middle|\; u_h|_\Gamma = 0 \quad \wedge \quad u_h|_T \in \mathbb{P}_1^2, \quad \forall T \in \mathcal{T}_{h/2} \right\}$$

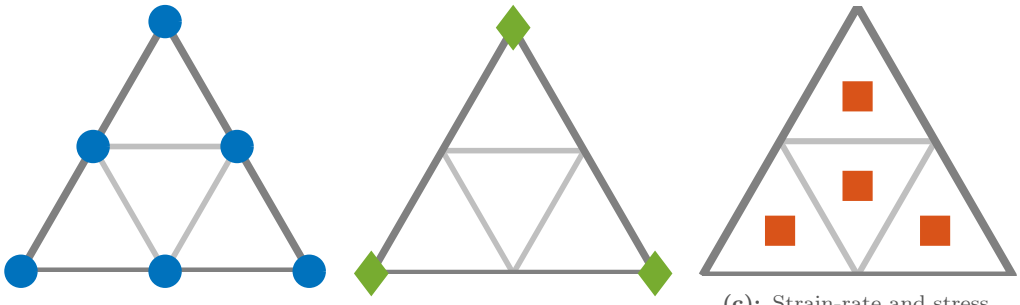

(a): Velocity nodes **(b):** Pressure nodes **(c):** Strain-rate and stress nodes

Figure 6.2: Finite elements for simulations of flows through two-dimensional cavities.

$$
\begin{aligned}
P_{0,h} &:= \left\{ p_h \in C(\bar{\Omega}) \;\middle|\; \int_\Omega p_h \,\mathrm{d}x = 0 \quad \wedge \quad p_h|_T \in \mathbb{P}_1, \quad \forall T \in \mathcal{T}_h \right\} \\
P_h &:= \left\{ p_h \in C(\bar{\Omega}) \;\middle|\; p_h|_T \in \mathbb{P}_1, \quad \forall T \in \mathcal{T}_h \right\} \\
Q_h &:= \left\{ \dot{\gamma}_h \in L^r(\Omega)^3 \;\middle|\; \dot{\gamma}_h|_T \in \mathbb{P}_0^3, \quad \forall T \in \mathcal{T}_{h/2} \right\} \\
S_h &:= \left\{ \tau_h \in L^{r^*}(\Omega)^3 \;\middle|\; \dot{\gamma}_h|_T \in \mathbb{P}_0^3, \quad \forall T \in \mathcal{T}_{h/2} \right\}.
\end{aligned}
$$

The triangulation $\mathcal{T}_{h/2}$ is obtained from $\mathcal{T}_h$ by connecting the edge midpoints in each triangle $T \in \mathcal{T}_h$.

With $u_{\mathrm{D},h} \in C(\Gamma)$ serving as an approximation to u_D that is linear on the triangle edges of $\mathcal{T}_{h/2}$ and that satisfies the same compatibility condition as u_D, we also introduce the convex set

$$
U_{*\mathrm{D},h} := \left\{ u_h \in C(\bar{\Omega})^2 \;\middle|\; u_h|_\Gamma = u_{\mathrm{D},h} \quad \wedge \quad u_h|_T \in \mathbb{P}_1^2, \quad \forall T \in \mathcal{T}_{h/2} \right\}
$$

The Bercovier-Pironneau elements and the piecewise constant elements for strain rate and stress are sketched in Figure 6.2.

The solvability of discrete analogues of the Stokes problems is non-trivial.

6.8 Proposition (Wellposedness of the Discrete Subproblems) *The discretised* Stokes *problems*

(a) find $(\hat{u}_h^{(k)}, \hat{p}_h^{(k)}) \in U_{*D,h} \times P_{0,h}$ *such that* $\forall u_h \in U_{*0,h}, \forall p_h \in P_h$

$$
\int_\Omega \mathcal{D}\hat{u}_h^{(k)} : \mathcal{D}u_h \,\mathrm{d}x - \int_\Omega \hat{p}_h^{(k)} \operatorname{div} u_h \,\mathrm{d}x = L^{(k)} \int_\Omega f \cdot u_h \,\mathrm{d}x
$$

$$+ \int_\Omega (\hat{\gamma}_h^{(k)} - L^{(k)} \hat{\tau}_h^{(k)}) : \mathcal{D}u_h \, \mathrm{d}x$$

$$\int_\Omega p_h \operatorname{div} \hat{u}_h^{(k)} \, \mathrm{d}x = 0.$$

(b) find $(\hat{u}_h^{(k)}, \hat{p}_h^{(k)}) \in U_{*D,h} \times P_{0,h}$ *such that* $\forall u_h \in U_{*0,h}, \forall p_h \in P_h$

$$\int_\Omega (\mathcal{H}_h^{(k)})^{-1} \mathcal{D}\hat{u}_h^{(k)} : \mathcal{D}u_h \, \mathrm{d}x - \int_\Omega \hat{p}_h^{(k)} \operatorname{div} u_h \, \mathrm{d}x = l^{(k)} \int_\Omega f \cdot u_h \, \mathrm{d}x$$

$$+ \int_\Omega ((\mathcal{H}_h^{(k)})^{-1} \hat{\gamma}_h^{(k)} - l^{(k)} \hat{\tau}_h^{(k)}) : \mathcal{D}u_h \, \mathrm{d}x$$

$$\int_\Omega p_h \operatorname{div} \hat{u}_h^{(k)} \, \mathrm{d}x = 0.$$

have a unique solution.

Proof. These results are a consequence of the fact that the Bercovier-Pironneau elements are stable, i.e. they satisfy the LBB condition. We refer to the corresponding proof in [208] for details. □

6.9 PCGU Algorithm for the Stokes problems For solving the Stokes problems that occur in each method, we apply the classical preconditioned conjugate gradient Uzawa (PCGU) method of Cahouet and Chabard [209, pp 892–893]. Glowinski [206, Sec 20–22] motivates this method by successively improving on the very basic Uzawa method for the Stokes problem. These step-by-step improvements on the speed of convergence of the algorithm are achieved by

(a) using conjugate gradients instead of steepest descent.

(b) performing an exact line search at every iteration instead of using the global Lipschitz constant of the dual gradient as a worst-case estimate. Since the problem is quadratic, the exact step size is straightforward to calculate.

(c) preconditioning the problem. While this is essential for the instationary generalisation of the Stokes problem, it is not beneficial for the stationary case that we consider here. With no time dependence, the suggested preconditioner would simply degenerate to a multiple of the identity. Looking at the discrete problem, one could interpret the occurrence of a mass matrix as preconditioning, though.

Since our algorithms implicitly assume that the proximal maps are evaluated exactly, we set a sharp tolerance on the dual gradient $\|\operatorname{div} \hat{u}_h^{(k)}\| \leq 10^{-12}$ for each solution of the Stokes problems. As the PCGU method converges at a linear rate for the Stokes problems [206, Ch IV], this tolerance is achievable relatively easily. Furthermore, we use 'warm starts' by initialising the solution of each Stokes problem with the converged pressure from the previous call. This way, the number of iterations for the PCGU method are initially in the order of ten, but only a couple of iterations are required once the outer optimisation algorithm has closely approached a solution.

Studying inexact methods would go beyond the scope of this project. Instead, we refer to [210], [211].

(B) Convergence Properties

6.10 Convergence of the Bercovier-Pironneau Elements For the convergence of the finite element discretisation to the solution $\bar{u}$ of the Bingham flow problem we have the following results [172]:

$$\|\mathcal{D}\bar{u}_h - \mathcal{D}\bar{u}\|_Q = O(\sqrt{h})$$
$$\|\bar{u}_h - \bar{u}\|_{L^2(\Omega)^2} = O(h).$$

Due to the higher regularity of solutions to the Casson and Herschel-Bulkley flow problems, we achieve a linear $O(h)$ rate even in the energy norm (cf [212]).

Convergence of the Optimisation Algorithms

For our numerical convergence studies in the two-dimensional case, we consider two different flow problems in a square reservoir: a force-driven and a boundary-driven flow.

In both cases, we define $\Omega := \Omega_h :=]0,1[^2$. We also set the viscosity parameters μ and κ to unity. To mesh the geometry, we proceed as follows: first, we generate a uniform grid of $1/h \times 1/h$ squares. Then we divide each square diagonally into four congruent triangles, the collection of which defines the coarse pressure grid $\mathcal{T}_h$.

For all accelerated methods, we compute the primal sequence from the leading points. Any variable metrics are computed by means of the diagonal preconditioner.

6.11 Convergence Rates In [186], De los Reyes and González Andrade simulate the flow of a Bingham fluid, which is driven by the force

$$f(x_1, x_2) := 300\,(x_2 - 0.5, 0.5 - x_1)^\top$$

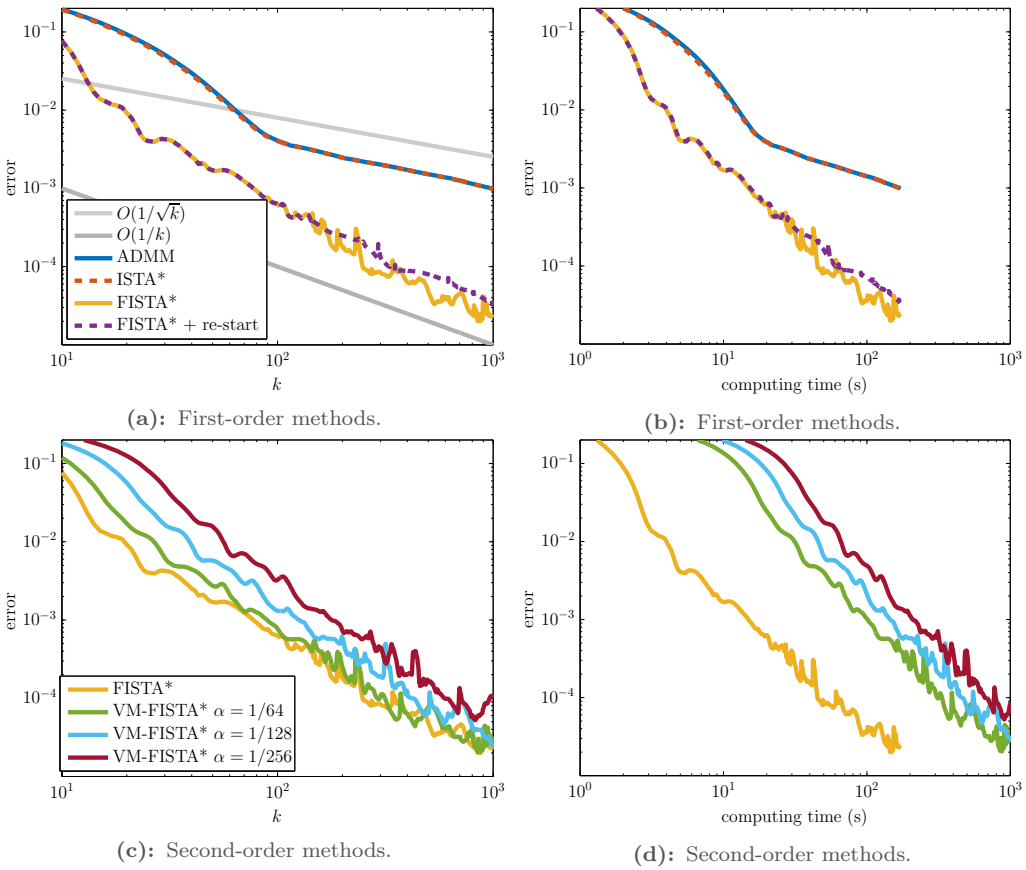

(a): First-order methods.

(b): First-order methods.

(c): Second-order methods.

(d): Second-order methods.

Figure 6.3: Convergence history for Bingham flow in a square reservoir.

almost everywhere in Ω, with yield stress $\tau_0 = 10\sqrt{2}$ and homogeneous boundary conditions. We use the same parameters, and additionally consider the corresponding Casson and Herschel-Bulkley flow problems ($r = 1.5$). Our simulations are carried out on the grid with $h = 1/32$.

As an approximation to the exact solution in the Bingham case, we compute our reference solution by 5,000 iterations with FISTA*. The method terminates with a residual of gradTol $= 8.6 \cdot 10^{-8}$. For the other fluids, we apply VM-FISTA* with $\alpha = 1/128$ instead, which results in final residuals of gradTol $= 8.0 \cdot 10^{-9}$ and gradTol $= 1.9 \cdot 10^{-4}$, respectively.

In Figure 6.3, we compare the convergence of ADMM, ISTA*, FISTA* and VM-FISTA* on this problem. Additionally, we show how the convergence of FISTA* is affected when the criterion (3.28) is monitored to trigger adaptive re-starts of the method.

In this setting, the accelerated methods achieve a convergence rate of order $O(1/k)$

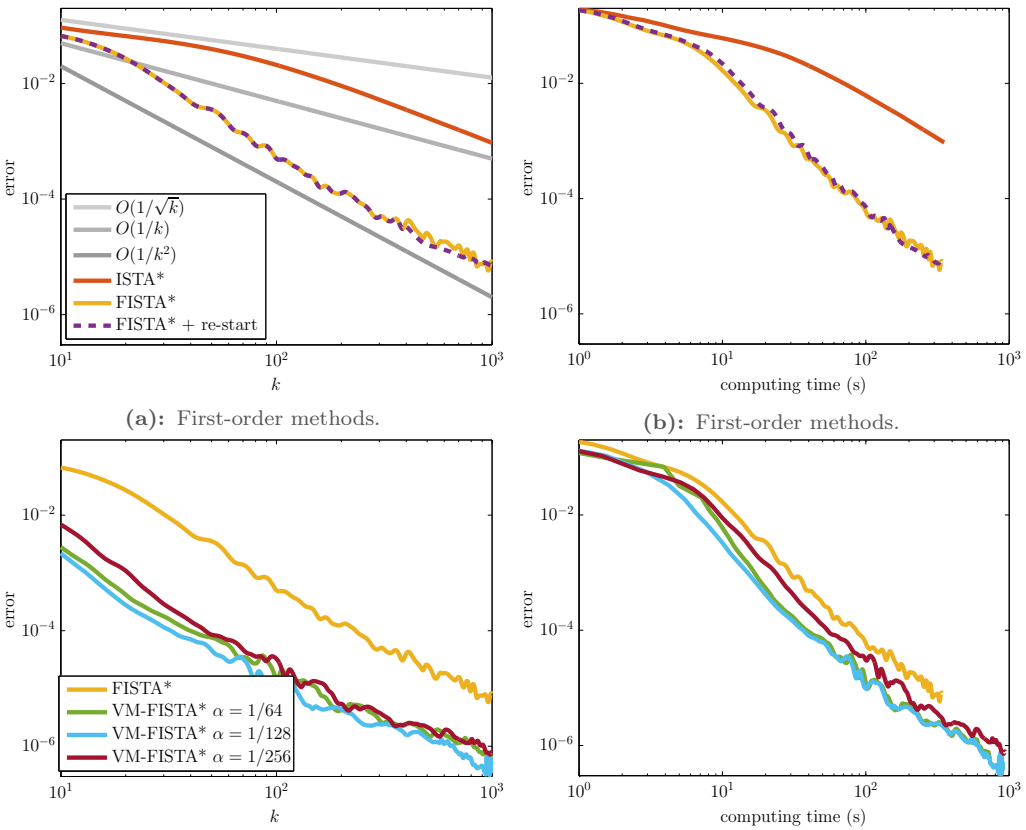

(a): First-order methods.

(b): First-order methods.

(c): Second-order methods.

(d): Second-order methods.

Figure 6.4: Convergence history for Casson flow in a square reservoir.

within only few iterations. ADMM and ISTA* also exhibit their worst-case convergence rate after a start-up phase. FISTA* with adaptive re-starting discards its previous momentum after the iterations $k = 144$ and $k = 351$. Although the descent is qualitatively more consistent, the method is not strictly monotonous and in absolute numbers, the errors lie above those that can be achieved without re-starting.

For these first-order methods, the plot over time exhibits the same features.

Preconditioning does not contribute to smaller errors. As can be seen from the convergence history over time, it is strongly advisable not to invest computational resources in assembling second-order information. These observations agree with those for Bingham flows though pipes.

Moving on to the results for the Casson fluid in Figure 6.4, fast optimisation algorithms show convergence of order $O(1/k^2)$. Surprisingly, even ISTA* appears to attain the same rate asymptotically. In contrast, the results suggest that re-starts of FISTA* after the

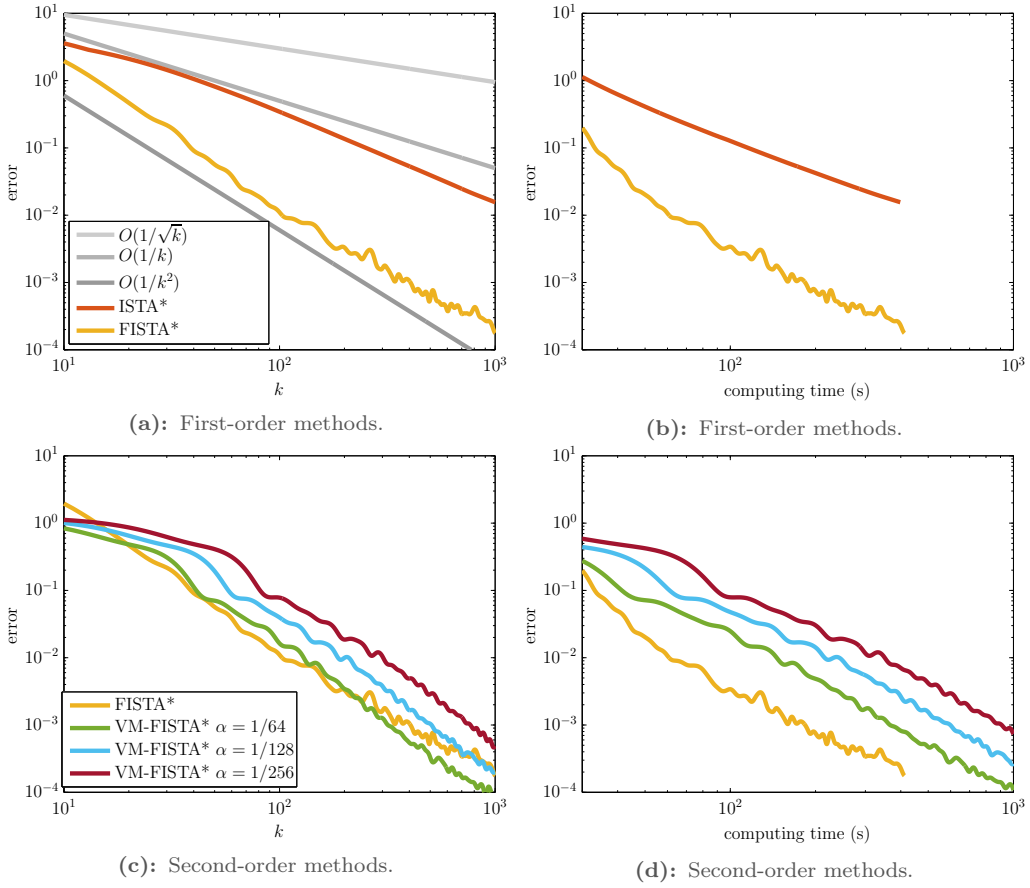

(a): First-order methods.

(b): First-order methods.

(c): Second-order methods.

(d): Second-order methods.

Figure 6.5: Convergence history for Herschel-Bulkley flow in a square reservoir ($r = 1.5$).

iterations with indices $k = 313$ and $k = 919$ decelerate the convergence rate down to $O(1/k)$. Nevertheless, the re-starting scheme effectively improves the monotonicity of the descent.

Evaluating the error as a function of k, Newton-type methods are clearly superior to FISTA* with fixed metric. The performance increase persists in the graph over time, but expectedly reduces in significance. For a weighting factor of $\alpha = 1/64$ or $\alpha = 1/128$, preconditioning allows for approximately five times more accurate results within the same computing time.

In Figure 6.5, we present the results for the simulations of a shear-thinning Herschel-Bulkley fluid. No re-starts of FISTA* occurred during the first 1,000 iterations. The results are otherwise similar to the Casson flow problem, with the exception that for all assessed values of α, the Newton-type methods struggle with improving on the

convergence of FISTA*.

6.12 Regimes of $O(1/k)$ and $O(1/k^2)$ Convergence Let us re-visit an interesting phenomenon which we have already observed on numerous occasions: both the conventional and the fast dual-based proximal gradient algorithms often appear to converge rather slowly initially, but then segue into a regime of significantly faster convergence. In the previous chapter, we hypothesised that this phenomenon may be linked to the accurate identification of the regions of shear flow and stagnation, i.e. the identification of the sparsity pattern in the strain rate. In order to investigate this effect numerically, we compare the convergence of the iterates with the measure of the misclassified regions over the first 1,000 iterations.

With the reference solution denoted by $\bar{\tau}_h$, we compute

$$\operatorname{meas}\left(\left\{\, |\tau_h^{(k)}| > \tau_0 \quad \wedge \quad |\bar{\tau}_h| \leq \tau_0 \,\right\} \cup \left\{\, |\tau_h^{(k)}| \leq \tau_0 \quad \wedge \quad |\bar{\tau}_h| > \tau_0 \,\right\}\right).$$

While we leave the geometry unchanged, we now set the inhomogeneity to zero and instead consider a moving lid:

$$u_{\mathrm{D}}(x) = \begin{cases} (1,0)^\top & \text{if } x_2 = 1 \\ (0,0)^\top & \text{otherwise} \end{cases}.$$

We point out that due to the discontinuities in the top corners, this choice violates our regularity assumption $u_{\mathrm{D}} \in U_{\mathrm{D}}$. The resulting singularities in the stress and pressure make this a classical benchmark problem for testing the stability of numerical schemes. Clearly, any piecewise linear approximation $u_{\mathrm{D},h}$ on a triangulation $\mathcal{T}_h$ does not cause actual singularities in the discrete problems, which are still well-posed for fixed $h > 0$.

For the three different parameters $\tau_0 \in \{\, 100, 200, 500 \,\}$, we simulate the flow of a Bingham fluid, this time on a finer mesh with $h = 1/64$. We carry out 5,000 iterations of FISTA* and set $\bar{u}_h := u_h^{(5{,}000)}$.

The top graph in Figure 6.6 depicts the decay of the errors $\|u_h^{(k)} - \bar{u}_h\|$. By adding up the number of triangles that are classified differently than for the reference solution and dividing through the total number of triangles, we obtain the results in the bottom graph (recalling $\operatorname{meas}(\Omega) = \operatorname{meas}(\Omega_h) = 1$).

Indeed, all three simulations show a very strong correlation between the two error measures. In all cases, the accuracy of yielded and unyielded regions does not improve by any noteworthy extent for a considerable number of iterations. Over exactly the same interval, the errors in the velocity fields decay at a moderate rate. An exact order is difficult to infer from the graph.

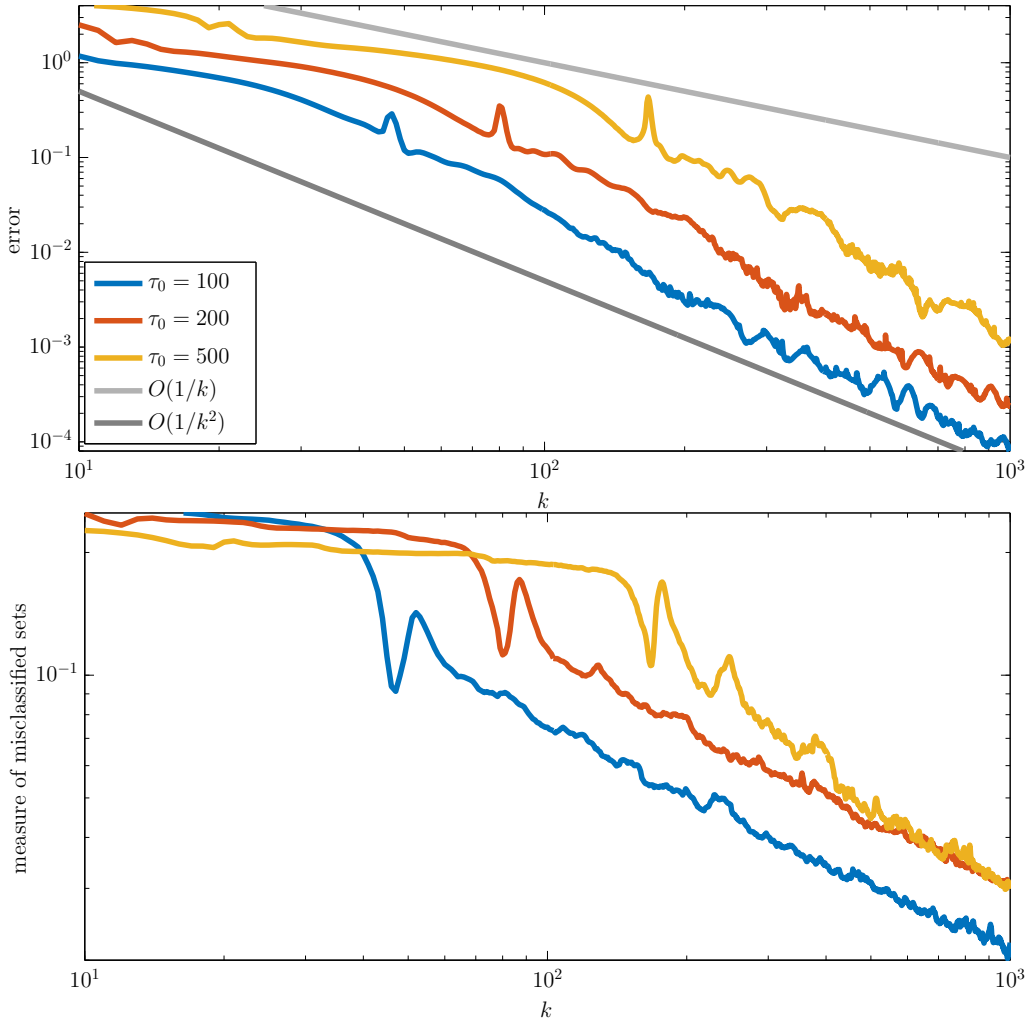

Figure 6.6: Convergence history for BINGHAM flow in the lid-driven cavity, $h = 1/64$.

It is not until k reaches a value of the order 100 until a sharp transition to more rapid descent takes place. This feature is visible in both diagrams.

These observations provide strong support for our hypothesis. The results suggest that an efficient method should ideally be able to quickly identify an accurate approximation to the actual sparsity pattern of $\dot{\gamma}$, as this promises faster convergence than predicted by the worst-case estimate.

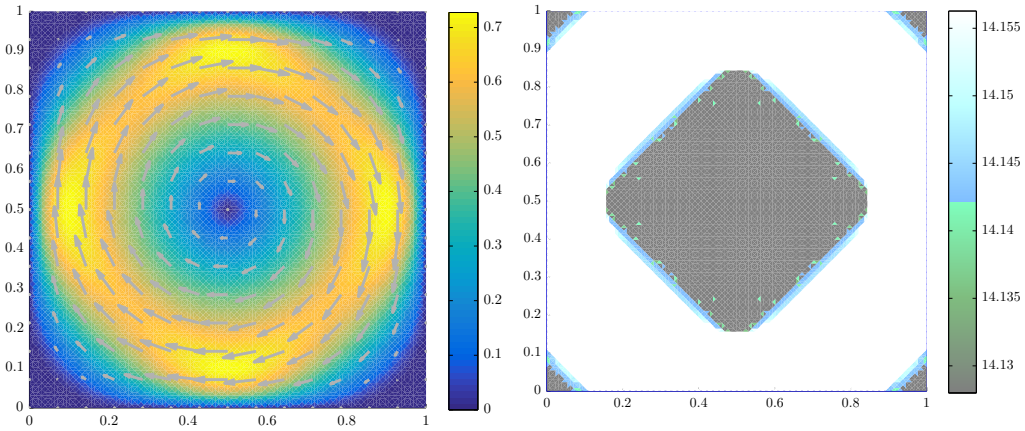

Figure 6.7: Flow velocity and plug flow zones for rotational Bingham flow in a square reservoir ($h = 1/32$).

(C) Numerical Experiments

Force-Driven Cavity

6.13 Yielded and Unyielded Regions Let us now compare the geometry of the stagnant zones as they are predicted by the genuinely nonsmooth methods of this work and the regularised approach of De los Reyes and González Andrade in [186]. Even though the authors study a time-dependent problem, they report that a steady state is quickly attained. This allows us to compare their results under the quasi-stationary regime with ours.

On the grid with $h = 1/32$, we determine the flow profile and the geometry of stagnant zones by using FISTA* with a stopping criterion of gradTol $= 10^{-6}$.

Upon comparing the results in Figure 6.7 with [186], we observe major differences. The central solid region of approximately square shape deviates significantly from the '+'-shape computed by De los Reyes and González Andrade. In our visualisation, it appears that the stress magnitude lies well below the yield stress, which indicates that those results should be reliable.

In the corresponding graphs for Casson flow (Figure 6.8) and Herschel-Bulkely flow (Figure 6.9) we recognise a similar pattern in the stress magnitude as the one found by De los Reyes and González Andrade. Still, our numerical results suggest that the actual unyielded region extends beyond the gray '+'.

On another hand, the flow field in the Bingham case computed by FISTA* agrees both qualitatively and quantitatively with the semismooth Newton method in [185]. This observation confirms once more that regularisation techniques are most appropriate

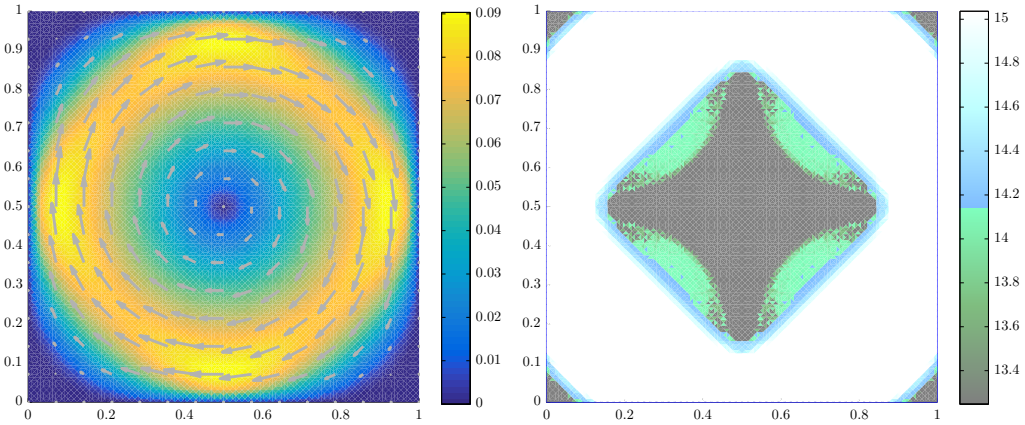

Figure 6.8: Flow velocity and plug flow zones for rotational Casson flow in a square reservoir ($h = 1/32$).

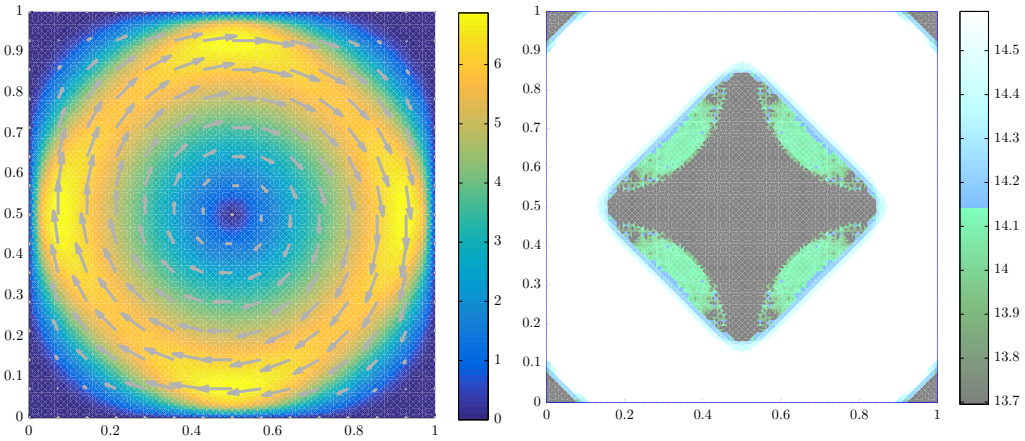

Figure 6.9: Flow velocity and plug flow zones for rotational Herschel-Bulkley flow in a square reservoir ($h = 1/32$).

if a simulation serves the purpose of finding an accurate approximation to the velocity field, but not necessarily of reflecting the exact sparsity pattern of the strain rate.

Lid-Driven Cavity

6.14 Iterations and computing times For a range of different grid sizes and values of the yield stress, we now compare how many iterations and how much time the four algorithms ADMM, ISTA*, FISTA* and FISTA* with re-starting require to compute a solution of the prescribed accuracy gradTol $= 10^{-4}$. We investigate the problem of Bingham flow in the lid-driven cavity.

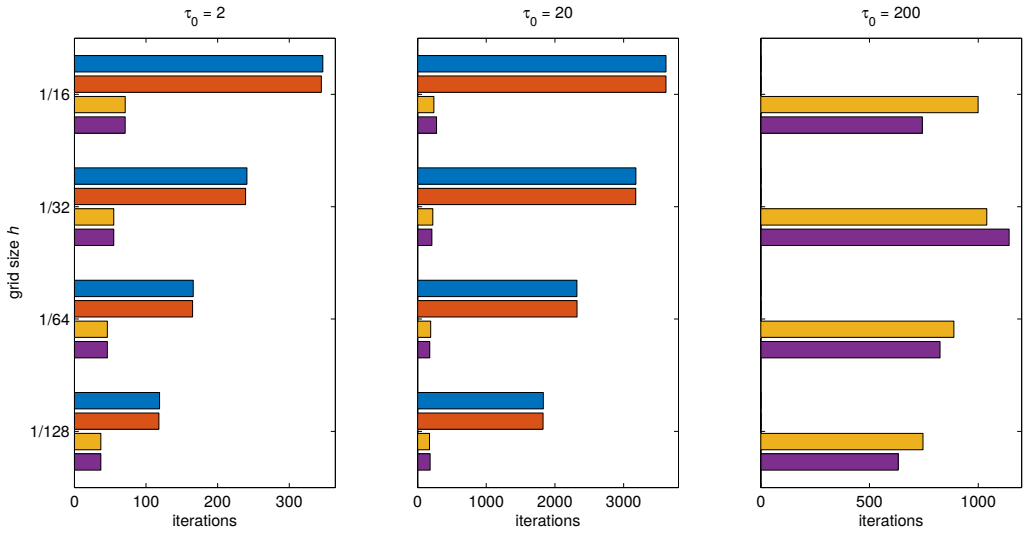

Figure 6.10: Iterations until convergence for different mesh sizes (of the coarse pressure grid) and yield stress parameters. ADMM (blue) and ISTA* (orange) failed to converge within 5,000 iterations for $\tau_0 = 200$, therefore only the results for FISTA* (yellow) and FISTA* with re-starts (purple) are shown here.

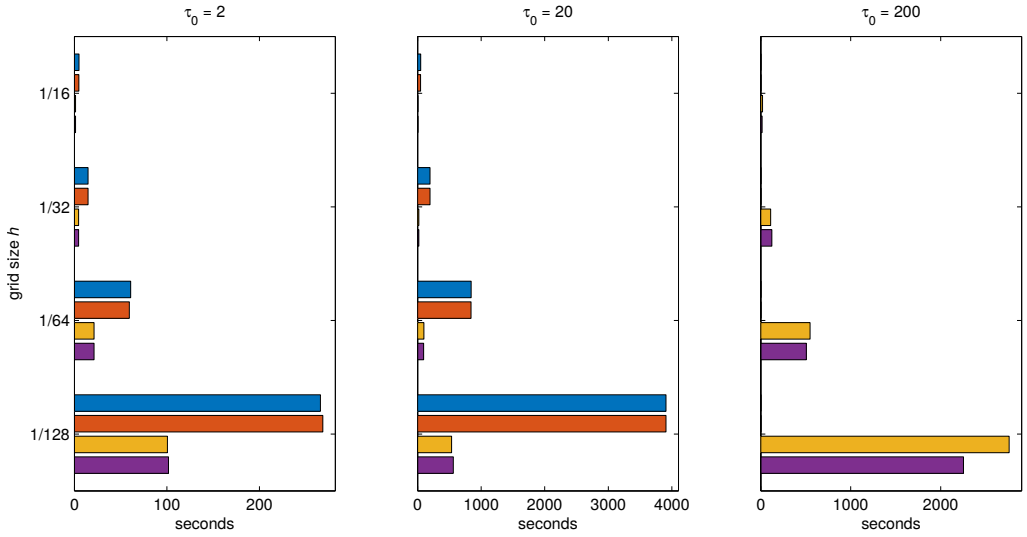

Figure 6.11: Computing times corresponding to the test runs in Figure 6.10.

It turns out again that by incorporating an acceleration scheme, the number of iteration is reduced significantly in every single case. For the largest value of the yield stress considered here, $\tau_0 = 200$, ADMM and ISTA* were still far from an optimal solution even after 5,000 iterations, which we consider as 'failed to converge'.

For the other cases where we have data for all algorithms available, FISTA* requires 83% fewer iterations and 79% less computing time than ADMM. The reduction in iteration numbers and CPU times for the re-starting adaptation are 83% and 78%, respectively. As can be seen from Figures 6.10 and 6.11, re-starting is worthwhile in certain examples, while it is the opposite in others.

6.15 Accurate Identification of Yielded and Unyielded Flow Regions As noted by Yu and Wachs [170], the precise resolution of yielded and unyielded regions becomes particularly challenging in case of larger values of the yield stress.

Solutions for the problem, using different computational techniques and different values of the yield stress, have been published by Begis [213], (see also [77, Ch 6]), Sanchez [214], Mitsoulis and Zisis [215], Yu and Wachs [170], Olshanskii [205], De los Reyes and González Andrade [185], dos Santos et al. [216], Syrakos et al. [217], Aposporidis et al. [177], and, for a non-zero body force term, Zhang [218].

From Figure 6.13 we observe that Algorithm FISTA* identifies the unyielded regions in agreement with the results published in the works cited above. The approximation computed with FISTA* including re-starts is overall similar. Nevertheless, the relatively large areas where the stress is very close to the yield stress make it difficult to detect where the stagnant flow region ends and where shearing begins. Overall, elements where $|\tau_h| \leq \tau_0$ clearly dominate in these areas, which should, indeed, be classified as unyielded.

Despite the identical stopping criterion in all cases, Algorithms ADMM and ISTA* clearly underestimate the regions occupied by unyielded fluid. While the approximation of the stress lies at least reasonably close to the yield stress in the blue areas, these two methods still fail to identify these as solid.

6.16 Model Reduction with Adaptive Finite Elements In past years, solutions on adaptive grids have already been successful at resolving the liquid-solid interface in fine detail, while reducing the substantial computational cost of simulations on uniform grids with the same fine resolution [218]–[221]. Similarly, our objective is to achieve a resolution of $h = 1/128$ in critical areas, while using a much coarser mesh with $h = 1/16$ where the residual is already comparatively small anyways.

For now, let us use the following ad hoc strategy:

- Solve the optimisation problem with one of the four algorithms until convergence.

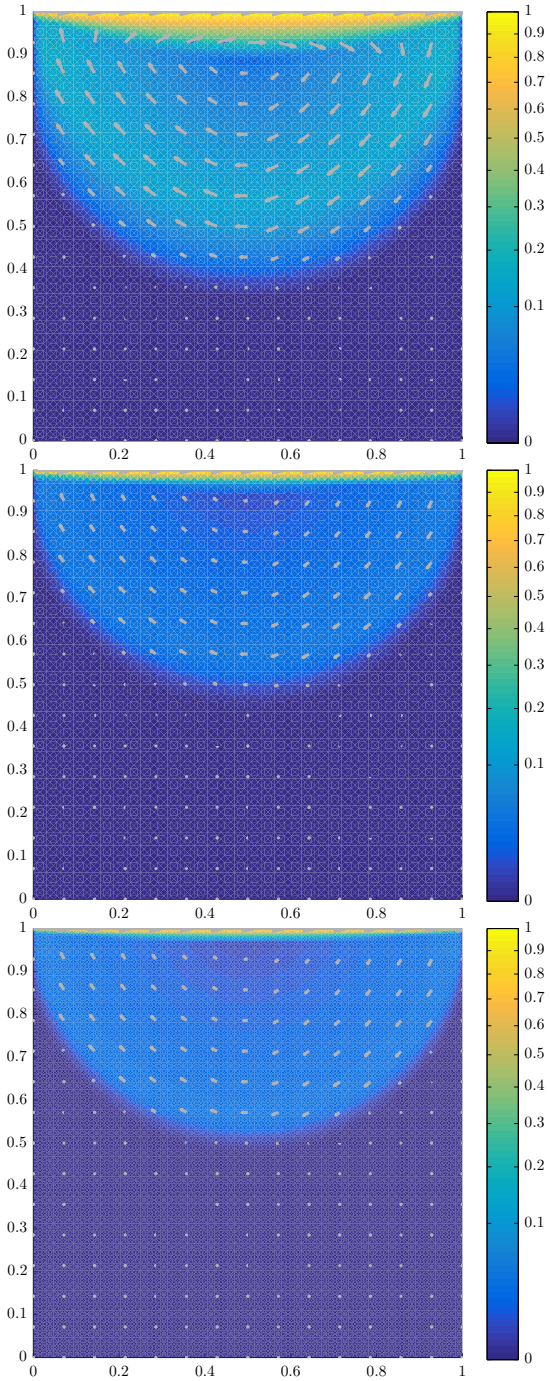

Figure 6.12: Velocity field for BINGHAM flow in the lid-driven cavity. The colourbar and the arrow lengths have been re-scaled by applying the square-root function to the magnitude of the flow field. From top to bottom: $\tau_0 = 20$, $\tau_0 = 200$, $\tau_0 = 500$. In all cases $h = 1/32$.

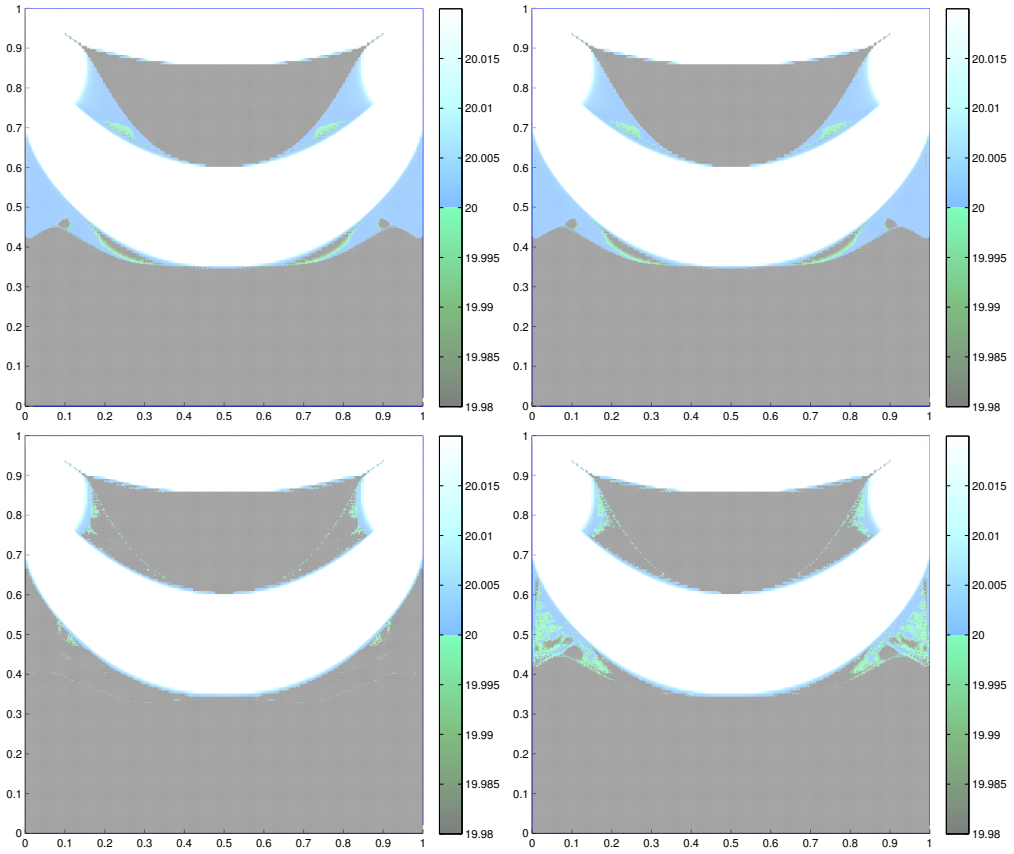

Figure 6.13: FROBENIUS norm of the stress $|\tau_h|$ near the yield stress τ_0. Top left to bottom right: ADMM, ISTA*, FISTA* and FISTA* with re-starts. Values outside the range of the colourbar have been projected onto the upper and lower end points, respectively ($\tau_0 = 20$, $h = 1/128$).

- Determine the 60th percentile of the FROBENIUS norm of the residual $|\mathcal{D}u_h^{(k)} - \dot{\gamma}_h^{(k)}|$ over all triangles and refine those $\sim 40\%$ of all triangles with the largest residual. Further refinements of neighbouring triangles are required to avoid hanging nodes.
- Interpolate the converged solution linearly to the refined grid.

In Figure 6.14, we tackled the problem with $\tau_0 = 20$ with ADMM and FISTA* once again, this time on a grid that was only locally refined. Starting from the uniform mesh with $h = 1/16$, we cycled through the above refinement procedure three times. We conclude that the quality of both results is very much comparable to the one of the corresponding graphs in Figure 6.13. Nevertheless, it took about 65% (ADMM) or 61% (FISTA*) less computing time, respectively, until convergence was achieved. Additionally,

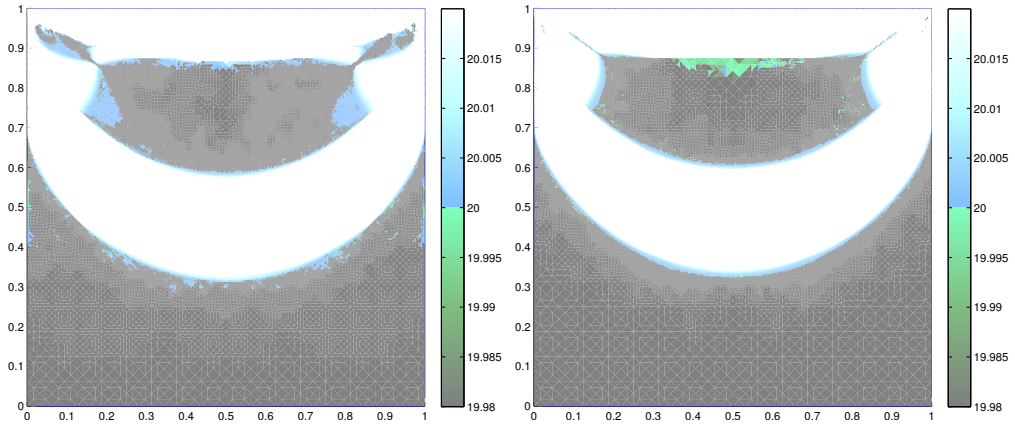

Figure 6.14: Adaptive finite elements for resolving the free boundary between yielded and unyielded regions. Stress magnitude $|\tau_h|$ computed by ADMM (left) and FISTA* (right) for the same problem as in Figure 6.13 ($\tau_0 = 20$).

the identification of the zero-flow region by ADMM has even improved considerably. The upper stagnant zone still exhibits many coarse artefacts, though.

Now that we can assume our methodology to be well validated, we apply it to the traditional challenge of predicting the yield surfaces when the yield stress is very large. We pick the two values $\tau_0 = 200$ and $\tau_0 = 500$ for which results have been published in the literature. We adaptively refine the initial homogeneous mesh with $h = 1/16$ five times. Our results are depicted in Figure 6.15.

Yu and Wachs [170] have used ADMM on a homogeneous grid with $h = 1/256$ to solve these two problems. Their results deviate from ours, those of Mitsoulis and Zisis [215] and Syrakos et al. [217]. Since both of the latter works solve regularised approximations of the Bingham flow problem, fine geometric features like sharp tips that are visible in our results, have already been smoothed out in the problem formulations of these authors.

Although this very basic approach to mesh adaptivity has proven to be effective, we anticipate even further improvements from more sophisticated, goal-oriented adaptive finite element methods like the DWR (dual weighted residual) method. We refer to the book of Suttmeier [222] for more details.

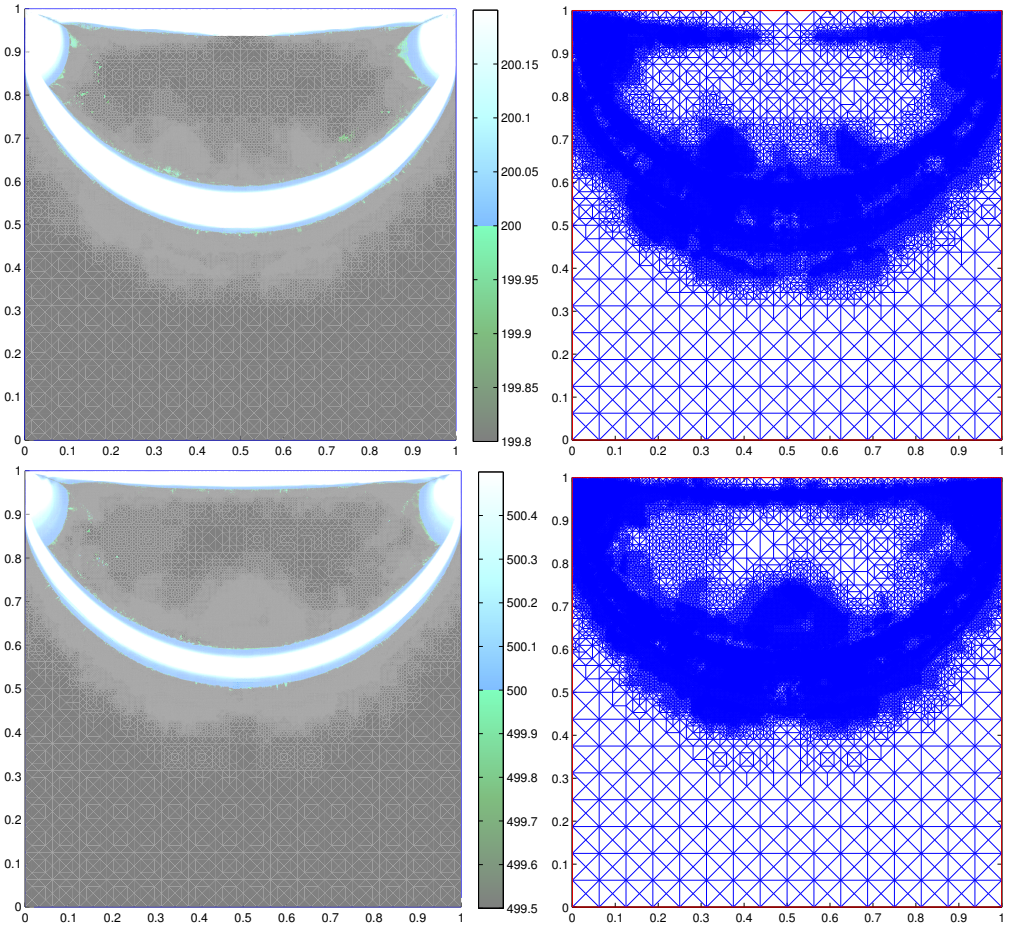

Figure 6.15: Predicting the yield surface for flows at high yield stress values with Algorithm FISTA* and adaptive finite elements. Top: $|\tau_h|$ and the corresponding grid when $\tau_0 = 200$. Bottom: $\tau_0 = 500$.

Chapter 7

Discretisation of Instationary Flow Problems

The numerical solution of a time-dependent viscoplastic flow problem can be decomposed into an iterative solution of modified steady flow problems. In principle, any scheme for integrating ordinary differential equations could equally be applied to semidiscretise the instationary flow problem (4.7) or (4.9) in time.

In practice, however, the large effort that is required for solving a steady viscoplastic problem at every snapshot in time implies that a suitable numerical scheme should be characterised by stability, even if large time steps are chosen.

In the literature on numerical methods in viscoplasticity, we can find several different approaches that may be grouped into two categories: operator splitting methods and multi-step methods, in particular backward differentiation formulas. Operator splitting methods are studied by Dean, Glowinski and co-workers [188], [206], [223], as well as by Sanchez [214]. We consider the second approach instead.

(A) Outline of the Method

7.1 Backward Differentiation Formulas Multi-step methods provide a natural generalisation of Runge-Kutta methods. Backward differentiation formulas are one particular instance of multi-step methods. To discretise the initial value problem

$$\frac{\mathrm{d}x}{\mathrm{d}t} = f(t,x) \qquad x(t_0) = x_0$$

a backward differentiation formula of order n uses not just one, but the last n time steps to compute the next approximate value of x.

The backward differentiation formula of order 2, BDF2, defines a recursion by

$$x_{j+2} - \frac{4}{3}x_{j+1} + \frac{1}{3}x_j = \frac{2}{3}\delta t f_{j+2} \tag{BDF2}$$

for $j \in \mathbb{N}$, $t_j := t_0 + j\delta t$, $f_j := f(t_j, x_j)$, $\delta t > 0$. [224, p 349]

BDF1 is equivalent to the backward Euler scheme:

$$x_{j+1} - x_j = \delta t f_{j+1} \tag{BDF1}$$

It is also used to initialise the point x_1 which is required for the first iteration of BDF2 by solving

$$x_{2/3} = x_0 + \frac{2}{3}\delta t f\left(t_0 + \frac{2}{3}\delta t, x_{2/3}\right)$$
$$x_{4/3} = x_0 + \frac{2}{3}\delta t f\left(t_0 + \frac{4}{3}\delta t, x_{4/3}\right)$$

and then setting $x_1 := (x_{2/3} + x_{4/3})/2$.

7.2 Properties of BDF2 The backward Euler method is well-known for its unconditional stability. It consequently enjoys great popularity in fluid mechanics, where small step sizes are often computationally infeasible.

A drawback consists in its poor convergence rate. The local discretisation error only decreases linearly in δt, i.e.

$$\|x_j - \bar{x}(t_j)\| = O(\delta t).$$

BDF2 unites the advantages of unconditional stability and a higher, quadratic rate of convergence [224]:

$$\|x_j - \bar{x}(t_j)\| = O(\delta t^2).$$

7.3 Semidiscretisation in Time In the context of numerical simulations of Newtonian flow, the backward differentiation formula BDF2 has appeared in [225]. In recent works of De los Reyes and González Andrade [186] and Muravleva [226] it has been applied to problems of Bingham flow. Also the backward Euler scheme has been investigated in viscoplastic applications [77], [172], [188], [227], [228].

Due to the typically large viscosity of viscoplastic fluids, phenomena of convection are minor in nature. It is therefore not normally sensible to apply nonlinear solvers for its resolution. Instead, it can either be neglected altogether, or it is discretised in an explicit fashion from previous time steps. In the interest of modelling physical phenomena with a certain accuracy, we opt for the latter approach.

It is standard to linearly extrapolate from the past two velocity iterates $u_{h,j+1}$ and $u_{h,j}$ in order to approximate the unknown $u_{h,j+2}$ by $2u_{h,j+1} - u_{h,j}$. This way, the convection term $c(2u_{h,j+1} - u_{h,j}, 2u_{h,j+1} - u_{h,j}, \cdot\,)$ can be absorbed in the inhomogeneity f. Only a constant mass matrix is added to the elliptic operator that already arises in the stationary problem.

In conclusion, only a shift in the STOKES operator distinguishes steady viscoplastic flow problems from instationary problems that have been semidiscretised in time in this manner. We refer to [186], [225] for full details and an analytical justification.

(B) Numerical Experiments

As a proof of principle for the efficiency of such a classical time-discretisation scheme coupled with an accelerated optimisation method, we re-visit the problem of force-driven flow in the square cavity.

7.4 Evolution of Yielded and Unyielded Flow Regions Applying the same meshing techniques as for the stationary problem, we consider the problem of instationary BINGHAM flow in $\Omega = \Omega_h =]0,1[^2$ with $h = 1/32$. While we impose a zero trace of the velocity on the boundary for all times $t > 0$, the density f of driving forces is now time-dependent:

$$f(t,x) := \begin{cases} 300\,(x_2 - 0.5, 0.5 - x_1)^\top & \text{if } t < 0.1 \\ 0 & \text{if } t \geq 0.1. \end{cases}$$

The flow starts from the state of rest at time $t = 0$. The yield stress $\tau_0 = 10\sqrt{2}$, as before. We solve the problems at each time step with FISTA* until the FROBENIUS norm of the dual gradient is smaller than gradTol $= 10^{-5}$. The results obtained by DE LOS REYES and GONZÁLEZ ANDRADE in [186] provide a reference solution.

As can be seen from Figure 7.1 on the next page, the rotational motion quickly accelerates over time. The corresponding regions of shear flow and plug flow are all qualitatively similar to one another, but the total area of stagnation decreases over time. This effect naturally agrees with physical expectations.

A comparison with the computational results of DE LOS REYES and GONZÁLEZ ANDRADE [186] admits analogous conclusions to the stationary setting: the predicted flow regions differ largely, while the velocity field appears to be equally well approximated by both methods.

7.5 Cessation of Flow In the outset of this project we have set ourselves the challenge to reproduce three features of viscoplastic fluids in numerical approximations. We have

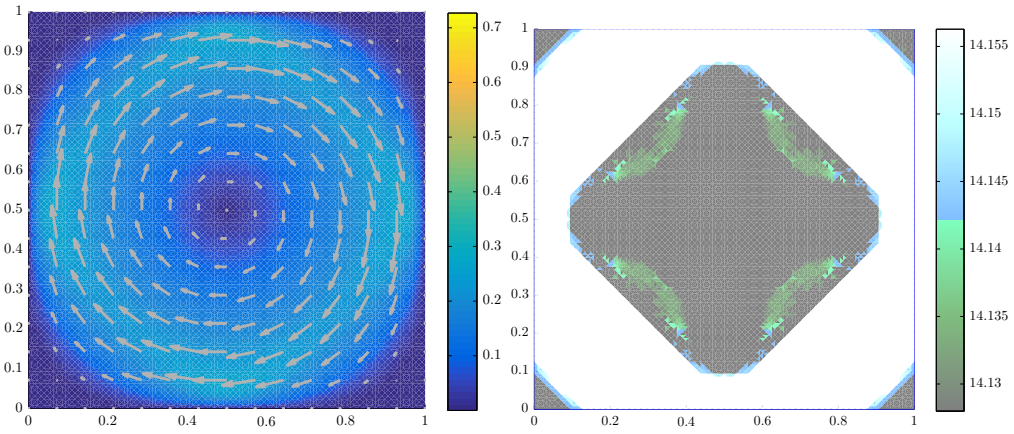

(a): $t = 0.01$.

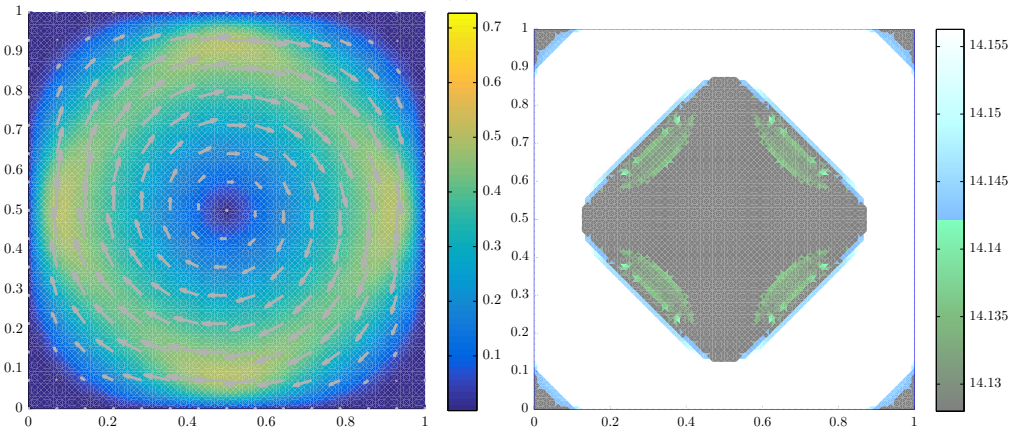

(b): $t = 0.03$.

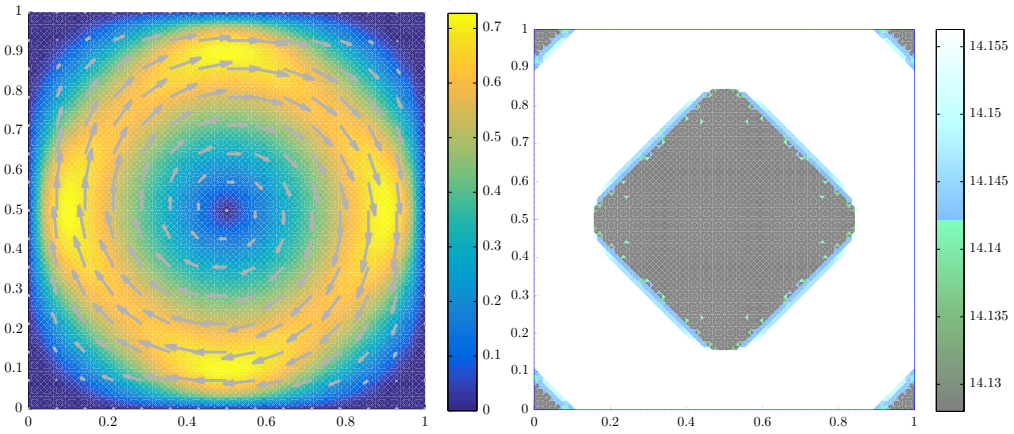

(c): $t = 0.1$.

Figure 7.1: Flow field and stagnant zones for the unsteady BINGHAM flow problem.

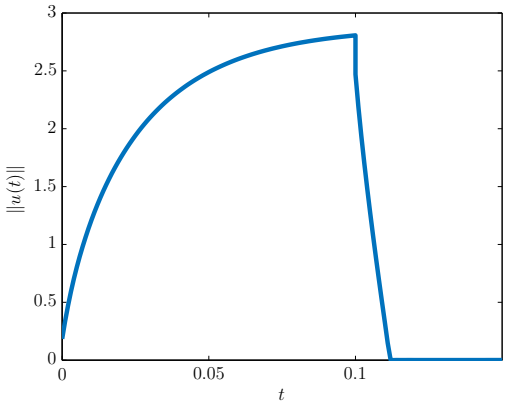

Figure 7.2: Energy norm of the flow velocity. Shortly after the driving forces are switched off at $t = 0.1$, the fluid returns to rest.

yet to confirm the third characteristic property, namely, cessation of flow within finite time if no driving forces remain.

Accordingly, the graph in Figure 7.2 visualises the evolution of the energy norm of the velocity field over the course of time. We conclude that after an initial transient phase, the fluid motion soon tends to become steady.

In the opposite event, however, the fluid returns to a state of rest not only asymptotically: for $t \geq 0.114$, the numerical method predicts a flow rate of exactly zero. Although no numeric value is reported in [186], the corresponding graph in their article shows good agreement with Figure 7.2. In conclusion, we may consider our numerical solutions to fully reflect crucial physical properties of the theoretical model also at the discrete level.

Conclusions and Future Directions

Computational simulations in viscoplasticity heavily rely on convex programming algorithms. The nature of viscoplastic flow problems demands for numerical methods, which are (i) suited for problems of very large scale, which (ii) resolve nonlinearities efficiently and which (iii) exhibit fast convergence.

Classical methods in viscoplasticity, primarily the alternating direction method of multipliers (ADMM), meet the first criterion effortlessly. These methods are, however, adversely affected by

(a) a suboptimal worst-case complexity bound, resulting in unnecessarily slow convergence

(b) nonlinear subproblems in every iteration, if the constitutive model is nonlinear

(c) very few results on preconditioning techniques.

Therefore, one can note a mismatch between the state of the art in viscoplasticity, and the state of the art in convex programming. This can be seen as the primary motivation for this interdisciplinary project.

Main Novelties

New Formulation Formulated in the primal variables, i.e. the flow velocity and strain-rate tensor, viscoplastic flow problems pose great obstacles to a direct numerical solution. Not only is the problem nonsmooth, it is also not amenable to proximal algorithms, as proximal maps are uneasy to evaluate.

The dual formulation proposed in this work effectively addresses both issues at once. Furthermore, the dual multiplier possesses the physical interpretation of a stress, the computation of which is desirable in many typical applications.

Contribution to Convex Programming The dual-based accelerated proximal gradient and NEWTON-type methods appear to be new in this form. By extrapolating from the last two iterates as in the fast iterative shrinkage-thresholding algorithm (FISTA), provably optimal worst-case convergence rates are established. For many problems, preconditioning with curvature information incorporated into a variable metric results in additionally improved convergence properties.

Although the new dual methods FISTA* and VM-FISTA* have been designed with viscoplastic applications in mind, the applicable problem structure is sufficiently general to admit further applications in other fields.

Identification of Sparsity Patterns Numerical viscoplasticity faces one of its greatest challenges on the problem of identifying regions of stagnation and shear flow. State-of-the-art methods that tackle regularised formulations can at best recover perturbed active and inactive sets. For the most relevant problems close to the plastic limit or at high yield stress, classical methods like ADMM have proved unable to converge to sufficiently accurate solutions within a practicable time frame. Therefore, the precise identification of active and inactive sets of the flow domain is generally considered an open problem.

It seems that the proposed accelerated algorithms are the first successful attempt for addressing this issue. Applied to traditional benchmark problems, we obtain computationally less demanding and/or more accurate results than those published in the literature. Previously infeasible simulations become viable by replacing ADMM in viscoplastic flow simulations with FISTA* or VM-FISTA*.

Further Contributions

Choice of Algorithms From the numerical results of this project we can draw several conclusions. First of all, adding inertia to the recursion of optimisation algorithms in viscoplasticity has turned out to yield greatly accelerated convergence with no exception. Moreover, problems of CASSON or HERSCHEL-BULKLEY flow additionally benefit from variable metrics, where diagonal preconditioning appears most advisable. Even for simple duct-flow problems, the full Hessian does not result in faster convergence over time. For higher-dimensional problems, diagonal preconditioners are the only computationally viable option. BINGHAM flow problems, however, are best approached with the basic proximal gradient method FISTA*.

Computational Techniques For dual-based accelerated schemes, three suitable primal sequences are considered. A definition in the sense of least squares allows for the strongest theoretical properties. For the computationally most inexpensive definition, a proof

or disproof of unconditional convergence is missing. In practice, however, no different convergence behaviour is noticeable.

Although adaptive re-starting of inertial algorithms has merit in various applications, no consistent benefits are observed in the context of this work. To the contrary, our simulations even indicate detrimental effects.

Residual-based mesh refinement contributes to achieving a locally high resolution while keeping the computational cost moderate overall. Adaptive finite elements are of particular interest for detecting stagnant zones as well as for problems with singularites, such as flow inside the lid-driven cavity. Furthermore, such strategies are crucial for simulations near the plastic limit, where the effective flow domain reduces to only a thin layer.

Links to Related Methods Detailed reviews of the state of the art in both convex optimisation and viscoplastic fluid mechanics have shed light on tight links to similar methods. Dual proximal NEWTON-type methods admit an interpretation as trust-region method—a concept that the early stages of this project were devoted to. Meanwhile, dual proximal gradient methods are closely related to other primal-dual algorithms, in particular ADMM, a splitting method of TSENG or the primal-dual algorithm of CHAMBOLLE-POCK. Additionally, the modified Hessians studied as preconditioners in this work share certain features with a preconditioned BINGHAM-flow solver of APOSPORIDIS and colleagues.

FISTA* and VM-FISTA* unite many benefits of all of these approaches.

Advantages of the Approach

Standard Subproblems From the viewpoint of convex optimisation, viscoplastic flow problems provide a specific set of applications. From the sole perspective of fluid mechanics, our approach relies on classical methods for the discretisation of each subproblem and their solution.

These are in fact most expedient features of our methodology:

- The convergence and performance of the underlying optimisation algorithms has been proven and meanwhile well understood.
- For implementing our suggested improvements in viscoplastic applications, no novel numerical techniques are required. Instead, we are confronted with classical STOKES-type problems for which most efficient solvers have already been developed for decades.

For numerical practitioners in fluid mechanics, these benefits imply that existing programs are straightforward to adapt, to (most likely) yield an immediate speedup.

Effective Acceleration The theoretical convergence analysis only admits statements on an improved worst-case convergence rate from $O(1/\sqrt{k})$ to $O(1/k)$. Our numerical studies suggest that the convergence rate actually increases beyond this estimate as soon as sparsity features in the solution have been approximated to a certain degree of accuracy.

Due to their slower convergence overall, methods without inertial extrapolation normally require a large number of iterations until this level of accuracy is attained.

In the examples studied here, accelerated methods reach this critical threshold within significantly fewer iterations. Even though we have found that a traditional method may asymptotically achieve convergence of order $O(1/k)$ or more, this regime will be out of reach for many practical applications. Consequently, algorithms that incorporate FISTA-type extrapolation can effectively achieve an acceleration from $O(1/\sqrt{k})$ to $O(1/k^2)$.

Open Problems

Uniformly Convex Problems in Banach Spaces Even though Herschel-Bulkley flow problems are not generally posed in Hilbert spaces, we can apply their advantageous features by considering discretised approximations in $\mathbb{R}^n$.

An analysis in the original function spaces introduces a few complications, as many notions that collapse in the Hilbert space setting have to be distinguished in the more general case. Actual difficulties are of numerical nature: the subproblems of every iteration are no longer of Stokes-type, but the elliptic operator becomes an r-Laplacian instead. It is at least questionable whether possible advantages of the 'first-optimise-then-discretise' approach can outweigh the implications of a significantly increased complexity per iteration.

For Herschel-Bulkley flow problems, it is expedient to replace the assumption of strong convexity with one on uniform convexity with respect to a polynomial Bregman function of the same exponent r. The acceleration of nonlinear proximal gradient algorithms of this kind still appears to be an open problem at this stage.

Inexact Proximal Evaluations One may anticipate that the efficiency of our algorithms offers room for further improvement. When the iterates of the outer optimisation method are still far from a solution, it appears unnecessary to evaluate the proximal map, i.e. the Stokes-type problems, to a very high accuracy. This motivates a more careful investigation of stopping criteria. Ideally, the proximal operators are evaluted sufficiently

accurately for fast convergence of the proximal algorithm, but not overly accurate in order to limit the cost of the initial iterations.

Inexact proximal gradient methods should be most relevant for complex problems of very large scale.

Three-Dimensional Flow Simulations Due to the limitations of existing numerical methods for viscoplastic flows, three-dimensional flow problems have only received very little attention so far. The large-scale nature of such problems implies the crucial role of model reduction by mesh adaptivity and parallelisation.

The CFD (Computational Fluid Dynamics) packages Rheolef [229] by Saramito and co-workers and PeliGRIFF [230], [231] by the group of Wachs implement, among other algorithms, the alternating direction method of multipliers for approximating viscoplastic fluid flows. Mesh adaptivity is a core feature of Rheolef. PeliGRIFF offers support for parallelisation with MPI and is specifically targeted towards particulate flows.

Combined with such sophisticated tools for discretisation and computing efficiency, accelerated convergence of the optimisation routine appears like a very promising attempt for tackling more general viscoplastic flow problems. Being able to simulate viscoplastic flows in three spatial dimensions will clearly set a milestone in the viscoplastic community. We can anticipate that the availability of previously infeasible simulations will not only facilitate optimised industrial processes, but also deepen our fluid mechanical understanding of viscoplastic phenomena.

Bibliography

[1] Clay Mathematics Institute. Millienium problems: Navier-Stokes equation. Retrieved on 13 November 2015., [Online]. Available: `http://www.claymath.org/millennium-problems/navier%E2%80%93stokes-equation`.

[2] H. A. Barnes, J. F. Hutton, and K. Walters, *An introduction to rheology*. Elsevier, 1989, vol. 3.

[3] R. S. Lakes, *Viscoelastic solids*. CRC press, 1998, vol. 9.

[4] H. Barnes and K. Walters, 'The yield stress myth?', *Rheologica acta*, vol. 24, no. 4, pp. 323–326, 1985.

[5] H. A. Barnes, 'The yield stress–a review or $\pi\alpha\nu\tau\alpha$ $\rho\varepsilon\iota$–everything flows?', *Journal of Non-Newtonian Fluid Mechanics*, vol. 81, no. 1, pp. 133–178, 1999.

[6] ——, 'The 'yield stress myth?' paper – 21 years on', *Applied Rheology*, vol. 17, no. 4, pp. 43 110–44 250, 2007.

[7] G. Astarita, 'Letter to the editor: the engineering reality of the yield stress', *Journal of Rheology*, vol. 34, no. 2, pp. 275–277, 1990.

[8] J. Schurz, 'The yield stress—an empirical reality', *Rheologica Acta*, vol. 29, no. 2, pp. 170–171, 1990.

[9] J. P. Hartnett and R. Y. Hu, 'Technical note: the yield stress—an engineering reality', *Journal of Rheology*, vol. 33, no. 4, pp. 671–679, 1989.

[10] R. Temam, *Navier-Stokes equations: theory and numerical analysis*. American Mathematical Society, 2001, vol. 343.

[11] E. C. Bingham, 'An investigation of the laws of plastic flow', *Bulletin of the Bureau of Standards*, vol. 13, no. 2, pp. 309–352, 1917.

[12] ——, *Fluidity and plasticity*. McGraw-Hill New York, 1922, vol. 1.

[13] R. B. Bird, G. Dai, and B. J. Yarusso, 'The rheology and flow of viscoplastic materials', *Rev. Chem. Eng*, vol. 1, no. 1, pp. 1–70, 1983.

[14] W. H. Herschel and R. Bulkley, 'Konsistenzmessungen von Gummi-Benzollösungen', *Kolloid-Zeitschrift*, vol. 39, no. 4, pp. 291–300, 1926.

[15] J. Málek, M. Růžička, and V. Shelukhin, 'Herschel–Bulkley fluids: existence and regularity of steady flows', *Mathematical Models and Methods in Applied Sciences*, vol. 15, no. 12, pp. 1845–1861, 2005.

[16] S. Basu and U. Shivhare, 'Rheological, textural, micro-structural and sensory properties of mango jam', *Journal of Food Engineering*, vol. 100, no. 2, pp. 357–365, 2010.

[17] F. De Larrard, C. Ferraris, and T. Sedran, 'Fresh concrete: a Herschel-Bulkley material', *Materials and Structures*, vol. 31, no. 7, pp. 494–498, 1998.

[18] V. Kelessidis, R. Maglione, C. Tsamantaki, and Y. Aspirtakis, 'Optimal determination of rheological parameters for Herschel-Bulkley drilling fluids and impact on pressure drop, velocity profiles and penetration rates during drilling', *Journal of Petroleum Science and Engineering*, vol. 53, no. 3, pp. 203–224, 2006.

[19] G. Vinay, A. Wachs, and J.-F. Agassant, 'Numerical simulation of weakly compressible Bingham flows: the restart of pipeline flows of waxy crude oils', *Journal of non-newtonian fluid mechanics*, vol. 136, no. 2, pp. 93–105, 2006.

[20] N. J. Balmforth, A. Burbidge, R. Craster, J. Salzig, and A. Shen, 'Visco-plastic models of isothermal lava domes', *Journal of Fluid Mechanics*, vol. 403, pp. 37–65, 2000.

[21] V. Manville, K. Hodgson, and J. White, 'Rheological properties of a remobilised-tephra lahar associated with the 1995 eruptions of Ruapehu volcano, New Zealand', *New Zealand Journal of Geology and Geophysics*, vol. 41, no. 2, pp. 157–164, 1998.

[22] R. Uzuoka, A. Yashima, T. Kawakami, and J.-M. Konrad, 'Fluid dynamics based prediction of liquefaction induced lateral spreading', *Computers and Geotechnics*, vol. 22, no. 3–4, pp. 243–282, 1998. DOI: http://dx.doi.org/10.1016/S0266-352X(98)00006-8.

[23] A. Kobayashi, I. Yamamoto, and T. Aoyama, 'Tribology of a snail (terrestrial gastropod)', *Tribology Series*, vol. 41, pp. 429–436, 2003.

[24] A. J. Apostolidis and A. N. Beris, 'Modeling of the blood rheology in steady-state shear flows', *Journal of Rheology*, vol. 58, no. 3, pp. 607–633, 2014.

[25] C. S. Lingle, T. J. Hughes, and R. C. Kollmeyer, 'Tidal flexure of Jakobshavns Glacier, West Greenland', *Journal of Geophysical Research: Solid Earth*, vol. 86, no. B5, pp. 3960–3968, 1981.

[26] N. Dubash and I. Frigaard, 'Conditions for static bubbles in viscoplastic fluids', *Physics of Fluids*, vol. 16, no. 12, pp. 4319–4330, 2004.

[27] S. Echendu, F. Belblidia, H. Tamaddon-Jahromi, and M. Webster, 'Modelling with viscous and viscoplastic materials under combining and separating flow configurations', *Mechanics of Time-Dependent Materials*, vol. 15, no. 4, pp. 407–428, 2011.

[28] N. Casson, 'A flow equation for pigment-oil suspensions of the printing ink type', *Rheology of disperse systems*, vol. 84, 1959.

[29] S. Charm and G. Kurland, 'Viscometry of human blood for shear rates of $0 - 100,000$ sec^{-1}', *Nature*, 1965.

[30] M. A. Rao, *Rheology of fluid and semisolid foods: principles and applications*. Springer Science & Business Media, 2010.

[31] W. Heinz, 'The Casson flow equation: its validity for suspension of paints', *Materialpruefung*, vol. 1, pp. 311–316, 1959.

[32] F. Mohos, *Confectionery and chocolate engineering: principles and applications*. John Wiley & Sons, 2010.

[33] S. Mizrahi and R. Firstenberg, 'Effect of orange juice composition on flow behaviour of six-fold concentrate', *Journal of Texture Studies*, vol. 6, no. 4, pp. 523–532, 1975.

[34] E.-K. Park and K.-W. Song, 'Rheological evaluation of petroleum jelly as a base material in ointment and cream formulations: steady shear flow behavior', *Archives of Pharmacal Research*, vol. 33, no. 1, pp. 141–150, 2010.

[35] L. Figura and A. A. Teixeira, *Food physics: physical properties-measurement and applications*. Springer Science & Business Media, 2007.

[36] K. A. Athanasiou and R. M. Natoli, *Introduction to continuum biomechanics*. Morgan & Claypool Publishers, 2008.

[37] E. Reher, D. Haroske, and K. Kohler, 'Flows of non-Newtonian liquids', *Chemische Technik*, vol. 21, no. 3, p. 137, 1969.

[38] R. Ofoli, R. Morgan, and J. Steffe, 'A generalized rheological model for inelastic fluid foods', *Journal of Texture Studies*, vol. 18, no. 3, pp. 213–230, 1987.

[39] A. N. Tikhonov and V. I. Arsenin, *Solutions of ill-posed problems*. Vh Winston, 1977.

[40] M. A. Treiber, *Optimization for Computer Vision: An Introduction to Core Concepts and Methods*, ser. Advances in Computer Vision and Pattern Recognition. Springer Science & Business Media, 2013.

[41] I. Daubechies, M. Defrise, and C. De Mol, 'An iterative thresholding algorithm for linear inverse problems with a sparsity constraint', *Communications on pure and applied mathematics*, vol. 57, no. 11, pp. 1413–1457, 2004.

[42] A. Beck and M. Teboulle, 'A fast iterative shrinkage-thresholding algorithm with application to wavelet-based image deblurring', in *IEEE International Conference on Acoustics, Speech and Signal Processing*, IEEE, 2009, pp. 693–696.

[43] L. I. Rudin, S. Osher, and E. Fatemi, 'Nonlinear total variation based noise removal algorithms', *Physica D: Nonlinear Phenomena*, vol. 60, no. 1, pp. 259–268, 1992.

[44] D. P. Bertsekas, 'Nonlinear programming', 1999.

[45] D. Gabay and B. Mercier, 'A dual algorithm for the solution of nonlinear variational problems via finite element approximation', *Computers & Mathematics with Applications*, vol. 2, no. 1, pp. 17–40, 1976. DOI: `http://dx.doi.org/10.1016/0898-1221(76)90003-1`.

[46] G. Ngwa, I. A. Frigaard, and O. Scherzer, 'On effective stopping time selection for visco-plastic nonlinear BV diffusion filters used in image denoising', *SIAM Journal on Applied Mathematics*, vol. 63, no. 6, pp. 1911–1934, 2003.

[47] I. Frigaard and O. Scherzer, 'Herschel-Bulkley diffusion filtering: non-Newtonian fluid mechanics in image processing', *ZAMM-Journal of Applied Mathematics and Mechanics/Zeitschrift fuer Angewandte Mathematik und Mechanik*, vol. 86, no. 6, pp. 474–494, 2006.

[48] A. Beck and M. Teboulle, 'A fast iterative shrinkage-thresholding algorithm for linear inverse problems', *SIAM Journal on Imaging Sciences*, vol. 2, no. 1, pp. 183–202, 2009.

[49] A. Chambolle and T. Pock, 'A first-order primal-dual algorithm for convex problems with applications to imaging', *Journal of Mathematical Imaging and Vision*, vol. 40, no. 1, pp. 120–145, 2011.

[50] Y. Kanno, *Nonsmooth mechanics and convex optimization*. CRC Press, 2011.

[51] D. P. Palomar and Y. C. Eldar, *Convex optimization in signal processing and communications*. Cambridge University Press, 2010.

[52] L. A. Vese and C. Le Guyader, *Variational methods in image processing*. CRC Press, 2015.

[53] L. C. G. Rogers and D. Talay, *Numerical methods in finance*. Cambridge University Press, 1997, vol. 13.

[54] P. Bühlmann and S. Van De Geer, *Statistics for high-dimensional data: methods, theory and applications*. Springer Science & Business Media, 2011.

[55] S. Sra, S. Nowozin, and S. J. Wright, *Optimization for machine learning*. The MIT Press, 2012.

[56] H. H. Bauschke and P. L. Combettes, *Convex analysis and monotone operator theory in Hilbert spaces*. Springer Science & Business Media, 2011.

[57] R. T. Rockafellar, *Convex analysis*. Princeton University Press, 1997.

[58] B. P. Rynne and M. A. Youngson, *Linear functional analysis*. Springer Science & Business Media, 2013.

[59] X. Chen, Z. Nashed, and L. Qi, 'Smoothing methods and semismooth methods for nondifferentiable operator equations', *SIAM Journal on Numerical Analysis*, vol. 38, no. 4, pp. 1200–1216, 2000.

[60] A. Dhara and J. Dutta, *Optimality conditions in convex optimization: a finite-dimensional view*. CRC Press, 2011.

[61] M. Hintermüller, K. Ito, and K. Kunisch, 'The primal-dual active set strategy as a semismooth Newton method', *SIAM J. Optim.*, vol. 13, no. 3, pp. 865–888, 2002.

[62] I. Ekeland and R. Témam, *Convex Analysis and Variational Problems*. Society for Industrial and Applied Mathematics, 1999. DOI: 10.1137/1.9781611971088.

[63] T. Schuster, B. Kaltenbacher, B. Hofmann, and K. S. Kazimierski, *Regularization methods in Banach spaces*. Walter de Gruyter, 2012, vol. 10.

[64] R. E. Megginson, *An introduction to Banach space theory*. Springer Science & Business Media, 2012, vol. 183.

[65] P. Kosmol and D. Müller-Wichards, *Optimization in function spaces: with stability considerations in Orlicz spaces*. Walter de Gruyter, 2011, vol. 13.

[66] R. Ioan-Bot, *Conjugate duality in convex optimization*. Springer Science & Business Media, 2009, vol. 637.

[67] J.-F. Bonnans, J. C. Gilbert, C. Lemaréchal, and C. A. Sagastizábal, *Numerical optimization: theoretical and practical aspects*. Springer, 2006.

[68] J. F. Bonnans, J. C. Gilbert, C. Lemaréchal, and C. A. Sagastizábal, 'A family of variable metric proximal methods', *Mathematical Programming*, vol. 68, no. 1-3, pp. 15–47, 1995.

[69] N. Karmitsa and M. M. Mäkelä, 'Limited memory bundle method for large bound constrained nonsmooth optimization: convergence analysis', *Optimization Methods & Software*, vol. 25, no. 6, pp. 895–916, 2010.

[70] J. V. Burke, A. S. Lewis, and M. L. Overton, 'A robust gradient sampling algorithm for nonsmooth, nonconvex optimization', *SIAM Journal on Optimization*, vol. 15, no. 3, pp. 751–779, 2005.

[71] K. C. Kiwiel, 'Methods of descent for nondifferentiable optimization', 1985.

[72] ——, 'Convergence of the gradient sampling algorithm for nonsmooth nonconvex optimization', *SIAM Journal on Optimization*, vol. 18, no. 2, pp. 379–388, 2007.

[73] N. Z. Shor, *Minimization methods for non-differentiable functions*. Springer Science & Business Media, 2012, vol. 3.

[74] A. S. Lewis and M. L. Overton, 'Nonsmooth optimization via quasi-Newton methods', *Mathematical Programming*, vol. 141, no. 1-2, pp. 135–163, 2013.

[75] H. Uzawa, 'Iterative methods for concave programming', *Studies in linear and nonlinear programming*, vol. 6, 1958.

[76] M. Fortin and R. Glowinski, *Augmented Lagrangian methods: applications to the numerical solution of boundary-value problems*. North-Holland, 1983.

[77] R. Glowinski and P. Le Tallec, *Augmented Lagrangian and operator-splitting methods in nonlinear mechanics*. SIAM, 1989, vol. 9.

[78] R. Glowinski and A. Marrocco, 'Sur l'approximation, par éléments finis d'ordre un, et la résolution, par pénalisation-dualité, d'une classe de problèmes de Dirichlet non linéaires', *Rev. Fran. d'Aut. Inf. Rech. Oper. Ana. Numer.*, vol. 9, no. 2, pp. 41–76, 1975.

[79] J. Douglas and H. H. Rachford, 'On the numerical solution of heat conduction problems in two and three space variables', *Transactions of the American mathematical Society*, vol. 82, no. 2, pp. 421–439, 1956.

[80] R. Glowinski, 'On alternating direction methods of multipliers: a historical perspective', in *Modeling, Simulation and Optimization for Science and Technology*, Springer, 2014, pp. 59–82.

[81] E. Esser, X. Zhang, and T. F. Chan, 'A general framework for a class of first order primal-dual algorithms for convex optimization in imaging science', *SIAM Journal on Imaging Sciences*, vol. 3, no. 4, pp. 1015–1046, 2010.

[82] X. Zhang, M. Burger, and S. Osher, 'A unified primal-dual algorithm framework based on Bregman iteration', *Journal of Scientific Computing*, vol. 46, no. 1, pp. 20–46, 2011.

[83] K.-J. Arrow, L. Hurwicz, and H. Uzawa, *Studies in linear and non-linear programming*, H.-B. Chenery, S.-M. Johnson, S. Karlin, and T. Marschak, Eds., ser. Stanford Mathematical Studies in the Social Sciences. Stanford University Press, 1958, vol. 2.

[84] M. Zhu and T. Chan, 'An efficient primal-dual hybrid gradient algorithm for total variation image restoration', *UCLA CAM Report*, pp. 08–34, 2008.

[85] T. Hohage and C. Homann, 'A generalization of the Chambolle-Pock algorithm to Banach spaces with applications to inverse problems', *arXiv preprint*, 2014. [Online]. Available: `http://arXiv.org/pdf/1412.0126`.

[86] A. Chambolle and T. Pock, 'On the ergodic convergence rates of a first-order primal-dual algorithm.', *preprint*, 2014.

[87] D. W. Peaceman and H. H. Rachford Jr, 'The numerical solution of parabolic and elliptic differential equations', *Journal of the Society for industrial and Applied Mathematics*, vol. 3, no. 1, pp. 28–41, 1955.

[88] M. Burger, A. Sawatzky, and G. Steidl, 'First order algorithms in variational image processing', *arXiv preprint*, 2014. [Online]. Available: `http://arxiv.org/pdf/1412.4237`.

[89] T. Goldstein, B. O'Donoghue, S. Setzer, and R. Baraniuk, 'Fast alternating direction optimization methods', *SIAM Journal on Imaging Sciences*, vol. 7, no. 3, pp. 1588–1623, 2014.

[90] S. Osher, M. Burger, D. Goldfarb, J. Xu, and W. Yin, 'An iterative regularization method for total variation-based image restoration', *Multiscale Modeling & Simulation*, vol. 4, no. 2, pp. 460–489, 2005.

[91] J.-J. Moreau, 'Proximité et dualité dans un espace hilbertien', *Bulletin de la Societe mathematique de France*, vol. 93, pp. 273–299, 1965.

[92] B. Martinet, 'Brève communication. régularisation d'inéquations variationnelles par approximations successives', *Rev. Fran. d'Aut. Inf. Rech. Oper. S. Rouge*, vol. 4, no. 3, pp. 154–158, 1970.

[93] R. T. Rockafellar, 'Monotone operators and the proximal point algorithm', *SIAM journal on control and optimization*, vol. 14, no. 5, pp. 877–898, 1976.

[94] Z. Opial, 'Weak convergence of the sequence of successive approximations for nonexpansive mappings', *Bulletin of the American Mathematical Society*, vol. 73, no. 4, pp. 591–597, 1967.

[95] D. Butnariu and A. N. Iusem, 'On a proximal point method for convex optimization in Banach spaces', *Numerical Functional Analysis and Optimization*, vol. 18, no. 7-8, pp. 723–744, 1997.

[96] R. S. Burachik and S. Scheimberg, 'A proximal point method for the variational inequality problem in banach spaces', *SIAM Journal on Control and Optimization*, vol. 39, no. 5, pp. 1633–1649, 2000.

[97] P. L. Combettes and J.-C. Pesquet, 'Proximal splitting methods in signal processing', in *Fixed-point algorithms for inverse problems in science and engineering*, Springer, 2011, pp. 185–212.

[98] D. P. Bertsekas, 'Incremental proximal methods for large scale convex optimization', *Mathematical programming*, vol. 129, no. 2, pp. 163–195, 2011.

[99] J. Peypouquet, *Convex optimization in normed spaces: theory, methods and examples*. Springer, 2015.

[100] J. M. Bioucas-Dias and M. A. Figueiredo, 'A new TwIST: two-step iterative shrinkage/thresholding algorithms for image restoration', *Image Processing, IEEE Transactions on*, vol. 16, no. 12, pp. 2992–3004, 2007.

[101] G. B. Passty, 'Ergodic convergence to a zero of the sum of monotone operators in Hilbert space', *Journal of Mathematical Analysis and Applications*, vol. 72, no. 2, pp. 383–390, 1979.

[102] P.-L. Lions and B. Mercier, 'Splitting algorithms for the sum of two nonlinear operators', *SIAM Journal on Numerical Analysis*, vol. 16, no. 6, pp. 964–979, 1979.

[103] P. Tseng, 'Applications of a splitting algorithm to decomposition in convex programming and variational inequalities', *SIAM Journal on Control and Optimization*, vol. 29, no. 1, pp. 119–138, 1991.

[104] P. Tseng and S. Yun, 'A coordinate gradient descent method for nonsmooth separable minimization', *Mathematical Programming*, vol. 117, no. 1-2, pp. 387–423, 2009.

[105] M. Schmidt, D. Kim, and S. Sra, 'Projected Newton-type methods in machine learning', in, S. Sra, S. Novozin, and S. J. Wright, Eds., ser. Optimization for Machine Learning. MIT Press, 2011.

[106] J. D. Lee, Y. Sun, and M. A. Saunders, 'Proximal Newton-type methods for minimizing composite functions', *SIAM Journal on Optimization*, vol. 24, no. 3, pp. 1420–1443, 2014.

[107] M. Fukushima and H. Mine, 'A generalized proximal point algorithm for certain non-convex minimization problems', *International Journal of Systems Science*, vol. 12, no. 8, pp. 989–1000, 1981.

[108] M. W. Schmidt, E. Berg, M. P. Friedlander, and K. P. Murphy, 'Optimizing costly functions with simple constraints: a limited-memory projected quasi-Newton algorithm', in *International Conference on Artificial Intelligence and Statistics*, 2009.

[109] M. Schmidt, 'Graphical model structure learning with $l1$-regularization', PhD thesis, University of British Columbia, Vancouver, 2010.

[110] S. Becker and J. Fadili, 'A quasi-newton proximal splitting method', in *Advances in Neural Information Processing Systems*, 2012, pp. 2618–2626.

[111] J. Burke and M. Qian, 'A variable metric proximal point algorithm for monotone operators', *SIAM Journal on Control and Optimization*, vol. 37, no. 2, pp. 353–375, 1999.

[112] P. L. Combettes and B. C. Vu, 'Variable metric forward–backward splitting with applications to monotone inclusions in duality', *Optimization*, vol. 63, no. 9, pp. 1289–1318, 2014.

[113] P. L. Combettes and B. C. Vu, 'Variable metric quasi-Fejér monotonicity', *Nonlinear Analysis: Theory, Methods & Applications*, vol. 78, pp. 17–31, 2013.

[114] S. Bonettini, F. Porta, and V. Ruggiero, 'A variable metric forward–backward method with extrapolation', *arXiv preprint*, 2015. [Online]. Available: `http://arXiv.org/pdf/1506.02900`.

[115] Y. Nesterov, *Introductory lectures on convex optimization: A basic course*. Springer Science & Business Media, 2013, vol. 87.

[116] A.-S. Nemirovsky, D.-B. Yudin, and E.-R. Dawson, *Problem complexity and method efficiency in optimization*, ser. Wiley-Interscience Series in Discrete Mathematics. John Wiley & Sons, Inc., Panstwowe Wydawnictwo Naukowe (PWN), 1982.

[117] Y. Nesterov, 'A method of solving a convex programming problem with convergence rate $O(1/k^2)$', in *Soviet Mathematics Doklady*, vol. 27, 1983, pp. 372–376.

[118] ——, 'Gradient methods for minimizing composite objective function', CORE and INMA, Université catholique de Louvain, Belgium, Tech. Rep., Sep. 2007. [Online]. Available: `http://www.ecore.be/DPs/dp_1191313936.pdf`.

[119] O. Güler, 'New proximal point algorithms for convex minimization', *SIAM Journal on Optimization*, vol. 2, no. 4, pp. 649–664, 1992.

[120] B. O'Donoghue and E. Candes, 'Adaptive restart for accelerated gradient schemes', *Foundations of Computational Mathematics*, pp. 1–18, 2013.

[121] A. Beck and M. Teboulle, 'Fast gradient-based algorithms for constrained total variation image denoising and deblurring problems', *Image Processing, IEEE Transactions on*, vol. 18, no. 11, pp. 2419–2434, 2009.

[122] A. Chambolle and C. Dossal, 'On the convergence of the iterates of the "fast iterative shrinkage/thresholding algorithm"', *Journal of Optimization Theory and Applications*, vol. 166, no. 3, pp. 968–982, 2015.

[123] D. Goldfarb, S. Ma, and K. Scheinberg, 'Fast alternating linearization methods for minimizing the sum of two convex functions', *Mathematical Programming*, vol. 141, no. 1-2, pp. 349–382, 2013.

[124] B. He and X. Yuan, 'On non-ergodic convergence rate of Douglas–Rachford alternating direction method of multipliers', *Numerische Mathematik*, pp. 1–11, 2012.

[125] ——, 'On the $O(1/n)$ convergence rate of the Douglas-Rachford alternating direction method', *SIAM Journal on Numerical Analysis*, vol. 50, no. 2, pp. 700–709, 2012.

[126] W. Deng and W. Yin, 'On the global and linear convergence of the generalized alternating direction method of multipliers', DTIC Document, Tech. Rep., 2012. [Online]. Available: `http://www.dtic.mil/cgi-bin/GetTRDoc?AD=ADA567407`.

[127] M. Hong and Z.-Q. Luo, 'On the linear convergence of the alternating direction method of multipliers', *arXiv preprint*, 2012. [Online]. Available: `http://arxiv.org/pdf/1208.3922`.

[128] D. Davis and W. Yin, 'Faster convergence rates of relaxed Peaceman-Rachford and ADMM under regularity assumptions', *arXiv preprint*, 2014. [Online]. Available: `http://arxiv.org/pdf/1407.5210`.

[129] D. Davis, 'Convergence rate analysis of the forward-Douglas-Rachford splitting scheme', *SIAM Journal on Optimization*, vol. 25, no. 3, pp. 1760–1786, 2015.

[130] ——, 'Convergence rate analysis of primal-dual splitting schemes', *SIAM Journal on Optimization*, vol. 25, no. 3, pp. 1912–1943, 2015.

[131] T. Pock and A. Chambolle, 'Diagonal preconditioning for first order primal-dual algorithms in convex optimization', in *IEEE International Conference on Computer Vision (ICCV) 2011*, IEEE, 2011, pp. 1762–1769.

[132] J. Nocedal and S. Wright, *Numerical Optimization*. New York: Springer, 2006.

[133] K. Ito and K. Kunisch, *Lagrange Multiplier Approach to Variational Problems and Applications*. Philadelphia: SIAM, 2008.

[134] R. Byrd, 'Robust trust region methods for constrained optimization', in *Third SIAM Conference on Optimization, Houston, Texas*, 1987.

[135] M. Lalee, J. Nocedal, and T. Plantenga, 'On the implementation of an algorithm for large-scale equality constrained optimization', *SIAM Journal on Optimization*, vol. 8, no. 3, pp. 682–706, 1998.

[136] Y. A. Abramovich and C. D. Aliprantis, *An invitation to operator theory*, 50. American Mathematical Soc., 2002.

[137] A. Beck and M. Teboulle, 'A fast dual proximal gradient algorithm for convex minimization and applications', *Operations Research Letters*, vol. 42, no. 1, pp. 1–6, 2014.

[138] D. Gabay, 'Augmented Lagrangian methods: applications to the numerical solution of boundary-value problems', in. Amsterdam: North-Holland, 1983, ch. IX: applications of the method of multipliers to variational inequalities, pp. 299–331.

[139] G. Bachmann and L. Narici, *Functional analysis*. Dover Publications, 2000.

[140] R. A. Adams and J. J. Fournier, *Sobolev spaces*. Academic press, 2003, vol. 140.

[141] M. Dobrowolski, *Angewandte Funktionalanalysis: Funktionalanalysis, Sobolev-Räume und elliptische Differentialgleichungen*. Springer-Verlag, 2010.

[142] H. Sohr, *The Navier-Stokes equations: An elementary functional analytic approach*. Springer Science & Business Media, 2001.

[143] J. Necas, *Direct methods in the theory of elliptic equations*. Springer Science & Business Media, 2011.

[144] F. Demengel, G. Demengel, and R. Erné, *Functional spaces for the theory of elliptic partial differential equations*. Springer, 2012.

[145] G. Duvaut and J. L. Lions, *Les inéquations en mécanique et en physique*. Dunod Paris, 1972, vol. 18.

[146] ——, *Inequalities in mechanics and physics*, ser. Grundlehren der mathematischen Wissenschaften. Berlin, Heidelberg, New York: Springer-Verlag, 1976.

[147] I. Basov and V. Shelukhin, 'Generalized solutions to the equations of compressible Bingham flows', *ZAMM – Journal of Applied Mathematics and Mechanics*, vol. 79, no. 3, pp. 185–192, 1999.

[148] V. Shelukhin, 'Bingham viscoplastic as a limit of non-Newtonian fluids', *Journal of Mathematical Fluid Mechanics*, vol. 4, no. 2, pp. 109–127, 2002.

[149] H. Eberlein and M. Růžička, 'Existence of weak solutions for unsteady motions of Herschel–Bulkley fluids', *Journal of Mathematical Fluid Mechanics*, vol. 14, no. 3, pp. 485–500, 2012.

[150] W. Layton, *Introduction to the numerical analysis of incompressible viscous flows*. SIAM, 2008, vol. 6.

[151] V. Girault and P.-A. Raviart, *Finite element methods for Navier-Stokes equations: theory and algorithms*. Springer Science & Business Media, 2012, vol. 5.

[152] R. Glowinski, J.-L. Lions, and R. Tremolières, *Numerical analysis of variational inequalities*, J.-L. Lions, G. Papanicolaou, and R. T. Rockafellar, Eds. Amsterdam, New York, Oxford: North-Holland, 1981.

[153] R. Huilgol and Z. You, 'Application of the augmented Lagrangian method to steady pipe flows of Bingham, Casson and Herschel-Bulkley fluids', *J. Non-Newtonian Fluid Mech.*, vol. 128, no. 2–3, pp. 126–143, 2005.

[154] R. Dautray and J. L. Lions, *Evolution Problems I*, ser. Mathematical Analysis and Numerical Methods for Science and Technology. Springer-Verlag, 1992.

[155] M. Köhne, *L_p-theory for Incompressible Newtonian Flows: Energy Preserving Boundary Conditions, Weakly Singular Domains*. Springer Science & Business Media, 2012.

[156] O. A. Ladyzhenskaya, 'On modifications of Navier-Stokes equations for large gradients of velocities', *Zapiski Nauchnykh Seminarov POMI*, vol. 7, pp. 126–154, 1968.

[157] O. Ladyzhenskaya and G. Seregin, 'On semigroups generated by initial-boundary value problems describing two-dimensional visco-plastic flows', *Translations of the American Mathematical Society, Series 2*, vol. 164, pp. 99–124, 1995.

[158] G. Seregin, 'On a dynamical system generated by the two-dimensional equations of the motion of a Bingham fluid', *Journal of Mathematical Sciences*, vol. 70, no. 3, pp. 1806–1816, 1994.

[159] G. A. Seregin, 'Continuity for the strain velocity tensor in two-dimensional variational problems from the theory of the Bingham fluid', *Italian Journal of Pure and Applied Mathematics*, pp. 141–150, 1997.

[160] M. Gutmann, 'An existence result for Herschel-Bulkley fluids based on the Lipschitz truncation method', Diploma Thesis, Freiburg University, 2009.

[161] M. Růžička, 'Analysis of generalized Newtonian fluids', in *Topics in Mathematical Fluid Mechanics*, Springer, 2013, pp. 199–238.

[162] M. Fuchs and G. Seregin, 'Some remarks on non-Newtonian fluids including nonconvex perturbations of the Bingham and Powell–Eyring model for viscoplastic fluids', *Mathematical Models and Methods in Applied Sciences*, vol. 7, no. 03, pp. 405–433, 1997.

[163] ——, 'Regularity results for the quasi–static Bingham variational inequality in dimensions two and three', *Mathematische Zeitschrift*, vol. 227, no. 3, pp. 525–541, 1998.

[164] ——, *Variational methods for problems from plasticity theory and for generalized Newtonian fluids*. Springer Science & Business Media, 2000.

[165] S. Volkwein, 'Mesh-independence for an augmented Lagrangian-SQP method in Hilbert spaces', *SIAM Journal on Control and Optimization*, vol. 38, no. 3, pp. 767–785, 2000.

[166] R. Herzog and K. Kunisch, 'Algorithms for PDE-constrained optimization', *GAMM-Mitteilungen*, vol. 33, no. 2, pp. 163–176, 2010.

[167] J. Cea and R. Glowinski, 'Méthodes numériques pour l'écoulement laminaire d'un fluide rigide visco-plastique incompressible', *International Journal of Computer Mathematics*, vol. 3, no. 1-4, pp. 225–255, 1972.

[168] M. Fortin and R. Glowinski, *Méthodes de Lagrangien augmenté: Application à la résolution numérique de problèmes aux limites*. Dunod, Paris, 1982.

[169] M. Moyers-González and I. Frigaard, 'Numerical solution of duct flows of multiple visco-plastic fluids', *J. Non-Newtonian Fluid Mech.*, vol. 122, no. 1, pp. 227–241, 2004.

[170] Z. Yu and A. Wachs, 'A fictitious domain method for dynamic simulation of particle sedimentation in Bingham fluids', *Journal of Non-Newtonian Fluid Mechanics*, vol. 145, no. 2, pp. 78–91, 2007.

[171] R. Glowinski, *Numerical methods for nonlinear variational problems*. Springer Verlag, 1984, 2008.

[172] R. Glowinski and A. Wachs, 'On the numerical simulation of viscoplastic fluid flow', in *Numerical Methods for Non-Newtonian Fluids*, ser. Handbook of Numerical Analysis, P. G. Ciarlet, Ed., vol. 16, Amsterdam: North-Holland, 2011.

[173] Y. Dimakopoulos, M. Pavlidis, and J. Tsamopoulos, 'Steady bubble rise in Herschel–Bulkley fluids and comparison of predictions via the augmented Lagrangian method with those via the Papanastasiou model', *Journal of Non-Newtonian Fluid Mechanics*, vol. 200, pp. 34–51, 2013.

[174] J. He and R. Glowinski, 'Steady Bingham fluid flow in cylindrical pipes: a time dependent approach to the iterative solution', *Numerical linear algebra with applications*, vol. 7, no. 6, pp. 381–428, 2000.

[175] A. Aposporidis, E. Haber, M. A. Olshanskii, and A. Veneziani, 'A mixed formulation of the Bingham fluid flow problem: analysis and numerical solution', *Comput. Methods Appl. Mech. Engrg.*, vol. 200, no. 29-32, pp. 2434–2446, 2011, ISSN: 0045-7825. DOI: 10.1016/j.cma.2011.04.004.

[176] A. Aposporidis, 'Numerical analysis of mixed formulations for Bingham fluids', PhD thesis, Emory University, 2012.

[177] A. Aposporidis, P. S. Vassilevski, and A. Veneziani, 'Multigrid preconditioning of the non-regularized augmented Bingham fluid problem', *Electronic Transactions on Numerical Analysis*, vol. 41, pp. 42–61, 2014.

[178] A. Beris, J. Tsamopoulos, R. Armstrong, and R. Brown, 'Creeping motion of a sphere through a Bingham plastic', *J. Fluid Mech.*, vol. 158, pp. 219–244, 1985.

[179] P. Szabo and O. Hassager, 'Flow of viscoplastic fluids in eccentric annular geometries', *J. Non-Newtonian Fluid Mech.*, vol. 45, no. 2, pp. 149–169, 1992.

[180] M. Bercovier and M. Engelman, 'A finite element method for incompressible non-Newtonian flows', *J. Comput. Phys.*, vol. 36, no. 3, pp. 313–326, 1980, ISSN: 0021-9991. DOI: 10.1016/0021-9991(80)90163-1.

[181] T. C. Papanastasiou, 'Flows of materials with yield', *J. Rheol.*, vol. 31, p. 385, 1987.

[182] R. Tanner and J. Milthorpe, 'Numerical simulation of the flow of fluids with yield stress', *Num. Meth. in Lam. and Turb. Fl.*, pp. 680–690, 1983.

[183] S. González-Andrade, 'Semismooth Newton and path-following methods for the numerical simulation of Bingham fluids', PhD thesis, EPN Quito, 2008.

[184] J. C. De los Reyes and S. González Andrade, 'Path following methods for steady laminar Bingham flow in cylindrical pipes', *ESAIM Math. Model. Numer. Anal.*, vol. 43, pp. 81–117, 01 Jan. 2009, ISSN: 1290-3841.

[185] ——, 'Numerical simulation of two-dimensional Bingham fluid flow by semismooth Newton methods', *J. Comput. Appl. Math.*, vol. 235, no. 1, pp. 11–32, 2010.

[186] J. C. De los Reyes and S. González Andrade, 'A combined BDF-semismooth Newton approach for time-dependent Bingham flow', *Numerical Methods for Partial Differential Equations*, vol. 28, no. 3, pp. 834–860, 2012.

[187] S. González-Andrade, 'A preconditioned descent algorithm for variational inequalities of the second kind involving the p-Laplacian operator', *arXiv preprint arXiv:1504.01429*, 2015.

[188] E. J. Dean, R. Glowinski, and G. Guidoboni, 'On the numerical simulation of Bingham visco-plastic flow: old and new results', *J. Non-Newtonian Fluid Mech.*, vol. 142, no. 1, pp. 36–62, 2007.

[189] R. Glowinski, Y. A. Kuznetsov, and T.-W. Pan, 'A penalty/Newton/conjugate gradient method for the solution of obstacle problems', *Comptes Rendus Mathematique*, vol. 336, no. 5, pp. 435–440, 2003.

[190] B. Dacorogna, R. Glowinski, Y. Kuznetsov, and T.-W. Pan, 'On a conjugate gradient/Newton/penalty method for the solution of obstacle problems. application to the solution of an eikonal system with Dirichlet boundary conditions', in *Conjugate Gradient Algorithms and Finite Element Methods*, Springer, 2004, pp. 263–283.

[191] R. Glowinski, L. J. Shiau, Y. M. Kuo, and G. Nasser, 'The numerical simulation of friction constrained motions (I): one degree of freedom models', *Applied Mathematics Letters*, vol. 17, no. 7, pp. 801–807, 2004.

[192] ——, 'The numerical simulation of friction constrained motions (II): multiple degrees of freedom models', *Applied Mathematics Letters*, vol. 18, no. 10, pp. 1108–1115, 2005.

[193] I. Frigaard and C. Nouar, 'On the usage of viscosity regularisation methods for visco-plastic fluid flow computation', *Journal of Non-Newtonian Fluid Mechanics*, vol. 127, no. 1, pp. 1–26, 2005.

[194] N. J. Balmforth, I. A. Frigaard, and G. Ovarlez, 'Yielding to stress: recent developments in viscoplastic fluid mechanics', *Annual Review of Fluid Mechanics*, vol. 46, pp. 121–146, 2014.

[195] M. Chatzimina, G. C. Georgiou, I. Argyropaidas, E. Mitsoulis, and R. Huilgol, 'Cessation of Couette and Poiseuille flows of a Bingham plastic and finite stopping times', *Journal of non-newtonian fluid mechanics*, vol. 129, no. 3, pp. 117–127, 2005.

[196] M. Chatzimina, C. Xenophontos, G. C. Georgiou, I. Argyropaidas, and E. Mitsoulis, 'Cessation of annular Poiseuille flows of Bingham plastics', *Journal of non-newtonian fluid mechanics*, vol. 142, no. 1, pp. 135–142, 2007.

[197] G. K. Batchelor, *An introduction to fluid dynamics*. Cambridge University Press, 2000.

[198] A. Wachs, G. Vinay, and I. Frigaard, 'A 1.5 d numerical model for the start up of weakly compressible flow of a viscoplastic and thixotropic fluid in pipelines', *Journal of Non-Newtonian Fluid Mechanics*, vol. 159, no. 1, pp. 81–94, 2009.

[199] P. G. Ciarlet, *The finite element method for elliptic problems*. Elsevier, 1978.

[200] G. Froishteter and G. Vinogradov, 'The laminar flow of plastic disperse systems in circular tubes', *Rheologica Acta*, vol. 19, no. 2, pp. 239–250, 1980.

[201] R. B. Bird, R. C. Armstrong, and O. Hassager, *Dynamics of polymeric liquids*, 2nd ed. New York: John Wiley & Sons, 1987, vol. 1.

[202] M. M.-S. Lih, *Transport phenomena in medicine and biology*. New York: John Wiley & Sons, 1975.

[203] C.-S. Zhang, 'Adaptive finite element methods for variational inequalities: theory and applications in finance', PhD thesis, University of Maryland, 2007.

[204] P. Mosolov and V. Miasnikov, 'Variational methods in the theory of the fluidity of a viscous-plastic medium', *Journal of Applied Mathematics and Mechanics*, vol. 29, no. 3, pp. 545–577, 1965.

[205] M. A. Olshanskii, 'Analysis of semi-staggered finite-difference method with application to Bingham flows', *Computer Methods in Applied Mechanics and Engineering*, vol. 198, no. 9, pp. 975–985, 2009.

[206] R. Glowinski, 'Numerical methods for fluids (part 3)', in *Handbook of Numerical Analysis*, P. G. Ciarlet and J.-L. Lions, Eds., vol. 9, Amsterdam: North-Holland, 2003.

[207] J. Donea and A. Huerta, *Finite element methods for flow problems*. John Wiley & Sons, 2003.

[208] M. Bercovier and O. Pironneau, 'Error estimates for finite element method solution of the Stokes problem in the primitive variables', *Numerische Mathematik*, vol. 33, no. 2, pp. 211–224, 1979.

[209] J. Cahouet and J.-P. Chabard, 'Some fast 3D finite element solvers for the generalized Stokes problem', *International Journal for Numerical Methods in Fluids*, vol. 8, no. 8, pp. 869–895, 1988.

[210] M. Schmidt, N. L. Roux, and F. R. Bach, 'Convergence rates of inexact proximal-gradient methods for convex optimization', in *Advances in Neural Information Processing Systems*, 2011, pp. 1458–1466.

[211] K. Jiang, D. Sun, and K.-C. Toh, 'An inexact accelerated proximal gradient method for large scale linearly constrained convex SDP', *SIAM Journal on Optimization*, vol. 22, no. 3, pp. 1042–1064, 2012.

[212] F. Brezzi and M. Fortin, *Mixed and hybrid finite element methods*. Springer Science & Business Media, 2012, vol. 15.

[213] D. Begis, 'Etude numérique de l'écoulement d'un fluide viscoplastique de Bingham par une méthode de Lagrangien augmenté', INRIA-Laboria, Tech. Rep. 42, 1979.

[214] F. Sanchez, 'Application of a first-order operator splitting method to Bingham fluid flow simulation', *Computers & Mathematics with Applications*, vol. 36, no. 3, pp. 71–86, 1998.

[215] E. Mitsoulis and T. Zisis, 'Flow of Bingham plastics in a lid-driven square cavity', *Journal of Non-Newtonian Fluid Mechanics*, vol. 101, no. 1, pp. 173–180, 2001.

[216] D. D. dos Santos, S. Frey, M. F. Naccache, and P. de Souza Mendes, 'Numerical approximations for flow of viscoplastic fluids in a lid-driven cavity', *Journal of Non-Newtonian Fluid Mechanics*, vol. 166, no. 12, pp. 667–679, 2011.

[217] A. Syrakos, G. C. Georgiou, and A. N. Alexandrou, 'Solution of the square lid-driven cavity flow of a Bingham plastic using the finite volume method', *Journal of Non-Newtonian Fluid Mechanics*, vol. 195, pp. 19–31, 2013.

[218] J. Zhang, 'An augmented Lagrangian approach to Bingham fluid flows in a lid-driven square cavity with piecewise linear equal-order finite elements', *Computer Methods in Applied Mechanics and Engineering*, vol. 199, no. 45, pp. 3051–3057, 2010.

[219] P. Saramito and N. Roquet, 'An adaptive finite element method for viscoplastic fluid flows in pipes', *Computer methods in applied mechanics and engineering*, vol. 190, no. 40, pp. 5391–5412, 2001.

[220] N. Roquet and P. Saramito, 'An adaptive finite element method for Bingham fluid flows around a cylinder', *Comput. Methods Appl. Mech. Engrg.*, vol. 193, pp. 3317–3341, 2003.

[221] A. Syrakos, G. C. Georgiou, and A. N. Alexandrou, 'Performance of the finite volume method in solving regularised Bingham flows: inertia effects in the lid-driven cavity flow', *Journal of Non-Newtonian Fluid Mechanics*, vol. 208, pp. 88–107, 2014.

[222] F.-T. Suttmeier, *Numerical solution of variational inequalities by adaptive finite elements*. Springer, 2008.

[223] E. Dean and R. Glowinski, 'Operator-splitting methods for the simulation of Bingham visco-plastic flow', *Chinese Annals of Mathematics*, vol. 23, no. 02, pp. 187–204, 2002.

[224] E. Süli and D. F. Mayers, *An introduction to numerical analysis*. Cambridge University Press, 2003.

[225] G. A. Baker, V. A. Dougalis, and O. A. Karakashian, 'On a higher order accurate fully discrete Galerkin approximation to the Navier-Stokes equations', *Mathematics of Computation*, vol. 39, no. 160, pp. 339–375, 1982.

[226] L. Muravleva, 'Uzawa-like methods for numerical modeling of unsteady viscoplastic Bingham medium flows', *Applied Numerical Mathematics*, vol. 93, pp. 140–149, 2015.

[227] L. Muravleva, E. Muravleva, G. C. Georgiou, and E. Mitsoulis, 'Unsteady circular Couette flow of a Bingham plastic with the augmented Lagrangian method', *Rheologica acta*, vol. 49, no. 11-12, pp. 1197–1206, 2010.

[228] ——, 'Numerical simulations of cessation flows of a Bingham plastic with the augmented Lagrangian method', *Journal of Non-Newtonian Fluid Mechanics*, vol. 165, no. 9, pp. 544–550, 2010.

[229] P. Saramito, 'Efficient C++ finite element computing with Rheolef', 2015.

[230] A. Wachs, 'PeliGRIFF, a parallel DEM-DLM/FD direct numerical simulation tool for 3D particulate flows', *Journal of Engineering Mathematics*, vol. 71, no. 1, pp. 131–155, 2011.

[231] A. Wachs, A. Hammouti, G. Vinay, and M. Rahmani, 'Accuracy of finite volume/staggered grid distributed Lagrange multiplier/fictitious domain simulations of particulate flows', *Computers & Fluids*, vol. 115, pp. 154–172, 2015.